AFFDL-TR-77-25

FAULT TOLERANT DIGITAL FLIGHT CONTROL WITH ANALYTICAL REDUNDANCY

HONEYWELL SYSTEMS & RESEARCH CENTER
MINNEAPOLIS, MINNESOTA 55413

MAY 1977

TECHNICAL REPORT AFFDL-TR-77-25
Final Report for Period 1 January 1976 to 1 February 1977

DDC
RECEIVED
OCT 19 1977
D

Approved for public release; distribution unlimited.

AIR FORCE FLIGHT DYNAMICS LABORATORY
AIR FORCE SYSTEMS COMMAND
UNITED STATES AIR FORCE
WRIGHT-PATTERSON AFB, OHIO 45433

SECURITY CLASSIFICATION OF THIS PAGE (WHEN DATA ENTERED)

REPORT DOCUMENTATION PAGE	READ INSTRUCTIONS BEFORE COMPLETING FORM

1. REPORT NUMBER	2. GOV'T ACCESSION NUMBER	3. RECIPIENT'S CATALOG NUMBER
AFFDL-TR-77-25		

4. TITLE (AND SUBTITLE)	5. TYPE OF REPORT PERIOD COVERED
Fault Tolerant Digital Flight Control with Analytical Redundancy	Final Report 1 January 1976 - 1 February 1977
	6. PERFORMING ORG. REPORT NUMBER

7. AUTHOR(S)	8. CONTRACT OR GRANT NUMBER(S)
Tom Cunningham, Don Carlson, Russ Hendrick, Don Shaner Gary Hartmann, Gunter Stein	F33615-76-C-3031

9. PERFORMING ORGANIZATIONS NAME/ADDRESS	10. PROGRAM ELEMENT, PROJECT, TASK AREA & WORK UNIT NUMBERS
Honeywell Systems & Research Center 2600 Ridgway Parkway Minneapolis, Minnesota 55413	Project 1987, Task 198701

11. CONTROLLING OFFICE NAME/ADDRESS	12. REPORT DATE
Air Force Flight Dynamics Laboratory Air Force Systems Command United States Air Force Base Wright-Patterson AFB, Ohio 45433	May 1977
	13. NUMBER OF PAGES
	377

14. MONITORING AGENCY NAME/ADDRESS (IF DIFFERENT FROM CONT. OFF.)	15. SECURITY CLASSIFICATION (OF THIS REPORT)
396p.	Unclassified
	15a. DECLASSIFICATION DOWNGRADING SCHEDULE

16. DISTRIBUTION STATEMENT (OF THIS REPORT)

Approved for public release; distribution unlimited.

17. DISTRIBUTION STATEMENT (OF THE ABSTRACT ENTERED IN BLOCK 20, IF DIFFERENT FROM REPORT)

18. SUPPLEMENTARY NOTES

19. KEY WORDS (CONTINUE ON REVERSE SIDE IF NECESSARY AND IDENTIFY BY BLOCK NUMBER)

Analytical Redundancy	Aircraft Simulation
Fault Tolerant Flight Control	Redundancy Management
Sensor Fault Detection	Estimation
Kalman Filtering	A-7D Aircraft

20. ABSTRACT (CONTINUE ON REVERSE SIDE IF NECESSARY AND IDENTIFY BY BLOCK NUMBER)

Analytical redundancy offers high potential for solving the sensor redundancy problem. The current state-of-the-art in analytical redundancy contains a number of candidate filters which are developed here from a fundamental relationship of variables through hybrid simulation. Three analytical redundancy concepts of varying complexity were developed for the A-7D aircraft. Two monitor techniques were used: a multiple trip level exceedance criteria currently

over

HD-166 REV 11/74

DD FORM 1473 1 JAN 73   EDITION OF 1 NOV 55 IS OBSOLETE

SECURITY CLASSIFICATION OF THIS PAGE (WHEN DATA ENTERED)

20. in use with voting systems, and a sequential likelihood ratio hypothesis test (SLRT) on the mean value of the error signal.

Results indicate that fault detection, whether designed by classical methods or Kalman filtering, perform similarly and that gust estimation improves fault detection performance. Also, failure isolation for a single set of unlike sensors is difficult to achieve with a reasonable computation load.

The output recommendation is to proceed to flight test with a set of nonlinear diagnostic filters to be used with comparison monitors for dual sensor failure isolation, creating a fail-operative dual sensor system. Fail-safe operation will also be achieved by continuing to monitor the filters and to detect, but not isolate, a second failure.

ACCESSION for

RTIS	White Section	X
DDC	Buff Section	☐
UNANNOUNCED		☐
JUSTIFICATION		

BY
DISTRIBUTION/AVAILABILITY CODES

Dist.	AVAIL. and/or SPECIAL	
A		

D D C

RECEIVED

OCT 19 1977

D

FOREWORD

This report discusses a design and simulation study of sensor redundancy through computer algorithms designed to determine faults analytically. The principal investigators were T. B. Cunningham and G. L. Hartmann of Honeywell Inc., Systems and Research Center. The project engineer was R. D. Poyneer of the Control Systems Development Branch of the Air Force Flight Dynamics Laboratory. Mr. Poyneer's valuable assistance in technical review and meeting coordination was greatly appreciated.

CONTENTS

CONTENTS (continued)

CONTENTS (continued)

CONTENTS (concluded)

LIST OF ILLUSTRATIONS

LIST OF TABLES

LIST OF TABLES (concluded)

LIST OF ABBREVIATIONS AND SYMBOLS

Abbreviations

A/D	Analog to Digital
ADC	Air Data Computer
AFCS	Automatic Flight Control System
ARS	Attitude Reference System
AOA	Angle-of-Attack
BW	Bandwidth
CAS	Control Augmentation System
D/A	Digital to Analog
dB	Decibels
dps	Degrees per Second
DF	Diagnostic Filter
DFBW	Digital Fly-By-Wire
DFCS	Digital Flight Control System
Fail-Op	Failure with Operational System Reversion Mode
FC	Flight Condition
fps	Feet per Second
H_i	Hypothesis Number i
H.O.	Hardover
HSI	Horizontal Situation Indicator
IMU	Inertial Measurement Unit
KF	Kalman Filter
Kts	Knots (Nautical Miles per Hour)
L-D	Lateral-Directional
LIM	Limit
LON	Longitudinal
MM	Multimode
M.T.	Multiple Trip
N/A	Not Applicable
PSD	Power Spectral Density
RMS	Root Mean Square
rps	Radians per Second
RR	Residual Ratio
RSS	Root Sum Square
SDF	Super-Diagnostic Filter
S.F.	Scale Factor
SLRT	Sequential Likelihood Ratio Test
SW	Switch

WRT	With Respect to
μsec	Microsecond (10^{-6} Second)
msec	Millisecond (10^{-3} Second)

Operators

$\sim N(a, b)$	Normal Distribution with Mean = a and Intensity = b
$\triangleq$	Definition
∇	Gradient Functional
Δ	Difference
Φ	Normal Distribution Function
π	Multiply
$(\hat{\ })$	Estimate
$(\bar{\ })$	Prediction
$(\tilde{\ })$	Measured
$(\ )^T$	Transpose
$(\ )^{-1}$	Inverse
$(\dot{\ })$	Derivative (WRT time)
$(\ )*$	Conjugate
$\cap$	Intersection
$\angle$	Angle
a:b	a given b
det( )	Determinant
E( )	Expected Value
F( )	Normal Probability Functional
f( )	Function
Ln	Natural Logarithms
P( )	Probability Functional
R( )	Joint Probability Functional
S( )	Joint Probability Functional
Tr( )	Trace

Greek Symbols (Upper Case)

Γ	Observability Matrix
Γ_i	Column i of Γ
ΔT	Sample Time Increment
Λ	Likelihood Ratio

Φ	Discrete Transition Matrix, Correlation Transfer Matrix
Σ	Summation

Greek Symbols (Lower Case)

α	Angle-of-Attack
β	Sideslip Angle
δ	Control Surface Deflection
$\delta a, \delta e, \delta r$	Aileron, Elevator, and Rudder Deflection, respectively
$\delta_{i,j}$	Kroneker Delta Function
$\delta(t)$	Dirac Delta Function
ϵ	Error
γ	Flight Path Angle
ξ	Noise (white)
η	Noise (white)
θ	Euler Pitch Angle
λ	Failure Rate, Eigenvalue, Quaternion Element
μ	Mean Value
ν	Kalman Filter Residual
π	PI, Noise (white)
ρ	Density
ρ_c	Correlation Coefficient
σ	Standard Deviation
τ	Time Constant
ϕ	Euler Roll Angle
ψ	Euler Yaw Angle
ω_s	Frequency
χ	Velocity Yaw Angle

Upper Case Symbols

A	Discrete System Dynamics Matrix
A_F	Discrete Filter Matrix
A_x, A_y, A_z	Forward, Lateral, and Vertical Body Accelerations, respectively
B, B_1	Discrete State Matrix WRT Control (Use B_1 when B_2 is also used)
B_2	Discrete State Matrix WRT Noise
B_D	Kalman Filter Residual Covariance Matrix (D = design)
$B*$	Kalman Filter Residual Covariance Matrix (* = optimal)

C	Comparison Monitor, Discrete Output Matrix WRT State Vector
C_x, C_y, C_z	Dimensionless Aerodynamic Coefficients (x, y, z) Directions, respectively
D, D_1	Discrete Output Matrix WRT Control (Use D_1 when D_2 is also used)
D_2	Discrete Output Matrix WRT Noise
E, E_1	Continuous Output Matrix WRT Control (Use E_1 when E_2 is also used)
E_2	Continuous Output Matrix WRT Noise
F	Continuous State Matrix
F_x, F_y, F_z	Forward, Lateral, and Vertical Body Forces, respectively
G, G_1	Continuous State Matrix WRT Control (Use G_1 when G_2 is also used); Gravity
G_2	Continuous State Matrix WRT Noise
H	Discrete Output Matrix WRT State
Hz	Hertz (cycles per second)
I_{xx}	Moment of Inertia About X-axis
I_{xz}	Cross Moment of Inertial (XZ axis)
I_{yy}	Moment of Inertia About Y-axis
I_{zz}	Moment of Inertia About Z-axis
K	Constant Gain
K*	Kalman Filter Gain
K_n	Noise Intensity
K_{sens}	Cross-Axis Sensitivity
L	Moment Applied About Body X-axis; Log Likelihood Function
L_N	Likelihood Function for a Sequence of N Data Points
L'_x	Roll Moment Coefficient WRT x ($x = \beta, \rho, r, \delta_a, \delta_r$, etc.)
M	Moment Applied About Body Y-axis; Kalman Filter Error Covariance Matrix--Before Update; Mach
M_P, M_Q, M_R	Roll, Pitch and Yaw Rate Scale Factor Errors, respectively
M_S	Error Covariance Matrix for Quaternions--Before Update
Mass	Vehicle Mass
M'_x	Pitch Moment Coefficient WRT x ($x = \alpha, Q, \delta_e$, etc.)
N	Moment Applied about Body Z-axis
N	General Integer Variable
N'_x	Yaw Moment Coefficient WRT x ($x = \beta, p, r, \delta_a, \delta_r$, etc.)
P	Body Roll Rate
P	Kalman Filter Covariance Matrix--After Update

LIST OF ABBREVIATIONS AND SYMBOLS (continued)

P_b	Roll Rate Bias
P_s	Error Covariance Matrix for Quaternions--After Update
Q	Vehicle Body Pitch Rate, Noise Intensity Matrix
Q_b	Pitch Rate Bias
Q_s	Probability of Sensor Failure
R	Vehicle Body Yaw Rate, Measurement Noise Intensity Matrix
R_b	Yaw Rate Bias
R_s	Measurement Noise Intensity Matrix for Quaternions
S	Sensor
S_A	Vehicle Characteristic Area
S_x, S_{x_O}, S_{x_I}	Sensor Outputs (During, Before, and After Fault)
U, V, W	Forward, Lateral, and Vertical Body Velocity States
U_T	Total Forward Speed
U_g, V_g, W_g	Forward, Lateral, and Vertical Components of Wind Gusts, respectively
V_x	Velocity in X Direction
V_o	Trim Velocity
V_T	Total Velocity Magnitude
X	Forward Position
X_e, Y_e, Z_e	Earth Referenced Forward, Lateral, and Vertical Positions, respectively
X_u	Roll Uplogic Variable
Y_x	Lateral Force Coefficient WRT χ ($\chi = \beta, p, r, \delta_a, \delta_r$, etc.)
Z	Total Covariance Matrix (State and Estimation Error)
Z_x	Vertical Force Coefficient WRT χ ($\chi = \alpha, Q, \delta_e$, etc.)

Lower Case Symbols

a_g	Gust Correlation Constant
a_w	Vertical Gust Correlation Constant
a_y	Acceleration (+Y Direction)
a_z	Acceleration (+Z Direction)
b	Wing Span
c	Command, Chord Length
e	Error
$\underline{e}$	Noise Vector
g	Gust Intensity

LIST OF ABBREVIATIONS AND SYMBOLS (concluded)

h	Altitude
i, j, k	Indexing Integers
ℓ_x	Normal Accelerometer Offset Distance
m	Measurement (subscript)
m_o	Trim Pitching Moment
n_r	Number of Responses
n_x	Number of States
n_y	Body Axis Lateral Acceleration
n_z	Normal Acceleration (-Z Direction)
p	Vehicle Body Roll Rate
q	Vehicle Body Pitch Rate
$\bar{q}_a$	Dynamic Pressure
$\bar{q}_c$	Dynamic Pressure (Measured)
q_b	Quaternion Rotation from Reference Frame a to b
r	Vehicle Body Yaw Rate
s	LaPlace Operator
t	Time
u	Control Vector
v	Lateral Direction (subscript), Kalman Filter Residual
w	Wing (subscript)
x	State Vector
y	Measurement Vector
z	Specialized State Vector

SECTION 1

INTRODUCTION AND PROGRAM OVERVIEW

1.1 THE SENSOR REDUCTION PROBLEM

Reliable digital flight control systems are burdened with large numbers of sensors which
are required for both quality and redundancy.

The demand for control quality has expanded the types of sensors used in basic augmen-
tation functions. The humble yaw damper, with a single rate gyro, for example, has
grown to be a sophisticated inertially coordinated CAS, requiring sensed rates, attitudes,
angle-of-attack and airspeed. The pitch damper has grown to be a complex multifunction
control law using several sensed quantities to drive multiple surfaces. The benefits
of this improved quality are dramatic (e.g., the A-7D Digital Multimode System), and
future aircraft are not likely to accept less.

At the same time, mission reliability requirements have forced duplication, triplication,
and even quadruplication of critical sensing systems. Hardware redundancy has grown
to the point where the potential for mismanagement alone represents a major concern
for flight safety.

These large sensor populations exact their toll in system cost. Also, many sensors
distributed throughout an airframe make wonderful antennas to aggravate lightning and
EMP susceptibility. They impose environmental problems, compromise vulnerability,
and constrain overall airframe design. Hence, there is ample motivation to reduce the
sensor population. Fortunately, there are reasons to believe that significant reductions
are possible. Present voting techniques, for example, waste as much as a full channel of
sensor hardware. The control laws themselves may also use excessive hardware in that
certain sensed signals may be replaceable with equivalent estimates.

1.2 STUDY GOALS

The purpose of this study was to demonstrate just how much sensor reduction is attain-
able in practice. Examinations of various techniques for achieving sensor reduction
were conducted, with particular emphasis on so-called "functional" or "analytical"

1

redundancy concepts. Three promising concepts were selected and evaluated through detailed design, computer cost effectiveness, and hybrid simulation for the A-7D air-craft. The most promising single concept was then selected from combinations of all three and recommended for flight test.

Initial investigations with the current A-7D sensor system resulted in two possible design goals:

1. Design to maintain current system reliability with associated sensor reduction, and

2. Design to upgrade system reliability to achieve improved mission standards with current sensor complement.

Of the two approaches, the second presents a greater technical challenge and is more compatible with current digital fly-by-wire mission standards. It is also implicit that development of the technology necessary to achieve the second design goal will encompass development of the first.

1.3   CONCEPT SELECTION

Two general techniques are recognized for sensor reduction:

1. Control Law Modification--Ensures that operational requirements can be met with the minimum number of sensors.

2. Fault Tolerant Design--Exploring all possible techniques for meeting relia-bility requirements of failure tolerance with a minimum number of sensors, the following potential solutions exist:
    *   Skewed and special sensors
    *   Integration for redundancy management (e.g., flight sensor sharing with navigation function)
    *   In-line sensor monitoring
    *   Analytical redundancy

Of these, analytical redundancy offers high promise for sensor reduction.

2

1.3.1   Analytical Redundancy

In general, analytical redundancy is approached using one of two basic building blocks:

- Diagnostic Filter (DF)--An assembly of sensors combined in some functionally related fashion such that a failure of any one can be diagnosed.

- Super-Diagnostic Filter (SDF)--An assembly of sensors combined in some functionally related fashion such that a failure of one can be detected and isolated to the specific faulted sensor.

Given these two definitions, one can use assemblies of diagnostic filters to construct a super-diagnostic relationship through truth table logic.

A literature survey was performed to examine currently available techniques that had promise of being able to detect and isolate faults in aircraft sensors and meet current on-board flight computer allocations.   All schemes fell into three basic categories:

1.   Failure detection with assemblies of diagnostic filters

2.   Specific diagnostic filter design techniques

3.   Explicit super-diagnostic filter design techniques

Three concepts were chosen for development through hybrid simulation.   These concepts are distinguished by design procedure and complexity.   The final recommended system is a combination of individual filters designed within these concepts.

Concept I.   Observer/Blender--Five diagnostic filters, which model physical relationships using sensor outputs, provide fault detection for nine sensors (n_z, P, Q, R, ϕ, θ, ψ, α, h).   Monitors use a three trip level exceedance criteria.   Trip boundaries are scheduled on sensor outputs to account for unmodeled dynamics and sensor anomalies.

Concept II.   Diagnostic Kalman Filters--Kalman filters with greater capability for modeling sensor anomalies in the filter, i.e., bias, scale factors, and estimation of wind gusts.   Fault detection is provided for sensors included in Concept I plus U_m and n_y.

Concept III.   Super-Diagnostic Design--Kalman filters using linear equations for pitch and lateral-directional dynamic equations of motion. Both detection and isolation are addressed. These filters contain gain-scheduled models for the A-7D. All inputs were prefiltered to eliminate low frequency dynamics.

1.3.2   Fail-Operational Followed by Fail-Safe Philosophy

Concepts I and II can operate with comparison monitors of dual sensors to isolate faults for a fail-operational capability. A fail-safe capability exists for Concepts I and II for all single sensors and for dual sensors after one failure.

1.3.3   Fault Detection Monitors

Fault detection monitors used in this study fall into three categories:

1.   Multiple trip monitors were designed for all concepts. These are fairly standard monitors. Scheduling trip boundaries on sensor values, to handle known sensor and modeling errors, was performed in Concept I. Pilot input command scheduling to handle aircraft transients was used in all concepts. The fault detection logic requires three consecutive trips for a fault to be declared.

2.   A sequential likelihood ratio test (SLRT) of the mean value was used in Concepts II and III along with multiple trip monitors. Theory based on hypothesizing a shift in the mean value of the filter error signals was used. .

3.   A SLRT on likelihood function differences was used with comparison monitors. This function isolates a faulted dual sensor by deciding which sensor channel has the fault once a miscompare has been declared.

1.3.4   A-7D Design Application

Concepts chosen for development were applied to the A-7D aircraft. The reasons for this choice were as follows:

4

- The A-7D is currently being flight tested with an all-digital CAS and multimode outer loop control design. The dual Honeywell 301 computers and dual acceleration and body rate sensor offer a good baseline for the design philosophy of this study.

- The HDC 301 computers currently on board the A-7D have residual core and calculation frame time which allow parallel programming of either Concepts I or II to conduct fail-operational (fail-op) and fail-safe experiments.

Another reason for choosing the A-7D aircraft and flight control system is the prospect of achieving a fairly dramatic improvement in mission reliability. The A-7D system with dual computers currently has fail-safe dual sensors and servos. Its mission abort probability is estimated at 12.6×10^{-4} per flight hour. Analytical redundancy operating at a 95 percent effectiveness cuts this to 6.6×10^{-4}. If the same 95 percent effective redundancy were achieved for the servos, the mission abort probability would be reduced to 0.8×10^{-4}.

1.4 CONCEPT DEVELOPMENT

The three selected concepts were developed for hybrid simulation of the A-7D. Key design issues addressed were the following:

- Appropriate monitor level scheduling in Concept I to account for filter modeling simplifications

- Kalman filter design modifications to insure that each sensor had a sufficient failure transient for failure detection

- Gain-scheduled Kalman filters which would generate consistent error signal statistics over the flight envelope

A pre-simulation analysis of fault detection monitors was also conducted to:

- Insure that the false alarm specification (<1 per 1000 flight hours) was met

- Investigate the impact of error signal autocorrelation on monitor performance

Sensor error and fault modeling requires careful treatment for fault detection because typical sensor models are not sufficient and fault characteristics are not well-defined. Key modeling issues are:

5

- Modeling of characteristics (particularly noise) based on an operational environment, and not on manufacturer's sales data

- Fault categories based on type and percentages of occurrence for each sensor

1.5 A-7D SIMULATION

Much attention was given to false alarm checkout. Monitors were adjusted based on filter responses to the following inputs:

- Random wind gusts (6 ft/sec)
- $60°$ in one second roll commands

- Two g pitch-up maneuvers
- "1-COS" and "β" gust inputs

Monitor adjustments included a roll uplogic, scheduled with stick commands, designed to handle high roll rate transients.

Fault runs consisted of subjecting the fault detection algorithms to a number of high probability faults:

1. Sensor hardover

2. Dead sensor

3. Dynamic response reduction (accelerometers only)

4. Scale factor changes

5. Bias shifts

1.6 CONCLUSIONS AND RECOMMENDATIONS

Results from the A-7D simulation offer a number of performance conclusions both on an absolute basis, i.e., which ones will work in the real-world environment of flight test, and on a relative basis, i.e., which ones work better than others.

On an absolute basis, Concept I works well for faults in all sensors (n_y and U_m not addressed) except α_m and has marginal performance for n_z. Concept II performs well for almost all sensors with marginal performance for n_y (this was anticipated at the outset).

6

Concept III results lead to a number of performance concerns and developmental needs. The basic notion of obtaining fault detection and isolation for a single set of unlike sensors (measuring different quantities) was addressed. Two areas of greatest difficulty for Concept III were:

- Accelerometer soft failure detection, e.g., dead sensor, scale factor faults, and dynamic response faults.*

- Fault isolation based on more than one filter detecting a given fault. This demonstrated some difficulty if both filters did not detect the failure at the same time.

Table I contains a subjective summary of the Concept I and II comparative results and a recommended system for further development through flight test.

TABLE 1. SUBJECTIVE COMPARISONS OF CONCEPTS I AND II

Sensor	Performance		Recommendation	Reason
	Concept I	Concept II		
1. n_{zm}	marginal	good	Concept II	Clear performance edge over Concept I.
2. α_m	poor	good		
3. h_m	good	good		
4. U_m	not addressed	good		
5. P_m	good	good	Concept I or II	Concept I is less complex with comparable performance. Concept II bias estimates can be used for slow bias faults.
6. ϕ_m	excellent	excellent		
7. Q_m	good	good		
8. θ_m	excellent	excellent		
9. R_m	good	good		
10. ψ_m	excellent	excellent		
11. n_{y_m}	not addressed	marginal	Retain Concept II filter for flight test	Retains the only n_y diagnostic. Offers some state reconstruction capability.

---

*All concepts failed to detect dynamic response faults.

7

A comparison of monitors shows that the sequential likelihood ratio test (SLRT) of residual mean values performed very well relative to the multiple trip monitor. SLRT caught hardover failures sooner (almost by definition, as the multiple trip monitor has a built-in delay). SLRT also showed good soft failure identification characteristics, particularly scale factor changes that escaped the multiple trip monitor.

Finally, state reconstruction was not addressed here since it was recognized early that this would not provide a fail-operational capability. Some consideration might be given to a fail-suboperational capability which would result in the replacement of a single failed sensor with an estimated sensor. This would be in lieu of automatically going from fail-op to fail-safe upon a second sensor failure. Retaining the lateral-directional gain-scheduled filter would provide an experimental base for this in addition to its own n_y fault diagnostic capability.

1.7 DOCUMENT ORGANIZATION

This document is organized into six sections. This section contains an introduction to sensor reduction and a program overview. Section 2 presents a detailed explanation of sensor reduction, a classification of techniques, and an overview of analytical redundancy. The rationale for the three concepts chosen for development is also given.

Section 3 covers sensor modeling, including basic measured quantities, sensor characteristics, fault models, and sensor simulation models. Section 4 contains design details for the various analytical redundancy filters and monitors and describes how they fit together into a fail-op/fail-safe system. Section 5 presents the simulation setup and results. Specific technical conclusions and recommendations are discussed in Section 6.

Cost effectiveness, i.e., what each system will cost in computer requirements and save in hardware costs, is presented in Appendix A. The hybrid computer simulation of the A-7D with CAS is discussed in Appendix B. Appendix C outlines an alternate scheme for Euler angle body rate fault detection using quaternions.

Finally, strip charts of aircraft and fault detection filter performance during simulation are presented in Appendix D. The fault detection algorithms are documented in Appendix E.

SECTION 2

CONCEPT SELECTION

2.1   SENSOR REDUCTION TECHNIQUES

There are two general techniques for reducing the number of sensors required for flight control.   One is to use fewer sensors in the basic simplex (single channel) control laws; i.e., redesign the controller to use fewer sensed quantities while achieving the same performance.   This we'll call "control law modification."   The second is to use fewer duplicate sensors in the redundancy management scheme, i.e., achieve the same level of redundancy with fewer hardware elements.   This we'll call "fault tolerant design." These techniques can be used together to minimize the overall sensor population.

2.1.1   Control Law Modification

Control law modifications reduce the number of sensor types required for a simplex control channel to a minimum.   This, in turn, reduces the number of redundant sensors required for system reliability.   In essence the technique implies better control law design.   These techniques are application dependent.

Signal synthesis is an example of a control law modification.   The number of sensors required is reduced by synthesizing a signal or group of signals from a reduced set. In the context of modern control theory, the synthesis elements are Kalman filters or Luenberger observers.   In a classical sense, the synthesis is achieved by dynamic compensation of the reduced sensor set.   In the final analysis, the two viewpoints are equivalent.

The issues are complexity and performance.   Reduction in the number of sensors is traded off against increased complexity of the control laws.   In analog systems this is an important tradeoff.   It is not nearly as critical when the system is implemented digitally.   Then system performance is the driver.   The quality of the synthesized signal must be equivalent to the sensor eliminated.   Primary quality parameters are DC accuracy, signal bandwidth, and noise content.   Observability theory tells us that the state variables of the system, and hence sensor outputs, can be reconstructed from a single hardware sensor if the system is completely observable from that sensor.   We

9

know that in a practical sense, however, the quality of the synthesized signal will suffer. Synthesizing rates from attitudes is an example. This requires high bandwidth filters approaching the quality of a differentiator over the control bandwidth. This is not realistic unless a very high quality (low noise, wide bandwidth) attitude signal is available. Thus, we must exercise practical judgment in applying signal synthesis techniques. Even the most sophisticated estimation theories cannot overcome basic physical limitations.

Integrated flight management is another control law modification technique. The idea is to combine subsystems which use common sensor types. For example, the ring laser gyro is being studied for joint applications of strapdown navigator and primary flight control (Reference 1). The quality of the rate and acceleration signals derived from the navigator is high. The signals can be used in flight control loops. The issue is cost. Normally the navigator is not flight critical and is not made redundant. Four navigation systems would be required for a system with dual-fail-operative capability (using voting techniques). How does this cost compare with one navigation system and triply redundant sensors? A second issue is multiple failures. Loss of one element of the navigation system, a gyro for example, means loss of both attitude and rate information.

The end product of control law modification is a better control system design with a minimum set of sensor types. No sensor can be removed from this set without unacceptably compromising control performance. Maintaining performance through state reconstruction and integrated flight management is a worthwhile goal. Sensor reduction, as it is addressed in this design study, begins after assuming that the minimum necessary sensor set for performance has been identified.

2.1.2   Fault Tolerant Design

Once a minimal simplex sensor set has been defined, fault tolerant design techniques can address the redundancy problem. Our goal is to eliminate the need for quad sensors currently dictated by dual-fail-operative requirements. Potential solutions are:

- Skewed and special sensors
- Integration for redundancy management
- In-line sensor monitoring
- Analytical redundancy

-

10

The first three of these approaches has been studied extensively (References 2, 3, 4). Where the technology is state-of-the-art, it is used here. Where not, the limitations are fundamental hardware limitations. Analytical redundancy is new and shows promise of payoff.

Skewed and Special Sensors--A skewed sensor arrangement can significantly reduce the number of sensors required for redundancy management. For example, with orthogonal gyros in a three-axis system, a total of 12 are required for a quad-redundant dual-fail-operative capability. The same system with skewed gyros requires only six for the same capability. Properly configured, any three gyros can be resolved to the required three orthogonal signals. After two failures (four remain), the fact that a third failure has occurred can be identified. The same savings apply for skewing accelerometers. With two-axis acceleration required, a_z and a_y skewing reduces the number of sensors from eight to five.

Table 2 shows the savings that can be accrued simply by skewing gyros and accelerometers. The sensor complement consists of the 12 instruments listed in the Request for Proposal. However, skewing has practical limitations. For gyros, the scale and resolution requirements are different for the three axes. In a conventional (orthogonal) system, the roll rate gyro must have a larger scale or range than the pitch rate gyro. Conversely, the pitch rate gyro requires more resolution. In a skewed arrangement all instruments must be the same. This will either limit the resultant signal quality or increase the component cost, potentially by more than the savings accrued by eliminating six conventional gyros.

A generalized form of skewing can be achieved with special sensors. In this case the measurements are skewed in measurement space (p, q, r, a_z, a_y,...) rather than geometrically. Special sensors measure linear combinations of variables. For example, in the pitch axis, special sensors can measure signals (m) of the form

$$m = Q + kA_z$$

Each sensor has a different, known, constant k. Any two sensors can span the Q-A_z subspace. Using this type of sensor, a conventional quad-redundant system requiring four pitch rate gyros and four normal accelerometers can be replaced by five special sensors.

11

TABLE 2.   SENSOR REDUCTION WITH SKEWING

| | Number Required | | |
Sensor	Baseline Quad.	Skewed	Skewed and Integrated
Gyros (3 axis)	12	6	5*
Accelerometers (2 axis)	8	5	4*
Altitude and Vertical Velocity	8	8	6**
Attitude (3 axis)	12	12	9**
Dynamic Pressure	4	4	4
Angle-of-Attack	4	4	4
Navigation System	0	0	1
Total Sensors	48	39	33 + Nav

*One sensor in Nav system used.
**One channel replaced with Nav system.

Why don't we build such sensors today? We do, but we throw them away! Component manufacturers work hard at building gyros that are not sensitive to acceleration (k = 0). In component testing, those with k ≠ 0 are rejected. The obvious problem in building such devices is consistency. In addition, special sensors tend to be unique for each application, which increases manufacturing costs.

Integration for Redundancy Management--Another way to reduce redundant sensors is through subsystem integration. This technique is currently being employed for redundancy management in the Space Shuttle flight control system. The concept uses sensor data from subsystems which are not normally functionally related for monitoring and tie breaking. In the case of the Space Shuttle, derived rates from the navigation system are used in the primary flight control system for voting. The concept is related to integrated flight management. In this case, the redundant subsystem signal is not used directly in the feedback loop because of signal quality limitations.

Table 2 shows the savings that can be accrued by skewing and integrating the navigation and flight control systems for redundancy management.

12

In-Line Monitoring--Still another way to achieve fault tolerant design is through in-line monitoring. It was determined in the F-4 DFCS study (Reference 5) that a triplex system with 95 percent self-test confidence can meet the dual-fail-operative failure rate requirements. The state-of-the-art is approaching 99 percent self-test confidence for servos and computers. Unfortunately, this is not true for sensors. The primary reason for the difference is that the input to the sensor is unknown and cannot be used for self test. For servos and computers, the inputs are available for use in self-test systems.

Some ad hoc approaches have been developed for in-line sensor monitoring of rate gyros and accelerometers. Partial self test of gyros can be achieved using a spinmotor rotation detector to ensure that the speed has not fallen below the minimum detectable level. To ensure gimbal freedom and proper output pickoff, a small-amplitude tracer monitor signal can be applied to a torquer winding. The dither signal is normally well outside the control system bandwidth. The dither technique is also applicable to accelerometers.

Nearly all failures that occur in the device stop the wire vibration in the wire gyros and accelerometers. Thus a test on the wire vibration is a good in-line self-test technique.

In-line sensor self-test feasibility is limited by several factors. The input to the sensor is unknown except when special test signals are introduced. Self-test techniques do not include sensor installation errors (base mounting). Finally, the additional complexity and cost associated with sensor self test may override the savings gained by reducing the number.

Analytical Redundancy--Up to this point we have discussed what might be called conventional approaches to sensor reduction: control law modifications, skewing, integration, and sensor self test. We have concluded that these techniques are fairly well understood. In particular we know what the payoff of each of these techniques will be and how to use them when hardware considerations permit.

The one remaining sensor reduction technique--analytical redundancy--is not nearly so well in hand. Various theoretical and simulation studies have shown that sensor failures can be detected by exploiting known functional relationships between different sensors. This possibility opens up a whole new approach to failure detection with significant savings potential. In the following subsection we explore analytical redundancy techniques in detail.

13

2.2 ANALYTICAL REDUNDANCY

The basic idea of analytical redundancy is to use known relationships between different sensors in order to detect failures. This idea has produced a growing variety of redundancy concepts, ranging from simple signal blenders to complex banks of Kalman filters. Each new investigator seems able to invent yet another scheme to add to the collection. This proliferation has obscured common basic features and has made comparisons and evaluations of competing approaches difficult. For this reason, we interpret "analytical redundancy" as a general failure detection concept. We can then examine specific approaches which are further classified for comparison.

2.2.1 The General Concept

Analytical redundancy hinges on the existence of two basic functions or "building blocks" which can be assembled in various ways to achieve fault detection. The building blocks are:

1. Diagnostic-Filter (DF)--This is an algorithm which processes data from a family of N functionally related sensors in order to estimate signals or states and also to assess the health of the sensor family. Outputs from a diagnostic filter are signal estimates plus one binary error flag which indicates "0" if all sensors are healthy and "1" if any one of them has failed.

2. Super-Diagnostic Filter (SDF)--This is an algorithm which performs the functions of a diagnostic filter but with enhanced capability to assess the health of individual sensors. Its outputs are signal estimates plus error flags for each sensor in the input family.

How these building blocks are actually constructed is discussed in a later subsection. First, however, we will consider how they may be assembled to provide fault detection.

Assemblies of Building Blocks--The way in which diagnostic or super-diagnostic filters can be combined for sensor fault detection depends upon the overall structure of the failure management approach, i.e., whether uniform redundancy requirements apply throughout the system or whether various reversion modes with different redundancy levels are allowed. We will first discuss assemblies for uniform requirements in two basic sensor groups and then turn to assemblies for reversion modes.

14

Interchangeable and Noninterchangeable Sensors--For redundancy requirements, flight control sensors can be grouped into two basic categories: interchangeable and non-interchangeable. The first group includes all sensors which can substitute for one another in the event of a failure. Any one can replace any other. Examples include skewed gyros or skewed accelerometers. When one sensor fails, another can be sub-stituted, provided only that the sensor-to-body coordinate transformation is appropri-ately modified. In contrast, the second category consists of sensors which must be replaced on an individual one-for-one basis. If one fails, only a duplicate can replace it without compromising estimator/control quality and performance. An example is the minimal sensor sets which remain after sensor reduction by control law modifica-tions, as described earlier.

Now suppose that N healthy sensors are needed in each of these categories in order to be operational. Then a minimum of $N + 2$ interchangeable sensors (two extras) and 3N noninterchangeable sensors (two extras of each type) is required for $(fail-op)^2$ perfor-mance. We know all too well, of course, that these minimum numbers are not sufficient for traditional voting redundancy techniques. These require $N + 3$ and 4N sensors, respectively, in order to resolve voting conflicts. With diagnostic or super-diagnostic filters, however, the minimum numbers will suffice.

This latter point is illustrated in Figure 1 which shows fault detection schemes using diagnostic filters. For simplicity, the figure is limited to fail-op performance with $N = 2$. It can be readily generalized to arbitrary N and to $(fail-op)^2$ performance.

Figure 1A treats the case of interchangeable sensors. Three sensors are required for fail-op performance and two diagnostic filters suffice to detect failures. This is verified by the truth table in the figure. In order to generalize, note that there are $N + 2$ columns in the truth table, one for each sensor failed individually $(N + 1)$ and one for the no-fail condition. Note also that each column corresponds to a unique binary "word" constructed from the error flag "bits" of the diagnostic filters. Since there are 2^M such words for M diagnostic filters, it follows that the necessary number of filters is

$$M = [\log_2 (N + 2)]*$$

---

*The brackets indicate the nearest larger integer.

15

A. INTERCHANGEABLE SENSORS

TRUTH TABLE

ERROR FLAGS	SENSORS FAILED			
	NONE	S1	S2	S3
E12	0	1	1	0
E23	0	0	1	1

B. NON-INTERCHANGEABLE SENSORS

TRUTH TABLE

ERROR FLAGS	SENSORS FAILED				
	NONE	$S1_1$	$S1_2$	$S2_1$	$S2_2$
E12	0	1	0	1	0
C1	0	1	1	0	0
C2	0	0	0	1	1
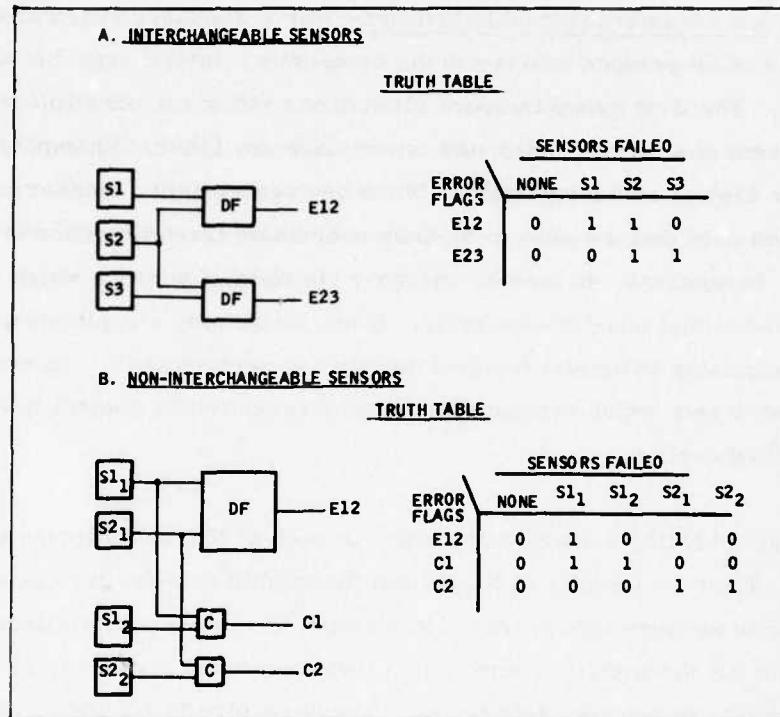
Figure 1. Fault Detection with Diagnostic Filters

We can further deduce from the truth table that the sensor inputs to each of these filters are uniquely determined by the unit entries in each row of the table. Hence, we have a completely general way to assemble diagnostic filters for interchangeable sensors:

1. Determine the number of sensors:

    N + 1 for fail-op

    N + 2 for (fail-op)^2

2. Determine the number of diagnostic filters:

    $[\log_2 (N + 2)]$ for fail-op

    $[\log_2 (N + 3)]$ for (fail-op)^2

3. Determine sensor inputs to each filter from the truth table. *

---

*This step offers some flexibility in the event that $[\log_2 (N + 2)] > \log_2 (N + 2)$. Then we have more potential columns and can choose the most convenient ones for filter mechanization.

The diagnostic filter arrangement for noninterchangeable sensors is shown in Figure 1B. Because duplicate sensors are available in this case, it is sufficient to use a single diagnostic filter plus two ordinary comparators. The filter monitors one channel of sensors while the comparators monitor the other. The fault detection capability of this arrangement is again verified by a truth table. The arrangement generalizes easily to larger N (one diagnostic filter plus N comparators) and also to $(fail-op)^2$ performance (add the third channel of sensors plus comparators to check against Channel 1 or Channel 2).

Similar arrangements can also be developed using the super-diagnostic filter building block. However, because this filter isolates individual sensor failures on its own, the arrangements become very simple. Only one super-diagnostic filter is needed in all cases. While this seems very attractive from the point of view of structure, it may not be justifiable in terms of complexity. The super-diagnostic filter must compete with a few ordinary diagnostic filters and a few comparators to achieve equal sensor reduction benefits.

The sensor reduction comparisons of SDF's and DF's are highlighted in Table 3. The table compares the number of building blocks required to achieve minimum sensor sets and also shows standard voting requirements. As we can see, the greatest sensor reduction benefit of analytic redundancy, no matter which building block is used, is realized for noninterchangeable sensors. In this case, one diagnostic filter plus 2N comparators achieves the same benefits as a single super-diagnostic filter. An SDF which is more complicated than this will not be competitive.

For the case of interchangeable sensors, the total sensor reduction benefits are smaller and more diagnostic filters are required to match the super-diagnostic filter. Again, however, very complicated SDF's will not be competitive. As will be shown later, several analytical redundancy schemes proposed in the literature violate these competitive realities.

Reversion Modes--So far we have treated only uniform redundancy schemes. All sensors had the same fail-op or $(fail-op)^2$ requirements. This is not typical of today's flight control systems. Rather, high levels of redundancy are usually required for critical inner loops with lower levels for outer loops. Flight operations consisting only of inner loops are then treated as "reversion modes" in the overall failure management scheme.

17

TABLE 3. SENSOR REDUCTION COMPARISONS FOR
ANALYTICAL REDUNDANCY BUILDING BLOCKS

	No. of SDF's	No. of DF's	No. of Comparators	No. of Sensors $(\text{fail-op})^2$
Interchangeable Sensors				
Detection with SDF's	1	0	0	N+2*
with DF's	0	$[\log_2(N+3)]$	0	N+2*
with Voting	0	0	N+4	N+3
Noninterchangeable Sensors				
Detection with SDF's	1	0	0	3N*
with DF's	0	1	2N	3N*
with Voting	0	0	3N	4N

*Minimum $(\text{fail-op})^2$ requirements.

While details tend to be application dependent, the basic building blocks of analytic
redundancy can be assembled to deal with these situations also. As an example, Figure
2 shows a failure detection scheme for a fail-op pitch inner loop with fail-safe attitude
and altitude hold modes. As in Figure 1, the fail-op function (assuming noninterchangeable
sensors) is accomplished with one diagnostic filter plus N comparators. The diagnostic
filter monitors one channel of sensors ($S3_1$, $S4_1$, $S5_1$) and the comparators monitor the
other. In order to implement the reversion modes, however, it is also necessary to
detect failures of the outer-loop instruments, S1 and S2, individually. This calls for
enough diagnostic filters to distinguish between four logic conditions: no failures, S1-
failed, S2-failed, and $S3_1$-, $S4_1$-, or $S5_1$-failed. Hence the number of filters must be

$$M = [\log_2 (\text{No. of logic conditions})] = 2$$

This formula is a generalization of the one derived earlier and can be used to determine
the minimum number of diagnostic filters required for various specific failure detection
problems. Once the number of filters is known, the sensor inputs for each are deter-
mined as before by the unit entries in rows of the truth table.

18

S1 — h

DF — E1345

S2 — θ

TWO FAIL-SAFE OUTER LOOPS
  (h), (θ)

$S3_1$ — δ

DF — E2345

$S4_1$ — q

ONE FAIL-OP INNER LOOP
  (δ, Q, n_z)

$S5_1$ — n_z

$S3_2$ — δ

C — C3

$S4_2$ — q

C — C4

$S5_2$ — n_z

C — C5
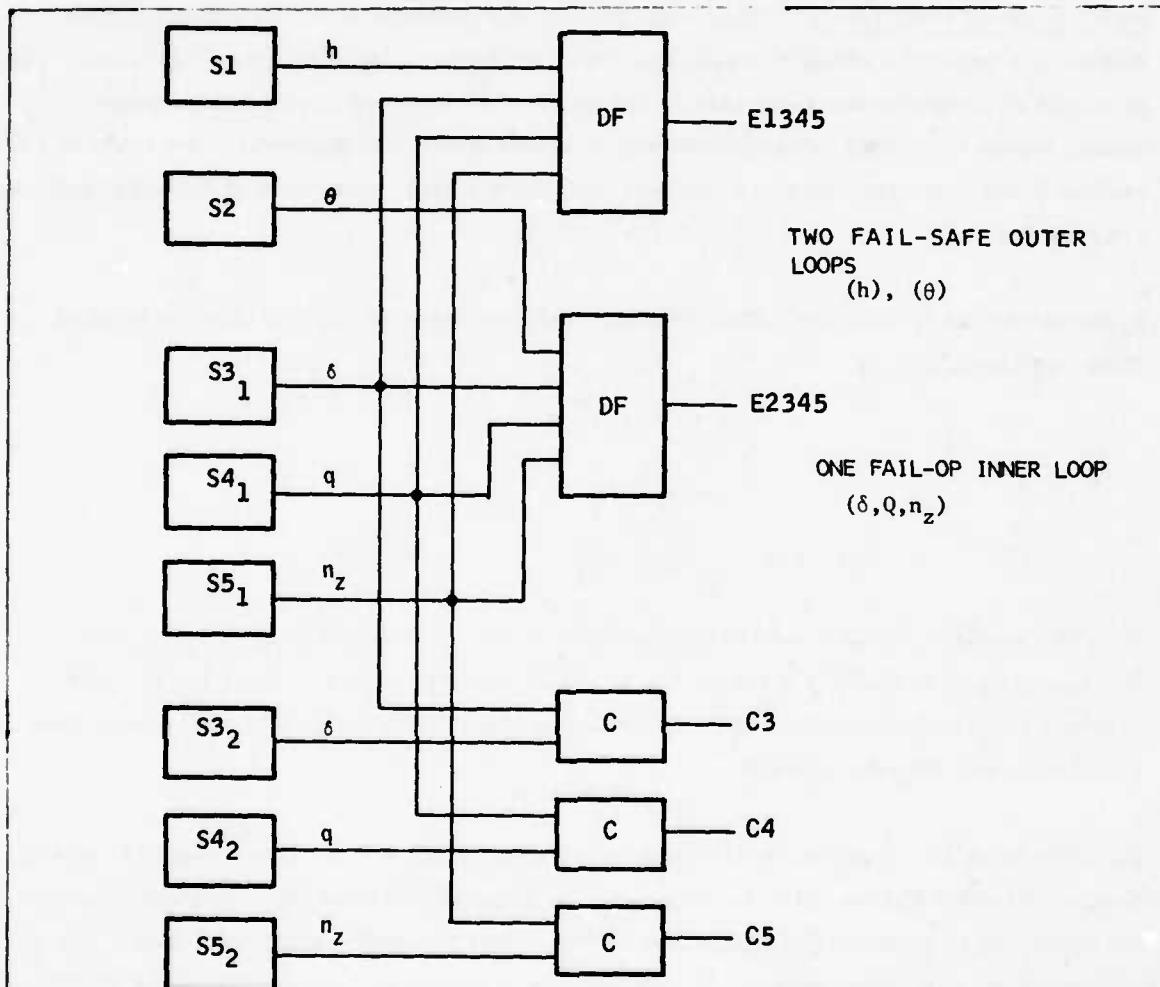
TRUTH TABLE

| ERROR FLAGS	NONE	S1	S2	$S3_1$	$S4_1$	$S5_1$	$S3_2$	$S4_2$	$S5_2$
E1345	0	1	0	1	1	1	0	0	0
E2345	0	0	1	1	1	1	0	0	0
C3	0	0	0	1	0	0	1	0	0
C4	0	0	0	0	1	0	0	1	0
C5	0	0	0	0	0	1	0	0	1

Figure 2. Example of Fault Detection with Reversion Modes

19

<u>Building Block Construction</u>--Discussed here is the problem of actually constructing computer algorithms which perform diagnostic or super-diagnostic filter functions. The principle of operation for each case is the same--test whether actual sensor outputs satisfy known functional relationships which exist between the sensors. The sensors are healthy if the relationships are satisfied; they have failed somewhere if the relationships are violated.

In mathematical terms, the known relations between sensors usually take the form of state equations, i.e.,

$$\dot{x} = f(x, u_c) + \xi$$

$$u = u_c + \eta_u$$

$$y = h(x) + \eta_h$$

Here the sensors are assumed to measure noise-corrupted inputs, $u = u_c + \eta_u$, and noise-corrupted outputs, $y = h(x) + \eta_h$, of the dynamic system $\dot{x} = f(x, u_c) + \xi$. The problem is to test whether measured inputs and outputs are consistent with constraints imposed by the dynamic system.

Possible tests for consistency can range all the way from simple signal blenders to full-fledged extended Kalman filters. Suppose, for example, that we use our knowledge of the dynamics to combine the inputs and all but one of the output signals in such a way as to predict the remaining output. In addition, we'll use an ordinary comparator to test consistency of the predicted N^{th} output with the actual one. Failures of any sensor should then produce a miscomparison, and it follows that we have built a diagnostic filter. * Its construction would be called "signal blending" in classical terminology or "observer design" in modern systems language.

The "observer design" approach in fact offers a complete hierarchy of diagnostic filters. This is illustrated in Figure 3. At the bottom of the hierarchy is a low-order observer of the type just discussed. Above it are higher-order observers which blend one subset

---

*This is only a conceptual argument, of course. Whether such a filter would actually produce strong enough miscomparisons for failure detection in noise is a key design question which must still be answered for each application.
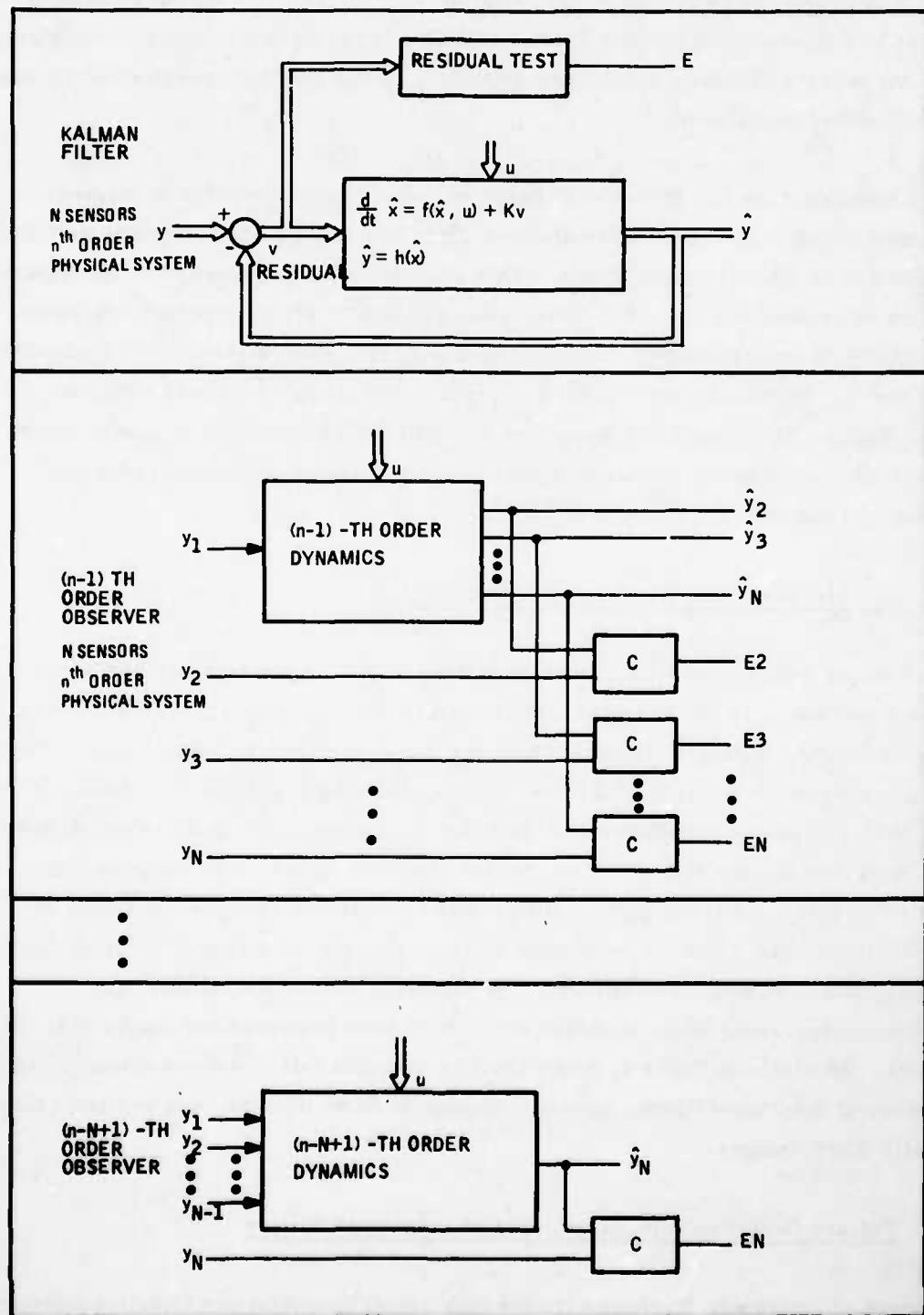
Figure 3. Diagnostic Filter Construction

21

of signals to predict and test consistency with another subset. At the very top of the hierarchy is the (extended) Kalman filter which blends all signals and uses consistency tests of the filter's residuals for failure detection. Some specific examples of residual tests will be discussed later.

Figure 3 highlights the fact that a wide range of complexity is possible in diagnostic filter construction. The most cost-effective filter can only be determined by detailed design studies on specific applications. This becomes even more apparent for super-diagnostic filter construction. For these more powerful building blocks there seems to be no unifying design approach. The literature suggests very sophisticated residual tests to isolate individual sensor failures, hypothesis testing with banks of filters, modified Kalman filter designs, parameter identification formulations, and so forth. These are discussed in the next section which surveys specific analytic redundancy techniques proposed in the literature.

2.2.2 Specific Analytical Redundancy Techniques

Thus far in our technical discussion we have defined the sensor reduction problem, discussed various ways for reducing numbers and types of sensors, and identified a diagnostic filter as a general building block for using functionally related data. We noted that the diagnostic filter can give a "yes" or "no" decision regarding the "health" of the sensor data it is processing. We also identified a super-diagnostic filter which can isolate individual sensor failures from the set of sensor data it is processing. We further noted that a super-diagnostic filter can be constructed from a collection of diagnostic filters and a simple truth table and that this places an upper limit on the viable complexity of super-diagnostic filters. The following subsection summarizes specific analytical redundancy concepts which have been proposed and analyzed in the literature. As shown in Table 4, these specific concepts fall into three major categories: assemblies of diagnostic filters, specific diagnostic filter designs, and explicit super-diagnostic filter designs.

2.2.3 Failure Detection with Assemblies of Diagnostic Filters

An example of combining diagnostic filters into a fault detection and isolation algorithm is given by Hartmann and Stein (Reference 8). The objective of this design is to make dual pitch-axis inner-loop sensors fail-operative. Therefore, only a single Kalman filter is required as a diagnostic device. The system is being applied to the NASA F-8

22

TABLE 4. FAULT DETECTION CONCEPTS*

<u>Failure Detection with Assemblies of DFs</u>

    Meier, et al.,[6] Maybeck[7] - Uses Kalman filter as a DF

    Hartmann, Stein[8] - Uses Kalman filter as a DF

    Clark, et al.[9] - Uses observer as a DF

<u>Specific DF Design Techniques</u>

    Kerr[10] - Uses an augmented suboptimal Kalman filter as a DF

    F-4 DFBW [5] - Uses simple blenders as a DF

    Mehra-Peschon[11] - Proposes several residual tests for a
                 Kalman filter

<u>Explicit SDF Design Techniques</u>

- Hypothesis testing methods:
  Montgomery et al.;[12,13] Athans-Willner[14]
  Lainiotis;[15] Buxbum-Haddad[16]

- Parameter identification:
  Mehra-Peschon;[11] Stein[17]

- General likelihood ratio methods:
  Willsky, et al.;[18,19] Deyst-Deckert[20]
  McAulay-Denlinger;[21] Sanyal-Shen[22]

- Modified Kalman filter designs:
  Jones;[23] Beard[24]

- Jump processes:
  Sworder;[25,26] Ratner;[27] Pierce;[28] Davis;[29]
  McGarty;[30] Chien[31]

*Superscripts indicate reference numbers.

DFBW. Its intended structure is shown in Figure 4 where it is noted that the DF is used to resolve sensor failures following a miscompare. The DF is a two-state representation of the short-period dynamics. The states are:

           Q   --pitch rate

           $\alpha + \alpha_{gust}$ --total angle-of-attack

           g/U   --trim $\dot{\alpha}$

           m_o --trim pitching moment

C = COMPARATOR
* 1 IF SENSOR SET 1
NOT CONSISTENT
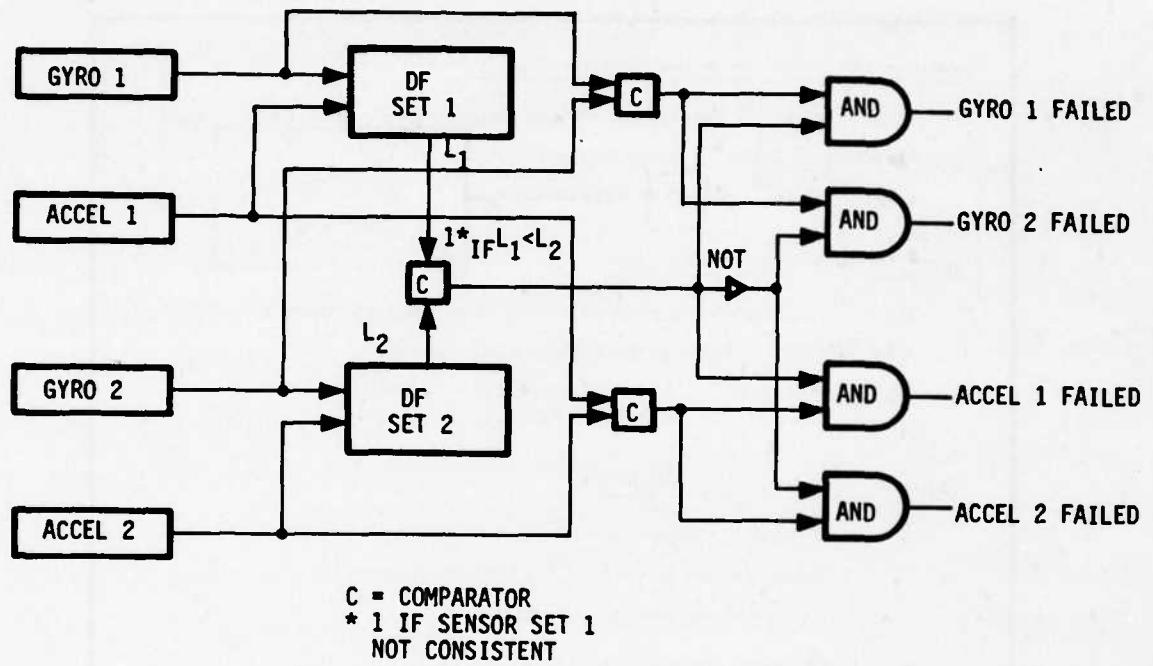
Figure 4. Two-Channel Fail-Operational Sensor Redundancy

The measurements are:

$$Q_m \text{ --pitch rate}$$

$$n_{z_m} \text{ --normal acceleration}$$

and the input is elevator surface position (δ_e). Thus, the filter has the structure shown in Figure 5. For this application, stored gains (K) are used and the matrices (F, G, H, E) are determined by a maximum likelihood identification process. These matrices change with flight condition in rather predictable ways so it is straightforward to schedule them with dynamic pressure and mach, for example, when these quantities are measured directly.

Note that Figure 4 uses a duplicate DF on each sensor set. The primary advantage of this configuration lies in setting residual thresholds. A likelihood function is computed for each sensor channel and, if a hardware comparison fails, the smaller likelihood function indicates the "healthy" sensor set. Each likelihood function is a weighted sum of squares of the individual residuals.

24
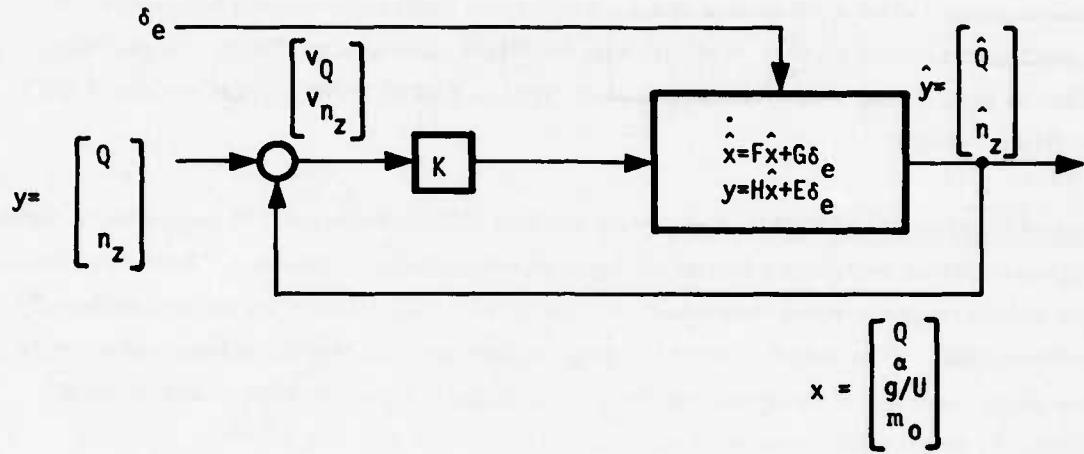
Figure 5.   Diagnostic Filter for F-8 DFBW

Results from this design demonstrate good failure detection and isolation when used with comparison monitors, thus providing a fail-operational capability for dual sensor sets. Classes of failures examined were dead, hardover and stuck sensors, and sensor scale factor changes.

Failure detection was also achieved using only analytical redundancy techniques without dual sensor channels, thus providing a fail-safe single sensor set.

2.2.4   Specific Diagnostic Filter Design Techniques

An example of designing a filter to check the operation of a specific sensor is provided by Kerr (Reference 10).   This study developed a special residual testing procedure for diagnostic Kalman filters.   The procedure is intended primarily for filters which are known to be suboptimal (i.e., reduced order) and hence do not produce "white" residuals by definition.   This is an important twist on standard theory since reduced-order models may be desirable (or mandatory) in many applications.   Basically, a low-order

Kalman filter is augmented with a few "failure states" and a function of the filter residuals is used to decide when a departure from a no-failure confidence region has occurred. This concept warrants further investigation for flight control application. A potential problem is that, if the sensor failure modes require adding many failure states, a high-order filter results.

Advanced Fighter (F-4 DFCS)--A study on the F-4 DFCS (Reference 5) suggested a number of diagnostic filter techniques based on "data reasonableness" checks. These are basically simple blenders (observers) that estimate one sensor output based on other functionally related sensors. They were developed using simple physical relationships and provide comparisons over some intermediate frequency range. Conceptually, these types of DF elements are the least complex and will be attractive for that reason. Specific blenders performed the following functions:

- Pitch rate estimation from two physically separated accelerometers

- Rate derivation from attitude references. This is also used in the shuttle flight control for tie breaking following a gyro failure. The NASA F-8 DFBW Phase I system also used this technique for obtaining rates.

- Rate and acceleration predictions from surface deflections

These schemes are attractive for their simplicity. Their performance remains to be thoroughly evaluated.

In addition to the above schemes, there are a number of simple "blenders" that can be devised using the equations of motion. We have categorized these as observers/blenders since both are designed without requiring a description of measurement noise or stochastic disturbances (gusts). An example of a "blender" is illustrated in Figure 6 where normal acceleration (n_z) is computed from two alternate relationships. A disagreement indicates that one (or more) of the input signals is in error. (Here Z_α and Z_δ might be scheduled with air data.)

Mehra-Peschon (Reference 11)--This report provided a survey of various residual tests for diagnostic Kalman filters. The basic approach is to treat fault detection via hypothesis testing, where normal operation is the null hypothesis and the error signal (or residuals) are tested against this hypothesis. Tests that apply are:
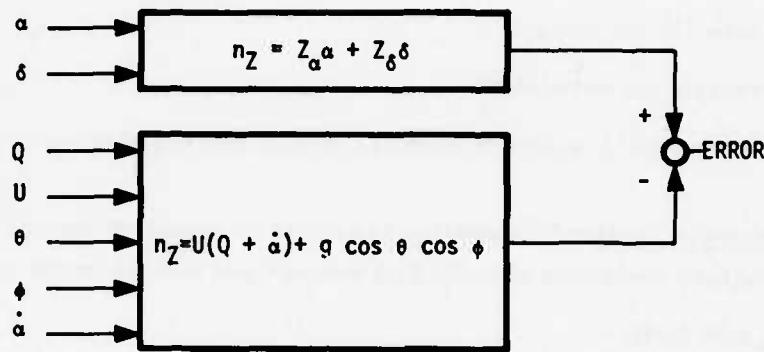
Figure 6.   Blender for n_z

1.   Tests of whiteness.   The residuals should be uncorrelated at different time instants:

   • Autocorrelations

   • Sample correlation coefficients

   • Tests of independence between different components of the error vector

2.   Tests of mean.   Compare sample mean with zero.

3.   Tests of covariance.   Compare covariance of residuals with an a priori value.

Another possibility not mentioned would be testing the orthogonality of the residual and the estimated measurement.

Explicit Super-Diagnostic Filter Design Techniques--Table 4 shows that the largest volume of research literature in analytical redundancy is devoted to super-diagnostic filters.   This is natural because these building blocks pose the most significant theoretical construction problems.   At the same time, however, they have ready competitors (as seen in Table 3) which sharply restrict the allowable complexity of viable designs. Five design approaches have been pursued to date for super-diagnostic filters:

   • Multiple hypothesis tests

   • Parameter identification

   • Generalized likelihood ratio methods

27

- Modified filter designs

- Jump process estimation

The status and principal features of each are briefly discussed below.

Multiple Hypothesis Tests--This approach is based on Bayesian statistical decision theory. The various failure conditions of individual sensors are used to define a set of hypotheses:

H_0 : No failures

H_1 : + Gyro hardover

H_2 : - Gyro hardover

H_3 : Gyro spinmotor inoperative

⋮

etc.

Each hypothesis is then tested against observed input/output measurements. The test involves a Kalman filter operation which generates sensor residuals under the assumption that a particular hypothesis is true. These residuals are accumulated into likelihood functions, and the minimum likelihood is selected to identify the currently valid hypothesis.

This approach has been studied extensively at NASA's Langley Research Center, with promising performance results on their F-8 simulator. However, complexity has so far ruled the concept out even for such powerful flight computers as the F-8's AP101. This problem is evident in Figure 7 which shows a block diagram of the algorithm. One Kalman filter is needed to test each hypothesis. This produces a large bank of filters, even for modest collections of failure modes. Since each of these filters is itself equal to a diagnostic filter in capability and complexity, it follows from earlier discussions that the approach represents an inefficient assembly of building blocks.

Parameter Identification--This approach uses explicit on-line parameter identification to detect individual sensor failures. Critical parameters of each instrument (for example, gain and bias) are selected as unknowns and estimated from input/output data. When these estimates deviate substantially from nominal values, a failure is declared. This approach was suggested originally by Mehra and Peschon (Reference 11) for the F-8 DFBW aircraft.
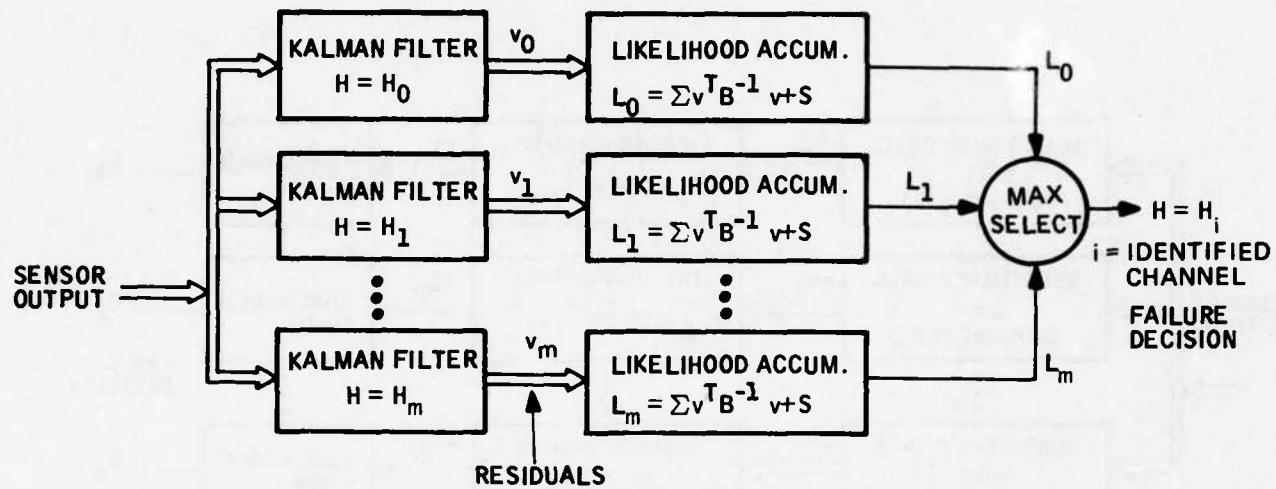
Figure 7. Multiple Hypothesis Test SDF

Viability of the approach depends largely on the complexity of the required identification algorithm. For example, if a one-step maximum likelihood identification procedure is used, the overall super-diagnostic filter algorithm will look like Figure 8. In structure, it matches the multiple hypothesis test. A bank of sensitivity calculations is required to evaluate likelihood gradients with respect to the unknown sensor parameters. Large gradients indicate failed conditions. One sensitivity calculation is required per parameter, and each calculation approximately matches the complexity of a Kalman filter. Hence, the approach not only looks like but also tends to be as inefficient as the multiple hypothesis test. Other identification algorithms are under investigation to reduce this complexity.

Generalized Likelihood Ratio Methods--Largely in response to the complexity of multiple hypothesis tests, a separate direction of failure detection research has been pursued by Willsky and Jones (Reference 19). This work begins with the constraints that only one Kalman filter will be available and that individual sensor failures must be detected

SENSITIVITY CALC. WRT PARAMETER 1 → ∇v_1 → LIKELIHOOD GRAD $\nabla L_1 = \Sigma v^T B^{-1} \nabla v_1$ → ∇L_1 → THRESHOLD COMP. → E_1

SENSOR OUTPUT

SENSITIVITY CALC. WRT PARAMETER 2 → ∇v_2 → LIKELIHOOD GRAD $\nabla L_2 = \Sigma v^T B^{-1} \nabla v_2$ → ∇L_2 → THRESHOLD COMP. → E_2

FAILURE DECISION

SENSITIVITY CALC. WRT PARAMETER m → ∇v_m → LIKELIHOOD GRAD $\nabla L_m = \Sigma v^T B^{-1} \nabla v_m$ → ∇L_m → THRESHOLD COMP. → E_m
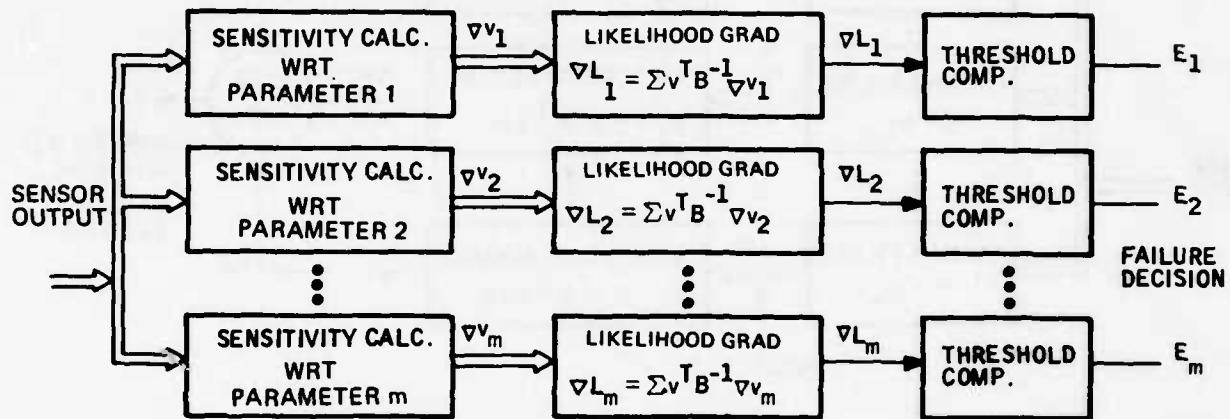
Figure 8. Parameter Identification SDF

by monitoring residuals from that filter alone. Hence, the research seeks a residual testing procedure powerful enough to turn ordinary diagnostic filters into super-diagnostic filters. Results show that this can indeed be done for a large class of failures.

Failures which can be detected from residuals of a single Kalman filter are those which leave recognizable "signatures" when they occur, i.e., characteristic transients in the residuals which can be recognized by correlation-like data processing. Examples are momentary jumps and step changes produced by open circuits or hardover failure conditions. These conditions are detected by statistically correlating the residuals with known signatures. The correlations are normalized by their expected no-failure value and then compared to preset threshold levels. If a particular normalized correlation (likelihood ratio) is sufficiently high, the corresponding failure event is declared.

A block diagram of the resulting super-diagnostic filter is shown in Figure 9. This diagram illustrates the potential complexity advantages of the generalized likelihood ratio approach. Only one Kalman filter is required to drive a bank of (potentially) simple

30
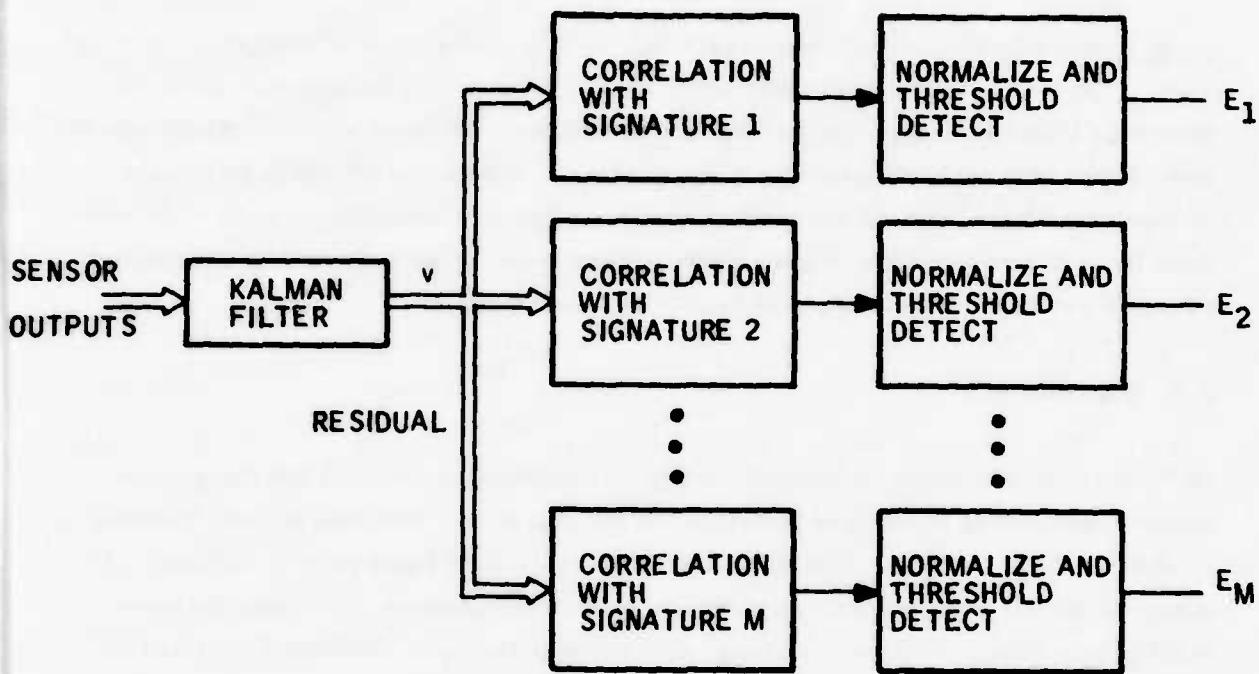
Figure 9.   Generalized Likelihood Ratio SDF

correlation operations.   We should recognize, however, that at the present state of
development the correlation operations themselves are fairly complex.

Both the time of occurrence and the magnitude of each signature are treated as unknowns,
so the correlation process must perform a maximization operation over these variables
before normalization and threshold comparison can take place.   Simplification procedures
for these operations are being investigated.

Modified Filter Design--Like the generalized likelihood ratio method, this approach also
starts with the constraint of permitting only one Kalman filter in the building block.
However, it does not treat the filter as a fixed element which accepts whatever failure
signature it produces.   Rather, the approach attempts to alter the filter gains in such a
way that failures produce strong, easily recognizable, and readily distinguishable signa-
tures.   While the state of development of this idea is still largely theoretical, it offers
a high potential for improving the detection capability of super-diagnostic filters.

31

Jump Process Estimation--This approach is also in an early stage of theoretical development. The idea is to represent failures as randomly occurring jump processes in an otherwise known stochastic system and to estimate times of occurrence and magnitude of these jumps with optimal stochastic filtering theory. Solutions turn out to be infinite dimensional filters, and the research literature is now concentrating on ways to approximate these filters without losing too much performance. Results from this direction of research require more development before they can be applied.

2.3 FEASIBILITY

So far we have discussed the general concept of analytical redundancy and the various specific approaches which have been taken in the literature. The next obvious question is whether these ideas are actually practical for real-world flight control systems. A complete answer has not been available; therefore, the question represents the main point of this study. We have, however, done some preliminary feasibility analyses to indicate that the study has a high potential for success.

To assess feasibility, we analyzed two requirements: performance (how well does an analytical redundancy concept have to work to be worthwhile), and computer resources (how much of a typical flight computer's capability would be required to mechanize a representative concept). Both analyses show reasonable results.

2.3.1 Performance

Performance requirements are most easily addressed in cases where analytical redundancy is applied to effectively eliminate one channel of sensors, i.e., reduce quad to triple, triple to dual, etc. In each case the necessary function is to isolate the failure.

Taking the quad case as an example, the usual approach to management of the set of four is to isolate the first and second failed sensors by majority vote, with the third failure (sensed by a miscomparison between the remaining two sensors) resulting in total disengagement. If the monitoring process is perfect, the probability of total failure of the set is approximated by $4Q_s^3$, where Q_s is the probability of failure of one of the sensors in the selected time period. Under the same assumption, the probability of failure of any two sensors is $6Q_s^2$, a number of significance to mission abort calculations.

32

In terms of current sensor failure rates, the above probabilities are exceedingly small numbers. Taking a rate gyro as an example with a failure rate of about 10^{-4} per hour (one of the worst of the sensor failure rates),

$$4Q_s^3 = 4 \times 10^{-12}$$

$$6Q_s^2 = 6 \times 10^{-8}$$

where each applies to a one-hour flight. Typical flight control system requirements for total failure and mission abort are on the order of 10^{-7} and 10^{-3}, respectively, for a one-hour flight. Assuming 10 quad sets of sensors and conservatively allocating only one-tenth of the system failure requirements to the sensors, per sensor set requirements of 10^{-9} for total failure and 10^{-5} for a dual failure (mission abort) result. Consequently, the quad sensor set (with perfect monitoring) exceeds requirements by about two orders of magnitude.

If a majority-voted triple set were hypothesized instead of the quad, however, the associated flight safety and mission abort probabilities of $3Q_s^2$ and $3Q_s$ would produce values of 3×10^{-8} and 3×10^{-4}, respectively, failing to meet above requirements by a factor of 30. The situation is simply that, with conventional comparison monitoring, triple is not good enough and quad is too good.

Complicating the above argument (and changing some of the conclusions) is the issue of imperfect monitoring, which in itself is difficult to deal with quantitatively. One attempt to do so argues that an undetected failure may cause quad set failure after the second sensor failure (instead of after the third), producing an added total failure contribution of $6Q_s^2 Q_m$, where Q_m is the probability of having the first failure occur without being detected and where both of the actual sensor failures are alike. The results of such a combination of events is that the quad voting logic cannot decide between two good like-sensors and two bad like-sensors. A common example of this situation is when two sensors fail dead in an interval where monitors fail to trip due to insufficient control activity (e.g., cruise). There are no data available to assign numbers to Q_m, but a parametric study of its potential effects shows that it is a significant and probably a dominant contributor to total failure rate. For example, speculated values for Q_m are on the order of 10^{-2}, making the $6Q_s^2 Q_m$ term (again for a rate gyro) equal to 6×10^{-9} for the one-hour flight, just within requirements. With imperfect monitoring considered, the quad set may no longer be "too good," but just good enough.

33

The relevance of the above discussion to analytical redundancy requirements lies primarily in the notion that imperfect monitoring (an element of redundancy mismanagement) is probably the pacing cause for failure of highly redundant sensor sets. The quality of the required analytical diagnostics must be viewed in this perspective. Consider, as an example, an analytical redundancy application wherein triple sensors are to be configured for dual-fail-op performance. The first failure will be "voted out" by comparison logic. The second failure will be detected by comparison monitoring and isolated by diagnostics. The resulting total failure rate is $Q_s^3 + 3Q_s^2 Q_D$, where $3Q_s^2$ represents the probability of a dual sensor failure and Q_D is the probability of failure of the diagnostics to pick the bad sensor. Judging the second term to be dominant and equating it to be the 10^{-9} requirement speculated above,

$$3Q_s^2 Q_D = 10^{-9}$$

or $Q_D = 0.033$ for a rate gyro set. This means that the diagnostics must be correct in about 97 percent of the decisions made to distinguish a good sensor from a bad sensor. This performance appears feasible. Note that the source of failure experienced in the conventional quad set due to imperfect monitoring is also present in the above triple set, but it is only half as probable in the triple. It may simply be included as a contribution to Q_D.

In terms of mission reliability, the triple set described above will be aborted after the second failure, a probability of $3Q_s^2$. This is lower than the quad set by a factor of two.

In summary:

1. The performance expected from analytical diagnostics must be based on a specific redundancy management strategy and realistically related to total flight control system requirements.

2. In specific cases the required ability of the diagnostics to satisfy system needs appears attainable.

3. Considering the reality of imperfect monitoring, analytical redundancy techniques are potentially equal or superior to conventional quad channel voting.

34

2.4 MOTIVATION

If analytical redundancy is both technically ready and feasible in the real world of on-board computations, then the basic issue is motivation. What is the payoff?

Total control system reliability, i.e., not just sensors but computers and servos, is the ultimate measure of success. An example would be the current A-7D multimode CAS. Without a fail-op capability (i.e., by analytical redundancy or a third sensor string), the mission reliability is as shown in Table 5, Column I.

Also shown in Table 5 is the improvement provided by redundancy. The full benefit of sensor redundancy, however, is not realized until extra effort is expended to back up the servos with effective redundancy (perhaps analytical). This is shown in Column III.

TABLE 5. A-7D MULTIMODE CAS MISSION RELIABILITY

Major Abort Causes	Probability (failures per flight hour)		
	Case I Current A-7D	Case II 95% Sensor Redundancy	Case III 95% Sensor and Servo Redundancy
(a) Either computer fails plus 95% effective self test*	0.2×10^{-4}	0.2×10^{-4}	0.2×10^{-4}
(b) Servo failure in any axis	6.0×10^{-4}	6.0×10^{-4}	0.3×10^{-4}
(c) Gyro failure in any axis	6.0×10^{-4}	0.3×10^{-4}	0.3×10^{-4}
(d) Normal accelerometer failure	0.4×10^{-4}	0.02×10^{-4}	0.02×10^{-4}
Total	12.6×10^{-4}	6.52×10^{-4}	0.82×10^{-4}

*Diagnosis and redundancy scheme are 95% effective.

2.5 CONCEPTS SELECTED FOR FURTHER STUDY

Having examined and classified the state-of-the-art in analytical redundancy, three concepts were chosen which cover a large breadth of sensor fault detection and isolation capabilities.

2.5.1 Filter Concepts

Table 6 displays the three basic concepts studied. Concept I specifically attempts to blend related sensors into a reconstructed output. An error signal is produced when the reconstructed output is compared with the actual sensed output. Low computational requirements are emphasized for later comparisons with the more complex Concept II. Sensor outputs which cannot easily be reconstructed through kinematic relationships are ignored (e.g., lateral acceleration).

TABLE 6. ANALYTICAL REDUNDANCY CONCEPTS SELECTED FOR DEVELOPMENT

Concept	Basic Classification	Complexity (Computer Requirements)	Reference * Similarity
I Observer/Blender	Specific DF Design	Low	F-4 DFBW[5]
II Diagnostic Kalman Filters	Assembly of DF's	Medium	Meier[6] and Maybeck[7]
III Super-Diagnostic Kalman Filter	Assembly of DF's	Medium to High	Hartmann, Stein[8]

*Superscripts indicate reference numbers.

36

Concept II uses an assembly of Kalman filters to produce a complete fault detection capability for a given set of sensors. Extra computational expense is used to investigate fault detection for difficult sensor combinations, i.e., gain-scheduled lateral-directional dynamic equations of motion to monitor lateral acceleration. Specific sensor anomalies such as body rate biases and scale factors are also treated to investigate early failure detection.

Concept III addresses the fault isolation problem as well as the detection problem-- producing a super-diagnostic filter. No computational restrictions are imposed. Concept III is further distinguished by the creation of an error signal for each sensor treated. Kalman filters with gain-scheduled longitudinal and lateral-directional axes dynamic equations are used to produce linear equations necessary for isolation of inner-loop sensors (n_z, n_y, P, Q, and R) in maneuvering flight.

2.5.2 Monitor Concepts

The choice of monitors for testing various error signals is critical to performance. Two basic monitor schemes were examined for detection capability: speed of response, and meeting the false alarm criterion, i.e., one false alarm per 1000 flight hours.* Table 7 briefly describes these monitors and the concepts to which they were applied. Section 4 contains a complete development of these monitors.

---

*This is used for individual sensors under 98 percent wind gust conditions (approximately 6 fps).

37

TABLE 7. FAULT DETECTION MONITORS

Monitor Description	Concepts
I. Multiple Trip--Delayed Declaration	
A. Constant monitor level	II and III
B. Monitor level scheduled on sensor output	I
C. Monitor level scheduled on stick input	I, II and III
II. Sequential Likelihood Ratio Test	
A. On error signals	II and III
B. On likelihood functions	II*

*Used with comparison monitors on dual sensors for fault isolation.

38

SECTION 3

SENSORS AND SENSOR MODELING

3.1   VEHICLE DYNAMICS

Analytical redundancy is based on combining known relationships of sensed variables.
These relationships can be broken into two groups: translational equations and rotational
equations.

I.   Translational Equations

   A.   Inertial Velocity-Body Velocity

$$\dot{X}_e = (\cos\theta\cos\psi)U + (\sin\phi\sin\theta\cos\psi - \cos\phi\sin\psi)V$$
$$+ (\cos\phi\sin\theta\cos\psi + \sin\phi\sin\psi)W \tag{1}$$

$$\dot{Y}_e = (\cos\theta\sin\psi)U + (\sin\phi\sin\theta\sin\psi + \cos\phi\cos\psi)V$$
$$+ (\cos\phi\sin\theta\sin\psi - \sin\phi\cos\psi)W \tag{2}$$

$$\dot{Z}_e = (-\sin\theta)U + (\sin\phi\cos\theta)V + (\cos\phi\cos\theta)W \tag{3}$$

   B.   Force Equations

$$\dot{U} = A_x - g\sin\theta - QW + RV \tag{4}$$

$$\dot{V} = A_y + g\cos\theta\sin\phi - RU + PW \tag{5}$$

$$\dot{W} = A_z + g\cos\theta\cos\phi - PV + QU \tag{6}$$

where

$$A_x = F_x/\text{Mass}$$

$$A_y = F_y/\text{Mass}$$

$$A_z = F_z/\text{Mass}$$

$$(F_x, F_y, F_z) = 1/2\rho V_T^2 S_A(C_x, C_y, C_z)$$

$$V_T^2 = U^2 + V^2 + W^2$$

39

II. Rotational Equations

A. Euler Rates/Body Rates

1. Euler Rate Formulation

$$\dot{\phi} = P + (Q \sin \phi + R \cos \phi) \tan \theta \tag{7}$$

$$\dot{\theta} = Q \cos \phi - R \sin \phi \tag{8}$$

$$\dot{\psi} = (Q \sin \phi + R \cos \phi) \sec \theta \tag{9}$$

2. Body Rate Formulation

$$P = \dot{\phi} - \dot{\psi} \sin \theta \tag{10}$$

$$Q = \dot{\theta} \cos \phi - \dot{\psi} \sin \phi \cos \theta \tag{11}$$

$$R = \dot{\psi} \cos \phi \cos \theta - \dot{\theta} \sin \phi \tag{12}$$

B. Moment Equations

$$L = \dot{P} I_{xx} - \dot{R} I_{xz} + QR (I_{zz} - I_{yy}) - PQ I_{xz} \tag{13}$$

$$M = \dot{Q} I_{yy} + PR (I_{xx} - I_{zz}) + (P^2 - R^2) I_{xz} \tag{14}$$

$$N = \dot{R} I_{zz} - \dot{P} I_{xz} + PQ (I_{yy} - I_{xx}) + QR I_{xz} \tag{15}$$

where

$$(L, N) = 1/2 \rho V_T^2 S_A b (C_\ell, C_n)$$
$$M = 1/2 \rho V_T^2 S_A c \, C_m$$

3.2 SENSOR COMPLEMENT

The basic sensor set identified for fault detection is as follows:

- Normal acceleration

  $$n_{z_m} = -a_z - G + \text{Errors}*$$

- Lateral acceleration

  $$n_{y_m} = a_y + \text{Errors}*$$

---

*Errors include noise, bias, scale factor, hysteresis, environmental effects, response dynamics, and unmodeled sensor inputs.

40

- **Angle-of-attack**

  $$\alpha_m = \sin^{-1}(W/V_T) - \alpha_w + \text{Errors}*$$

- **True airspeed**

  $$U_m = U - U_w + \text{Errors}*$$

- **Altitude**

  $$h_m(\text{BARO}) = -Z_e + \text{Errors}*$$

- **Three body rate**

  $$(P_m, Q_m, R_m) = (P, Q, R) + \text{Errors}*$$

- **Three Euler angles**

  $$(\phi_m, \theta_m, \psi_m) = (\phi, \theta, \psi) + \text{Errors}*$$

This represents a realistic set of motion and position quantities, identical to those used in the A-7D multimode system with the exception of true heading, ψ, which must be added to current interfaces. The set also indirectly encompasses other types of input variables used in other applications:

1. Dynamic pressure $(\bar{q})$, comparable to $1/2\rho V_T^2$ via altitude and true air speed functions.

2. Altitude rate $(\dot{h})$, comparable to a blend of derived altitude rate from altitude, normal acceleration, pitch attitude, and roll attitude. The actual function depends on the method used in deriving altitude rate for the specific application.

3. Mach number comparable to true airspeed with an error of less than 10 percent.

Input quantities not encompassed by the sensor set include:

1. Pilot inputs such as stick and pedal forces and position, trim, heading select, etc.

---

*Errors include noise, bias, scale factor, hysteresis, environmental effects, response dynamics, and unmodeled sensor inputs.

2. Error signals which occur only when certain modes are selected by the pilot, e.g., altitude hold and heading hold (i.e., clutched outputs).

Other means must be used to detect faults in these signals (e.g., in-line testing) or an associated failure must be accommodated by suitable design features such as signal limiting.

3.2.1 Significance and Summary of Sensor Modeling

Analysis and verification of the various fault tolerant concepts by simulation require adequate models of the sensors or signals involved. These sensor models are required to contribute pertinent and appropriate dynamics and anomalies to the problem, as well as to allow the introduction of sensor failure modes to evaluate the fault detection capability of a particular concept. Further, recognition and identification of sensor characteristics--noise and other anomalies--allow the definition of monitor threshold or detection levels which will pass these "normal" irregularities but will still indicate "failure" when they should.

It is possible, of course, to simulate the mechanization of a sensor complete with springs, vanes, spinmotors, gimbals, etc. This approach is particularly appealing if one considers the relative ease of inserting realistic failures of a sensor into the simulation; however, this approach was not used. Instead, this study relied on analytical models--transfer functions--coupled with superposition of the fault.

In all cases of sensor modeling, an attempt is made to generalize the model. That is, specifics which would make the sensor unique to a given vehicle are avoided. Also, wherever possible and without giving up the desired generality, the sensor data associated with the A-7D Multimode DFCS are used. A case in point is the bandwidth and damping ratios assumed for the A-7D analytical sensor models, all of which are considered to be representative of typical fighter aircraft sensors.

3.2.2 Simulation Modeling Approach

The normal sensor operating characteristics outlined in Table 8 include a definition of appropriate sensor dynamics, i.e., frequency and damping ratios for use in idealized second-order modeling. It is seen that the sensor bandwidths are from 5 to 50 hertz, much greater than the approximately 2 Hz bandwidth expected to be used in the fault tolerant monitor concepts.

42

TABLE 8.   MODEL PARAMETER VALUES FOR NORMAL OPERATING SENSORS

		P_m (o/s)	Q_m (o/s)	R_m (o/s)	n_{z_m} (g's)	n_{y_m} (g's)	ϕ_m (deg)	θ_m (deg)	ψ_m (deg)	U_m (ft/sec)	h_m (ft)	α_m (deg)
Basic Sensor	x_1	P_m (o/s)	Q_m (o/s)	R_m (o/s)	n_{z_m} (g's)	n_{y_m} (g's)	ϕ_m (deg)	θ_m (deg)	ψ_m (deg)	U_m (ft/sec)	h_m (ft)	α_m (deg)
Cross-Axis Variable	x_2	Negligible	P	P	N_y	N_z	-	-	-	-	-	-
Noise Level	K_N^*(RMS)	1.1	0.4	0.4	0.03	0.03	0.75	0.75	0.75	2.5	25	0.08
Mis-alignment	Δ (deg)	0.43	0.43	0.43	0.36	0.36	-	-	-	-	-	-
Bias	Δx^*	0.5	0.08	0.08	0.05	0.0025	1.6	1.6	0.75	7.9	25	0.36
Scale Factor Error	K_{SF} (% full scale)	5.5	5.5	5.5	5.4	5.4	-	-	-	-	25 ft or 0.25% h	-
Natural Frequency	ω_x(rps)	50(2π)	20(2π)	20(2π)	30(2π)	16(2π)	5(2π)	5(2π)	5(2π)	5(2π)	5(2π)	1.6(2π)
Damping Ratios	ζ_x	0.7	0.7	0.7	1.0	1.2	0.7	0.7	0.7	0.7	0.7	(1st Order)
Sensor Limit	LIM*	±200	±30	±30	+10 -4	±0.5	±180	±180	360	Upper 1000 Lower 197	Upper 50,000 Lower -1,000	+30 -10

*Units same as sensor

43

In the following discussions, normal and faulted sensor models for the simulation are presented. They will be implemented digitally but are shown in block diagram format for better visualization.

3.2.3 Normal Operating Characteristics Modeling

Each sensor model will include those errors considered normal or acceptable for a population of sensors:

- Scale factor error

- Null error

- Alignment (cross-axis sensitivity) error

- Noise

A basic difference between fault tolerant concepts is the means of accommodating these errors while indicating faults for genuine failures. The simplest concepts use monitor thresholds statistically fixed to fit the sensor population while the more sophisticated concepts, through predictive techniques, set thresholds to suit the given sensor set.

Comparative evaluations of fault tolerant concepts use identical "seeded" values of the above anomalies. Figure 10 is a simplified mathematical model of the normal sensor operating characteristics. Table 8 shows the variations in parameters appropriate to the normal sensor.

3.2.4 Fault Categories

As a first step, faults are categorized as open-loop or closed-loop faults. In the case of open-loop faults, the sensor can be assumed to be out of the loop, and its normal output can be replaced by something completely independent of its input. Faults in this category may include:

1. Zero output (dead sensor)

2. Step output to maximum level (hardover)

3. Stuck at transient value (stuck output)

4. Drift or randomly varying output

44
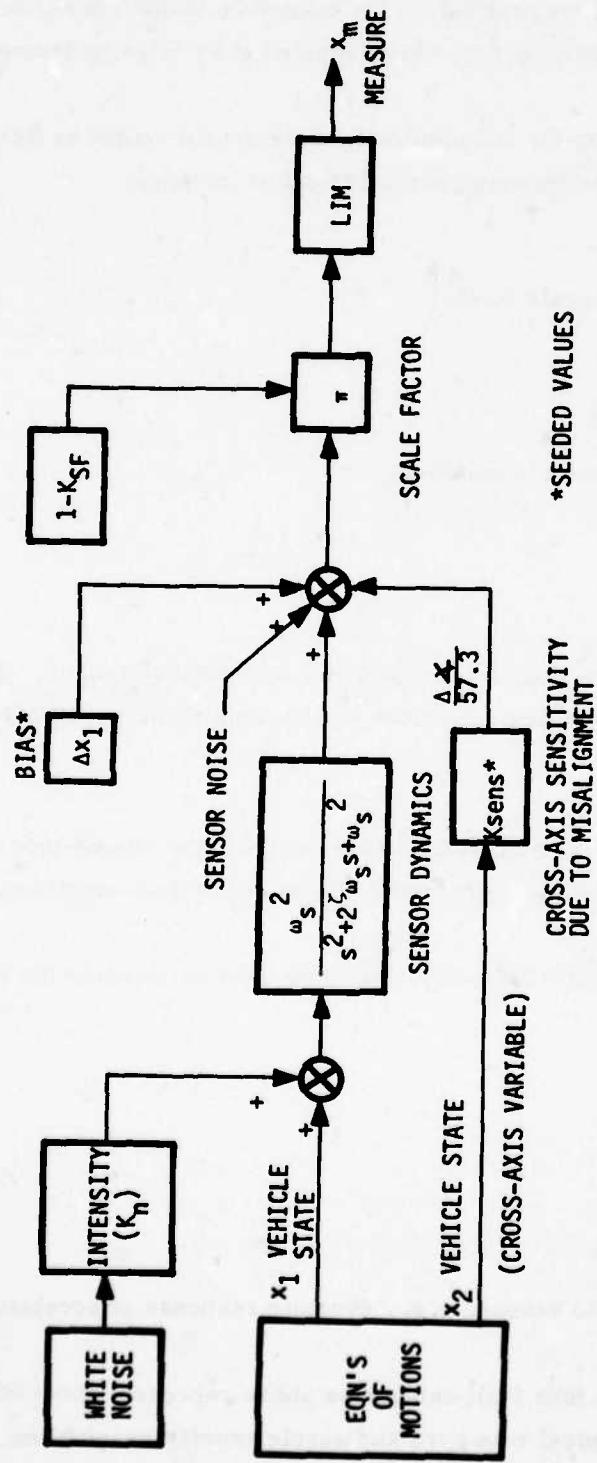
Figure 10. Generalized Simulation Model of Normal Sensor Operating Characteristics

These faults are introduced to the problem in the open-loop fashion described. Also, turbulence and unmodeled structural noise are assumed to be missing from the output.

Closed-loop faults are based on the assumption that the sensor output is following the input, but with errors added or superimposed. This list includes:

5. Hysteresis

6. Low (or high) gain (scale factor)

7. Bias or null offsets

8. Stiction or deadspot

9. Misalignment (cross-axis coupling)

10. Noise

11. Resolution

All of the above items are present, to some degree, in a normal sensor. They become "faults" when they exceed their nominal values and become dominant terms in the error equations.

Statistical summations of the nominal values were used for the closed-loop characteristics given above to determine the detection levels in the various monitors.

In our simulations the following fault categories were used to exercise the fault detection monitors:

1. Zero output

2. Hardover

3. Gain error

4. Bias

5. Other (as specific to sensor, e.g., dynamic response of accelerometers)

It will be shown that the first four fault categories above represent about 90 to 95 percent of the expected failures in typical rate gyro and accelerometer assemblies. Further, all the earlier listings of potential failure categories are shown to be embodied or represented since many potential faults are merely variations of gain or bias errors.

Of particular interest is field and analytical experience with the various sensors. In general, it is difficult to accumulate this information. Furthermore, the data will generally reflect the failure modes of associated electronics as well as the actual sensor. Analysis of the resultant sensor/circuitry will usually result in the conclusion that any failure mode is possible. An attempt was made to assemble data to determine the probability of failure modes by examining test data and Failure Mode and Effects Analyses (FMEA). Table 9 is such a compilation for a three-axis rate gyro package, a three-sensor normal accelerometer package, and a two-sensor lateral accelerometer package.

TABLE 9.   FAILURE MODE AND EFFECTS ANALYSIS (FMEA)
FOR HIGH PERFORMANCE JET AIRCRAFT

Failure Mode	System		
	3 Axis Gyro Package (Spring Restrained)	3 Unit Normal Acceleration (Pendulous)	2 Unit Lateral Acceleration (Force Rebalance)
Failure Rate of Assembly (Including Electronics)	14.5% / 1000 hrs	5.13% / 1000 hrs	3.42% / 1000 hrs
Failures:			
1. Zero or very low gain	75.6%	1.1%	
2. Very high gain	0.4	0.3	
3. Moderate high gain	1.1	0.2	
4. Moderate low gain	1.3	0.9	
5. Dynamic response	3.4	11.3	
6. Null offset out of spec	1.2	17.4	
7. Hardover	16.5	68.8	
8. Mech play, hyst, stuck	-	-	
9. Self-test failure	0.5	-	
	100.0%	100.0%	

Table 10 groups the data from Table 9 into our five fault categories. Also included are air data angle-of-attack and attitude gyro fault categories. Fault data for these sensors are more scarce than rate gyro/accelerometer percentages; therefore, the degree of confidence is lower.

A generalized fault model to be simulated is shown in Figure 11 with parametric fault values and model states shown in Table 11.

TABLE 10. SUMMARY OF SENSOR FAILURE MODES

Fault Category	Spring (1), (2) Restrained Gyro	Pendulous Force Rebalance Accelerometers	Air Data Comp. True Airspeed	(3) Altitude
1. Zero output	76%	1%	34%	21%
2. Hardover	17	69	5	6
3. Gain errors	3	1	} 61[4]	} 73[4]
4. Null or bias	1	18		
5. Other	3	11		
	100%	100%	100%	100%

NOTES:

(1) By similarity, the gyro failure modes shown will be assumed for platform attitude signals ϕ, θ, ψ.

(2) The angle of attack sensor, assumed to be the vane type, will use the gyro failure modes shown since zero output is expected to be the dominant fault. Null offsets or biases would be common for pressure balance types.

(3) Exclusive of Air Data Computer inputs (static and total pressure and total temperature).

(4) Listed in data source as "degraded." We will assume equal distribution between gain and null errors.

48

TABLE 11.   MODEL PARAMETER VALUES FOR SENSOR FAILURE MODES

Fault / Sensor			P_m (deg/sec)	Q_m (deg/sec)	R_m (deg/sec)	n_{z_m} (g)	n_{y_m} (g)	e_m (deg)	θ_m (deg)	ψ_m (deg)	U_m (ft/sec)	h_m (ft)	α_m (deg)
Zero Output	SW at B	ΔX	0	0	0	0	0	0	0	0	0	0	0
Hardover	Open-Loop Sensor	ΔX	200	30	30	10	0.5	180	180	360	1,000 197	50,000 -1,000	30 -10
Bias	SW at A	ΔX	◄——————— Ramp Drift ———————————————————►										
Scale Factor	Closed-Loop Sensor	K_{SF}	◄——————— 25% or 50% Full Scale —————————►										

3.3   SENSOR DATA

3.3.1   Normal Operating Characteristics

Gain, Null and Alignment Errors--From various sources (manufacturers' specifications, procurement specifications, etc.) for similar applications (e.g., F-18, F-14, JA-37), errors and tolerances for the selected sensors have been established.   These are summarized in Tables 12 through 15.   The values shown are felt to be typical of high performance aircraft equipment.   The applicability to the A-7D Multimode DFCS is seen from comparison of total errors to Multimode DFCS monitor thresholds (Tables 12 and 13).   Comparison monitor threshold for two like sensors would be the RSS of the two individual errors.

Gain, null, and alignment errors are shown in their component parts; however, the RSS totals of each are used in the sensor models.

Noise--It is generally acknowledged that any sensor output will contain elements categorized as noise, that is, external corruption independent of the quantity being measured. However, universal agreement on the definition of noise is not available.   In many applications, sensor signal noise is a limiting factor on potential control performance. Classic examples such as localizer beam-following could be cited.
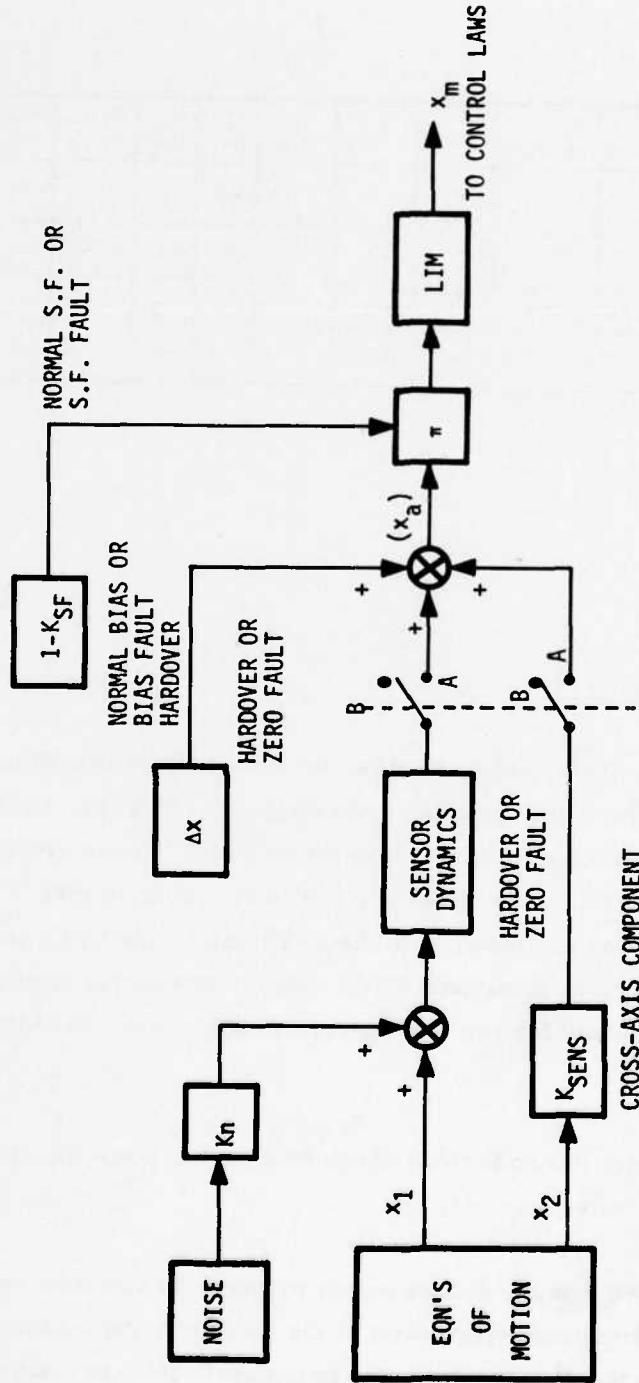
Figure 11. Generalized Simulation Model of Sensor Faults

TABLE 12.   ACCELEROMETER ERRORS/TOLERANCES

Characteristic	Normal	Lateral
*Input Range	+10, -4 g's	±0.5 g's
Gain Errors (% F.S.) Scale Factor Linearity Prefilter RSS	 5.0 1.0 1.9 $\overline{5.4}$%	 5.0 1.0 1.9 $\overline{5.4}$%
Null (Bias) Errors (% F.S.) Offset Hysteresis Threshold RSS X F.S.	 0.5 0.05 0.02 $\overline{0.50}$% 0.05 g's	 0.5 0.05 0.01 $\overline{0.50}$% 0.0025 g's
Alignment (deg) Internal Case RSS	 0.1 0.35 $\overline{0.36}$ deg	 0.1 0.35 $\overline{0.36}$ deg
RSS of Gain and Null Errors	5.4% F.S.	5.4% F.S.
*Actual A-7D Multimode Threshold	7.5% F.S.	25% F.S.

*Known A-7D values. Other parameters estimated from similar
 equipment and application.

TABLE 13.   NORMAL RATE GYRO ERRORS/TOLERANCES

Characteristic	Roll	Pitch	Yaw
Input range	±200 deg/sec	±30 deg/sec	±30 deg/sec
Gain errors (% F.S.) Scale Factor Linearity Prefilter RSS	 5.0 1.0 2.0 5.5%	 5.0 1.0 2.0 5.5%	 5.0 1.0 2.0 5.5%
Nulls (Bias) (% F.S.) Offset Resolution RSS X Full Scale	 0.25 0.016 0.25% 0.5 deg/sec	 0.25 0.025 0.25% 0.08 deg/sec	 0.25 0.025 0.25% 0.08 deg/sec
Alignment (deg) Internal Case RSS	 0.25 0.35 0.43	 0.25 0.35 0.43	 0.25 0.35 0.43
RSS of gain and null errors	5.5%	5.5%	5.5%
Actual threshold in A-7D multimode	7.5% of full scale		

51

TABLE 14. AIR DATA ERRORS/TOLERANCES AND ANGLE
OF ATTACK SENSOR (KNOWN A-7D VALUES)

Characteristics	Altitude (h_m)	True Airspeed (U_m)	Angle-of-Attack Sensor
Range	-1000 to 50,000 ft	118 to 600 KTS	+30, -10 deg
Accuracy	Below 10,000 ft ± 25 ft Above 10,000 ft ± .25% h	±4 KTS (h < 20,000) ±4.74 KTS (h ≥ 20,000)	0.36 deg
Resolution	25 ft	1 KT (1.7 ft/sec)	

TABLE 15. PLATFORM CHARACTERISTICS

Characteristic	Roll Attitude, ϕ	Pitch Attitude, θ	Heading, ψ
Range	360°	360°	360°
Accuracy*	1.6 deg	1.6 deg	0.75 deg

*Presumed to include resolution, linearity, etc.

Proper noise modeling is especially critical in the design of Kalman filters for fault detection. The fault detection capabilities are highly related to the filter bandwidth. This bandwidth is explicitly determined as a function of the process-to-measurement noise ratios.

Consequently, a special analysis was performed to get closer to real life noise existing on body axis rate gyros and accelerometers.

Noise Definitions--It is postulated that the output of a body-mounted gyro or accelerometer will contain the components identified in Figure 12, which are briefly defined below:

1. Internal Sensor Noise--Usually modeled in simulations as filtered white noise with a bandwidth defined by the sensor (on the order of 100 rps) with an RMS level of 0.25 percent of sensor full scale output (flight condition independent).

2. External Sensor Noise--A "steady-state" output induced by power plant, generators, and other machinery vibrating the aircraft structure. For a given engine power setting, the output is assumed steady, with components over the full sensor range of frequencies (assumed flight condition independent).
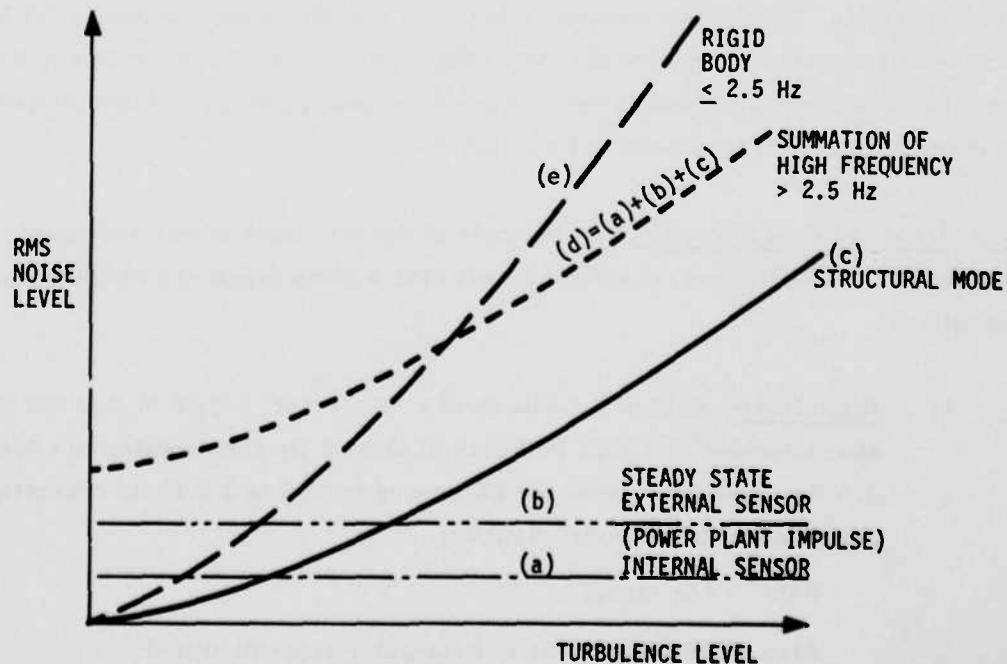
Figure 12. Postulated Gyro and Accelerometer Spectral Noise Content

53

3.   Structural Mode Inputs--This component of sensor output assumes that the
     aircraft structural modes are excited by turbulence and are flight condition
     dependent. However, as the results will show, this dependence on turbulence
     is not obvious in the data, at least not to the degree implied in Figure 12.
     Also, we do not know, except by qualitative implication, what the turbulence
     levels were during the data taking.

     This lack of turbulence dependence follows from the Mil Spec 8785-B (Reference
     33) definition of wind turbulence bandwidth. Dryden models normally cut off
     turbulence at 0.02 to 0.16 Hz, depending on altitude and velocity. Our analysis
     separates rigid body from "high frequency" at 2.5 Hz. Thus we could expect
     turbulence to excite rigid body modes, with significantly less influence at the
     structural modes, even if they are lightly damped.

4.   Total High Frequency--This quantity, deduced from the power spectral density
     plots, will be plotted on subsequent graphs. As noted, it is composed of the
     three noise components discussed above.

5.   Rigid Body--Normally, this is adequately simulated by turbulence in the
     equations of motion.

To summarize, at very low turbulence levels, we would expect structural (or high
frequency) spectra to dominate the total RMS, with the rigid body (or 10 rps frequency)
dominating at high turbulence levels. The cross-over point and relative slopes are
undefined, but the trend seems to be established.

Data Input and Data Reduction--An example of the data input to this analysis is shown in
Figure 13. The RMS level of sensor output over a given frequency range was determined
as follows:

1.   Rigid Body--Most of the data show a "clear-cut" region of data out to 2.5 Hz,
     characterized by a high PSD peak at about 1 Hz and dropping to a low value at
     2.5 Hz. The area under the PSD curve from 0 to 2.5 Hz is converted by
     definition to "rigid-body" RMS by:

$$RMS^2 = 1/\pi \ (area) \tag{16}$$

$$Area = (PSD \ max)(2.5)/2 \ \ (triangular \ approximation) \tag{17}$$

$$RMS = \sqrt{(PSD \ max)(2.5)/2\pi} \ rad/sec \tag{18}$$

54
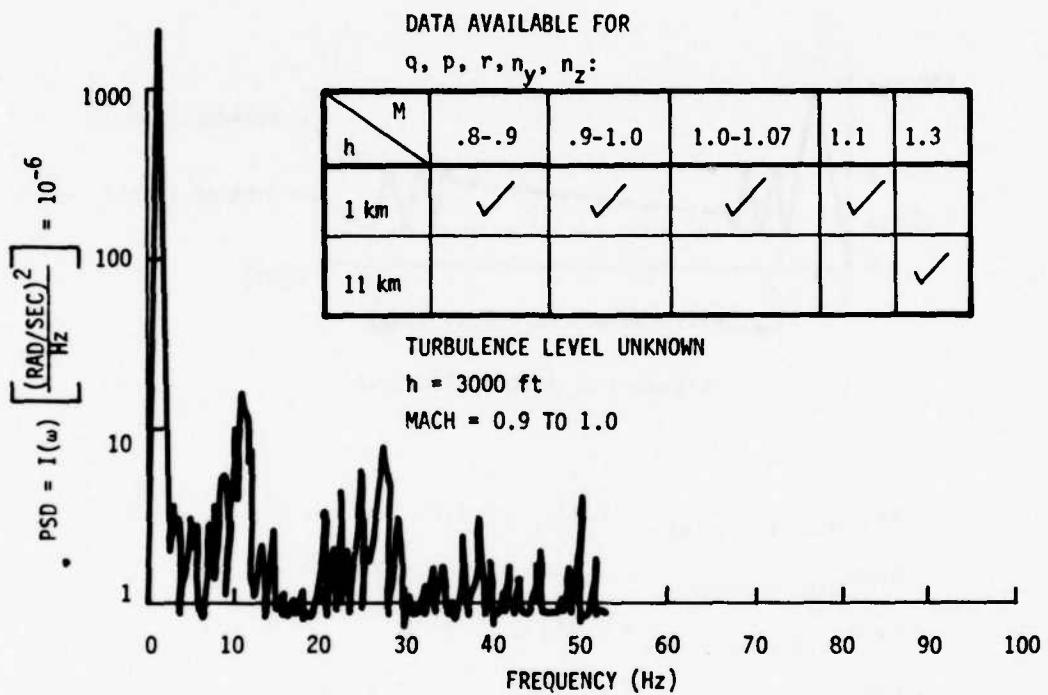
Figure 13. Pitch Rate Power Spectral Density (Flight Test Record)*

"PSD max" is read off the curves directly. If more than one peak occurs,
they are averaged, and this average is used in Equation (18) on the preceeding
page.

2. <u>High Frequency</u>--The area under the PSD curve is laborious to compute
manually with high precision. Several approximations were used, giving
fair correlation. The following method was finally applied to all curves.
The average value of the peaks was computed.

The spread of PSD data was noticed to be about 12 dB. That is, the minimum
valleys were about 25 percent of the maximum peaks, giving the graph in
Figure 14, after the averaging process:

---

*Sensor data taken from the SAAB JA-37 aircraft.

55
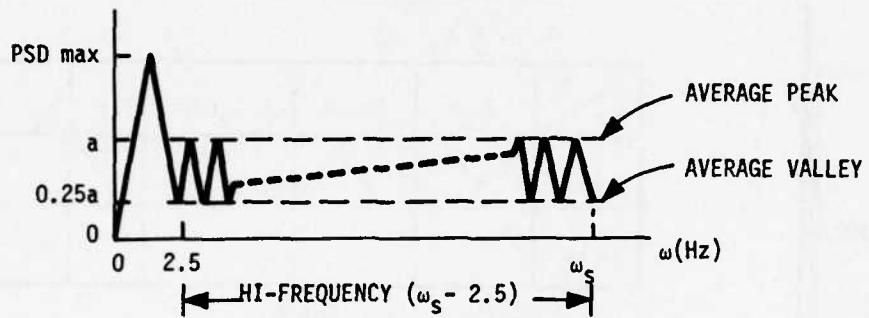
Figure 14. RMS Calculation

$$\text{Area}_{\text{High Frequency}} = 1/2(\omega_s - 2.5)(0.75a) + 0.25a \, (\omega_s - 2.5) \tag{19}$$

$$\text{Area}_{\text{High Frequency}} = (\omega_s - 2.5)[0.75a/2 + 0.25a] \tag{20}$$

$$\text{Area}_{\text{High Frequency}} = 0.63a \, (\omega_s - 2.5) \tag{21}$$

$$\text{RMS} = \sqrt{0.63a(\omega_s - 2.5)/\pi} \ \text{rps} \tag{22}$$

Admittedly, the method may give some numerical errors in the results; however, the data trends for the results should be indicative of real life.

3.3.2   Results and Recommended Sensor Noise Models

The results of the data reduction from PSD plots to RMS noise levels are summarized in Figure 15. Some highlights are:

- Turbulence level is not defined but one can deduce that, between Mach. 0.9 and 1.0, the turbulence is high and is low elsewhere (see n_z and Q plots).

- N_z shows little effect of high turbulence on high frequency noise.

- Note that, at high Mach, N_z high frequency dominates in a region where we can infer low turbulence, as earlier postulated.

Normal Acceleration, n_{zm} --High frequency noise seems relatively constant, independent of flight condition and turbulence level. (We assumed high vertical turbulence between M = 0.9 and 1.0.)

RMS = 0.03 g's
BW = 100 Hz (see Figure 16)

56
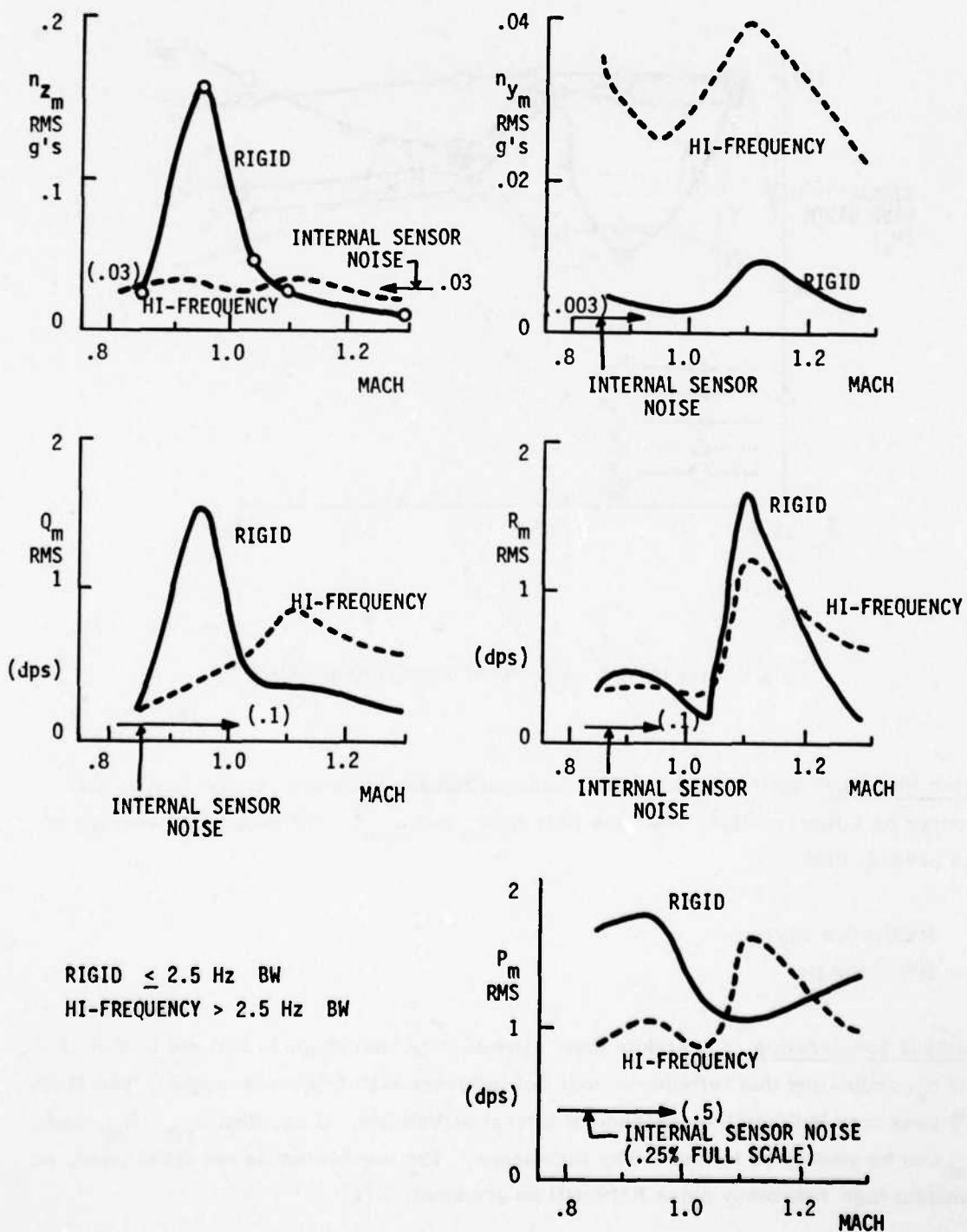
Figure 15. Sensor Spectral Noise Content
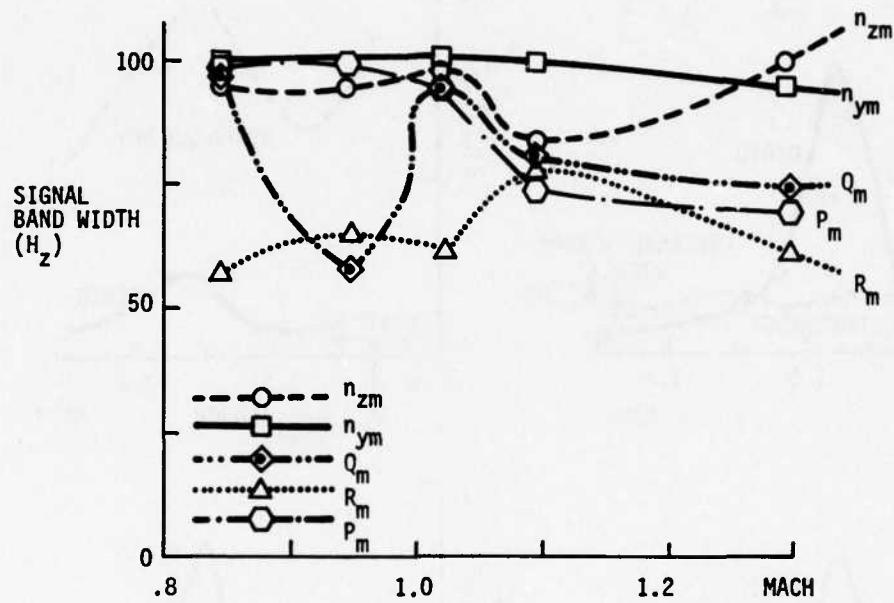
Figure 16. Measured Signal Bandwidth

Pitch Rate, Q--Again, there is no obvious turbulence influence, except maybe that induced by lateral motions (note the peak in R_m and n_{ym}). We assume an average of 0.5 percent RMS.

    RMS = 0.4 deg/sec
    BW = 100 Hz

Lateral Acceleration, n_{ym} --Note that, subsonically, the shape is inverse to that of q and n_z, indicating that turbulence does not influence high frequency output. The Mach 1.1 peak may indicate the presence of lateral turbulence. If so, then n_{ym}, R_m, and Q_m can be seen to be influenced by turbulence. The mechanism is not understood, so constant high frequency noise RMS will be assumed.

    RMS = 0.03 g's
    BW = 100 Hz

58

<u>Yaw Rate, R_m</u>--Similar to above comments.

 RMS = 0.4 deg/sec

 BW = 65 Hz

<u>Roll Rate, P_m</u>--Similar to above comments.

 RMS = 1.1 deg/sec

 BW = 100 Hz

From Figures 15 and 16 it is possible to pick out an RMS level and BW for each flight condition; however, average levels were selected which stressed the subsonic regime, which is pertinent to the A-7D application.

SECTION 4

CONCEPT DEVELOPMENT

4.1 DESIGN PHILOSOPHY

The design philosophy chosen for this study is largely independent of the design application. However, it is best explained using an example of how analytical redundancy blends with typical on-board computing functions and capabilities.

4.1.1 Analytical Redundancy for the A-7D

Analytical redundancy techniques were applied to the A-7D Multimode system to enable utlimate evaluation under realistic constraints and environments. To achieve benefits from this application, either added system capability or reduced system cost must be realized. The current system has a mixture of fail-operative and fail-safe hardware. The dual computers are fail-operative to a degree dependent on the self-test coverage. The sensors and servos are fail-safe; servos are made fail-safe through a combination of comparison monitoring (of like devices), validity testing, and signal limiting.

Sensors currently on board the A-7D are shown in Table 16. By application of analytical redundancy, some of these like sensors (rate gyros, a normal accelerometer, and an angle-of-attack sensor) could be eliminated and still maintain fail-safe operation. Alternatively, the mission reliability of the system could be improved with the current complement of sensors by providing fail-operative mission-essential sensors. Of these two options, the latter is selected for the design application because it is somewhat more demanding technically; furthermore, the resulting system is more in keeping with current operational requirements.

4.1.2 Design for Mission Reliability

There are many options for structuring the redundancy management which produce alternate performance qualities. Significant issues include:

1. Number of failure combinations possible before loss of function (success paths)

60

TABLE 16. SIGNAL AVAILABILITY ON A-7D AND F-4 DFCS

Sensor	Output	Variable Symbol	A-7D Available on Aircraft	A-7D AFCS Interface	F-4 DFCS* Available on Aircraft	F-4 DFCS* AFCS Interface	Study List
Inertial Measurement Unit or Attitude Reference System	Euler Angles	θ	X	X	X	X	X
		ϕ	X	X	X	X	X
IMU or HSI	Angles	** ψ	ψ	$\Delta\psi$	N/A	$\Delta\psi$	X
Normal Accelerometer	Normal Acceleration	n_z	X	X	X	X	X
Lateral Accelerometer	Lateral Acceleration	n_y	X	X	X	X	X
Pitch Rate Gyro	Body Axis Pitch Rate	Q	X	X	X	X	X
Roll Rate Gyro	Body Axis Roll Rate	P	X	X	X	X	X
Yaw Rate Gyro	Body Axis Yaw Rate	R	X	X	X	X	X
Air Data Computer Sensor Inputs • Static Pressure • Total Pressure • Total Temperature	True Air Speed	U	X	X	X	X	X
	Altitude	h	h	Δh	h	Δh	X
	Altitude Rate	$\dot{h}$	X	N/A	X	X	N/A
	Pilot Differential Pressure	$\bar{q}_c$	X	N/A	X	X	N/A
	Mach	M	X	X	X	X	N/A
AOA Indicator	Angle-of-Attack	α	X	X	X	X	X
Sideslip Indicator	Sideslip Angle	β	(Boom)X	N/A	X(ADC)	X	N/A

*Analysis performed on two aircraft; both originally considered for the design application. F-4 DFCS is included to demonstrate uniform treatment for both aircraft.

**ψ – North ref.; $\Delta\psi$ – Set-in ref.; h – total altitude; Δh – Set-in or synch. ref.

2. Dependency on monitoring quality

3. Fail safety versus mission reliability (generally conflicting requirements)

4. Cost effectiveness (mission reliability gained for added fault detection and isolation capability)

The sensor complement of the A-7D Multimode System and its related functions are presented in Table 17.

TABLE 17. A-7D MULTIMODE SENSORS RELATED TO FLIGHT CONTROL FUNCTION

Signal	Pitch CAS	Lateral-Directional CAS	Yaw Stability	Pitch Multimodes	Lateral-Directional Multimodes	Pitch Autopilot	Lateral-Directional Autopilot	Loss Consequence
Roll Rate		X			X		X	Abort
Pitch Rate	X			X	X	X		Abort
Yaw Rate		X	X		X		X	Abort
Normal Acceleration	X			X	X	X		Abort
Lateral Acceleration		X			X			Continue mission, degraded
Roll Attitude				X	X	X	X	Continue mission on CAS
Pitch Attitude				X	X	X		Continue mission on CAS
Yaw Attitude						X		Continue mission on pitch MM, lateral-directional CAS
Altitude					X	X		Continue mission on pitch MM, lateral-directional CAS
True Airspeed				X	X			Continue mission on CAS
Angle-of-Attack					X			Continue mission on pitch MM, lateral-directional CAS

Note that only the first four sensors are mission essential from the standpoint of flight control; the others are not required for Level 1 (Mil-Std 8785) handling qualities.

The primary gain in mission reliability is realized by structuring the system such that a single failure does not cause an abort. This means that mission essential elements must be fail-operative. It also suggests that the cause of a mission abort will be due to a pair of faults, generally an equipment failure, plus some isolation defect. There is therefore very little to be gained (reduction in abort probability) in complicating the redundancy management such that more than one sensor fault can be accommodated. Consequently, the following design approach was selected for the A-7D application:

1.   The current capability of fail-operative computers is retained.

2.   The mission essential sensors (pitch rate, roll rate, yaw rate, and normal acceleration) are fail-operative.

3.   The "performance enhancement" sensors (platform angles, angle-of-attack, true airspeed, and altitude) are at least fail-safe.

4.   If a computer fails, the added complication of retaining fail-operative sensors is not provided.

Assuming that the fault isolation is 95 percent effective for all cases, an abort will be caused by the following (servos and hydraulics excluded):

1.   Loss of either computer, plus a deficient self-test ($2 \times 2 \times 10^{-4} \times 0.05 = 2 \times 10^{-5}$ failures for one hour).

2.   Loss of any rate gyro (out of six) plus a deficient diagnosis ($6 \times 10^{-4} \times 0.05 = 3 \times 10^{-5}$ failures for one hour).

3.   Loss of either normal accelerometer plus deficient diagnosis ($2 \times 2 \times 10^{-5} \times 0.05 = 0.2 \times 10^{-5}$ failures for one hour).

The above three probabilities of failure total 5.2×10^{-5} for a one-hour flight, a small number compared to most mission reliability allowances. Note that several other contributions to mission abort have been neglected because of their size. For example,

1.   Computer/sensor combinations--failure of either computer followed by any mission essential sensor ($2 \times 2 \times 10^{-4} \times 6.0 \times 10^{-4} = 2.4 \times 10^{-7}$ failures for one hour).

2. Failure of both computers $(2 \times 10^{-4})^2 = 4 \times 10^{-8}$ failures for one hour.

3. Failure of two like rate gyros in any axis: $3(10^{-4})^2 = 3 \times 10^{-8}$ failures for one hour.

4. Failure of both normal accelerometers $(2 \times 10^{-5})^2 = 4 \times 10^{-10}$ failures for one hour.

4.1.3 Sensor Interfaces

A simplified diagram of the multimode system defining the interfaces of the studied sensors is shown in Figure 17. All sensors are applied to each computer channel. In the case of the dual sensors, however, signal conversion is only performed by the associated computer if both computers are operative.

Each computer receives the foreign sensor data by the serial data exchange. By taking the average of the dual sensor inputs, each computer operates on identical data. If one computer fails and is disabled, the remaining computer converts both channels of dual sensor data and continues to operate on the average.

In the case of single sensors, each computer will receive and convert the data. The converted data will be exchanged and averaged to maintain identical inputs to the control law in each channel. If a computer fails and is disabled, the remaining channel will use only its own converted single sensor data.

As indicated in Figure 17, the sensor diagnosis performed in each channel is based only on the local dual sensor data (e.g., a sensor with computer A). This means that, if a computer fails, the diagnosis of the associated sensors will also be lost. This approach is consistent with the single-fail-operative design philosophy (fail-safe sensors after a computer failure).

4.1.4 Fail-Operative Sensor Logic

Of the options available for achieving fail-operative sensors, the proposed approach is one which favors fail-safe operation with minimum dependency on diagnostic quality. This logic is illustrated in Figure 18. Note that the diagnostic filters are used as
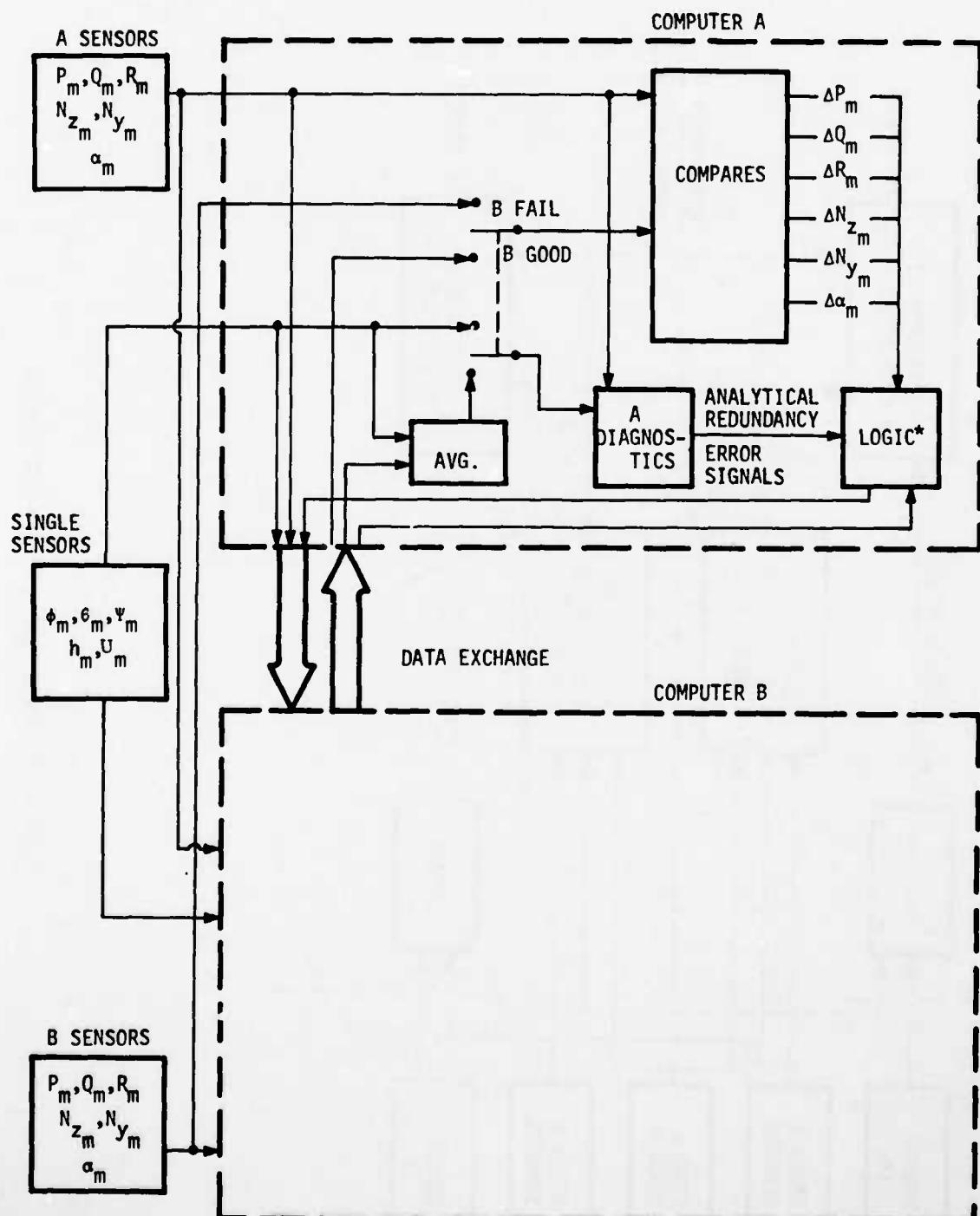
*LOGIC INCLUDES MONITOR TESTS AND FAULT ISOLATION.

Figure 17. A-7D Sensor Interfaces

65
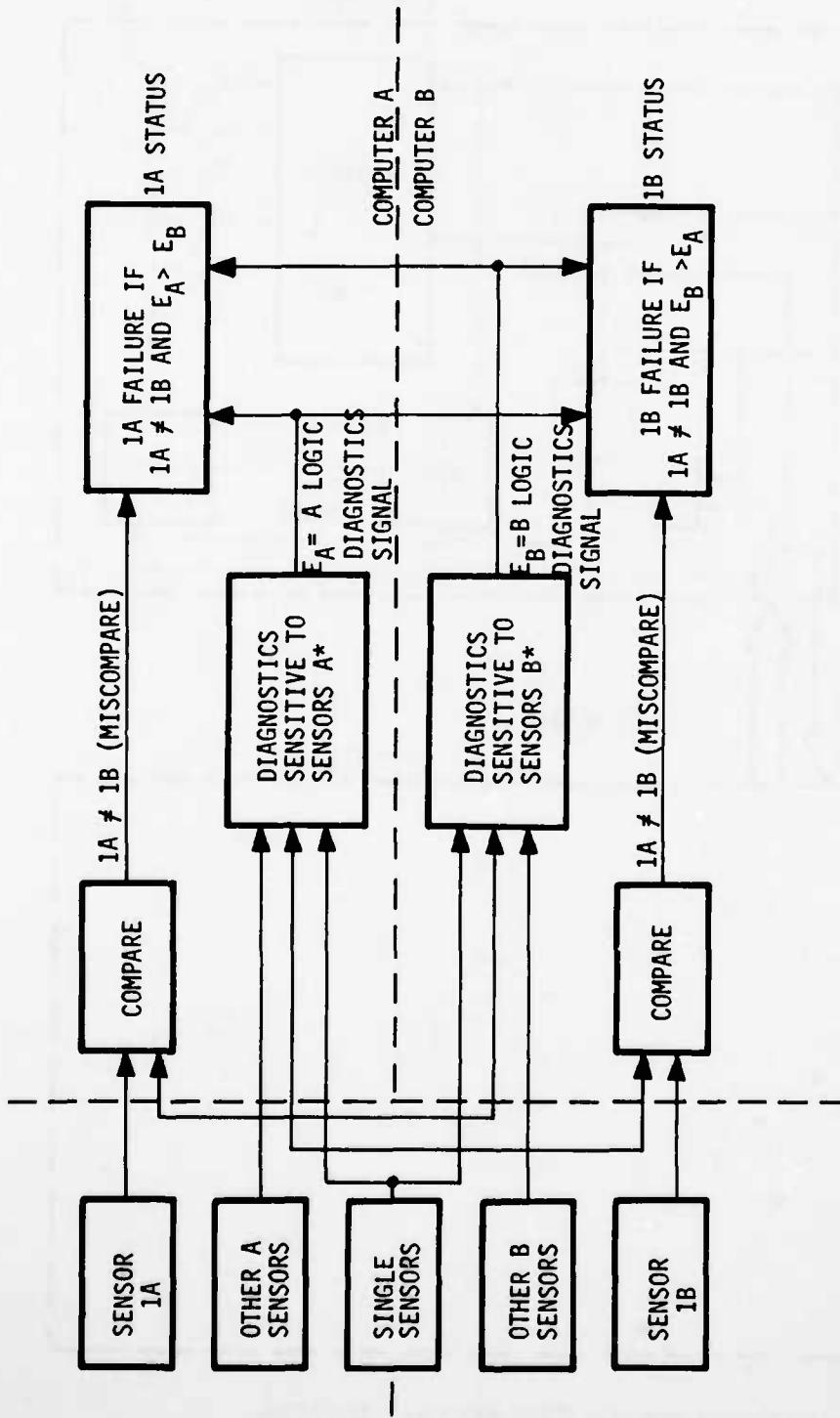
Figure 18. Fail-Operative Sensor Logic

66

failure isolators after a miscompare between like-sensors is signaled. The isolation can be based on relative magnitudes of diagnostic errors or a specifically designed monitor to compare like-diagnostic-filter assemblies. Both approaches avoid dependence on a predetermined failure threshold (with associated tolerance problems) for the diagnostics for the first-failure detection in a dual sensor set.

A diagnostic failure threshold will be required for detection of second like-faults and for first faults in single sensors.

Note that both diagnostic errors are not available if one computer has failed, requiring a shutdown if the dual inputs miscompare. This again is consistent with the fail-operative design philosophy.

It is anticipated that the miscompare discretes will be generated after three consecutive difference signals which exceed a preset level are received, as is currently done in the A-7D Multimode System.

4.1.5   Fail-Safe Sensor Logic

Three types of fail-safe sensor logic are required for the subject application:

1. Comparison monitoring of dual like-signals without a related diagnostic function (analytical redundancy). Examples include lateral acceleration (for which there is only a marginal diagnostic capability) and the other dual sensors after either failure of one computer or failure of an input to the relevant diagnostic filter.

2. Monitoring of the level of a diagnostic error function after failure of one sensor in a dual set. For example, if the pitch rate gyro in Channel A fails, the condition of the pitch rate gyro in Channel B is monitored by the relevant diagnostic filter.

3. Monitoring of a single sensor by its associated diagnostic filter. The approach here is to require (in the absence of other faults) a failure indication from both computers to avoid fault indication due to failure of a dual sensor; that is, a dual sensor failure yet to be detected by a comparison monitor would be detected in only one computer.

67

The first two logic types are fairly obvious, but the third is somewhat dependent on the specific diagnostic test used.

Note that the general approach is to indicate faults by sensor groups rather than attempt more isolation by less reliable logic combinations. Whereas the latter could be used in theory, marginal failure situations could result in faulty isolation. This conclusion is tested with Concept III. Furthermore, there is not a great deal to be gained from better isolation from the standpoint of the flight control data usage. For the A-7D, it is noted that:

- If the platform fails, there is no use for TAS or altitude.

- If TAS fails, the platform and altitude are only good for autopilot modes. A full CAS can be safely tried by using limited authority outer-loop inputs.

- If altitude fails, the pitch MM could still be used (which is not known without isolation to the altitude fault). The lateral-directional MM are lost regardless. Autopilot modes may be safely tried (altitude hold won't work).

4.2 CONCEPT I--THE OBSERVER/BLENDER

The basic relationships and goals of the concepts for development were laid out in Section 2. One of the key objectives of Concept I was to examine how cheaply (computationally) a diagnostic filter could be implemented. Also, a design technique based mostly on frequency domain considerations was tested indirectly.

The basic operation of the observer/blender is to blend state and state derivative into a consistent error function. For example, the relationship between a scalar position and velocity is

$$V_x = \dot{X} \tag{23}$$

If both position and velocity are measured quantities (or combinations of measurements), X_m and V_m respectively, then a consistent error function would be

$$e = \frac{1}{\tau s+1} V_{xm} - \frac{s}{\tau s+1} X_m \tag{24}$$

where the time constant, τ, is a design parameter.

68

Two important characteristics are observed:

1. Information about both state and derivative is available.

2. The describing Equation (23) is exact.

The first characteristic is significant only where both state and derivative are not available (as in the case of lateral acceleration, n_y).

The second characteristic is important because, for perfect measurements and perfect continuous filtering,

$$e = 0$$

The error is non-zero because of three real-world situations:

1. X_m and V_{x_m} are not perfect representations of X and V_x.

2. There is digital integration with associated sampling effects.

3. There are faults in X_m and/or V_{x_m}.

The goal of analytical redundancy in this case is to simply distinguish the first two situations from the third situation.

4.2.1   Concept I Candidate Filters

Matching the available sensors of Table 16 with the equations of motion, (1) through (15), the candidate error signals were proposed as shown in Table 18.

Of the nine candidate diagnostic filters, five were developed for evaluation. Anticipated fault diagnosis capabilities are also listed in Table 18. Within the final set of five algorithms, a good diagnostic filter exists for each sensor in Table 18 except n_{y_m} and V_m.

Lateral acceleration, N_{y_m}, fault diagnosis is very difficult because of its low range of magnitudes ($\pm 1/2g$) and because the required state to be used for blending (namely, β) is not available. High-passing the sideslip measurement β_m, as suggested in Algorithm 7, is not advisable because of the low quality signal of β_m and gust information, i.e.,

69

TABLE 18. CANDIDATE CONCEPT I ERROR SIGNALS

Observer/Blender Error Signal Relationship	Equation of Motion Represented in Equation	Symplifying Assumptions	Estimation Assumptions	Sensors Diagnosed	
				Primary Diagnosis	Secondary Diagnosis*
1. $P_\epsilon = P_m - \hat{\dot{\phi}} + \hat{\dot{\psi}}\sin\theta_m$	(10)	None	$\hat{\dot{\phi}} = \frac{s}{\tau s+1}\phi_m$	P_m, ϕ_m	θ_m, ψ_m
2. $Q_\epsilon = Q_m - \hat{\dot{\theta}}\cos\phi_m + \hat{\dot{\psi}}\sin\phi_m\cos\theta_m$	(11)	None	$\hat{\dot{\theta}} = \frac{s}{\tau s+1}\theta_m$	Q_m, θ_m	ϕ_m, ψ_m
3. $R_\epsilon = R_m - \hat{\dot{\psi}}\cos\phi_m\cos\theta_m + \hat{\dot{\theta}}\sin\phi_m$	(12)	None	$\hat{\dot{\psi}} = \frac{s}{\tau s+1}\psi_m$	R_m, ψ_m	ϕ_m, θ_m
4. $n_{z_\epsilon} = n_{z_m} - U_m(Q_m - \hat{\dot{\alpha}}_m) - g(\cos\theta_m\cos\phi_m - 1)$	(6)	V=0	$\hat{\dot{\alpha}} = \frac{s}{\tau s+1}\alpha_m$	N_{z_m}, Q_m, α_m	U_m, θ_m, ϕ_m
5. $\dot{h}_\epsilon = \hat{\dot{h}} - U_m(\sin\theta_m - \alpha_m\cos\phi_m\cos\theta_m)$	(3)	$\alpha = \frac{W}{U}, V=0$	$\hat{\dot{h}} = \frac{s}{\tau s+1}h_m$	h_m, θ_m, α_m	U_m, ϕ_m
6. **$n_{z_\epsilon} = n_{z_m} - \frac{C_L\hat{\bar{q}}A}{mass} + g$	(6) $\bar{q} = \frac{1}{2}\rho V_T^2$	Approximate C_L	$\hat{\bar{q}} = \frac{1}{2}\hat{\rho}U_m^2$ $\hat{\rho} = f(h_m)$	N_{z_m}, U_m	α_m, Q_m, h_m
7. **$n_{y_\epsilon} = n_{y_m} - U_m(\hat{\dot{\beta}} + R_m - P_m\alpha_m) + g\cos\theta_m\sin\phi_m$	(5)	$\beta = \frac{V}{U}, \alpha = \frac{W}{U}$	$\hat{\dot{\beta}} = \frac{s}{\tau s+1} - \beta_m$	n_{y_m}, R_m, β_m	$U_m, P_m, \alpha_m, \phi_m, \theta_m$
8. **$\dot{h}_\epsilon = \hat{\dot{h}}_m - \hat{\dot{h}}$	N/A	None	$\hat{\dot{h}}_m = \frac{s}{\tau s+1}h_m$	$\dot{h}_m, h_m$	
9. **$n_{y_\epsilon} = n_{y_m} - \frac{C_y\hat{\bar{q}}S_A}{mass}$	(5) $\bar{q} = \frac{1}{2}\rho V_T^2$	Approximate C_y	$\hat{\bar{q}} = \frac{1}{2}\hat{\rho}U_m^2$ $\hat{\rho} = f(h_m)$	n_y, U_m	α_m, P_m, R_m, h_m

*Fault diagnosis is possible but not expected or necessary.
**Initial feasibility examined but not developed.

$\beta_m = \beta$ + lateral gust. A recommendation to add a more effective sideslip indicator might be in order; however, the goal of this study is not to add sensors. Also, as indicated in Table 17, n_y is not mission-critical. Therefore, its diagnostic is not considered crucial to the system.

Airspeed, U_m, is also directly unaccounted for in Concept I. Diagnostic Filters 4 and 5 might provide a low level fault detection capability due to the minor U_m role.

Filter 6 would provide a much better capability for detecting airspeed measurement faults; however, the complexity is considered excessive and counter to the goal of simplicity for Concept I.

Both n_y and U_m are addressed in Concept II. Both are considered to have minor impact on mission reliability; therefore diagnosis in Concept I is not critical.

Block diagrams for Filters 1 through 5 are shown in Figures 19 through 23.
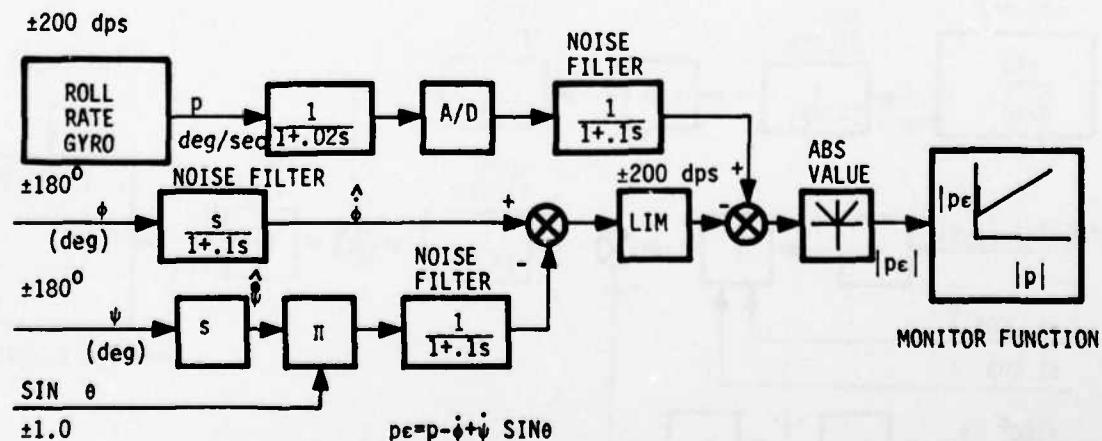
Figure 19. Filter I-1: Roll Rate Observer/Blender

71
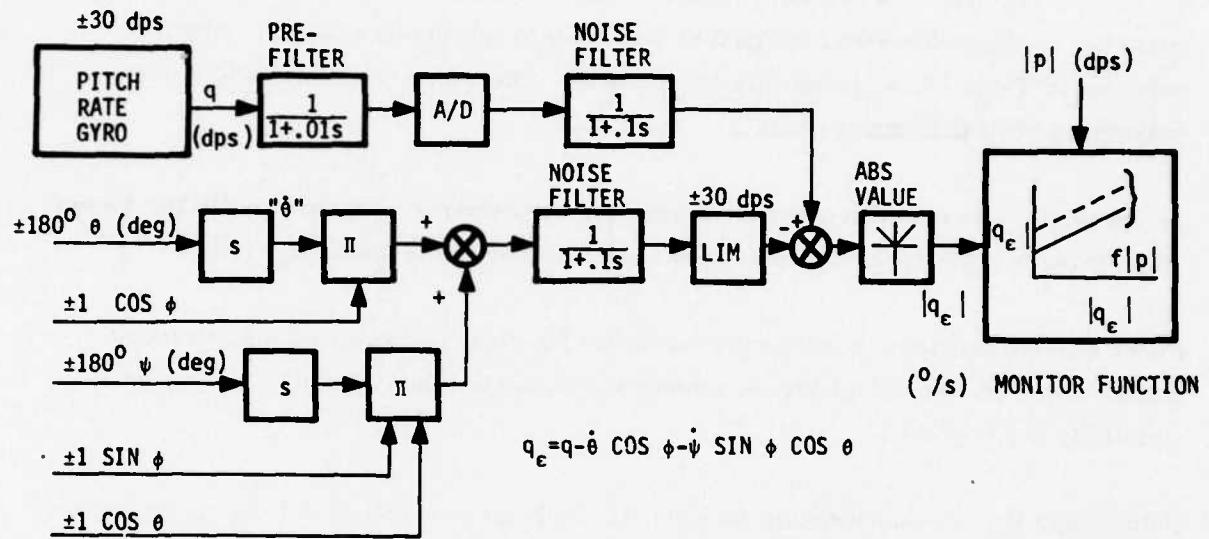
Figure 20. Filter I-2: Pitch Rate Observer/Blender

The equation shown in the figure: $q_\epsilon = q - \dot\theta \cos\phi - \dot\psi \sin\phi \cos\theta$
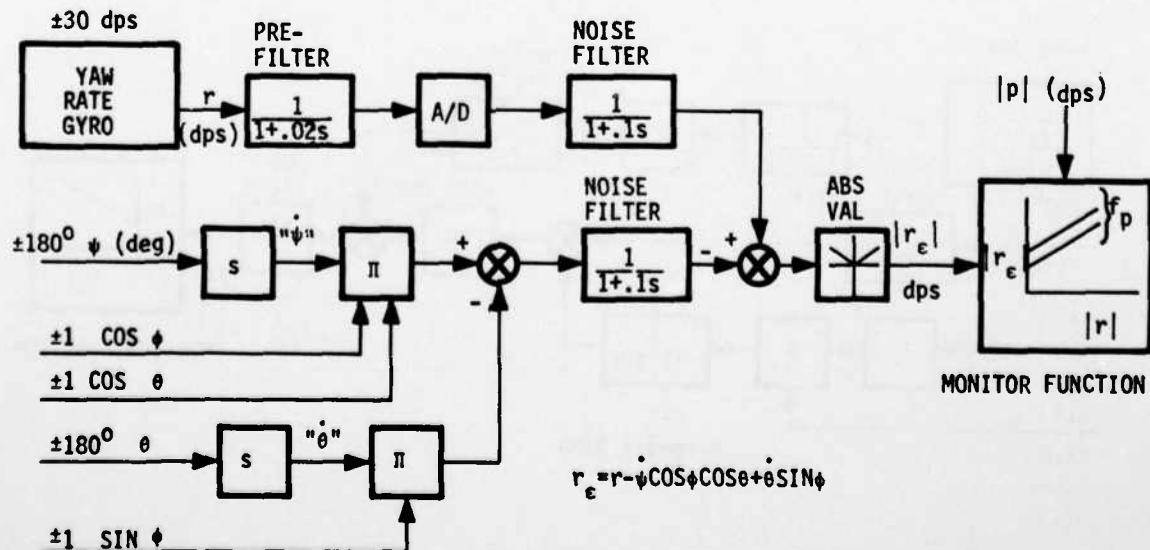
Figure 21. Filter I-3: Yaw Rate Observer/Blender

The equation shown in the figure: $r_\epsilon = r - \dot\psi \cos\phi \cos\theta + \dot\theta \sin\phi$
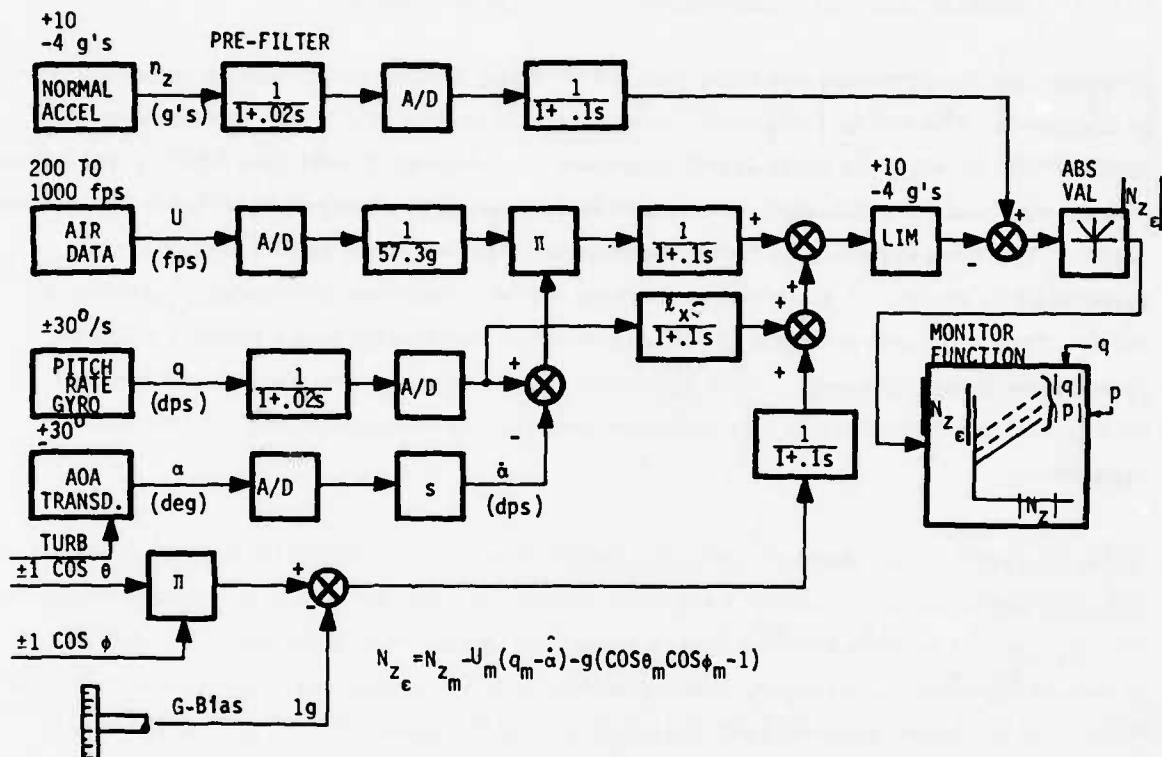
Figure 22. Filter I-4: Normal Acceleration Observer/Blender

$$N_{z_\epsilon} = N_{z_m} - U_m(q_m - \hat{\dot{\alpha}}) - g(\cos\theta_m \cos\phi_m - 1)$$

$$\dot{h}_\epsilon = \hat{\dot{h}} - U_m(\sin\theta_m - \alpha_m \cos\phi_m \cos\theta_m)$$
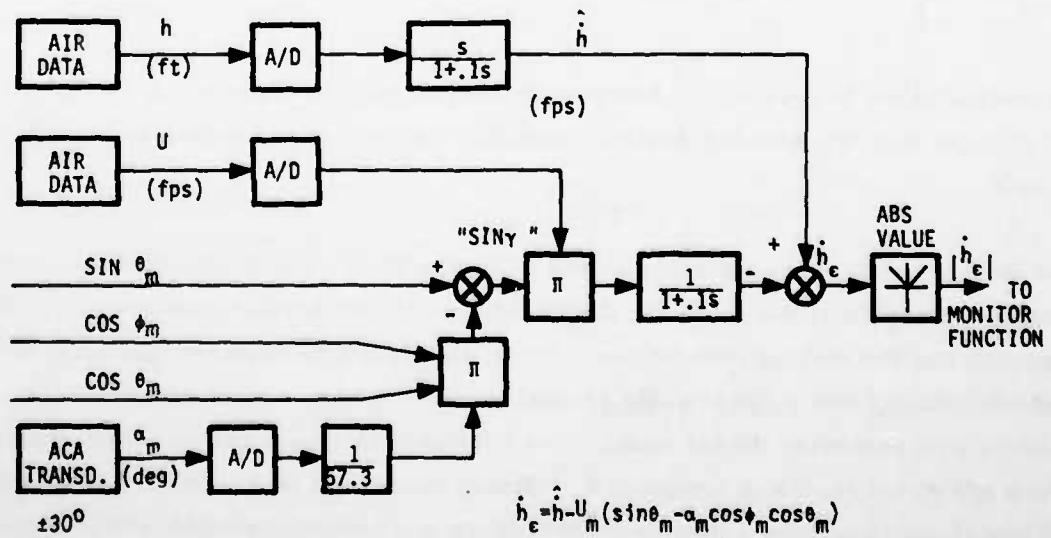
Figure 23. Filter I-5: Altitude Observer/Blender

73

4.2.2   Observer/Blender--Monitor Levels and Fault Detection

Monitor functions for Concept I are derived by using the individual sensor characteristics in Section 3. The key to "adequate" monitoring, of course, is highly dependent on the monitor trip levels. As these levels increase, the monitor finally gets to the point where "hardovers" only are detected or extreme maneuvering is required to activate the monitor output. The first approach to fixing the monitor trip level was to RSS all the errors introduced by imperfect state measurements (nulls, resolution hysteresis, turbulence, etc.). This approach attempts to define a monitor level which has a definite relation to nuisance disengagements. This approach results in some relatively large monitor trip levels, particularly when 3σ gusts are included as an error in the measurement algorithms.

Table 19 contains the monitor functions for the five Concept I algorithms. In general, the algorithms for derivation of body rates from platform-derived Euler angles (Figures 19, 20, and 21) provide monitor levels somewhat tighter than those possible with dual sensor comparators. Further, these algorithms provide good hardover and dead sensor failure detection for both the body rate sensor and the equivalent derived Euler rate, e.g., pitch rate, Q, and Euler rate, $\dot{\theta}$ (hence Euler attitude θ). Dead-faults are detected with reasonable maneuvering control inputs. This is also demonstrated in Table 19 by comparing these monitor levels with the dual sensor comparison monitor levels.

The minor terms in the monitor functions do not provide good monitoring in themselves, but because they are included they will provide a tighter monitor tolerance for the primary signals.

The normal acceleration algorithm shown in Figure 22 is a kinematic approach, converting angular rates and resolving the gravity vector into normal acceleration. This approach has two serious deficiencies. First, the algorithm requires kinematic velocity (vehicle velocity with respect to the ground), but the air data sensor gives vehicle velocity with respect to the air mass. The difference is steady and turbulent winds, which are direct errors in computed n_z. Steady winds aloft (e.g., jet stream or its influence), which could be a significant part of the total vehicle velocity, are treated as a percentage error on n_z ($0.35\,n_z$ in the monitor function). The second major deficiency is the derived angle-of-attack rate which is rich in turbulence-induced noise. If the

74

TABLE 19.   PRELIMINARY OBSERVER/BLENDER MONITORS

Algorithm	Monitor Level
1. P_ϵ (deg/sec)	Trip $\geq 3.74 + 0.0596/P_m/$ CM* Trip $\geq 5.12 + 0.0842/P_m/$
2. Q_ϵ (deg/sec)	Trip $\geq 0.54 + 0.039/Q_m/ + 0.0053/P_m/ + 0.0197/R_m/$ CM Trip $\geq 0.76 + 0.0484/Q_m/ + 0.0075/P_m/$
3. R_ϵ (deg/sec)	Trip $\geq 0.63 + 0.0378/R_m/ + 0.0050/P_m/ + 0.0197/Q_m/$ CM Trip $\geq 0.89 + 0.046/R_m/ + 0.0071/P_m/$
4. n_{z_ϵ} (g's)	Trip $\geq 0.65 + 0.35/n_{z_m}/ + 0.015/\dot{Q}_m/$ $\qquad + \dfrac{U_m}{57.3\,g}\,[0.54 + 0.0342/Q_m/ + 0.0353/P_m/]$ CM Trip $\geq 0.082 + 0.076/n_{z_m}/ + 0.005/q/$
5. h_ϵ (ft/sec)	Trip $\geq 2.7 + 0.0281/U_m/ + 0.35/\dot{h}/ +21$

*Comparison Monitor

system is designed to tolerate Mil-Spec 8785 gusts (21 ft/sec, 3σ), then inspection of the algorithm reveals that the 21 ft/sec vertical velocity is sensed directly by the monitor as $21/32.2 = 0.65$ g's. This g-level will be modified eventually, depending on the turbulence bandwidth and algorithm filtering. Worst case analysis was used here. This is also reflected in Table 19 by comparing the first terms monitor level for n_{z_e} with that for the dual sensor comparison monitor.

Consideration of winds aloft and turbulence seriously degrades the efficiency of this algorithm in detecting faults. In general, it will detect pitch rate (Q) and normal acceleration (n_z) hardovers and dead faults, but airspeed and angle-of-attack faults will escape detection except under certain restrictive conditions.

The final algorithm, Figure 23, monitors the altitude sensor. Although the algorithm appears in another mechanization, it was not effectively monitored there. In fact, steady state or absolute altitude monitoring is not provided. Thus, sensor faults resulting in altitude "drifts" within the defined tolerances will not be detected.

The altitude algorithm again is "kinematic" and will develop errors in proportion to steady winds and turbulence, similar to the normal acceleration mechanization discussed earlier. Vertical gust components sensed by the angle-of-attack vane (21 ft/sec - 3σ) will necessitate a higher monitor level to account for this. This is probably an unacceptable altitude monitor as it stands. A wind estimation input (if available) would be a significant improvement and may offer some hope. Integration of the derived altitude rate to provide a reference absolute altitude is intuitively unworkable, even with periodic updates, when considering steady wind errors (which in general cannot be estimated from the assumed sensor complement).

In operation, an error signal must trip (exceed) its monitor level three consecutive times for a fault declaration. This allows a low monitor level while maintaining the required false alarm probability (i.e., one false alarm per 1000 flight hours). Multiple trips, signal correlation, and false alarms are discussed further in Section 5.

4.3   CONCEPT II: DIAGNOSTIC KALMAN FILTERS

4.3.1   Equivalence of Observer/Blender and the Kalman Filter

The observer/blender idea in Concept I was characterized by simplicity and utilization of classical frequency domain techniques. By comparison, Concept II allows more complexity, albeit more performance expectations. Also, a time domain approach is used here.

Comments on these two guidelines are in order. First, simplicity versus complexity is not implied by the difference in design technique. Indeed, if the design goals of Concept I are repeated in the monitor (i.e., accountability for sensor characteristics such as bias, scale factor, and wind gusts), a Kalman filter approach would produce the same filters in structure as Concept I. Figure 24 uses the same position-velocity example presented earlier to demonstrate the equivalence of the classical approach addressed in Concept I with a steady state Kalman filter designed in the continuous time domain.

The equivalence, in structure, leaves only one difference between the construction of an observer/blender error signal function and a Kalman filter residual: the value of the feedback gain K $(1/\tau)$. In Concept I, a value of τ = 0.10 sec was chosen to differentiate

Basic Physical Relationship

$$\dot{x} = V_x$$

Available Measurements

1. Position

$$X_m = X + \eta_x \; : \; \eta_x \sim N(0, \; \sigma_x) \text{ white}$$

$$V_{x_m} = V_x + \eta_v \; : \; \eta_v \sim N(0, \; \sigma_v) \text{ white}$$

Observer/Blender Error Signal

$$e(s) = \frac{1}{\tau s + 1} V_{x_m} - \frac{s}{\tau s + 1} X_m$$

Kalman Filter Design

1. State Space Solution

$$\dot{\hat{X}} = K(\nu) + V_{x_m}$$

where the filter residual

$$\nu = X_m - X \quad \text{(residual)}$$

$$K = \text{steady state Kalman gain}$$

2. Frequency Domain Transfer Function

$$\nu(s) = \frac{sX_m}{s+K} - \frac{V_{x_m}}{s+K}$$

Let

$$\tau = \frac{1}{K}$$

Then

$$e = -K\nu$$

Figure 24. Equivalence Between the Observer/Blender and the Kalman Filter
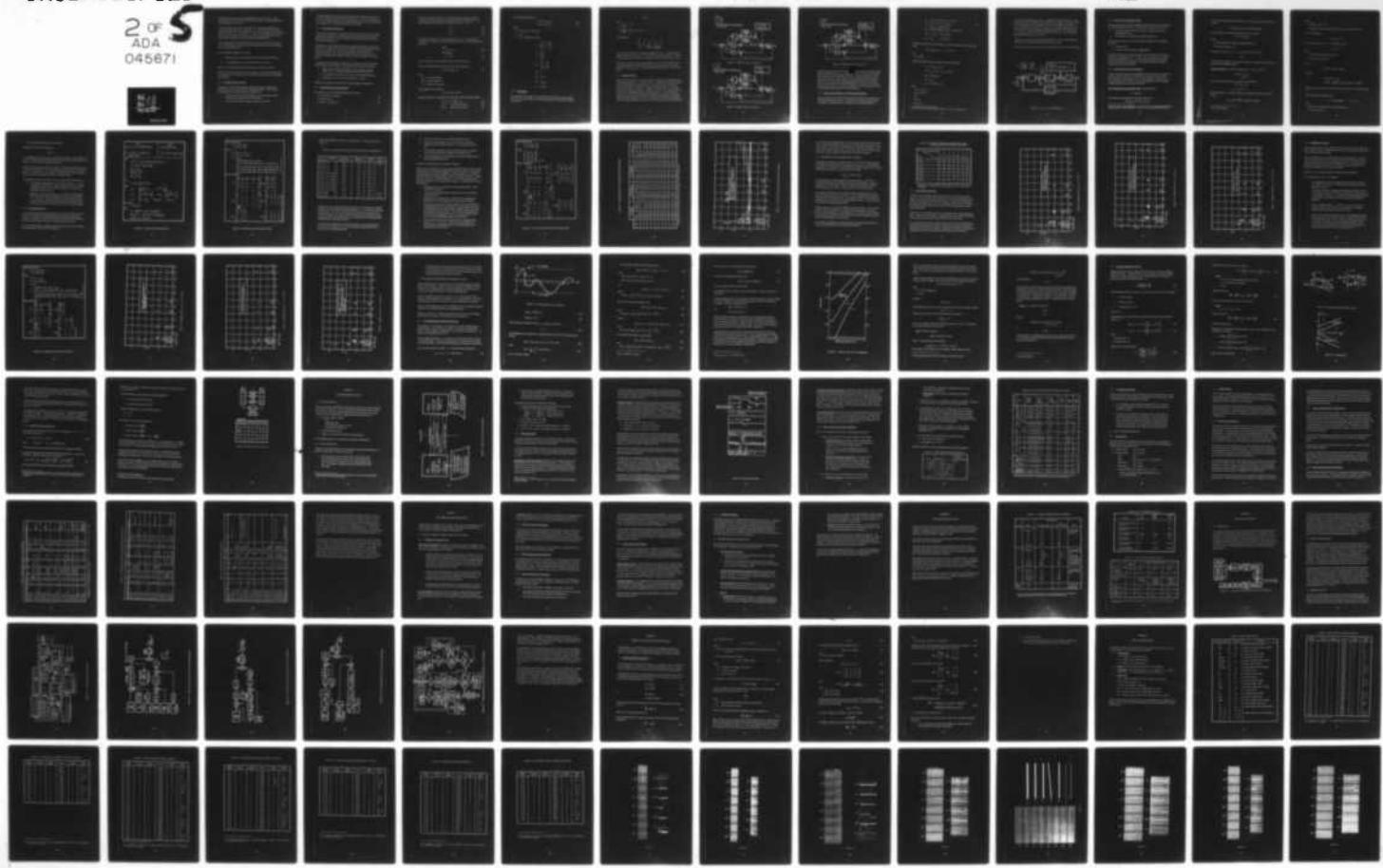
(by high-pass filters) frequencies in the rigid body motion of the aircraft. Is this the optimum time constant for fault detection? If not, what is? Note that Equation (24) is valid regardless of the value of τ.

In the Kalman filter sense, a small time constant τ (a high gain K) implies greater confidence in the measurement X_m relative to V_{x_m}. This gain value is proportional to the ratio of σ_x^2/σ_v^2. If X_m is a far cleaner (i.e., less noise) signal than V_{x_m}, the Kalman filter uses much more X_m in lieu of V_{x_m}. The limit is an infinite gain which means that no filter is necessary because X_m is a perfect representation of X.

The underlying premise of analytical redundancy is to use V_{x_m} to verify X_m and vice versa. An infinite gain (or in a practical sense a high gain) results in an overwhelming trust in X_m including its faults.

The conclusions for diagnostic filter design,

1.   Neither choosing τ to differentiate the rigid body frequencies (Concept I),

2.   Nor calculating K solely on noise ratios (Concepts II and III),

guarantee a successful design which meets the goals of analytical redundancy.

However, Kalman filtering does have one nice property: a residual (error signal) with low autocorrelation. The significance of this will be demonstrated later in discussions about monitors.

4.3.2   Concept II Performance Goals

Complexities in the Kalman filter designs result from attempts to provide better accountability for sensor characteristics in the diagnostic filters. This results in lower monitor levels. Specific extensions in Concept II are:

- Body rate bias and scale factor estimation to reduce monitor levels and investigate bias estimation for bias fault detection.

- Gust estimation to enhance diagnosis of angle-of-attack faults.

78

Additional complexity also results from scheduling a KF on dynamic pressure for the
lateral-directional acceleration equations of motion: (5), (13), and (15).   The goal here
is to create a diagnosis capability for lateral-acceleration (n_{y_m} is not checked in Concept
I) and airspeed (U_m is addressed only indirectly in Concept I).

4.3.3   Euler Angles and Body Rates

A specific goal of Concept II is to relieve the monitor of certain error sources outlined
in the Concept I discussions for the formulation of the Euler angle-body rate filters--
Equations (10) through (12).   These error sources are bias and scale factor errors in
body rate gyros (P_m, Q_m, R_m).

Another important consideration is the impact of the extensive nonlinear nature of the
equations.   An ultimate treatment would involve extended Kalman filtering with continual
gain calculations based upon error covariance updating.   This approach would
provide the best estimates and the lowest monitor levels for fault detection.   The
computational expense of this, however, would far exceed its usefulness for detecting
faults.

An approach taken by Montgomery (Reference 13) is to design by using constant filter
gains but nonlinear update equations.   This approach has many attractive features:

- Monitor levels based upon residual mean value, although they include
  nonlinearities, are consistent enough to provide good fault detection.

- The computational expense is far less than a full extended Kalman filter.

- Kalman gains can still be changed (scheduled) on key inputs.

Examples of this approach are included in the specific designs discussed below.

4.3.4   Euler Angle--Body Rate Kalman Filter

The equations of motion relating Euler angles to body rates are:

$$\dot{\phi} = P + (Q \sin \phi + R \cos \phi) \tan \theta \tag{7}$$

$$\dot{\theta} = Q \cos \phi - R \sin \phi \tag{8}$$

$$\dot{\psi} = (Q \sin \phi + R \cos \phi) \sec \theta \tag{9}$$

79

In order to calculate the filter gain, a nominal design must be chosen. Although schedules on ϕ and θ are possible, the implementation would be cumbersome. The initial design therefore is based upon a simplified system ($\theta = \phi = 0$), or

$$\dot{\phi} = P \tag{25}$$

$$\dot{\theta} = Q \tag{26}$$

$$\dot{\psi} = R \tag{27}$$

Working with just Equation (7), the filter design becomes one of estimating ϕ with a known driver P; however, roll rate is not known without error. The equations therefore become:

State:
$$\dot{\phi} = P_m - P_e \tag{28}$$

Measurement:
$$\phi_m = \phi + \phi_e \tag{29}$$

where "e" refers to the measurement errors associated with P and ϕ.

In order to incorporate important body rate errors, P_e is expanded to

$$P_e = P_b + M_p P_m + \eta_p \tag{30}$$

where

P_b is roll rate null bias

M_p is a scale factor error

η_p is random $\sim N(0, \sigma_p)$ white

The roll angle error is modeled as

$$\phi_e = \eta_\phi; \ \eta_\phi \sim N(0, \sigma_\phi) \text{ white}$$

where the roll angle, ϕ, can therefore be modeled with a third order representation:

$$\dot{\phi} = P_m - P_b - M_p P_m - \eta_p \tag{31}$$

$$\dot{P}_b = 0 \qquad (P_b \text{ assumed constant}) \tag{32}$$

$$\dot{M}_p = 0 \qquad (M_p \text{ assumed constant}) \tag{33}$$

80

The state space description is:

$$\dot{x} = Fx + G_1 u + G_2 \eta \qquad (34)$$

$$y = Hx + E_1 u + E_2 \eta \qquad (35)$$

where

$x^T = (\phi, P_b, M_p) \quad$ (state vector)

$u = P_m$

$y = \phi_m \quad$ (measurement vector)

$$F = \begin{bmatrix} 0 & -1 & -P_m \\ 0 & 0 & 0 \\ 0 & 0 & 0 \end{bmatrix}$$

$$G_1 = \begin{bmatrix} 1 \\ 0 \\ 0 \end{bmatrix}$$

$$G_2 = \begin{bmatrix} -1 & 0 \\ 0 & 0 \\ 0 & 0 \end{bmatrix}$$

$$E_1 = 0$$

$$E_2 = (0, 1)$$

$$\eta^T = (\eta_p, \eta_\phi)$$

$$H = (1, 0, 0)$$

4.3.5 Observability

The treatment of this problem is directly affected by the observability of the system.
Given that P_m is time varying, one must apply the appropriate observability criterion
(Reference 32):

81

where

$$\Gamma = [\Gamma_1, \Gamma_2, \ldots, \Gamma_n]$$

$$\Gamma_1 = H^T(t)$$

$$\Gamma_k = \frac{\partial \Gamma_{k-1}}{\partial t} + F^T(t) \, \Gamma_{k-1} \quad (k = 2, \ldots, n)$$

For this problem

$$\Gamma = \begin{bmatrix} 1 & 0 & 0 & \ldots & 0 \\ 0 & -1 & 0 & \ldots & 0 \\ 0 & -P_m & \dfrac{-\partial P_m}{\partial t} & \ldots & \dfrac{-\partial^{n-2} P_m}{\partial t^{n-2}} \end{bmatrix}$$

The rank of Γ depends entirely on the time-varying nature of P_m. A design based on an assumed steady value of P_m, i.e., $\partial^{k-2} P_m / \partial t^{k-2} = 0$, would be unobservable. Likewise a time-varying filter would exhibit weak reconstruction for periods of low roll activity.

The approach taken here is to employ logic based on body rate and Euler angle activity to switch alternately from bias estimation for low ϕ_m and P_m activity to scale factor estimation for high P_m activity. The same procedure also holds for "θ - Q" and "ψ - R" filters.

4.3.6   Estimator Design

Use of rate noise parameters, presented in Section 3, incorporates unmodeled dynamics into the problem solution, i.e., structural modes. A standard rule of thumb for attitude errors (0.25 percent of full scale) was used. The bias gain can be calculated with Kalman filtering theory by using one of a number of ad hoc methods, e.g., fictitious noise inputs or assumed correlation. The goal here, however, is to maintain estimation accuracy with a reasonable bandwidth for the bias estimation. The procedure used, therefore, was to select a bias gain based on bandwidth. Block diagrams of diagnostic filters are shown in Figures 25, 26, and 27. The residual RMS did not change appreciably over the optimum design case; that is, no bias or scale factor errors were assumed.

82

$K_1 = 0.229$

$K_2 = 0.075$

CLOSED-LOOP EQUIVALENT CONTINUOUS ROOTS
  -4.75, -0.358

$\Delta T[P_m + (Q_m SIN\phi_m + R_m COS\phi_m) TAN\theta_m]_1$

$\bar{M}_{P,1}$ UNIT DELAY

$P_{m,1}$

$K_2/P_{m,1}$

$+\hat{M}_{P,1} = \bar{M}_{P,(1+1)}$

Σ

Π

$/P_{m,1}/>.1$

$P_{b,1}$ UNIT DELAY

$\phi_{m,1}$

$+$ v_1

Σ

$\bar{\phi}_1$

$/P_{m,1}/\leq.1$

K_2

Σ

$\hat{P}_{b,1} = \bar{P}_{b,1+1}$

$\bar{\phi}_{1+1}$

Σ

UNIT DELAY

$\bar{\phi}_1$

K_1

Σ

$\hat{\phi}_1$
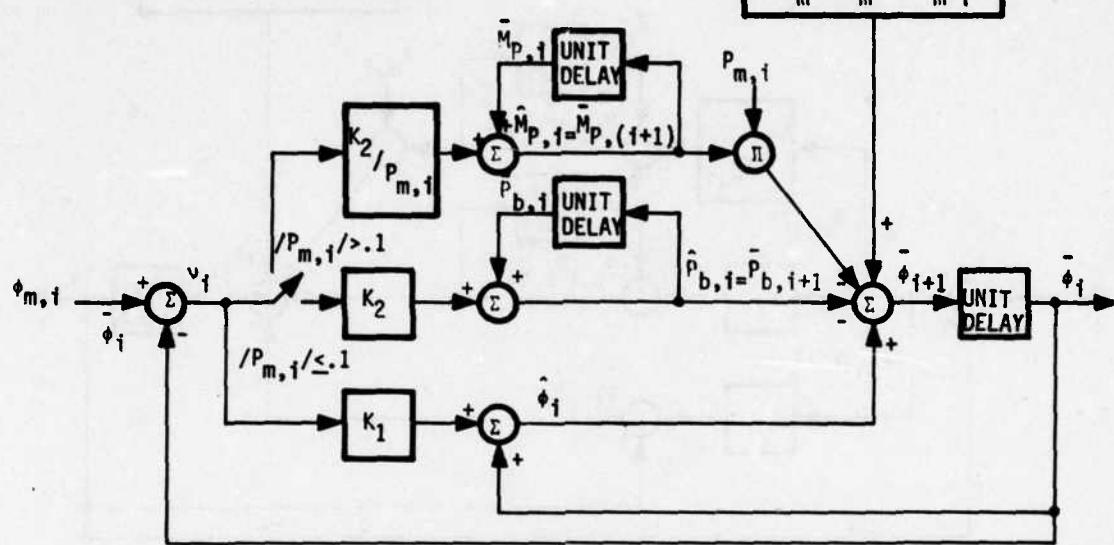
Figure 25. Diagnostic Filter for Equation (7)

$K_1 = 0.1131$

$K_2 = -0.03$

CLOSED-LOOP EQUIVALENT CONTINUOUS ROOTS
  -2.06, -0.309

$\Delta T[Q_m COS\phi_m - R_m SIN\phi_m]_1$

$\bar{M}_{Q,1}$ UNIT DELAY

$Q_{m,1}$

$K_2/Q_{m,1}$

$+$ $\hat{M}_{Q,1} = \bar{M}_{Q,1+1}$

Σ

Π

$/Q_{m,1}/>.1$

$Q_{b,1}$ UNIT DELAY

$\theta_{m,1}$

$+$ v_1

Σ

$\bar{\theta}_1$

$/Q_{m,1}/\leq.1$

K_2

Σ

$+$ $\hat{Q}_{b,1} = \bar{Q}_{b,1+1}$

$\bar{\theta}_{1+1}$

Σ

UNIT DELAY

$\bar{\theta}_1$

K_1

Σ

$\hat{\theta}_1$
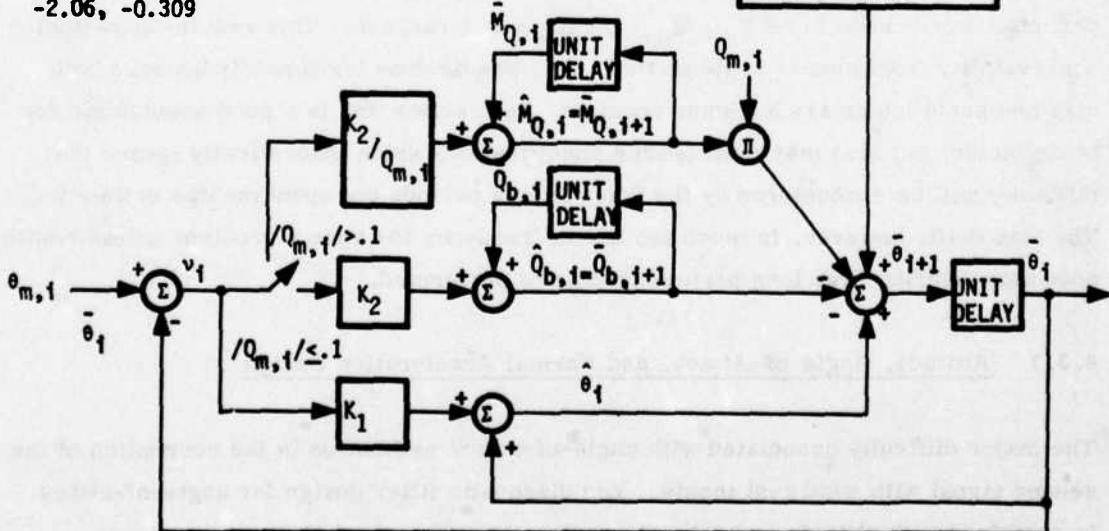
Figure 26. Diagnostic Filter for Equation (8)

$K_1 = 0.1563$

$K_2 = -0.05$

CLOSED-LOOP EQUIVALENT CONTINUOUS ROOTS
-2.97, -0.365
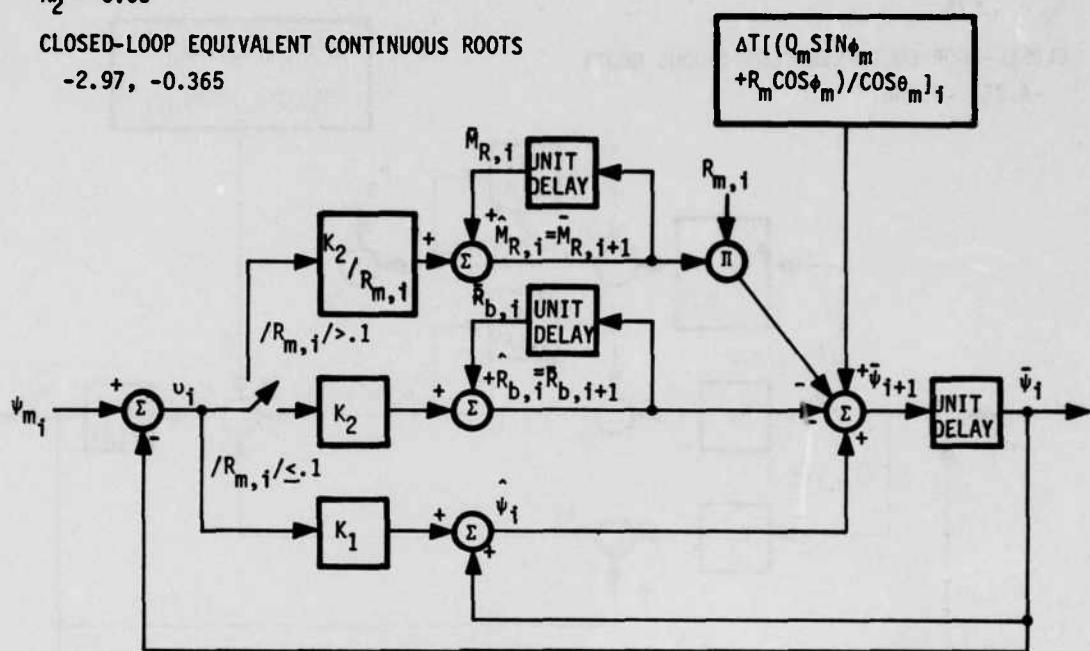
Figure 27. Diagnostic Filter for Equation (9)

Scale factor estimates result from switching . . . the bias estimates during high activity periods, chosen here to be P_m, Q_m, and $R_m \geq 0.1$ rad/sec. This results in switching observability from bias to scale factor. This can be done legitimately because both bias and scale factor are assumed constant. In practice this is a good assumption for scale factor, but bias may drift (within specification) which theoretically means that difficulty will be encountered by the filter during periods not spent on bias estimation. The bias drift, however, is much too low in frequency to cause a problem unless continuous maneuvering over long periods of time is performed.

4.3.7 Altitude, Angle-of-Attack, and Normal Acceleration Design

The major difficulty associated with angle-of-attack estimation is the corruption of the sensed signal with wind gust inputs. The diagnostic filter design for angle-of-attack is combined with altitude and normal acceleration using the following equations:

84

$$\dot{h} = U \sin \theta - W \cos \theta \cos \phi - V \cos \theta \sin \phi$$

$$\dot{W} = A_z + g \cos \theta \cos \phi - PV + QU \tag{6}$$

$$h_m = h + \eta_h \qquad : \eta_h \sim N(0, \sigma_h) \text{ white}$$

$$\alpha_m = \tan^{-1}[(W - W_g)/U_a^*] + \eta_\alpha : \eta_\alpha \sim N(0, \sigma_\alpha) \text{ white}$$

$$n_{z_m} = -A_z + \eta_{n_z} - g : \eta_{n_z} \sim N(0, \sigma_{n_z})$$

$$\theta_m = \theta + \eta_\theta \qquad \eta_\theta \sim N(0, \sigma_\theta)$$

The introduction of the vertical wind gust, W_g, results in having to account for this in the design:

$$\dot{W}_g = -a_w W_g + g_w \eta_w \qquad : \eta_w \sim N(0, 1)$$

where

$$g_w = \sigma_g \sqrt{2a_w}$$

Simplifying the equations results in design models for steady gains.

$$\dot{h} = W + U_m \theta_m - U_m \eta_\theta$$

$$\dot{W} = -n_{z_m} + U_m Q_m - \eta_{n_z} - U_m \eta_q + g$$

$$\dot{W}_g = -a_w W_g + g_w \eta_w$$

$$h_m = h + \eta_h$$

$$\alpha_m = (W - W_g)/U_m + \eta_a$$

where

$$\sin \theta \cong \theta; \cos \theta \cong 1$$

$$\sin \phi \cong \phi; \cos \phi \cong 1$$

$$PV = 0$$

$$U_a = U_m$$

$$\tan \alpha_m = \alpha_m$$

---

*U_a refers to forward velocity relative to wind, i.e., $U_a = U$ - forward wind.

Two inputs of consequence are θ_m and U_m. Although this filter does not address either sensor directly, fault detection for both is promising. Pitch angle, in particular, drives the filter significantly and would logically result in some high filter activity during a fault. One area of interest would be θ_m bias errors. It has been demonstrated earlier that filters like the Euler angle-body rate designs previously discussed will high pass θ_m, ϕ_m, and ψ_m. Bias errors will go undetected in these filters. The current application will be sensitive to θ_m bias errors.

Airspeed, U_m, enters into the current formulation twice. Expectations of detecting airspeed faults are reserved at best (simulation results were good).

Figure 28 contains the mechanization of this filter designed with discrete Kalman filtering.
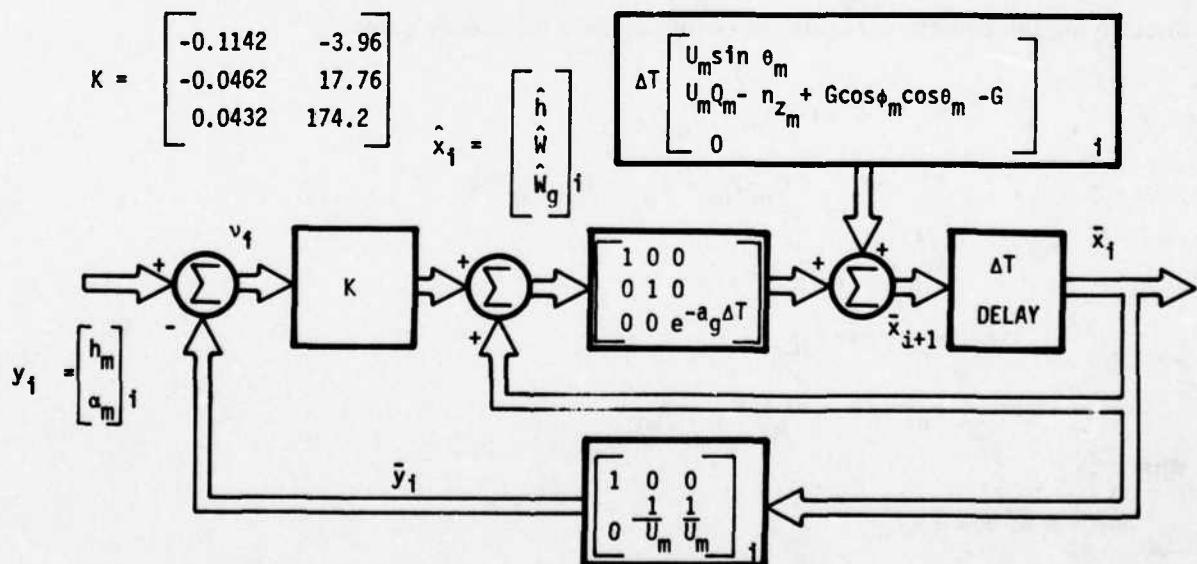
Figure 28. h_m, n_{z_m}, α_m Diagnostic Filter

4.3.8   Lateral Acceleration Diagnostic Filter

Concept I discussions revealed that handling fault detection of the lateral accelerometer, n_{y_m}, should be relegated to Concept II.   Previous issues discussed were as follows:

- The lack of necessary information, namely β, reduces the prospect of identifying faults in n_{y_m}.

- Fail operation in a degraded mode is possible without n_{y_m}.

The task of determining n_{y_m} faults was undertaken, nonetheless, with the following disclaimers:

- It might not work.

- If it does, it will be expensive (computationally).

The required design effort involves constructing a gain-scheduled lateral-directional Kalman filter using Equations (5), (7), (13), and (14).   The design exercise, however, has more implications than just n_{y_m}.   Concept III relies heavily on gain-scheduled acceleration equations for fault diagnosis.   The foregoing design can be considered preliminary to Concept III development.

4.3.9   Gain Scheduling and Filter Performance

In order to evaluate the impact of gain scheduling (or the lack of it) upon a Kalman filter design for sensor fault detection, a suitable evaluation criteria must be developed. Since all advanced schemes considered rely on filter residuals as a monitor input, the study concentrates on this variable.   Two such criteria might be a minimal residual covariance response ratio and residual correlation.

Minimal Residual Covariance Response Ratio--Letting the equation

$$B^* = E[\nu_i \nu_i^T]$$

be the residual covariance matrix for the optimal filter, then

$$\text{RMS ratio} = \text{tr}\{B^{*-1} E[\nu_i \nu_i^T]_D\}/n_r^\dagger$$

---

†Subscript D refers to the design filter.   In practice this may be the optimum for another flight condition or a gain schedule of some sort, or it may be completely arbitrary.

For a gain schedule approaching the ideal plant, i.e., one for which a Kalman filter is designed,

$$\text{tr } \{B^{*-1} E[\nu_i \nu_i]\} \rightarrow n_r \text{ (number of measurement)}$$

For this analysis, the following evaluation parameter can be used:

$$RR = \text{tr } \{B^{*-1} B_D\}/n_r$$

where

$$B_D \overset{\Delta}{=} E[\nu_i \nu_i^T]_D \text{ for the proposed suboptimal filter design}$$

$$RR \overset{\Delta}{=} \text{residual response ratio}$$

It should be noted that if $B_D = B^*$, i.e., the optimum filter itself, then

$$RR = 1$$

The closeness or "goodness" of a given filter design can be evaluated with this parameter relative to other suboptimal designs.

<u>Residual Correlation</u>--The optimum design produces a "white" residual, i.e.,

$$E[\nu_i \nu_j^T] = B^* \text{ for } i = j$$
$$= 0 \text{ for } i \neq j$$

Given an arbitrary filter gain, K, used with the following filter:

$$\hat{x} = \bar{x}_i + K(y - C \bar{x}_i)$$

$$\bar{x}_{i+1} = A \hat{x}_i + B u_i$$

and assuming that A, C, and $D_2^\dagger$ are identical to actual plant process, the correlation becomes

$$E[\nu_{i+1} \nu_i^T] = CA[MC^T - K(CMC^T + D_2 Q D_2^T)]$$

---

†Filter assumed stable.

88

where

$$M \stackrel{\Delta}{=} E[(\bar{x}_i - x_i)(\bar{x}_i - x_i)^T]$$

$$Q \stackrel{\Delta}{=} \text{diagonal matrix containing process and measurement noise variances}$$

For $K = K^*$ (optimum),

$$E(\nu_{i+1} \nu_i^T) = 0$$

It is hypothesized that ν_i is an n_r^{th} order Markov process

$$\nu_{i+1} = \Phi \nu_i + \pi_i$$

where

$$\Phi \stackrel{\Delta}{=} \text{correlation transfer matrix } (n_r \times n_r)$$

$$\pi_i \stackrel{\Delta}{=} \text{white noise driving term}$$

Then

$$E[\nu_{i+1} \nu_i^T] = \Phi E[\nu_i \nu_i^T] + E[\pi_i \nu_i]$$

Therefore,

$$\Phi = E[\nu_i \nu_i^T]^{-1} E[\nu_{i+1} \nu_i^T]$$

$$= [CMC^T + D_2 Q D_2^T]^{-1} CA[MC^T - K(CMC^T + D_2 Q D_2^T)]$$

The eigenvalues of Φ provide useful information about the correlation of a given residual set.

The ith eigenvalue in continuous form is

$$\lambda_i^c = (-1/\Delta T) Ln[\lambda_i^D(\Phi)] \qquad i = 1, 2, \ldots, n_r$$

where

$\lambda_i^D(\Phi)$ is the corresponding i^{th} discrete eigenvalue of Φ

ΔT is the sample rate

89

λ_i^c is the equivalent continuous system eigenvalue

The goal is to achieve white residuals or

$$\text{all } \lambda_i^c\text{'s} \to \infty$$

As the eigenvalues, λ_i^c's, move closer to the origin, the process is more correlated. In any case, an eigenvalue which indicates that the correlation occurs within the plant band-width (i.e., $\lambda_i^c > -10$ rad/sec) would be unacceptable.

These two evaluation criteria indicate the ability of a suboptimal filter design to perform relative to the real optimum case. The development allows analysis for an arbitrary K; however, a more general case also includes a completely arbitrary plant description. Figure 29 outlines the equivalent procedure for an arbitrary filter.

The application of this parameter sensitivity analysis has the following limitations:

- It is theoretically applicable only to discrete plant changes, i.e., a linear filter applied to a linear plant. Dynamic pressure variations are assumed low enough in frequency to be valid for such analysis. A more general nonlinearity would not be valid.

- Postulating a stochastic control input, u_i, is necessary for evaluating the effect of mismatches between scheduled and actual control effectiveness, i.e., ΔB_1 and ΔD_1. An approach might be to model the human operator as a correlated noise input, but this would not account for feedback control. In any case, this analysis is really not convenient for such a determination.

4.3.10 Gain Scheduling the A-7

The use of acceleration equations in Concept II (for n_y fault detection) and Concept III require that the implications of scheduling gains and aerodynamic coefficients be examined. The approach taken here was to use linear analysis techniques described in the previous subsection for the lateral-directional fault tolerant design.

For ease of understanding, the state space equations of motion are given in continuous time representation. These are shown in Figure 30.

90

Plant	Filter
$x_{i+1} = Ax_i + B_1 u_i + B_2 \omega_i \,(\text{order } n_x)$	$\bar{x}_{i+1} = A_F \hat{x}_i + B_{1F} u_i$
$y_i = Cx_i + D_1 u_i + D_2 \omega_i \,(\text{order } n_r)$	$\hat{x}_i = \bar{x}_i + K(y_i - C_F \bar{x}_i - D_{1F} u_i)$
$E[\omega_i \omega_j] = Q \delta_{ij}$	

Let

$$z_i^T = (x_i^T, \ e_i^T) \,(\text{order } 2n_x) \text{ where } e_i = \bar{x}_i - x_i$$

$$z_{i+1} = A_T z_i + B_{T1} u_i + B_{T2} \omega_i$$

$$\Delta A = A - A_F$$
$$\Delta B_1 = B_1 - B_{1F}$$
$$\Delta C = C - C_F$$
$$\Delta D_1 = D_1 - D_{1F}$$

and

$$\nu_i = C_T z_i + D_{1T} u_i + D_{2T} \omega_i$$

Then

$$A_T = \begin{bmatrix} A & 0 \\ A_F K \Delta C - \Delta A & A_F(I - KC_F) \end{bmatrix}$$

$$B_{1T} = \begin{bmatrix} B_1 \\ A_F K \Delta D_1 - \Delta B_1 \end{bmatrix} \quad ; \quad B_{2T} = \begin{bmatrix} B_2 \\ A_F K D_2 - B_2 \end{bmatrix}$$

$$C_T = \begin{bmatrix} \Delta C , & -C_F \end{bmatrix} \quad ; \quad D_{1T} = \Delta D_1 \quad ; \quad D_{2T} = D_2$$

Therefore if

$$Z = E[z_i z_i^T]$$

then

$$R_T = E[\nu_i \nu_i^T] = C_T Z C_T^T + D_{2T} Q D_{2T}^T$$

$$E[\nu_{i+1} \nu_i^T] = C_T A_T Z C_T^T + C_T B_{2T} Q D_{2T}^T$$

$$\text{and } \Phi_T = R_T^{-1} E[\nu_{i+1} \nu_i^T]$$

Figure 29. Estimation Filter Performance

91

Open-Loop System

$$\dot{x} = Fx + G_1 u + G_2 \eta$$
$$y = Hx + E_1 u + E_2 \eta$$

where

$$x^T = (\beta, p, r, \phi, \beta_g)$$
$$y^T = (n_{y_m}, p_m, r_m, \phi_m)$$
$$u^T = (\delta_r, \delta_a)$$

$$\eta = \begin{bmatrix} \eta_g ; \text{gust driver} \sim N(0, 1) \text{ white} \\ \eta_{n_y} ; n_y \text{ measurement noise} \sim N(0, 1.0 \text{ ft/sec}^2) \text{ white} \\ \eta_p ; p \text{ measurement noise} \sim N(0, 0.0192 \text{ rad/sec}) \text{ white} \\ \eta_r ; r \text{ measurement noise} \sim N(0, 0.00698 \text{ rad/sec}) \text{ white} \\ \eta_\phi ; \phi \text{ measurement noise} \sim N(0, 0.00436 \text{ rad}) \text{ white} \end{bmatrix}$$

Matrix Definitions

$$F \triangleq \begin{bmatrix} \dfrac{Y_\beta}{V_o}, & \dfrac{Y_p}{V_o}, & \dfrac{Y_r}{V_o} - 1.0, & \dfrac{-g}{V_o}, & \dfrac{Y_\beta}{V_o} \\ L'_\beta, & L'_p, & L'_r, & 0, & L'_\beta \\ N'_\beta, & N'_p, & N'_r, & 0, & N'_\beta \\ 0 & 1 & 0 & 0 & 0 \\ 0 & 0 & 0 & 0 & -a_g \end{bmatrix} ; \quad G_1 \triangleq \begin{bmatrix} \dfrac{Y_{\delta r}}{V_o}, & \dfrac{Y_{\delta a}}{V_o} \\ L'_{\delta r}, & L'_{\delta a} \\ N'_{\delta r}, & N'_{\delta a} \\ 0 & 0 \\ 0 & 0 \end{bmatrix}$$

$$G_2 \triangleq \begin{bmatrix} 0 & 0 & 0 & 0 & 0 \\ 0 & 0 & 0 & 0 & 0 \\ 0 & 0 & 0 & 0 & 0 \\ 0 & 0 & 0 & 0 & 0 \\ \sigma_g \sqrt{\dfrac{2}{a_g}} & 0 & 0 & 0 & 0 \end{bmatrix} ; \quad H \triangleq \begin{bmatrix} Y_\beta & Y_p & Y_r & 0 & Y_\beta \\ 0 & 1 & 0 & 0 & 0 \\ 0 & 0 & 1 & 0 & 0 \\ 0 & 0 & 0 & 1 & 0 \end{bmatrix}$$

$$E_1 \triangleq \begin{bmatrix} Y_{\delta r}, & Y_{\delta a} \\ 0 & 0 \\ 0 & 0 \\ 0 & 0 \end{bmatrix} \qquad E_2 \triangleq \begin{bmatrix} 0 & 1 & 0 & 0 & 0 \\ 0 & 0 & 1 & 0 & 0 \\ 0 & 0 & 0 & 1 & 0 \\ 0 & 0 & 0 & 0 & 1 \end{bmatrix}$$

Figure 30. Preliminary Lateral-Directional Model

Eleven flight conditions were chosen for design/analysis.   These are summarized in
Table 20.

TABLE 20.   ELEVEN CHOSEN FLIGHT CONDITIONS FOR GAIN SCHEDULING

FC	Mach	Altitude (ft)	Dynamic Pressure (lb/ft^2)	Angle-of -Attack (deg)	Airspeed (ft/sec)	Gross Weight (lb)
1	0.3	0	133.3	9.28	355.1	25,338
2	0.6	0	533.2	3.26	670.2	"
3	0.9	0	1199.8	2.20	1005.2	"
4	0.4	15,000	133.7	8.45	423.2	"
5	0.6	15,000	300.9	4.36	634.8	"
6	0.9	15,000	677.0	2.75	952.2	"
7	1.1	15,000	1011.3	2.90	1163.8	"
8	0.6	35,000	125.5	8.60	583.9	"
9	0.9	35,000	282.4	4.13	876.0	"
10	0.227	0	76.3	10.10	253.6	29,240
11	0.227	0	76.3	5.36	253.6	20,350

Preliminary results using this model showed that there was great difficulty maintaining
stability in the filter despite extensive gain scheduling (i.e., all aerodynamic coefficients
and filter gains).   This is due to the presence of the Spiral Root near the origin in all
11 open-loop models.   The closed-loop design for each condition maintained a root near
the origin (rationalized as a high pass on ϕ_m), and subsequent gain scheduling produced
unstable filters for many flight conditions.

The solution to this problem was to remove the roll angle, ϕ, from the measurement
set and use it as an input instead.   This not only removes the Spiral Root from the
model but also has the following benefits:

93

- The order reduction is always a worthwhile computational goal.

- Roll angle is a good candidate because its dynamics are separated in frequency from the dominant system roots, i.e., they have much lower root.

- The roll angle measurement has lower measurement noise; therefore, it does not cause deterioration of the Kalman filter performances.

- As will be demonstrated, gain scheduling can be greatly simplified without substantial performance penalties.

The filter can now be based on the model shown in Figure 31.

Design results were obtained for a number of gain-scheduling schemes. These schemes represent a hierarchy of schedules ranging from exact gain and plant model reconstruction (impossible from a practical standpoint) to a constant parameter, i.e., gain and model of the filter (the simplest possible). Results are presented in Table 21. Residual ratio data in Table 21 are presented in Figure 32. The trend lines demonstrate the performance degradation at the extremes of the conditions. Interpretations of the results are as follows:

- The Kalman gain, K, can be fixed at some mean flight condition. (Flight Condition #2 is used here.)

- A full model gain schedule produces consistent results across the range of dynamic pressure.

- Scheduling only the input matrix, C_F, demonstrates some performance degradation but it may be adequate for fault detection and estimation.

- A constant gain system (FC #2's optimal design in this case) demonstrates unacceptable performance at the $\bar{q}$ extremes. Figure 32 shows this for the residual response ratio and Table 2 shows residual correlation roots within the bandwidth of the aircraft system. This is likewise unacceptable since the filter residual should appear "white" to the system dynamics; that is, the correlation bandwidth should be higher than the system.

- None of the above designs include the effects of gain scheduling the input dynamics, i.e., δ_r, δ_a, or ϕ_m. This would have to be checked out in simulation since no reasonable method for including their effects was determined in the linear analysis.

94

Open-Loop System

$$\dot{x} = Fx + G_1 u + G_2 \eta$$
$$y = Hx + E_1 u + E_2 \eta$$

where

$$x^T = (\beta, \ p, \ r, \ \beta_g)$$
$$y^T = (n_y, \ p_m, \ r_m)$$
$$u^T = (\delta_r, \ \delta_a, \ \phi_m)$$
$$\eta^T = (\eta_g, \ \eta_{n_y}, \ \eta_p, \ \eta_r, \ \eta_\phi)$$

Matrix Definitions

$$F \triangleq \begin{bmatrix} \dfrac{Y_\beta}{V_o}, & \dfrac{Y_p}{V_o}, & \dfrac{Y_r}{V_o} - 1.0, & \dfrac{Y_\beta}{V_o} \\[2mm] L'_\beta, & L'_p, & L'_r, & L'_\beta \\[2mm] N'_\beta, & N'_p, & N'_r, & N'_\beta \\[2mm] 0 & 0 & 0 & -a_g \end{bmatrix} ; \quad G_1 \triangleq \begin{bmatrix} \dfrac{Y_{\delta_r}}{V_o}, & \dfrac{Y_{\delta_a}}{V_o}, & \dfrac{-g}{V_o} \\[2mm] L'_{\delta_r}, & L'_{\delta_a}, & 0 \\[2mm] N'_{\delta_r}, & N'_{\delta_a}, & 0 \\[2mm] 0 & 0 & 0 \end{bmatrix}$$

$$G_2 \triangleq \begin{bmatrix} 0 & 0 & 0 & 0 & \dfrac{g}{V_o} \\[2mm] 0 & 0 & 0 & 0 & 0 \\[2mm] 0 & 0 & 0 & 0 & 0 \\[2mm] \sigma_g \sqrt{\dfrac{2}{a_g}} & 0 & 0 & 0 & 0 \end{bmatrix}$$

$$H \triangleq \begin{bmatrix} Y_\beta, & Y_p, & Y_r, & Y_\beta \\ 0 & 1 & 0 & 0 \\ 0 & 0 & 1 & 0 \end{bmatrix} ; \quad E_1 \triangleq \begin{bmatrix} Y_{\delta_r}, & Y_{\delta_a} & 0 \\ 0 & 0 & 0 \\ 0 & 0 & 0 \end{bmatrix}$$

$$E_2 \triangleq \begin{bmatrix} 0 & 1 & 0 & 0 & 0 \\ 0 & 0 & 1 & 0 & 0 \\ 0 & 0 & 0 & 1 & 0 \end{bmatrix}$$

Figure 31. Final Lateral-Directional Filter Design Plant

TABLE 21. GAIN SCHEDULING PERFORMANCE COMPARISONS*

FC	K Constant; A, C Exact		K Constant; A, C Gain Scheduled		A, K Constant; C Gain Scheduled		A, C, K Constant	
	RR	Max λ^c	RR	Max λ^c	RR	Max λ^c	RR	Max λ^c
1	1.0396	-35.92	1.1795	-62.34	1.3333	-45.79	1.7402	-12.62
2	1.000	-∞	1.2156	-62.95	1.0175	-69.58	1.000	-∞
3	1.0332	-27.36	1.0567	-39.01	1.5911	-57.34	1.9469	-25.96
4	1.0174	-65.08	1.1689	-65.27	1.2556	-76.44	1.4854	-20.77
5	1.0138	-60.08	1.1995	-51.63	1.1462	-53.97	1.1526	-63.18
6	1.0348	-30.98	1.0429	-35.77	1.0810	-40.55	1.1022	-58.05
7	1.0894	-20.57	1.1237	-27.25	1.3849	-37.22	1.5449	-46.87
8	1.0220	-64.44	1.625	-62.75	1.5372	-66.30	1.6159	-19.02
9	1.0235	-46.54	1.0430	-49.14	1.0649	-41.09	1.0745	-50.77
10	1.0886	-27.26	1.1923	-45.61	1.7245	-30.37	2.7536	-6.30
11	1.0283	-37.97	1.4547	-24.65	1.8453	-16.78	2.3675	-6.12

*Constant values were obtained from optimum design at Flight Condition #2.
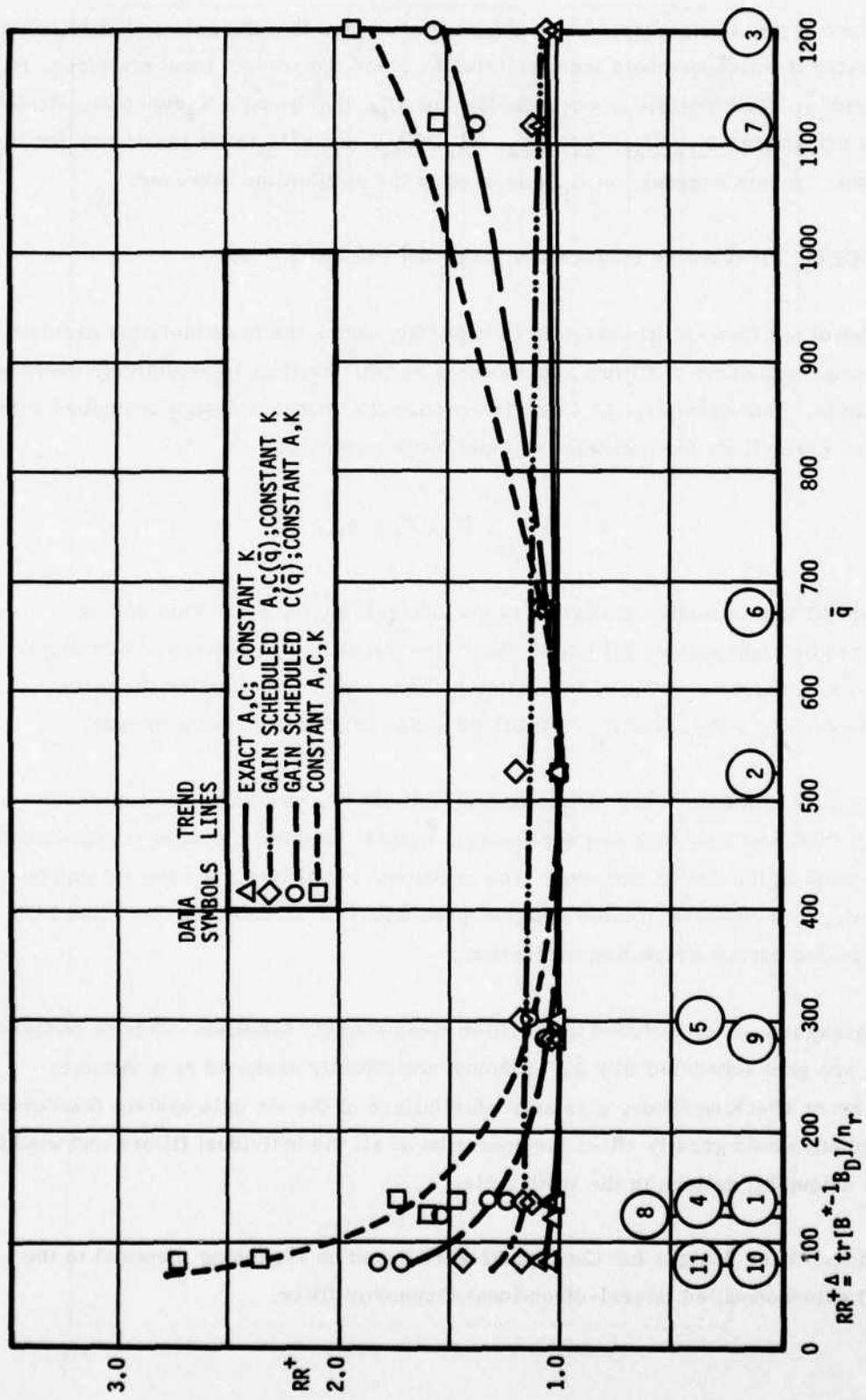
Figure 32. A-7D Lateral-Directional Axes Filter Gain Schedules

97

The net effect of this design exercise is a recommendation that the gain schedule consist of only varying the measurement input matrix, C_F, and the control input matrices, B_{IF} and D_{IF}, with $\bar{q}$. This results in one schedule for C_F, that being a Y_β function. Also, a total of six schedules--Y_{δ_r}/U_o, L'_{δ_r}, L'_{δ_a}, N'_{δ_r}, N'_{δ_a}, and g/U_o--are necessary for the control input. A gain schedule on A_F was used in the simulation, however.

4.4   CONCEPT III--FAULT ISOLATION KALMAN FILTERS

The purpose of the Concept III design is to explicitly attack the fault isolation problem by increasing the number of filters and choosing sensor families to selectively exclude measurements. For example, the lateral-directional Concept II design described earlier will produce error flags for a number of input measurements:

$$y^T = (n_{y_m}, \ P_m, \ R_m, \ \phi_m, \ \bar{q})$$

For Concept III this is modified slightly to exclude roll angle, ϕ_m. This can be accomplished by high-passing all inputs above the Spiral Root frequency. Working in conjunction with two other filters, this filter provides fault isolation for the three measurements, n_{y_m}, P_m, and R_m. Table 22 shows this in truth table format.

The longitudinal axis filters are also included in Table 22, yielding a total of seven filters. Of this total only four are necessary. LON #1 is shown because it represents a starting point in the design process. The additional two filters, one lateral and one longitudinal, were added to provide a higher probability of success. L-D #3 and LON #3 were eliminated during simulation evaluation.

Dynamic pressure, $\bar{q}$, is included in all filter measurement families. This is because all filters are gain scheduled with $\bar{q}$. Although not directly designed as a dynamic pressure error checking filter, a catastrophic failure of the air data system (hardover or zero output) would greatly affect the operation of all the individual filters and would produce a unique bit pattern in the truth table.

The individual filter designs for Concept III were based on reasoning identical to the Concept II gain-scheduled lateral-directional diagnostic filter.

TABLE 22. CONCEPT III CANDIDATE DIAGNOSTIC FILTERS
FOR SUPER-DIAGNOSTIC FILTER CONSTRUCTION

Measurements/Flags Filter	a_{y_m}	P_m	R_m	n_{z_m}	Q_m	α_m	$\bar{q}$
L-D #1	1	1					1
L-D #2	1		1				1
L-D #3		1	1				1
LON #1*				1	1	1	1
LON #2				1	1		1
LON #3				1		1	1
LON #4					1	1	1

*Designed as a starting point for other designs and is not a candidate for
Concept III.

4.4.1 Lateral-Directional Filters

Four filters have been designed using lateral-directional acceleration and moment
equations. The roll angle input into the equations is removed by high-passing the input
signals and controls above the Spiral Root frequency. In design, this eliminates the
roll angle measurement noise from the set of driving noise sources shown in Figure 31.
Roll angle measurement noise only minutely affected the total estimation error and
residual RMS values.

Figures 33, 34, and 35 present results from the design of these reduced measurement
filters. Unlike the Concept II design, it seems likely that a gain-scheduled plant matrix,
$A(\bar{q})$, will be necessary to insure filter performance across the $\bar{q}$ range.

The optimal gain matrices ($K^{*'}$s) proved to be quite close to the Concept II gain values.
This will reduce the on-board core which is necessary to perform the calculations by
eliminating new gain values for each filter. Note that only two filters are necessary for
fault isolation (L-D #3 was eventually eliminated during simulation evaluation).
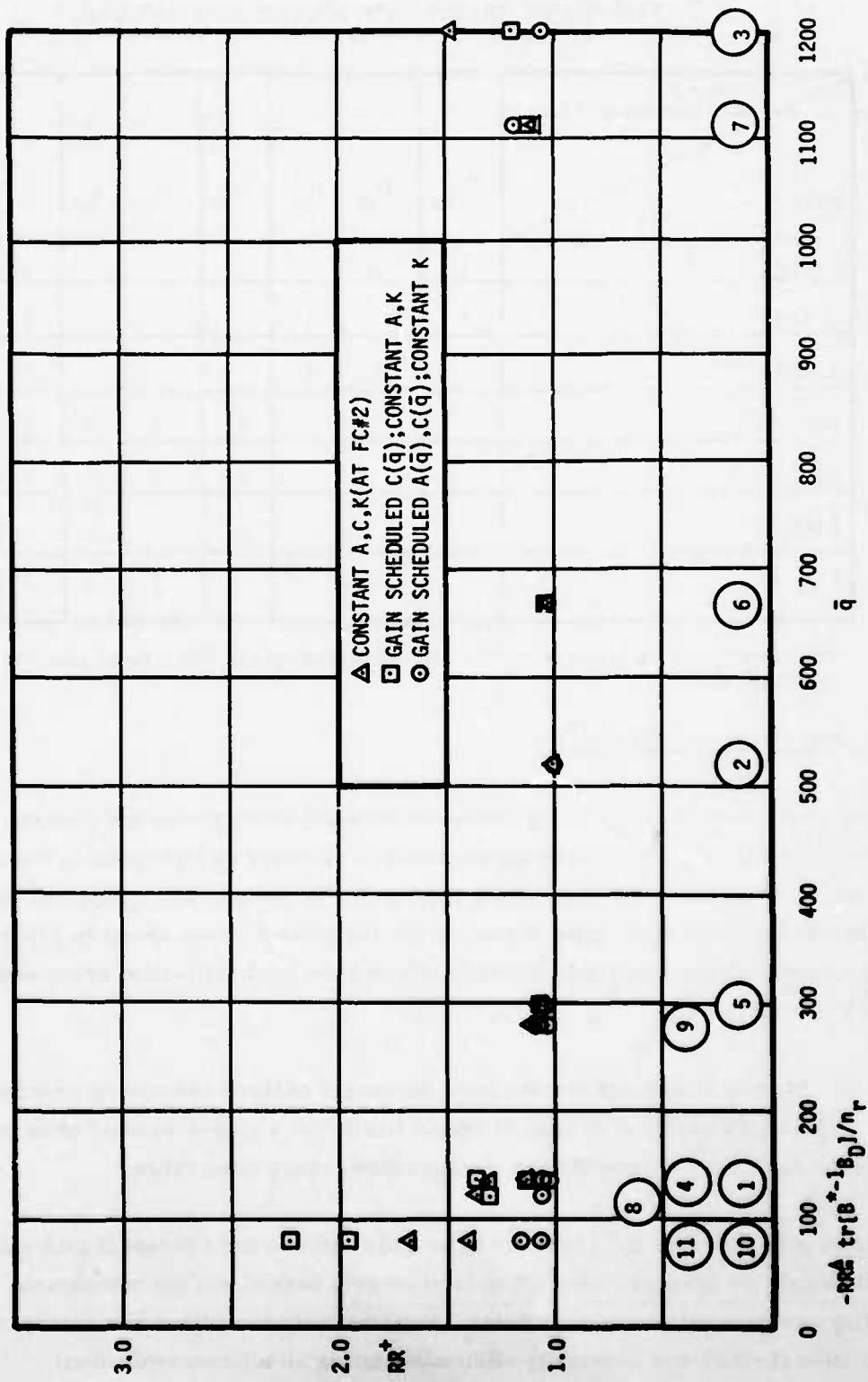
Figure 33. Diagnostic Filter for n_y, P, $\bar{q}$ (L-D #1)

△ CONSTANT A,C,K(AT FC#2)
▣ GAIN SCHEDULED C($\bar{q}$);CONSTANT A,K
⊙ GAIN SCHEDULED A($\bar{q}$),C($\bar{q}$);CONSTANT K

100
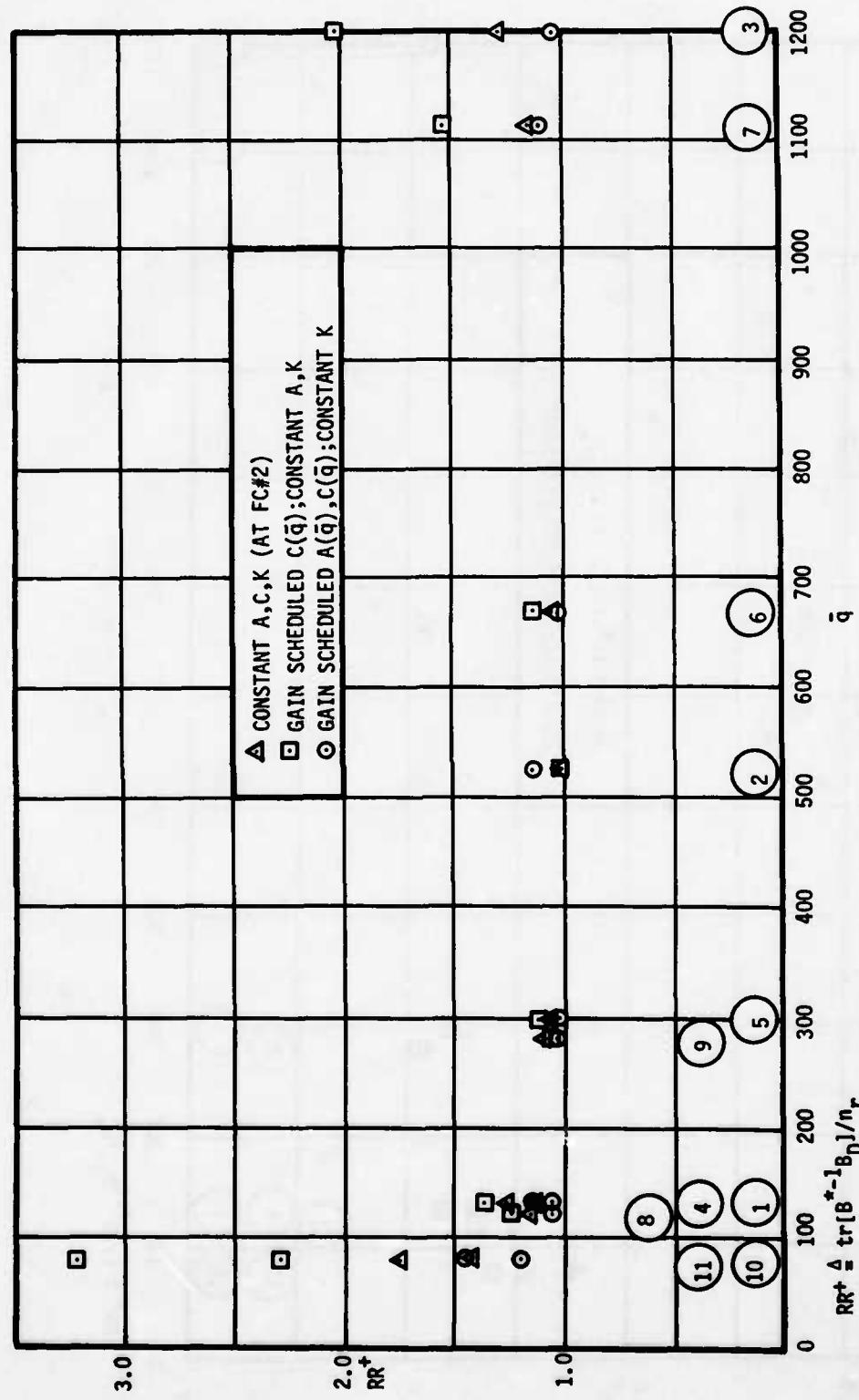
Figure 34. Diagnostic Filter for n_y, r, $\bar{q}$ (L-D #2)

101
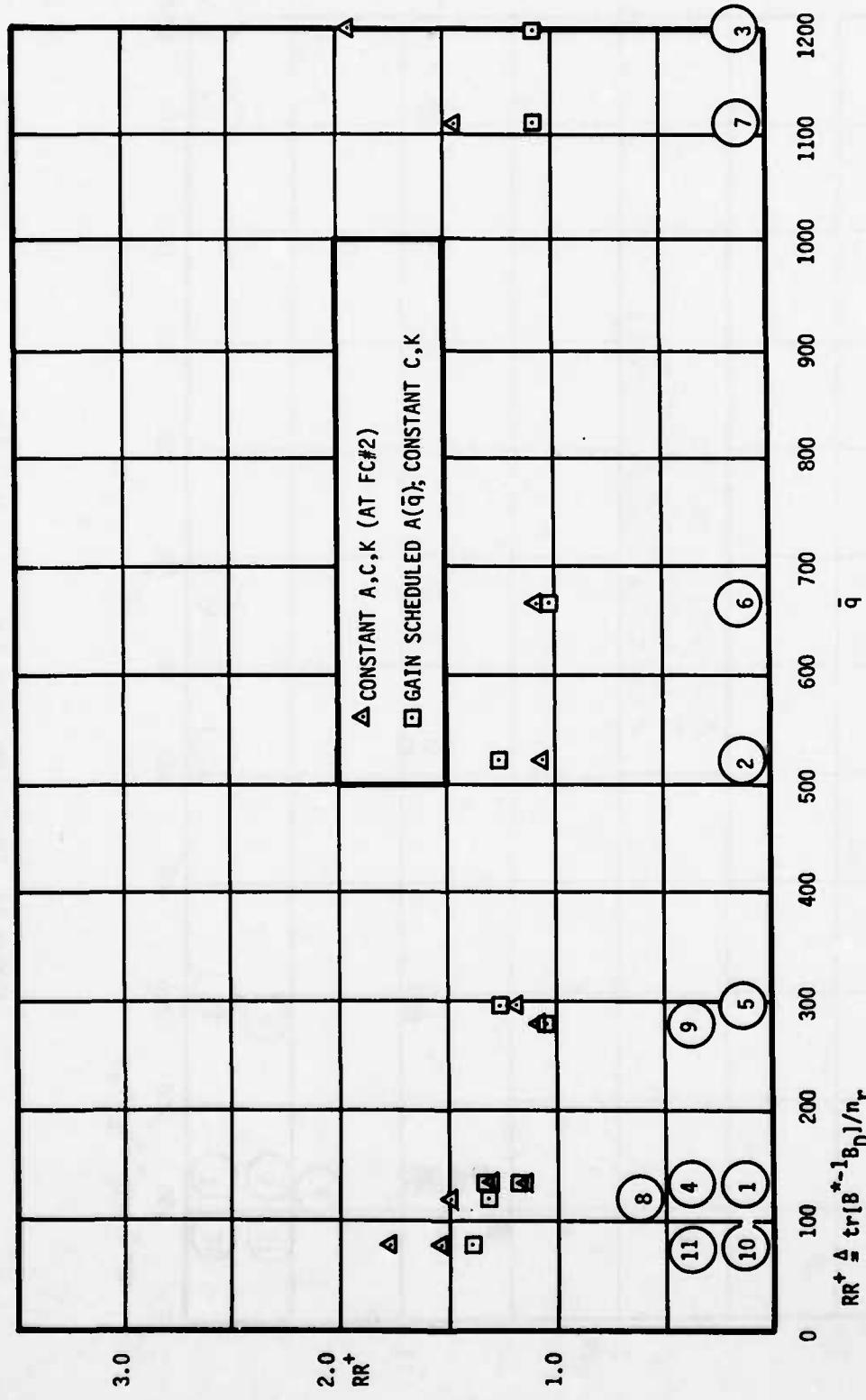
Figure 35. Diagnostic Filter for P, r, and $\bar{q}$ (L-D #3)

102

4.4.2 Longitudinal Axis Filters

Figure 36 shows the continuous representation of the A-7D pitch axis design model used for the Concept III designs. Phugoid oscillations and trim are eliminated by high-passing all measurements and control inputs.

Again, the constant gain, K, for Flight Condition #2 proved to be the best. Attempts were made to gain-schedule K over the flight envelope, but plots of gain values versus dynamic pressure produced extremely confusing gain patterns. A gain schedule for K would at best be highly complex functions that would not produce significantly better performance commensurate with this extra complexity.

Figures 37, 38, and 39 display residual ratio performance of these filters.

Some additional observations are the following:

1. The landing approach (FC #11) design evaluations produced poor residual ratio responses in some cases. These also demonstrated poor correlation properties (not shown).

   A redesign of the gains for landing approach is probably indicated; however, it is of interest to see how effectively this design procedure indicates good or bad performance in simulation. A gain change for landing approach can easily be implemented. For example, this can be done along with landing gear deployment.

2. The extra longitudinal filter, i.e., LON #3 for n_z and α, was eliminated. Repeated attempts to make this filter behave properly across the flight envelope produced instabilities at one point or another.

3. Figure 39 results show an interesting trade-off. The landing approach filter performance is poor when the filter is designed assuming the actual expected measurement noise values. This is due to the fact that stability is low for this condition. By increasing the measurement noise RMS in the design, parameter sensivity is decreased due to better filter pole placement (i.e., a pole near the origin was moved to a more stable position).

103

Open-Loop Systems

$$\dot{x} = Fx + G_1 u + G_2 \eta$$
$$y = Hx + E_1 u + E_2 \eta$$

where

$$x^T = (\alpha, q, \alpha_g)$$
$$y^T = (n_{z_m}, q_m, \alpha_{T_m})$$
$$u = (\delta_e)$$

$$\eta = \begin{bmatrix} \eta_g; \text{ gust driver} \sim N(0, 1) \text{ white} \\ \eta_{n_z}; \eta_{z_m} \text{ measurement noise} \sim N(0, 1.0 \text{ ft/sec})^2 \text{ white} \\ \eta_q; q_m \text{ measurement noise} \sim N(0, 6.98 \times 10^{-3} \text{ rad/sec}) \text{ white} \\ \eta_\alpha; \alpha_m \text{ measurement noise} \sim N(0, 1.309 \times 10^{-3} \text{ rad}) \text{ white} \end{bmatrix}$$

Matrix Definitions

$$F \triangleq \begin{bmatrix} \dfrac{Z_\alpha}{V_o}, & \dfrac{Z_q}{V_o}+1.0, & \dfrac{Z_\alpha}{V_o} \\ M'_\alpha, & M'_q, & M'_\alpha \\ 0, & 0, & -a_g \end{bmatrix}; \qquad G_1 \triangleq \begin{bmatrix} \dfrac{Z_{\delta e}}{V_o} \\ M'_{\delta e} \\ 0 \end{bmatrix}$$

$$G_2 \triangleq \begin{bmatrix} 0 & 0 & 0 & 0 \\ 0 & 0 & 0 & 0 \\ \sigma_g\sqrt{\dfrac{2}{a_g}} & 0 & 0 & 0 \end{bmatrix}; \qquad H \triangleq \begin{bmatrix} Z_{\alpha'}, & Z_{q'}, & Z_\alpha \\ 0 & 1 & 0 \\ 1 & 0 & 1 \end{bmatrix}$$

$$E_1 \triangleq \begin{bmatrix} Z_{\delta_e} \\ 0 \\ 0 \end{bmatrix}; \qquad E_2 \triangleq \begin{bmatrix} 0 & 1 & 0 & 0 \\ 0 & 0 & 1 & 0 \\ 0 & 0 & 0 & 1 \end{bmatrix}$$

Figure 36. Longitudinal Axis (Short Period) Model

104
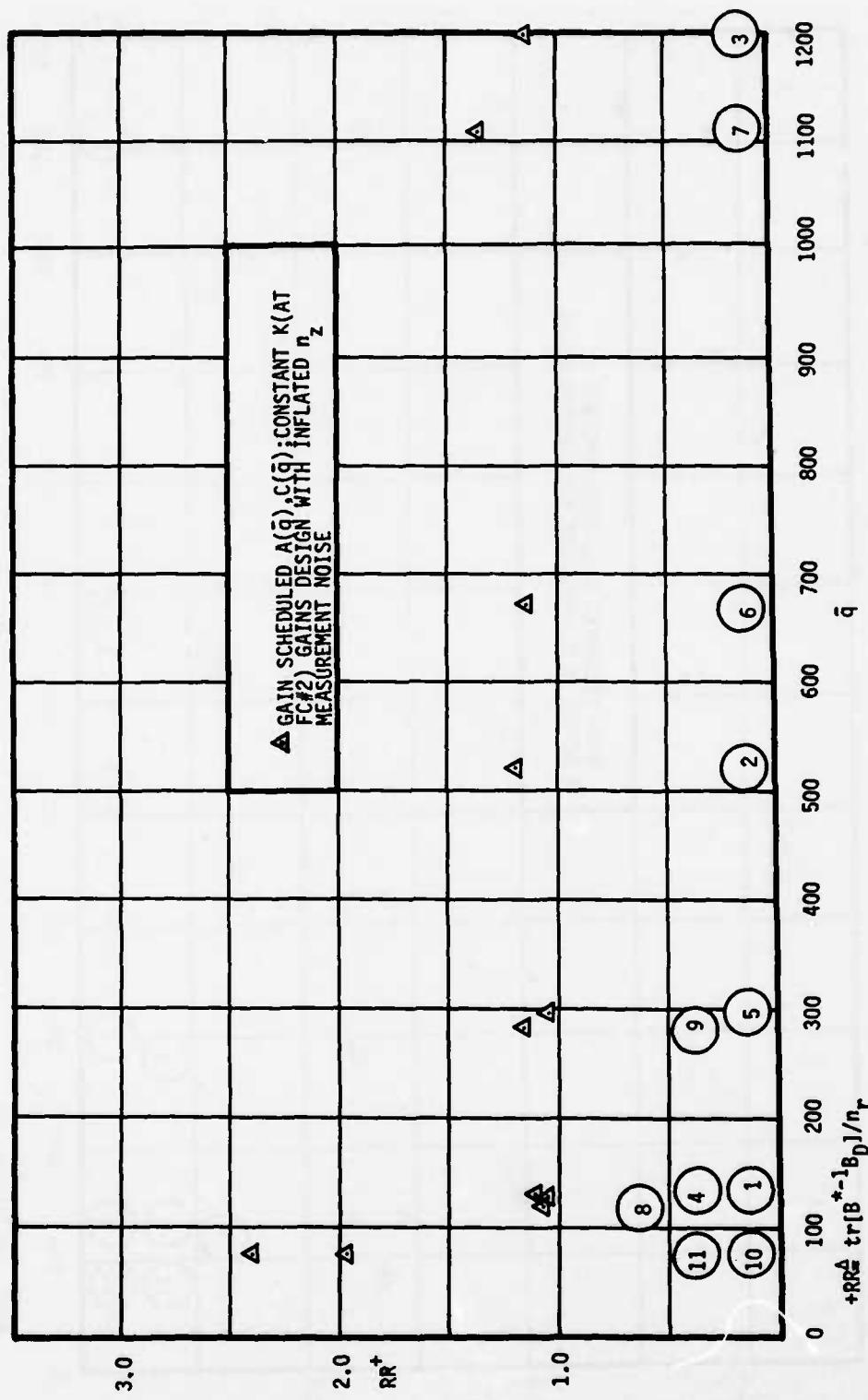
Figure 37. Diagnostic Filter for n_z, q, α, $\bar{q}$ (LON #1)

105
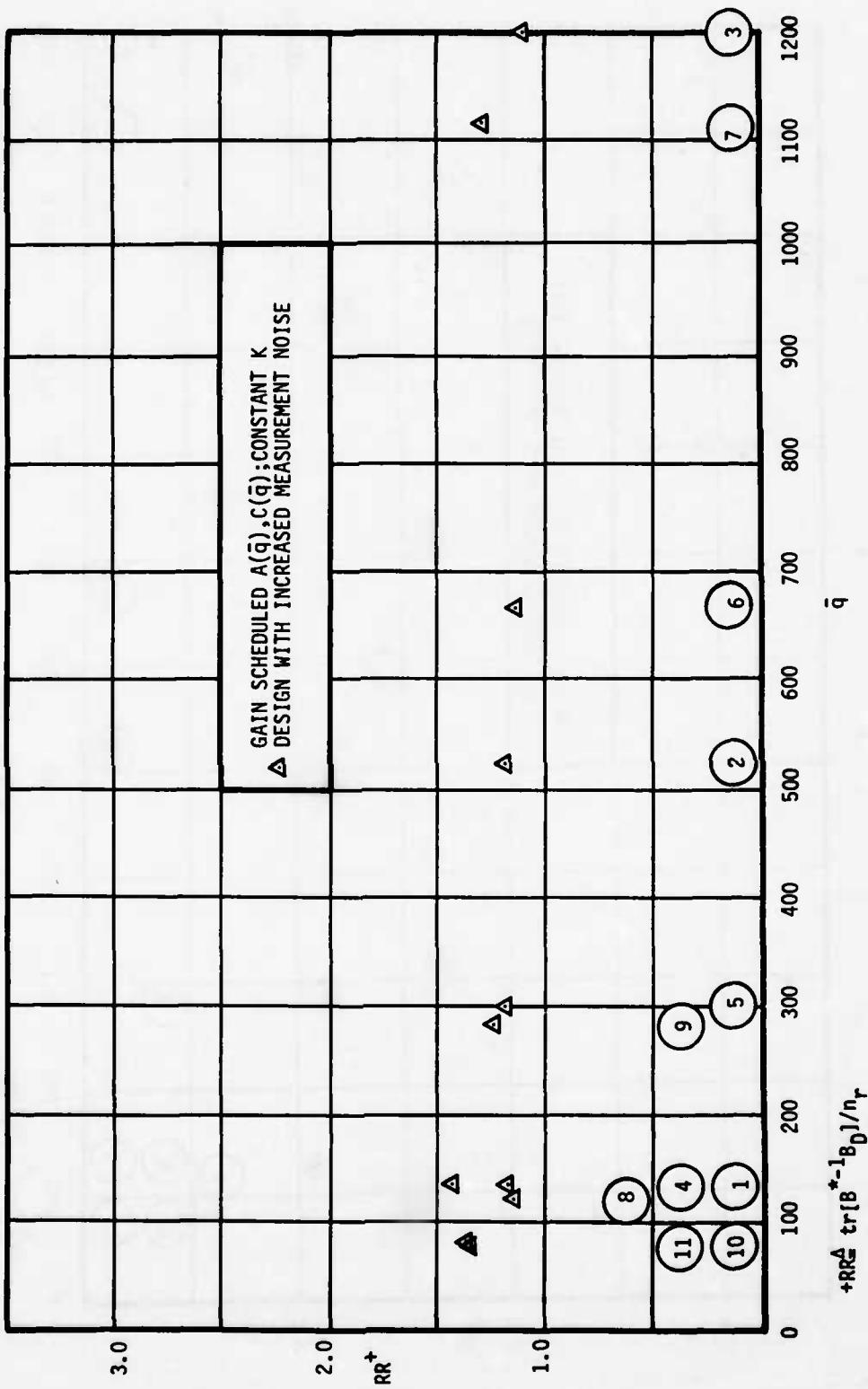
Figure 38. Diagnostic Filter for n_z, q, $\bar{q}$ (LON #2)
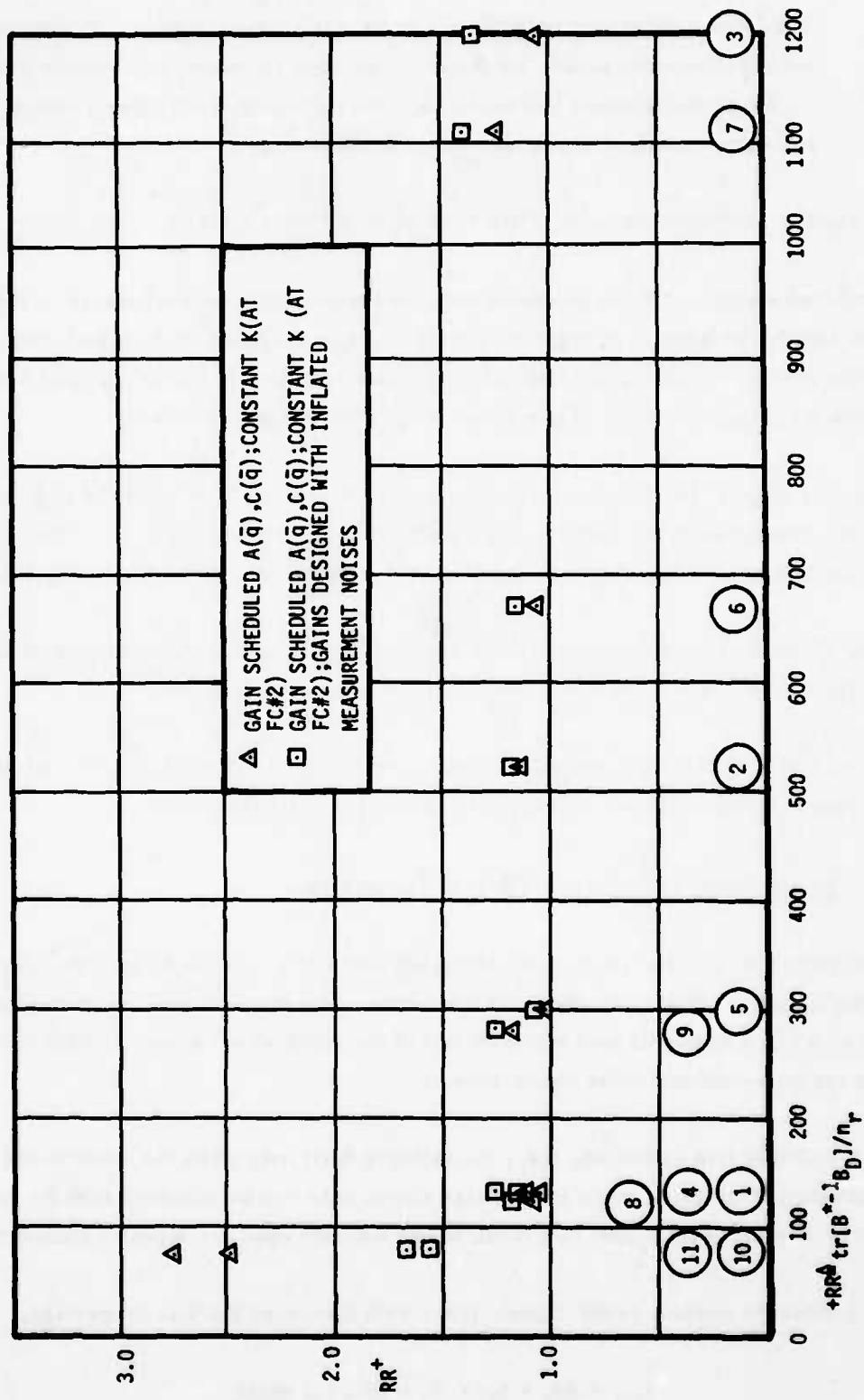
Figure 39. Diagnostic Filter for q, α, q̄ (LON #4)

107

This idea also makes intuitive sense for fault identification. By increasing the measurement noise, the filter relies less on the measurements and more on the process model to reconstruct the signal, thus ensuring a longer, more pronounced failure transient when a fault occurs.

4.5 FAULT DETECTION MONITORS FOR CONCEPTS II AND III

Design considerations for various monitors used with analytical redundancy schemes require careful attention. It might be said that, once the filter is designed, then half the battle is won. Design goals are accurate fault detection in minimum time after fault with an acceptable false alarm rate (one per 1000 flight hours).

Two basic categories of monitors are examined. First, a set of limits is chosen, based on assumed unfailed statistical properties, i.e., means and RMS. The impact of error signal autocorrection is examined since it affects delayed fault declarations.

Second, sequential likelihood ratio tests are designed for mean value testing of analytical redundancy error signal and differences in likelihood functions.

The choice of a monitor for analytical redundancy schemes is critical to the ultimate performance of any scheme. Various monitor ideas are being tried.

4.5.1 Error Signal Monitor with Delayed Declaration

The simplest test one can apply to an error signal is to check its magnitude against predefined limits. Figure 40 shows this scheme. The monitor level magnitude is placed at a value specified as a multiple (m) of the unfailed error signal RMS (σ). m is chosen for an acceptable false alarm rate.

Using a multiple trip criterion, i.e., declaring a fault only when the limit is exceeded "n" consecutive times, a much lower false alarm rate can be achieved than by using a first trip monitor level. Just how much lower depends upon the signal's autocorrelation.

Given a discrete random error signal, i.e., with Gaussian Markov properties,

$$e_{i+1} = Ae_i + \eta_i \quad : \quad \eta_i \sim N(0, \sigma_\eta) \text{ white} \tag{36}$$
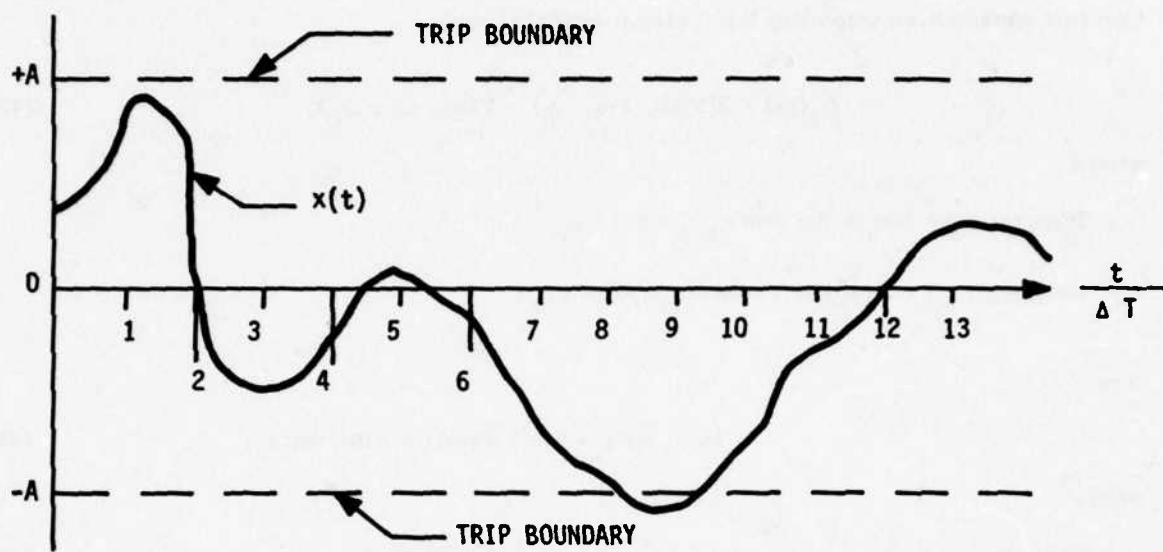
Figure 40. Trip Boundaries for Error Signals

$$E[e_{i+1}^2] = E[e_i^2] = \sigma_e^2 \tag{37}$$

$$E[e_{i+1}e_i] = A\sigma_e^2 \tag{38}$$

The correlation coefficient between ρ_c, e_i, and e_{i+1} is therefore

$$\rho_c = A \tag{39}$$

The probability that an unfailed error signal will exceed a level $m\sigma$ (indicating a false alarm) is

$$P(m) = P(e_i > m\sigma \text{ or } e_i < -m\sigma) = 2[1 - \Phi(m)] \tag{40}$$

where

$$\Phi(m) = \frac{1}{\sqrt{2\pi}} \int_{-\infty}^{m} \exp(-z^2/2)\,dz \tag{41}$$

and z is a dummy variable.

109

For two consecutive trips the false alarm probability is

$$P_2(m) = 2[P(m, +m; \rho_c) + P(m, -m; \rho_c)] \tag{42}$$

where

$$P(m, m; \rho_c) = P(e_i > m\sigma \text{ and } e_{i+1} > m\sigma : \rho_c)^*$$

$$P(m, -m; \rho_c) = P(e_i > m\sigma \text{ and } e_{i+1} < -m\sigma : \rho_c)$$

Now

$$P(m, m; \rho_c) = 1 - 2\Phi(m) + F(m, m; \rho_c) \tag{43}$$

where

$$F(m, m; \rho_c) = \frac{1}{2\pi} \int_{-\infty}^{m} \int_{-\infty}^{m} \exp\left[-(x^2 - 2\rho_c xy + y^2)/2\right] dx\, dy \tag{44}$$

but this can be transformed (Reference 35)

$$F(m, m; \rho_c) = \Phi^2(m) + R(m, +m; \rho_c) \tag{45}$$

where

$$R(m, +m; \rho_c) = \frac{1}{2\pi} \int_{0}^{\rho_c} \exp\left[-m^2/(1 + z)\right] (1 - z^2)^{-\frac{1}{2}} dz \tag{46}$$

Likewise

$$P(m, -m; \rho_c) = 1 - 2\Phi(m) + \Phi^2(m) - R(m, -m; \rho_c) \tag{47}$$

where

$$R(m, -m; \rho_c) = \frac{1}{2\pi} \int_{0}^{\rho_c} \exp\left[-m^2/(1 - z)\right] (1 - z^2)^{-\frac{1}{2}} dz \tag{48}$$

We can finally express $P_2(m)$ in terms of $P(m)$

$$P_2(m) = P^2(m) + 2S(m; \rho_c) \tag{49}$$

where

$$S(m; \rho_c) = \frac{1}{2\pi} \int_{0}^{\rho_c} \left\{ \exp\left[-m^2/(1 - z)\right] - \exp\left[-m^2/(1 - z)\right] \right\} (1 - z^2)^{-\frac{1}{2}} dz \tag{50}$$

$^*P(x:y)$ = probability of x given y.

110

For three consecutive trips using the Markovian property,[*]

$$P_3(m) = P_2^2(m)/P(m) \qquad (51)$$

A recursive relationship exists from here on:

$$P_k(m) = P_{k-1}(m) \cdot P_2(m)/P(m) \qquad (52)$$

where k = number of consecutive trips ($k \geq 2$).

The correlation enters in the $S(m; \rho)$ term of Equation (50). This must be integrated numerically.

False alarm probabilities for various monitor levels and correlations are shown in Figure 41. Results demonstrate a deteriorating performance in the monitor for increasing correlation. The bounds on performance are:

$$P_n(m) = P(m)^n \quad \text{for } \rho_c = 0$$

and

$$P_n(m) = P(m) \quad \text{for } \rho_c = 1$$

Analytical redundancy modeling simplifications, such as neglecting nonlinearities, unavailable inputs, and wind gusts, result in increases in both RMS and correlation in the error signal during application. RMS increases can be handled by scheduling the monitor level with the maneuver variables; however, care must be taken to ensure that the monitor level is not driven further than the error during a fault.

Choosing the number of consecutive trips involves a trade-off between model error insensitivity and fault detection reaction time. Three consecutive trips are commonly used for sensor comparison monitors; however, multiple threshold levels, i.e., higher threshold levels with less delay, might prove beneficial for catching catastrophic faults such as hardovers while lower threshold levels with delay would be more sensitive to slow failures such as a bias drifting out of specification.

---

[*]$P(X_n : X_{n-1}, X_{n-2}, \ldots, X_1) = P(X_n : X_{n-1})$

111
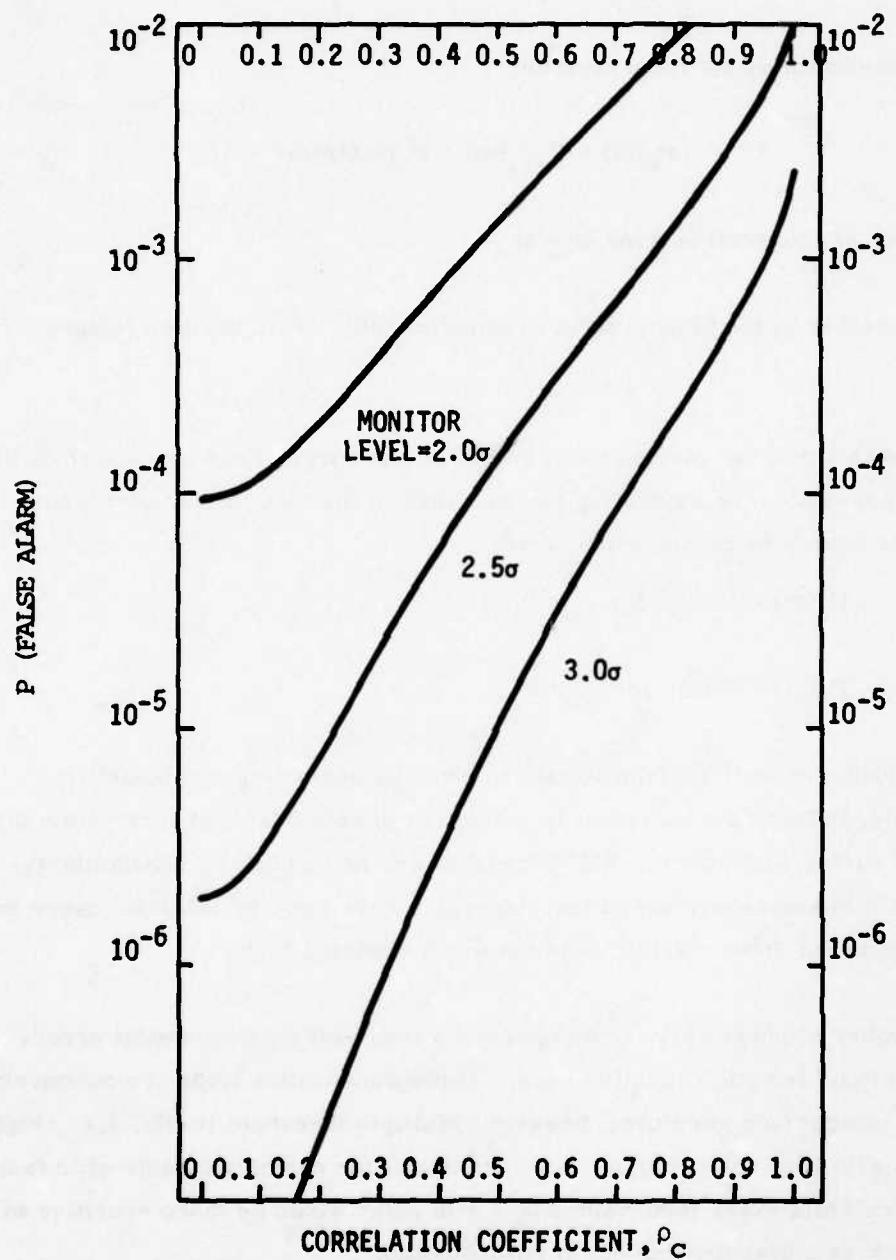
Figure 41. Monitor False Alarm Probabilities

112

Thus far the discussion of monitors has been concerned with exceeding trip boundaries and the impact of signal correlation on accidentally tripping a number of times consecutively. We now need to examine the number of boundary crossings over a given period of time.

Using the required false alarm rate of one per 1000 flight hours, the false alarm specification for one hour of flight is given by the following Poisson distribution calculation:

$$P(0) = P(\text{zero false alarms}) = e^{-\lambda T}$$

where

$\lambda = 1 \times 10^{-3}$ (1 failure/hour)

$T = 1$ hour

Therefore,

$$P(0) = 0.999$$

This probability must match up with the probability that the sequence of random variables

$$X_i; \, i = 1, \ldots, n$$

representing a sampled error signal stays within the trip boundary, i.e.,

$$P(\bigcap_{i=1}^{n} X_1) = e^{-\lambda T}$$

for a one-hour flight with 20 samples taken per second and $n = 72,000$. If the sequence is uncorrelated (independent), then we have

Case I: Independent sequence

$$P(\bigcap_{i=1}^{n} X_1) = \prod_{i=1}^{n} P(X_1) = n \, P(X_1)$$

Finally, the required false alarm boundary is

$$P(|X_i| > m\sigma) = 1 - (e^{-\lambda T}) \frac{1}{n} = 1.39 \times 10^{-8}$$

This low figure would require "m" to be very high.* Using a triple trip criteria,

_____

*Normal probability tables do not give numbers in this extreme range.

113

$$P(|X_i| > m\sigma; \text{3 consecutive times}) = (1.39 \times 10^{-8})^{\frac{1}{3}}$$
$$= 2.40 \times 10^{-3}$$

This corresponds to

$$m \cong 3.1$$

As noticed earlier, adding correlation into the sequence shows a monitor performance deterioration. However, the correlation impact on the number of boundary crossings for the entire sequence (1 hour) shows some improvement. This is because, although the time spent above the trip boundary is longer for a correlated sequence, the number of crossings is lower. Plotting values of monitor level versus correlation necessary to meet the false alarm specification is difficult. The upper bound can be calculated, however:

   Case II: $\rho_c = 1$ total sequence dependence

$$\text{Lim } n = 1$$
$$\rho_c \to 1$$

Therefore

$$P(|X_i| > m\sigma; \text{3 times}) \cong P(|X_i| > m\sigma; \text{1 time})$$
$$\cong 1 - e^{-\lambda T} = 10^{-3}$$

or

$$m \cong 3.3$$

From this analysis, it is hypothesized that one needs to set a triple trip monitor above 3.3σ[*] for a given error signal to meet the false alarm rate specification of one trip allowed per 1000 flight hours.

_____

[*]3.5 used in simulation.

4.5.2   Sequential Likelihood Ratio Tests

Hypothesis testing is a popular technique for monitor design for analytical redundancy (References 8 and 36).   Likelihood ratio tests are based upon two hypothesized density functions of a random variable $f_0(x)$ and $f_1(x)$.   The likelihood ratio is expressed as a function of the random variable observations, x_1's:

$$\Lambda_n = \frac{f_0(x_1, x_2, \ldots, x_n)}{f_1(x_1, x_2, \ldots, x_n)} \tag{53}$$

The hypothesized outcomes, H_0 and H_1, are accepted or rejected based on the following:

1.   Accept H_0 if $\Lambda_n \leq A$

2.   Accept H_1 if $\Lambda_n \geq B$

3.   No decision if $A < \Lambda_n < B$

where $B > A$.

One good hypothesis test situation involves testing the mean value (μ) of a given error signal (e_i), i.e.,

$$f_0(e_1, e_2, \ldots, e_n) = c \, \exp\left[-\sum_{i=1}^{n} (e_i - \mu_0)^2 / 2\sigma^2\right] \tag{54}$$

$$f_1(e_i, e_2, \ldots, e_n) = c \, \exp\left[-\sum_{i=1}^{n} (e_i - \mu_1)^2 / 2\sigma^2\right] \tag{55}$$

where

H_0 implies $E(e_i) = \mu_0$

H_1 implies $E(e_i) = \mu_1$

Setting up the no decision criterion

$$A < \frac{\exp\left[-\sum_{i=1}^{n} (e_i - \mu_0)^2 / 2\sigma^2\right]}{\exp\left[-\sum_{i=1}^{n} (e_i - \mu_1)^2 / 2\sigma^2\right]} < B \tag{56}$$

115

Using the natural log of this is more convenient.

$$\text{Ln } A < \sum_{i=1}^{n} \left[(e_i - \mu_1)^2 - (e_i - \mu_0)^2 \right] / 2\sigma^2 < \text{Ln } B \qquad (57)$$

Case I:

$\mu_0 = 0$: Process proceeding normally with no failure

$\mu_1 = m\sigma$: Process mean has shifted

$A = 1/B$

Equation (57) becomes

$$\frac{mn\sigma}{2} - \frac{\sigma \text{Ln } B}{m} < \sum_{i=1}^{n} e_i < \frac{mn\sigma}{2} + \frac{\sigma \text{Ln } B}{m} \qquad (58)$$

Figure 42a shows the decision criteria as a function of n.

Case II:

$(\mu_0 = 0, \ \mu_1 = -m\sigma, \ A = 1/B)$

Equation (57) becomes

$$-\frac{mn\sigma}{2} - \frac{\sigma \text{Ln } B}{m} < \sum_{i=1}^{n} e_i < -\frac{mn\sigma}{2} + \frac{\sigma \text{Ln } B}{m} \qquad (59)$$

Figure 42b shows this case.

In application, a combination of Case I and Case II is used. Let $B = 20,000$ and $m = 4.0$. A combined test consists of:

1.   Accept H_0 if $\left| \sum_{i=1}^{n} e_i \right| \leq (2.00n - 3.13)\sigma$

2.   Accept H_1 if $\left| \sum_{i=1}^{n} e_i \right| \geq (2.00n + 3.13)\sigma$

3.   Make no decision if $(1.95n - 1.95)\sigma < \left| \sum_{i=1}^{n} e_i \right| < (2.00n + 3.13)\sigma$

Figure 43 shows this graphically.
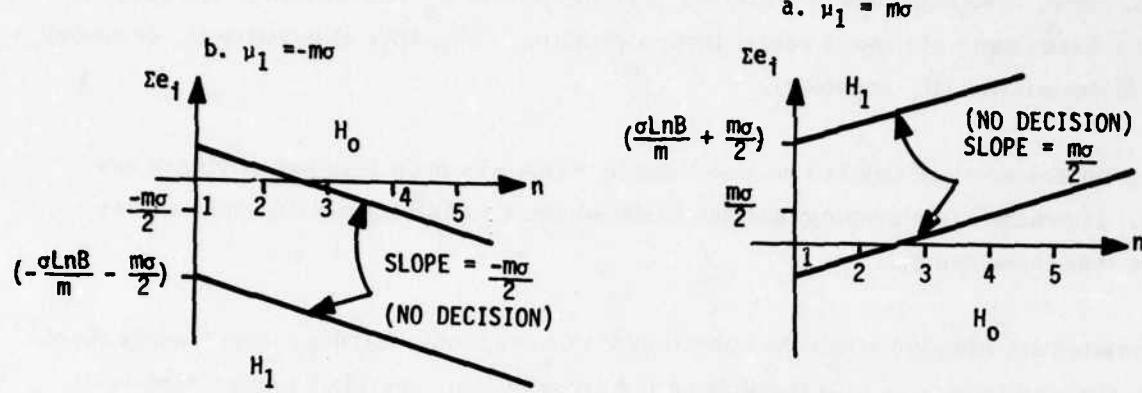
Figure 42. Sequential Likelihood Ratio Test of Mean
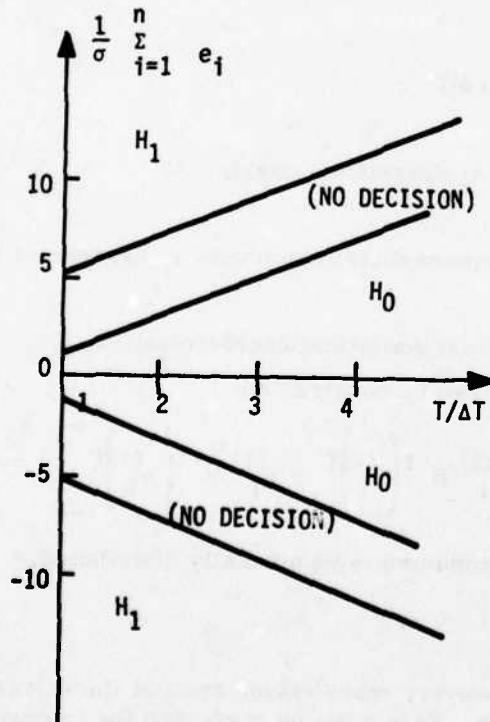
Figure 43. Combined SLRT

The testing procedure consists of initializing at n=1 and updating the sum each computational cycle. The sequence is restarted when hypothesis H_0 is accepted or the process runs a fixed length of time (1 sec) without a decision. The other alternative is, of course, a fault declaration (H_1 accepted).

Frequent restarts are desired because lengthy sequences show less sensitivity to new data. In practice this problem has not surfaced since restarting usually occurs after no more than three sums.

Correlated signals also affect the operation of this monitor. Although theoretically there is no change in the false or missed detection probabilities, correlated error signals do affect restart frequency. An uncorrelated sequence reaches a decision, either H_0 or H_1, with probability 1 (Reference 36). This cannot be demonstrated for correlated signal samples.

4.5.3 Comparison of Likelihood Functions

For a given set of n Kalman filter residual (n_r-vector) sequences ν_i; i = 1, 2, ..., n, the log likelihood function is

$$L_n = -\tfrac{1}{2} \sum_{i=1}^{n} (\nu_i B^{-1} \nu_i^T + Ln \det B) \tag{60}$$

where $\qquad B = E[\nu_i \nu_i^T]$ $\qquad$ (n_r x n_r covariance matrix)

The random variable L_n has a chi-square distribution with n_r degrees of freedom.

Using a second sensor set with identical statistical characteristics, i.e., noise, bias, scale factor, a likelihood difference can be constructed:

$$\Delta L_n = L_n^{(1)} - L_n^{(2)} = \tfrac{1}{2} \sum_{i=1}^{n} \left[\nu_i^{(2)} B^{-1} \left(\nu_i^{(2)} \right)^T - \nu_i^{(1)} B^{-1} \left(\nu_i^{(1)} \right)^T \right] \tag{61}$$

From a practical standpoint this is assumed to be normally distributed.*

---

*This distribution is symmetric; however, more values exist at the extremes about the mean than for a normal distribution. This must be accounted for in monitor level calculations.

The above error signal is used along with comparison monitors to provide a fail-op dual sensor set (Figure 44).

The two hypotheses, however, differ from previous applications:

1. H_0 implies sensor set 1 has failed.

2. H_1 implies sensor set 2 has failed.

A sequential likelihood ratio test of mean value results in

$$\mu_0 = + m\sigma$$
$$\mu_1 = - m\sigma$$

This results in one of the following decisions:

1. Accept H_o if $\Delta L_n \geq \frac{\sigma \, Ln \, B}{2m}$

2. Accept H_1 if $\Delta L_n \geq \frac{\sigma \, Ln \, A}{2m}$

3. Make no decision if $\frac{\sigma \, Ln \, A}{2m} < \Delta L_n < \frac{\sigma \, Ln \, B}{2m}$

As before, the logic will proceed to a decision (H_o or H_1) with probability 1.[*] Because the no-failed hypotnesis is not included, the test can only proceed when a failure is known to have occurred. The failure indication is supplied by the comparison monitors.

Using a delayed declaration on the comparison monitors, the likelihood mean test is initiated after the first trip. If the third consecutive trip occurs, resulting in a fault declaration, the hypothesis (H_o versus H_1) test is initiated to isolate the faulted sensor.

The net effect of this arrangement is two error flags, as shown in the truth table in Figure 44. Because the likelihood functions used can only increase[**] in a fault situation, the direction (+ or -) of the test sequence provides the extra information needed to determine which set contains the failed sensor.

---

[*]Assuming an uncorrelated sequence.

[**]Assuming the Kalman filter model correctly represents the physical system.

Figure 44.   Likelihood Difference Monitor
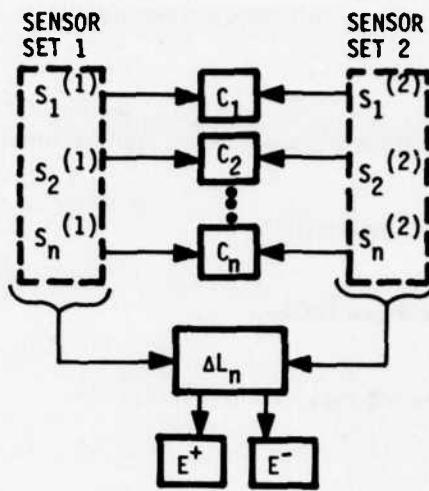
TRUTH TABLE

FAULTS / FLAGS	NONE	$S_1^{(1)}$	$S_2^{(1)}$	$S_n^{(1)}$	$S_1^{(2)}$	$S_2^{(2)}$	$S_n^{(2)}$
C_1		1			1		
C_2 ... C_n			1			1	
				1			1
E^+					1	1	1
E^-		1	1	1			

SECTION 5

A-7D SIMULATION EVALUATION

5.1 SIMULATION SETUP

The three concepts were simulated on a double hybrid computer setup* with the workload split as shown in Figure 45. The use of two digital computers afforded extra core and frame time to perform the aircraft dynamic simulation, fault detection, and monitor schemes, plus some added evaluation capability and record keeping such as:

- Statistical analysis of signals
    - Mean
    - Standard deviation
    - Peak values and time of occurrence
    - Autocorrelation calculations

- Monitor flag history record

- Parallel concept evaluation (Concept I versus Concept II)

A more detailed discussion of the simulation setup appears in Appendix B.

5.2 FALSE ALARM TESTS

Perhaps the most demanding aspect of the simulation was the false alarm analysis conducted on the algorithms. The reasons for this are:

1. Careful analysis of such runs must be made to determine the exact nature of the trip and the corrective action. Fault evaluation runs, on the other hand, were pretty much "let-the-chips-fall-where-they-may" since redesign of a monitor level was precluded after the false alarm tests.

---

*The simulation used two separate hybrid computers, each with an analog and digital portion, connected through an analog link.

121
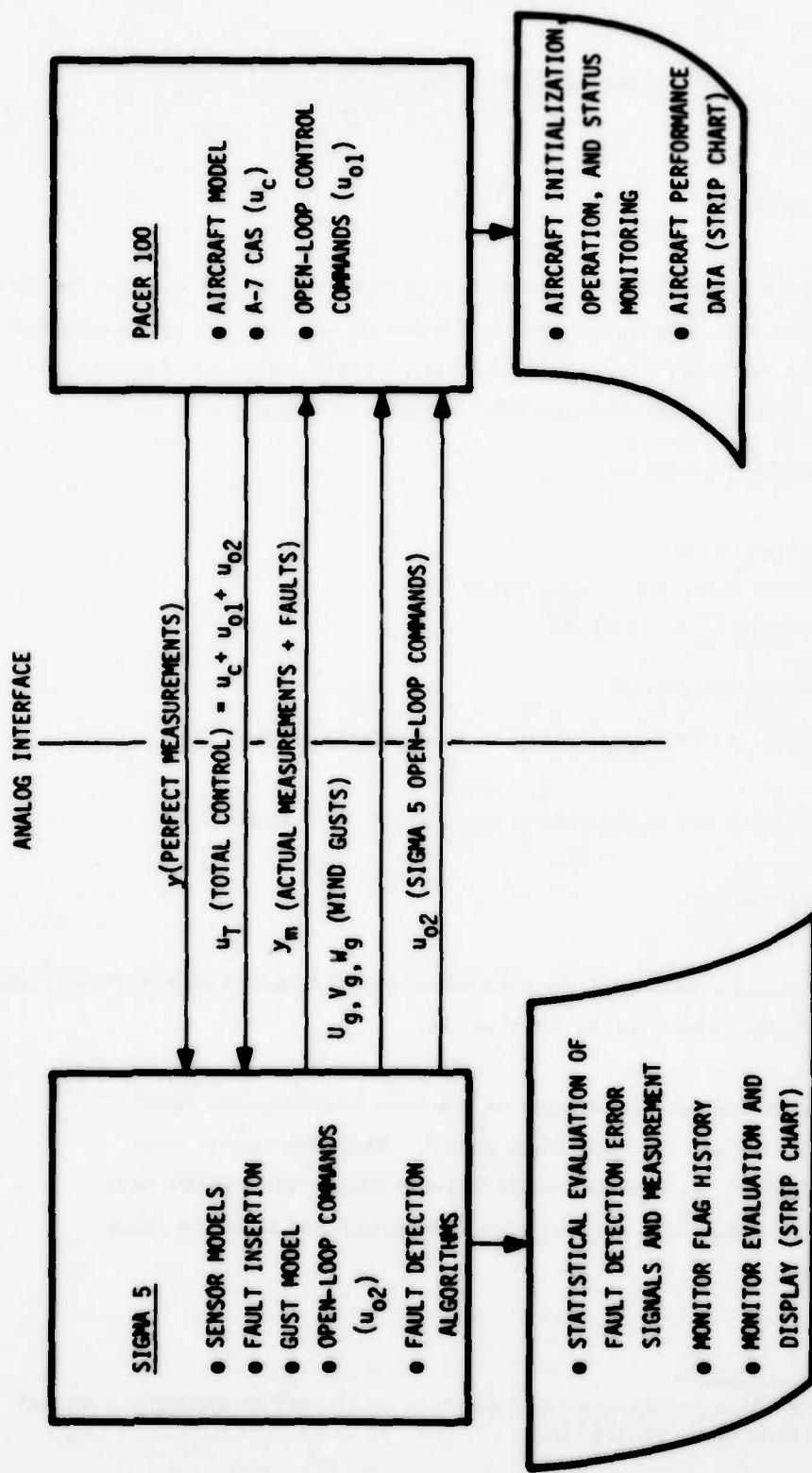
Figure 45. Sigma 5--Pacer 100 Hybrid Simulation

2. Fault detection runs are generally shorter in length, i.e., most were under 12 seconds in duration. False alarm runs included $1\frac{1}{2}$ hours worth of noise test for each concept (30 min at each of three flight conditions) plus numerous deterministic tests.

False alarm inputs include combinations of the following:

- Six ft/sec random gust runs at three flight conditions for $\frac{1}{2}$ hour each (a total of 6 million random numbers generated):
  - Low $\bar{q}$:   h = 1,000'; U_o = 335.1 ft/sec (M = 0.3)
  - Medium $\bar{q}$: h = 15,000'; U_o = 750.0 ft/sec (M = 0.6)
  - High $\bar{q}$:   h = 2,000'; U_o = 1,005 ft/sec (M = 0.9)

- Pitch maneuvers up to 2 commands

- Roll maneuvers (60° roll in 1 sec)

- 30 ft/sec "1-cos" α gusts at three flight conditions ($\omega = 2\pi$ rad/sec)

- 30 ft/sec "1-cos" β gusts at three flight conditions ($\omega = 2\pi$ rad/sec)

5.2.1 False Alarm Results

The results of false alarm tests are a set of nominal monitor values, some monitor schedules, and a performance disclaimer about discrete gusts at low dynamic pressure. Final monitor values are given at the end of this subsection.

All runs were made with different random numbers. Nominal sensor characteristics were chosen at random at the start of each run using RMS values for bias, scale factor, and misalignment listed in Section 3. High-frequency noise was inserted during each time frame.

$\bar{q}$ Schedules on Acceleration Residuals--Evaluation of all concepts took place at three flight conditions: low, medium, and high dynamic pressure. Certain residuals on accelerations for Concepts II and III (all associated with the gain-scheduled filters)* exhibited increased acceleration responses. This result was expected since residual covariance responses obtained during design predicted this. The trend is very consistent and predictable with $\bar{q}$.

---

*Both Concept I's (α, n_z) and Concept II's (h, α, n_z) filters were unaffected by dynamic pressure changes.

123

A $\bar{q}$ monitor schedule for these residuals was designed. The alternative of running the monitors at the constant high level (at high $\bar{q}$) demonstrates poorer monitor performance at lower $\bar{q}$ flight conditions. Much of the fault evaluation for acceleration failures, therefore, took place at the high $\bar{q}$ condition.

Roll Monitor Uplogic--Generally speaking, the guidelines for adjusting monitors during maneuvers consisted of increasing individual levels until acceptance was achieved. One difficulty encountered during the roll maneuver, however, so affected all lateral-axis monitors in all three concepts that a special adjustment was in order. When the monitor logic was set at values determined by other inputs, i.e., random gusts, "1-cos" β gusts, and pitch maneuvers, the filters responded well to inputs. However, the 60° in one second roll maneuver resulted in relatively severe transients in all monitors associated with the following roll variables:

- The error signal on the P filter in Concept I.

- Residuals on ϕ, n_y, P, and R filters in Concept II.

- Residuals on n_y, P, and R filters in Concept III.

The reasons for the excessive transients (in some cases five times the value needed to handle random gusts) were a combination of sample rate and hybrid computer Euler angle integration. One notion was to increase the sampling frequency; however, this resulted in increased error signal correlation (resulting in the need to increase monitor levels) and it reduced the available computer frame time.

The solution was to employ known information about maneuvers but not sensor information, i.e., the roll command. Figure 46 outlines the design used to "up" roll monitor magnitudes during pilot maneuvers.

The design is based on stepping up the affected monitors immediately upon receiving a roll command from the pilot. The magnitude of the uplogic is proportional to the stick command rate. The logic is designed to maintain a constant level of monitors "up," i.e., at a higher monitor level, for the duration of the residual transient (taken to be about 1 sec). If no further pilot commands are given, which would result in the uplogic staying "up," the monitor decays ($_{\tau}$ = 0.33 sec) to its original value.

The addition of a "fix" of this type carries with it a natural concern for the system performance during piloted maneuvers. For this reason, many of the fault evaluations for the affected monitors were conducted during the roll maneuver.

124
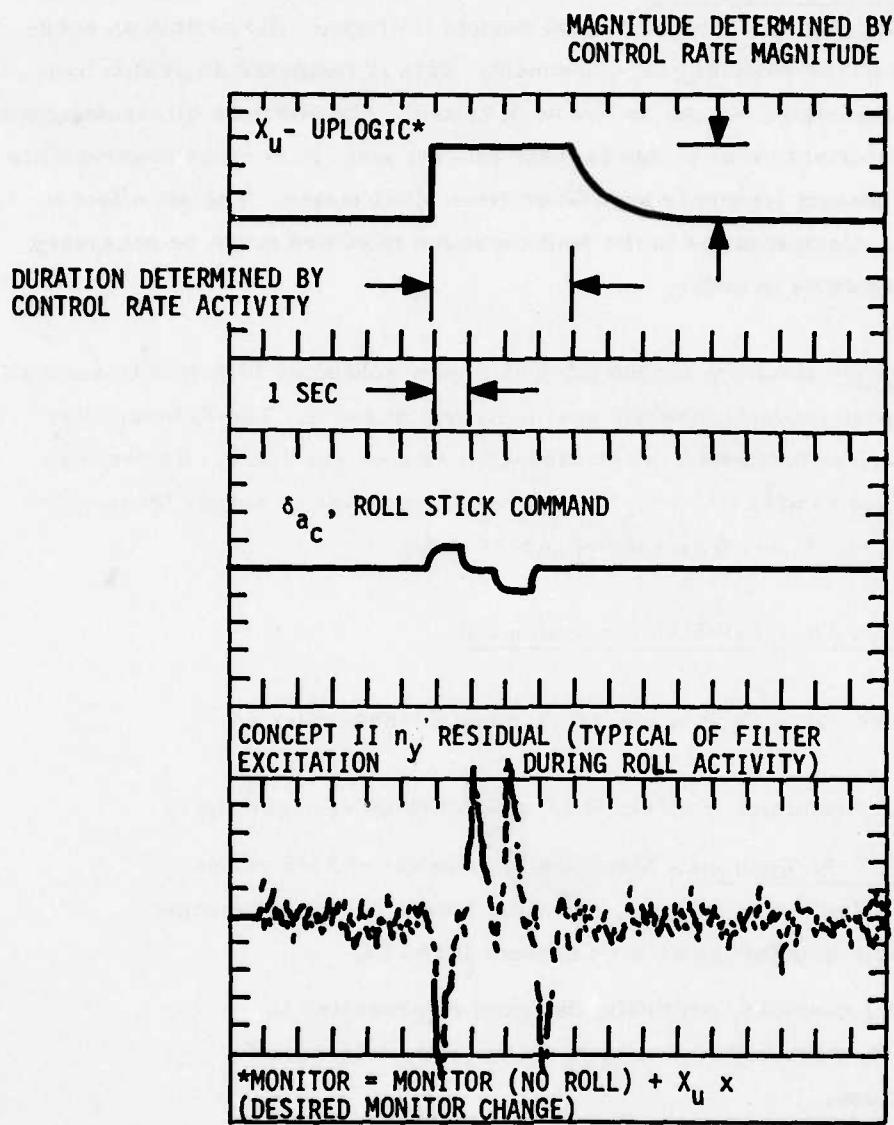
Figure 46. Roll Monitor Uplogic

h_m Uplogic on Vertical Gust Estimators--Although it was never really evaluated, it should be noted that during landing approach some gust models (Reference 38) contain an ever-increasing bandwidth on the vertical gust component. This is tempered somewhat by a lower RMS, but time constants can get as low as 0.11 sec. The effect on filters designed with vertical gust estimators, even if this is taken into account, is to cause observability problems, i.e., no inherent frequency separation from other states. The net effect is higher residual RMS. Compensation in the fault detection monitors might be necessary and an h_m schedule would be in order.

"1-cos" α Gust at Low $\bar{q}$--Monitors for the pitch axis gain-scheduled filters in Concept III did not successfully pass the 1 Hz discrete gust input test at low $\bar{q}$. The Kalman filter design process resulted in decreasing filter bandwidth with decreasing $\bar{q}$. Rather than increase monitor values to pass this test, the approach taken was to simply ignore performance for this magnitude and frequency of gust at low $\bar{q}$.

5.2.2   Monitor Values After False Alarm Evaluation

Monitors were adjusted during false alarm tests using various criteria:

1.   Random Gust Evaluation (6 ft/sec RMS - $1\frac{1}{2}$ hours on each concept).

    ● Multiple Trip Monitors - Statistically determined RMS values and the false alarm analysis in Section 4 were used to determine acceptable monitor levels for Concepts II and III.

    Concept I monitors, originally designed as presented in Section 4, were adjusted to meet statistically determined RMS values.

    ● Sequential Likelihood Ratio Tests (SLRT) - Concepts II and III were run with residuals operating on both the multiple trip monitors and the SLRT monitors. Using the basic development of Section 4, individual monitors were adjusted; however, final monitor levels were affected more by maneuvers than by turbulence.

2.   Pitch Maneuver (2-g pitch command at three flight conditions).

    ● Multiple Trip Monitors - All concepts were unaffected by

126

pitch maneuvers. Residual values stayed within monitor levels determined by random gusts.

- **SLRT Monitors** - Some monitors in Concept III needed slight adjustment.

3. Roll Maneuver (60° in 1 sec command at three flight conditions). All monitors on roll variables had to be adjusted to account for this maneuver.

4. Discrete α gust ($W_g = 30$ ft/s $[1 - \cos(2\pi t)]$ for 1 sec). Concept III pitch axis filters failed this test for the low $\bar{q}$ flight condition. Redesign was not performed due to the low probability of this input in real situations. This input, therefore, provides the limiting condition for Concept III pitch axis designs. Optimum bandwidths (based on random gusts) are too low to effectively counter this high-frequency gust.

5. Discrete β gust ($V_g = 30.0$ ft/s $[1 - \cos(2\pi t)]$ for 1 sec). Monitor adjustments on lateral axis gain-scheduled filters in Concepts II and III passed this test.

6. Other maneuvers that performed with no nuisance trips were:

- Roll to 70° in five seconds, and

- Coordinated turn at $\phi = 40^o$.

Tables 23 and 24 show the monitor values used for fault detection evaluation.

TABLE 23. FINAL MONITOR LEVELS (CONCEPT I)

Filter	Monitor Level	Roll Monitor Level (Δ/unit roll up logic)
1. P_ϵ (deg/sec)	$4.0 + 0.055/P_m/$	30.0
2. Q_ϵ (deg/sec)	$3.5 + 0.055/Q_m/ + 0.0053/P_m/$	-
3. R_ϵ (deg/sec)	$4.0 + 0.055/R_m/ + 0.0053/P_m/$	-
4. n_{z_ϵ} (g's)	$3.0 + 0.015/Q_m/ + 0.35/n_{z_m}/$ $+ U_m(0.54 + 0.0342/Q_m/$ $+ 0.0353/P_m/)/(32.17 \times 57.3)$	-
5. h_ϵ (ft/sec)	$721.0 + 0.028/U_m/ + 3/\dot{h}/$	-

127

TABLE 24. FINAL MONITOR LEVELS* (CONCEPTS II AND III)

CONCEPT	FILTER	RESIDUAL OR ERROR SIGNAL	6 ft/sec GUST INPUT RMS MED. q̄/HIGH q̄	LEVEL FOR MULTIPLE TRIP MONITOR	HIGH q̄ MONITOR LEVEL	SLRT MONITOR LEVEL	ROLL MONITOR LEVEL
II	$\phi_m - P_m$	1. ν_ϕ (rad)	0.00321	0.0033		0.0033	0.017
	$\theta_m - Q_m$	2. ν_θ (rad)	0.00279	0.0033		0.0033	
	$\psi_m - R_m$	3. ν_ψ (rad)	0.00276	0.0030		0.0030	
	h_m, α_m, n_{z_m}	4. ν_h (ft)	31.2	40.0		40.0	
		5. ν_α (rad)	0.00320	0.0050		0.0070	
	$n_{y_m}, P_m, R_m, \phi_m$	6. νn_y (ft/sec²)	1.09/1.43	1.20	2.0	1.5	3.0
		7. ν_P (rad/sec)	0.0023	0.030		0.04	0.15
		8. ν_R (rad/sec)	0.0084	0.012		0.015	0.10
III	n_{z_m}, Q_m	1. ν_{n_z} (ft/sec²)	2.62/5.67	4.3	6.2	4.8	
		2. ν_Q (rad/sec)	0.0080/.010	0.012		0.012	
	Q_m, α_m	3. ν_Q (rad/sec)	0.0086/.0130	0.020		0.020	
		4. ν_α (rad/sec)	0.0035/.0037	0.0035		0.0050	
	n_{y_m}, R_m	5. ν_{n_y} (ft/sec²)	1.15/1.47	1.25	2.0	1.25	1.4
		6. ν_R (rad/sec)	0.0076/.0077	0.010		0.010	0.04
	n_{y_m}, P_m	7. ν_{n_y} (ft/sec²)	1.16/1.52	1.25	2.5	1.25	1.4
		8. ν_P (rad/sec)	0.022/.022	0.025		0.025	0.30
F A I L O P	$P_{m_1} - P_{m_2}$ Compare	ΔP (rad/sec)	0.0136	0.018		N/A	
	$Q_{m_1} - Q_{m_2}$ Compare	ΔQ (rad/sec)	0.0050	0.006		N/A	
	$R_{m_1} - R_{m_2}$ Compare	ΔR (rad/sec)	0.0050	0.006		N/A	
	Likelihood Difference	ΔV_L (rad²)	0.171	N/A		0.5	

*Monitor levels are defined here to be the RMS values sent to the multi-trip monitor and sequential likelihood ratio test routines. Scaling as per Section 4 development was then performed.

5.2.3   Fail Operational Monitors

Some minor adjustments on the fail-operational comparison monitors were made during
the false alarm runs. These monitors are the constant level, triple trip type. Actual
A-7D monitor levels were not used for two reasons:

1. A-7D comparison monitors operate at higher sample rates. If allowed
    to operate at the sample rate used in this study, their thresholds would
    probably be too high.

2. The objective of this design is to evaluate the SLRT for differences of
    likelihood functions (as described in Section 4). There is only one real
    issue. When asked to decide which diagnostic filter contains this fault,
    this monitor can do one of three things: decide on the right sensor set,
    decide on the wrong sensor set, or decide later. The ability to make
    the right isolation decision at the earliest time was the test objective.

5.3   FAULT DETECTION SIMULATION

5.3.1   Fault Insertion

Section 3 outlines the various faults encountered by each sensor. For purposes of
simulating these faults in a fashion best suited to evaluation, the following faults were
inserted at prescribed insertion times:

- Hardover (plus): $\quad S_{x_O}$ = max value

- Hardover (minus): $\quad S_{x_O}$ = min value

  Dead: $\quad S_{x_O} = 0$

  Bias: $\quad S_{x_O} = S_{x_I} + t\sigma_b$ (i.e., 1 σ_b of bias/sec)

  Scale Factor 1: $\quad S_{x_O} = .75\, S_{x_I}$

  Scale Factor 2: $\quad S_{x_O} = .50\, S_{x_I}$

  Dynamic Response: $S_{x_O} = S_{x_I}/(\tau_c s + 1)$: $\quad \tau_c = 1$ sec

    where S_{x_O} is the sensor output after failure input, and
    S_{x_I} is the sensor input.

129

5.3.2 Recovery Modes

Recovery modes consisted of simply removing the fault. For redundant sensors (n_{z_m}, n_{y_m}, P_m, Q_m, R_m) this simulated replacing the bad sensor with a good one. For non-redundant sensors the insertion of the original sensor has no meaning other than to signify that the fault was detected for plotting purposes.

Recovery modes deserve more careful attention than was given them in this study. Although unsophisticated, the scheme used, when operating with a sensor consistency monitor (discussed next), performed adequately in all cases with no catastrophic transient resulting from the recovery. A recommended alternative which was not tried will be discussed later.

5.3.3 Sensor Consistency Monitor

At the outset of this study, the baseline constraint on the analytical redundancy algorithms was that the recommended system be implemented into the A-7D on-board computer (Honeywell-301). Due to this constraint, it was necessary to keep the sample rate as low as possible. At 20 samples/sec, the fault tolerant algorithms have a built-in delay in identifying faults, particularly if multiple trips are used to declare a fault. It is likely that if catastrophic faults, i.e., hardover sensors, are allowed to pass through the computer, a difficult recovery task results regardless of how well the monitor works.

The algorithms tested were supplemented by a sensor consistency monitor which compared the data from each sensor with past inputs. If the new value is not within some prescribed deviation from the immediate past value, the old data point is substituted for it. This procedure possesses no performance problem if the fault is discovered quickly, but it would cause problems if the fault were not detected.

The simulation allowed the entire fault to reach the control system for one entire sample time of the fault diagnosis frame. This roughly simulates the fault detection schemes operating at a much lower sample rate than the control schemes. It is recommended that the sensor consistency monitor be implemented at the highest sample rate, thereby not allowing any sensor hardovers to propagate into the control scheme.

It is further recommended that this scheme be investigated as a possible recovery mode transition filter. Instead of substituting a past value when an inconsistency is discovered,

130

one should substitute the previous value plus some portion of the current measurement. This would then operate completely independently of the fault detection schemes and force a gradual recovery from a dead sensor to its substitute which may be at a much larger magnitude by the time a fault is detected. Admittedly, some portion of a hardover sensor output would also propagate through the system and thus a design trade-off for choosing these levels should be performed.

5.3.4 Fault Detection Evaluation (Concepts I and II)

The procedure for performing fault evaluation runs for Concepts I and II was aided by the capability to run these two concepts in parallel. First a complete fault insertion set of runs was made using Concept I monitors for recovery. Then the procedure was switched to Concept II recovery monitors using sequential likelihood ratio test (SLRT) monitors. For all runs, both concepts were evaluating the faults with a running history of error flags being recorded for printout at the end of a given fault run. Concept II also ran with both monitors (multiple trip and SLRT) evaluating filter residuals. This procedure obtained two sets of fault evaluations.

For all runs, the random gust generator was set to a value of 3 ft/sec for all three axes gust components. The goal here was to not assist the fault detection with high gust levels.

Results for the Concept I and II evaluation are shown in Table 25. Complete strip chart outputs appear in Appendix D.

Not shown in Table 25 are the results from the SLRT test of likelihood functions of two sets of sensors with identical filters (body rate Euler angle filters). The main issue here was whether this test would provide the fault isolation necessary for the fail-op capability. In all cases the decision was made within one extra sample frame from the time the comparison monitor asked for a decision.

5.3.5 Fault Detection and Isolation (Concept III)

Concept III results are shown in Table 26. This evaluation took place for six sensors: α_m, n_{z_m}, n_{y_m}, P_m, Q_m, and R_m. Two additional sensors can be added to this list by using Concept II's LON #2 filter for Q_m faults and the lateral axis filter for ϕ_m faults.

131

TABLE 25. CONCEPTS I AND II SIMULATION COMPARISONS

FLIGHT CONDITION, MANEUVER	SENSOR	FAULT	CONCEPT I	CONCEPT II-MONITORS SLRT	CONCEPT II-MONITORS MULTI-TRIP (MT)	RECOVERY	SUBJECTIVE CONCEPT WINNER	COMMENTS
High $\bar{q}$, none	n_{z_m}	H.O.	4^2*	5^1	S^2	Good	II - SLRT	
High $\bar{q}$, pitch up	n_{z_m}	Dead	4^3	5^1	S^2	Adequate	II - SLRT	
High $\bar{q}$ pitch up	n_{z_m}	Dynamic Response	Not caught	Not caught	Not caught	N/A	All lose	105 sec detect time
High $\bar{q}$, none	n_{z_m}	Bias	4^3	5^1	S^1	Good	II - SLRT or MT	
High $\bar{q}$, 8 lb pitch	n_{z_m}	25% S.F.	Not caught	Not caught	Not caught	N/A	All lose	
High $\bar{q}$, 8 lb pitch	n_{z_m}	50% S.F.	Not caught	5^1	5^1	Good	II - SLRT	
Med. $\bar{q}$, None	q_m	H.O.	2^2	2^1	2^3	Adequate	II - SLRT	
Med. $\bar{q}$, Pitch up	q_m	Dead	2^1	2^1	2^1	Adequate	Tie	
Med. $\bar{q}$, None	q_m	Bias	2^3	2^1	2^2	Good	II - SLRT	56.70 sec detect time
Med. $\bar{q}$, Pitch up	q_m	25% S.F.	Not caught	2^1	Not caught	Good	II - SLRT	
Med. $\bar{q}$, Pitch up	q_m	50% S.F.	Not caught	2^1	2^2	Good	II - SLRT	
Med. $\bar{q}$, None	θ_m	H.O.	2^1	2^1	2^1	N/A	All good	
Med. $\bar{q}$, None	θ_m	Dead	2^1	2^1	2^1	N/A	All good	
Med. $\bar{q}$, None	θ_m	Bias	Not caught	5^2	5^1	N/A	II - M.T.	41.6 sec
Med. $\bar{q}$, Pitch up	θ_m	25% S.F.	Not caught	Not caught	Not caught	N/A	All lose	
Med. $\bar{q}$, Pitch up	θ_m	50% S.F.	2^1	2^1	2^1	N/A	All good	
Low $\bar{q}$, None	α_m	H.O.	Not caught	5^1	5^2	N/A	II - SLRT	Concept 1 Expected result
Low $\bar{q}$, Pitch up	α_m	Dead	Not caught	5^1	5^2	N/A	II - SLRT	
Low $\bar{q}$, None	α_m	Bias	Not caught	Not caught	Not caught	N/A	All lose	Expected result
Low $\bar{q}$, Pitch up	α_m	25% S.F.	Not caught	Not caught	Not caught	N/A	All lose	
Low $\bar{q}$, Pitch up	α_m	50% S.F.	Not caught	5^1	Not caught	N/A	II - SLRT	
Low $\bar{q}$, None	h_m	H.O. (-)	5^2	5^1	S^2	N/A	II - SLRT	Expected result
Low $\bar{q}$, None	h_m	Bias	Not caught	Not caught	Not caught	N/A	All lose	
Low $\bar{q}$, None	U_m	H.O. (+)	Not caught	5^1	S^2	N/A	II - SLRT or M.T.	Works good
Low $\bar{q}$, None	U_m	Dead	Not caught	5^1	S^2	N/A	II - SLRT or M.T.	
Med. $\bar{q}$, 60° Roll	P_m	H.O.	1^1	$7^1, 1^1$	$7^2, 1^2$	Good	I and II - SLRT	Gain Sched.
Med. $\bar{q}$, 60° Roll	P_m	Dead	1^1	$7^2, 1^2$	$7^3, 1^3$	Good	I - M.T.	
Med. $\bar{q}$, 60° Roll	P_m	Bias	1^1	N/A	g^2	Good	I - M.T.	Surprisingly good Concept I Performance
Med. $\bar{q}$, 60° Roll	P_m	25% S.F.	1^1	1^2	Not caught	Good	I - M.T.	
Med. $\bar{q}$, 60° Roll	P_m	50% S.F.	1^1	1^2	7^3	Good	I - M.T.	

*n^m notation: n refers to the corresponding error signal or residual number in Table 23 for the concept indicated. m refers to the order in which detection occurs. Ties are indicated with the same number.

132

TABLE 25. CONCEPTS I AND II SIMULATION COMPARISONS (concluded)

FLIGHT CONDITION, MANEUVER	SENSOR	FAULT	CONCEPT 11-MONITORS			RECOVERY	SUBJECTIVE CONCEPT WINNER	COMMENTS
			1	SLRT	MULTI-TRIP (MT)			
Med. $\bar{q}$, Roll	θ_m	H.O.	1^1	1^1	1^1	N/A	All good	Expected result
Med. $\bar{q}$, Roll	θ_m	Dead	1^1	1^1	1^1	N/A	All good	
Med. $\bar{q}$, None	θ_m	Bias	Not caught	6^1	6^2	N/A	11 - SLRT	
Med. $\bar{q}$, Roll	θ_m	25% S.F.	Not caught	1^1	Not caught	N/A	11 - SLRT	
Med. $\bar{q}$, Roll	θ_m	50% S.F.	Not caught	1^1	1^1	N/A	11 - SLRT or M.T.	
Med. $\bar{q}$, Roll	R_m	H.O.	3^1	3^2, 8^2	3^3, 8^3	Good	1 - M.T.	
Med. $\bar{q}$, Roll	R_m	Dead	3^1	3^2	3^3	Good	1 - M.T.	
Med. $\bar{q}$, None	R_m	Bias	3^2	N/A	11^1	Good	Bias Estimation	42.95 sec detect time
Med. $\bar{q}$, Roll	R_m	25% S.F.	Not caught	Not caught	Not caught	N/A	All lose	
Med. $\bar{q}$, Roll	R_m	50% S.F.	3^1	3^2	3^3	Good	1 - M.T.	
Med. $\bar{q}$, Roll	ψ_m	H.O.	3^1	3^1	3^1	N/A	All good	Expected result
Med. $\bar{q}$, Roll	ψ_m	Dead	3^2	3^1	3^2	N/A	11 - SLRT	
Med. $\bar{q}$, None	ψ_m	Bias	Not caught	Not caught	Not caught	N/A	All lose	
Med. $\bar{q}$, Roll	ψ_m	25% S.F.	Not caught	Not caught	Not caught	N/A	All lose	
Med. $\bar{q}$, Roll	ψ_m	50% S.F.	Not caught	3^1	Not caught	N/A	11 - SLRT	
High $\bar{q}$, Roll	n_{ym}	H.O. (+)	N/A	6^1	6^2	Good	11 - SLRT	
High $\bar{q}$, Roll	n_{ym}	H.O. (-)	N/A	6^1	6^2	Good	11 - SLRT	
High $\bar{q}$, Roll	n_{ym}	Dead	N/A	Not caught	Not caught	N/A	All lose	
High $\bar{q}$, Roll	n_{ym}	Dynamic Response	N/A	Not caught	Not caught	N/A	All lose	
High $\bar{q}$, None	n_{ym}	Bias	N/A	8^1	8^2	Good	11 - SLRT	Surprising-29.7 sec (Very quick)
High $\bar{q}$, Roll	n_{ym}	25% S.F.	N/A	Not caught	Not caught	N/A	All lose	
High $\bar{q}$, Roll	n_{ym}	50% S.F.	N/A	Not caught	Not caught	N/A	All lose	

133

TABLE 26. CONCEPT III SIMULATION EVALUATION

Flight Correction, Maneuver	Sensor	Fault	CONCEPT III OUTCOME Detect	Isolate	Comments
High $\bar{q}$, None	n_{z_m}	H.O. (+)	Good	Good	
High $\bar{q}$, None	n_{z_m}	H.O. (-)	Good	Good	
High $\bar{q}$, 8 lb Pitch up	n_{z_m}	Dead	Good	Good	Considerable n_z required
High $\bar{q}$, 8 lb Pitch up	n_{z_m}	Dynamic Response	Not caught	Not caught	
High $\bar{q}$, 8 lb Pitch up	n_{z_m}	25% S.F.	Not caught	Not caught	
High $\bar{q}$, 8 lb Pitch up	n_{z_m}	50% S.F.	Not caught	Not caught	
Med. $\bar{q}$, None	Q_m	H.O. (+)	Good	Adequate	Decided n_{z_m} first and switched after .05 sec
Med. $\bar{q}$, 8 lb Pitch up	Q_m	Dead	Good	Adequate	1. Considerable pitch up required
Med. $\bar{q}$, 8 lb Pitch up	C_m	25% S.F.	Not caught	Not caught	2. Decided n_{z_m} first and switched after .10
Med. $\bar{q}$, 8 lb Pitch up	Q_m	50% S.F.	Not caught	Not caught	
Low $\bar{q}$, None	α_m	H.O.	Good	Good	
Low $\bar{q}$, 8 lb Pitch Up	α_m	Dead	Good	Good	
Low $\bar{q}$, 8 lb Pitch up	α_m	25% S.F.	Good	Good	
Med. $\bar{q}$, 60°/sec Roll	P_m	H.O. (+)	Good	Good	
Med. $\bar{q}$, 60°/sec Roll	P_m	H.O. (-)	Good	Good	
Med. $\bar{q}$, 60°/sec Roll	P_m	Dead	Good	Good	
Med. $\bar{q}$, 60°/sec Roll	P_m	25% S.F.	Good	Good	
Med. $\bar{q}$, 60°/sec Roll	R_m	H.O. (+)	Good	Good	
Med. $\bar{q}$, 60°/sec Roll	R_m	H.O. (-)	Good	Good	
Med. $\bar{q}$, 60°/sec Roll	R_m	Dead	Not caught	Not caught	
Med. $\bar{q}$, 60°/sec Roll	R_m	25% S.F.	Not caught	Not caught	
Med. $\bar{q}$, 60°/sec Roll	R_m	50% S.F.	Not caught	Not caught	
High $\bar{q}$, 60°/sec Roll	n_{y_m}	H.O. (+)	Good	Good	
High $\bar{q}$, 60°/sec Roll	n_{y_m}	H.O. (-)	Not caught	Not caught	High-pass break frequency is too high
High $\bar{q}$, 60°/sec Roll	n_{y_m}	Dead	Not caught	Not caught	
High $\bar{q}$, 60°/sec Roll	n_{y_m}	Dyn. Resp.	Not caught	Not caught	
High $\bar{q}$, 60°/sec Roll	n_{y_m}	25% S.F.	Not caught	Not caught	
High $\bar{q}$, 60°/sec Roll	n_{y_m}	H.O. (-)	Not caught	Not caught	
High $\bar{q}$, 30°/sec Roll	n_{y_m}	H.O. (-)	Not caught	Not caught	
High $\bar{q}$, None	n_{y_m}		Good	Good	Good n_y residual match up
High $\bar{q}$, 30°/sec Roll	P_m	50% S.F.	Good	Good	25% S.F. Not caught

The filters were originally operated with second order high-pass filters at 2 rad/sec. The results from initial fault runs were so poor that the high-pass frequency was moved to 1 rad/sec. This shift produced the results shown in Table 26. Failure to achieve fault detection in many cases resulted from the fault transient being high-passed away too quickly. The low frequency inputs into the longitudinal axis, i.e., Phugoid motion and trim changes, preclude lowering the current high-pass frequency. Low frequency lateral-directional inputs, spiral mode motion and control effectiveness input mismatches are less severe. This would probably allow the frequency of the high-pass filter to be lowered.

Fault isolation logic requires observation of faults in various filters in order to identify the failed sensor. In practice, each filter's monitor levels were dictated by false alarm runs. This results in some delay in making the right fault decision. For example, pitch rate, Q_m, faults must show up in two filters, filters III-1 and III-2. If the fault is detected in filter III-1, the first decision is that n_{z_m} has failed. If it shows up first in filter III-2, the α_m is bad. The alternative of waiting for both filters to respond before a decision is made will delay n_{z_m} and α_m fault diagnosis. An approach of letting the isolation logic decide immediately and then switch if a change occurs was used.

SECTION 6

CONCLUSIONS AND RECOMMENDATIONS

Results presented in Section 5 yield a number of comments and recommendations. These will be provided in two groups: specific technical observations and conclusions and recommendations for future development through flight test.

6.1   SPECIFIC TECHNICAL OBSERVATIONS AND CONCLUSIONS

6.1.1   Comparisons of Concepts I and II

Euler Angles and Body Rates--In general, the performance of the two concepts was very close. This fact would favor Concept I because of the implementation simplicity; however, a number of considerations should be examined:

1.   The bias estimators of Concept II performed well in catching bias errors even though they were not originally designed to be monitored. The yaw rate, R_m, bias estimation was the most precise bias estimate of those designed because of its low gain. Concept II's bias fault detection capability was also excellent. Regardless of how long the bias errors propagate, the recovery impact and total net effect on the aircraft are minimal.

2.   Another choice for the high-pass time constant for Concept I would reduce the autocorrelation of error signals without sacrificing performance. This would allow the use of the sequential likelihood ratio test monitors with Concept I filters (SLRT does not like correlation).

3.   Euler angle fault detection proved to be easy for both concepts. Concept II performed better, based on the strength of the SLRT monitor performance.

n_z, α, and h Filters--Concept II was the clear winner. Ignoring wind gust correlation in Concept I produced high autocorrelation and high RMS. The key to the Concept II success was the gust estimation. Also, as predicted, Concept I missed the α_m hardover fault.

136

U_m Faults--Concept II's (n_z, α, h) filter proved surprisingly good at diagnosing airspeed faults. The gain-scheduled lateral-directional filter was expected to provide some diagnosis capability (and it did), but the primary performance came from (n_z, α, h).

6.1.2 Monitor Performance Comparisons

The two monitors used were the multiple-trip-level exceedance (with and without sensor scheduling) versus the sequential likelihood ratio test (SLRT). This idea is a computationally simplified version of one used previously (Reference 8). The SLRT monitor performed well. The monitor demonstrated adeptness at catching hardover faults quickly, plus detecting other faults (particularly scale factor changes) that escaped the multiple trip monitor.

More understanding of how this monitor works is needed because setting the necessary parameters for false alarm requirements is difficult.

6.1.3 SLRT of Likelihood Function Difference

As originally discussed in Section 2, the decision as to which sensor family (determined by the diagnostic filters) contained the faulty output was to be performed on a relative performance basis, i.e., which set of sensors performed the best when the comparison monitor declared a failure. The SLRT monitor used here provides a more formal way of isolating the failed sensor. Expansion to n_{z_m} and n_{y_m} fault isolation should be made.

6.1.4 Lateral Accelerometer Fault Detection

As expected, n_{y_m} faults were difficult to diagnose. The inclusion of a completely gain-scheduled third-order filter perhaps is not justified considering the return. The filter did supply some other benefits:

- Good fault detection of body rate signals, P_m and R_m, was observed.

- ϕ_m bias faults were detected (although eventual flight tests may have to include low frequency high-pass filters to wash-out modeling errors).

- Some detection capability for airspeed faults was observed.

137

The need for this type of filter goes beyond the current application. State reconstruction for control law modification is an issue discussed but not addressed in the current study. It has been demonstrated that this filter can perform well with reduced sets of measurements. For example, if the loss of an inner-loop signal, i.e., n_{y_m}, P_m, or R_m, occurs, this filter could be used to reconstruct the missing output.

The key issue (and the major reason why this was not addressed in the current study) is performance. It is likely that the performance required by the primary flight control system will not be obtained. Reconstruction, however, could supply a fail-sub-operational capability, a level of performance which would be a reversion mode that could be used before fail-safe is necessary.

6.1.5   Sample Rate and Fault Detection

The desire to operate at a low sample rate is strong due to a lack of computer core and time. Also, the longer the algorithms take to make a decision the better they will perform. The key issues are fault detection algorithms and flight control performance. Two modifications to the concepts studied provide the justification for retaining the 0.05 sec sample time.

Sensor Consistency Check--A simple check of sensor consistency from sample to sample gives the fault detection algorithms valuable time to make decisions, particularly during hardover failures. It is recommended that this sort of check be applied at the flight control sample rates to ensure that sensor hardover failures do not enter into the control law. This scheme could also be modified to provide a recovery mode capability. The one used in this study is not being recommended as a usable recovery process.

Roll Monitor Uplogic--The use of uplogic for certain monitors scheduled on roll command effectively solved a difficult problem. Use of a different Kalman filter integration scheme is recommended; a trapezoid integration scheme will reduce the effect of high roll rates and will provide quicker fault propagation into the detection scheme for certain sensors.

Simulation results verified that the roll monitor uplogic does not compromise fault detection during maneuvers.

138

6.1.6   Concept III Conclusions

Concept III results were less encouraging than results from Concepts I and II.   Detecting
and isolating faults produced marginal success.   Hardover fault detection posed the
fewest problems.   Referring to the concept selection discussions in Section 2, the
Concept III filters would have to be augmented with specific algorithms hypothesizing
various faults.   Either multiple hypothesis Kalman filters (Reference 12) must be
installed (with associated extra filtering) or signature tests for specific faults (Reference
19), also computationally expensive, must be explored.

6.2   RECOMMENDATIONS FOR FLIGHT TEST

Results from the evaluation of Concepts I and II and fail-op monitor selection evaluation
were encouraging.   The following recommendations can be made:

1.   Euler Angle-Body Rate Filters

   - Either Concept I body rate observer/blenders can be used with slight
     modification to run with SLRT, or

   - Concept II Euler angle Kalman filters operating with bias estimation
     (scale factor estimation should be dropped) can also be used with monitors
     on bias estimates to diagnose bias faults.

2.   Altitude, Normal Acceleration, and Angle-of-Attack--The Concept II filter
     includes gust estimation and demonstrated superior performance over the
     Concept I equivalent.   This should be used in flight test experiments.   This
     filter will also diagnose airspeed faults.

3.   Lateral Acceleration--The gain-scheduled Kalman filter for n_y, P, and R
     measurement fault detection should be retained.   In addition to n_{y_m} errors,
     this filter has growth potential into state reconstruction experiments.

4.   Monitors

   - Fail Operational--Dual sensor sets (n_{y_m}, n_{z_m}, P_m, Q_m, R_m, and α_m)
     should retain current comparison monitors.   A sequential likelihood ratio
     test of the mean value of the difference of likelihood functions should be

used to compare error signals from parallel analytical redundancy schemes operating with dual computers. This scheme as outlined in Section 2 offers high promise of providing a fail-op capability in lieu of the third set of redundant sensors which is currently needed.

● Fail-Safe--The sequential likelihood ratio test of residual mean value demonstrated superior performance over multiple trip monitors. This monitor should be investigated further in flight tests.

Cost-effectiveness analysis of the three concepts is discussed in Appendix A. The proposed flight test concept (with additional monitor logic for roll inputs and $\bar{q}$ changes plus sensor consistency checks) will use about the same computer requirements as Concept II. Additional consideration should be given to retaining multiple trip monitors for experimental comparisons with the SLRT monitors in flight test.

A subset of the Concept III longitudinal axis filter, i.e., one filter with multiple gain sets, could also be flight tested at minimum expense, allowing investigation of gain-scheduled pitch axis filters for fault detection and state reconstruction.

APPENDIX A

COST-EFFECTIVENESS ANALYSIS

The cost-effectiveness of analytical redundancy techniques to detect and isolate faults depends to a great extent upon how much computational space is available in the on-board computers. Designing detection schemes which are both effective and computationally cheap has been an underlying goal throughout this study.

The residual core of the HDC 301 is typical of the space available for current on-board processors for this type of application.

Computer sizing results for the three concepts investigated are shown in Table A.1. Concepts I and II easily fit into an HDC 301 processor on board the A-7D. Concept III barely meets the computer capability available, but simulation adjustments not taken into account here will make this application difficult.

Replaceable redundant sensors are shown in Table A.2 along with cost data. Projected cost savings due to analytical redundancy are shown in Table A.3. The design philosophy taken in this study is not to replace these sensors but to view the cost savings as the price one pays to add a triple redundant set of mission critical sensors, i.e., P_m, Q_m, R_m, n_{z_m}, and n_{y_m} (subcritical).

Sensor reduction is not possible in all cases due to the existence of non-redundant outputs, e.g., U_m, α_m, h_m, ϕ_m, θ_m, or ψ_m, for the A-7D. Analytical redundancy provides a higher level of fail-safe reliability for these sensors.

TABLE A.1. CONCEPT COMPUTER COST COMPARISON

| Concept | Algorithm | Requirements | | Notes |
		Equivalent Adds	Total Memory (Words)	
I	Overhead	98	52	Uses multiple trip criteria monitor.
	$\dot{P}$	51	76	
	$\dot{Q}$	69	88	
	$\dot{R}$	61	76	
	$\dot{\alpha}$	115	110	
	$\dot{h}$	77	84	
	Totals*	471	486	
II	Overhead	81	77	Uses sequential likelihood ratio test. (Euler angle schemes are check combined for comparison with quaternion scheme below.)
	ϕ	121 ⎫	123 ⎫	
	θ	93 ⎬ 327	115 ⎬ 316	
	Ψ	113 ⎭	78 ⎭	
	h, α, n_z	180	112	
	n_y, P, R	436	324	
	Totals*	1024	829	
III	Overhead	81	77	Uses sequential likelihood ratio test.
	n_z, α, Q	457	560	
	n_y, P, R, ϕ	971	727	
	θ (Concept II)	93	115	
	Totals*	1602	1479	
Quaternion	Total	775	631	Compare with ϕ, θ, Ψ of Concept II.

*At an iteration rate of 20 per second, the remaining capacity of the A-7D HDC301 computer is approximately 3500 adds at 5 μsec/add and 1500 words.

142

TABLE A.2. A-7D SENSOR COST DATA

SENSOR	WT (lbs)	POWER RQMT (watts)	TYPICAL COST ($)
Normal Accelerometer (Bourns Inc.)	0.75	1	500
Lateral Accelerometer (Bourns Inc.)	1.0	1	500
Pitch & Yaw Rate Gyro (Lear-Seigler)	0.5 (each)	3.5 (each)	600 (each)
Roll Rate Gyro (Lear-Seigler)	0.5	3.5	600
Inertial Measurement Unit (ASN-50)	20	Unknown	Unknown
Air Data Computer-h, TAS (Air Research)	17	Unknown	Unknown

TABLE A.3. COST-EFFECTIVENESS ANALYSIS

Item	Concepts / Factors	Comparison Baseline System	Analytical Redundancy Concepts		
			Concept I	Concept II	Concept III
1	Computer Load (70 KOPS Available)	10.6 KOPS	10 KOPS	22 KOPS	35 KOPS
2	Memory (Words) (1500 Available)	481	471	829	1479
3	Sensor* Reduction		3 Rate Gyros 1 Normal Acceleration	3 Rate Gyros 1 Normal Acceleration 1 Lateral Acceleration	3 Rate Gyros 1 Normal Acceleration 1 Lateral Acceleration
4	Weight Reduction (lbs)		2.25	3.25	3.25
5	Power Reduction (watts)		11.5	12.5	12.5
6	Hardware Cost Reduction		$2,300	$2,800	$2,800

*Reduction assumes only one angle-of-attack indicator (i.e., A-7D). In cases where two exist, one could be eliminated.

143

APPENDIX B

SIMULATION DESCRIPTION

B.1 INTRODUCTION

A six-degree-of-freedom real-time simulation of the A-7D aircraft and control system was implemented on a PACER 700 hybrid computing system. The PACER system is comprised of a digital computer (16K memory, 32-bit word) with teletype, card reader, line printer and moving head disk, two parallel analog processors, and an interface providing data exchange capabilities between analog and digital. Additional data channels allow interfacing with external processors such as the Sigma 5 hybrid computing system. Figure B.1 provides a functional block diagram of how the PACER 700 is integrated with the Sigma 5.
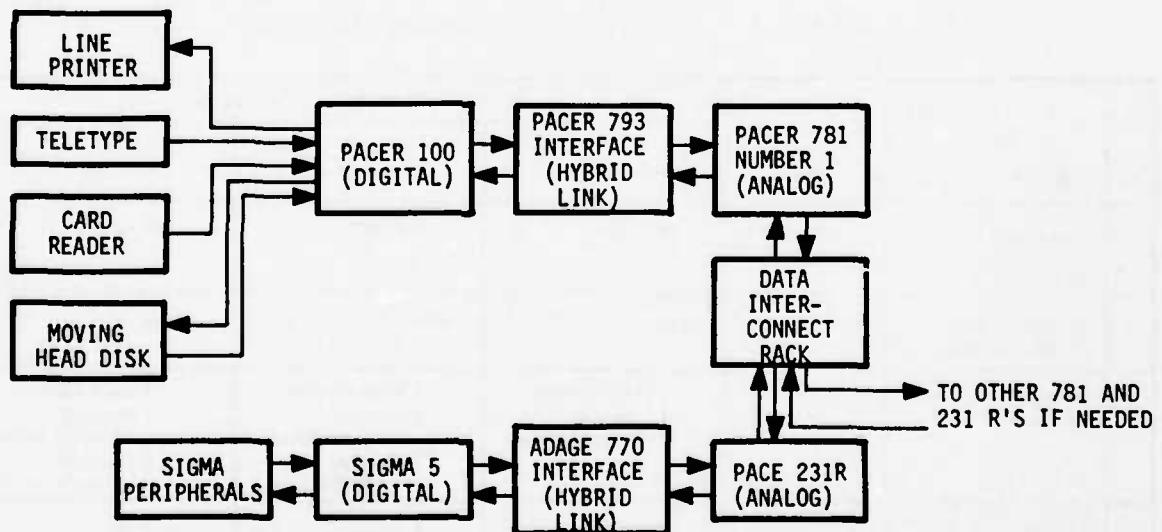
Figure B.1.   PACER 700 Computing System Interfaced with SIGMA 5

The real-time aircraft was implemented on the hybrid computer in a way that best utilized the high-speed characteristics of an analog and the accuracy and data storage capability of a digital computer. An all-digital aircraft simulation would require a sample rate of less than 10 cycles/second to process data in a real time frame, while an all-analog simulation is inherently less accurate and more cumbersome to initialize. By programming the higher frequency components of the equations of motion on the analog and using the digital subsystem for lower frequency computations, an accurate real-time simulation with a digital sample rate of 20 cycles/second was achieved. Figure B.2 is a block diagram of the A-7D simulation showing the digital/analog partitioning.

B.2 HYBRID IMPLEMENTATION

The digital computer, programmed with Fortran, is used to store aerodynamic data tables, provide function table look-ups of the aerodynamic coefficients, and process low-frequency aircraft dynamics. It computes earth axis aircraft velocities ($\dot{X}$, $\dot{Y}$, $\dot{h}$) and integrates to position (X, Y, h). Euler angles (ϕ, θ, ψ) are computed via quaternion integration. Other computed parameters are flight path and heading angles (γ, χ). Digital routines are also used to provide data input/output capabilities, initialize the simulation, compute initial trim conditions, and provide master control over the entire simulation. A subroutine which inputs programmed maneuvers to the control system was added before making final production runs to ensure consistency between runs.

The analog subsystem computes all aerodynamic forces and moments and evaluates the equations of motion for $\dot{u}$, $\dot{v}$, $\dot{w}$, $\dot{p}$, $\dot{q}$, and $\dot{r}$. Analog integration of these accelrations provides the corresponding translational and rotational velocities. Other aircraft parameters, angle-of-attack, sideslip angle, attack-of-angle rate, and total velocity (α, β, $\dot{\alpha}$, V_T) are computed on the analog computer. An analog control system provides basic rate and acceleration feedbacks to the actuators. Models of the pilot stick dynamics are also implemented in the pitch and roll axes. Block diagrams of the control system are shown in Figures B.3, B.4, and B.5.

B.3 PROGRAM CONTROL

The PACER 100 digital computer provides master control of the entire simulation. Figure B.6 shows how the digital control ties all pieces of the simulation together. By selecting sense switches on the computer consoles, the operator can start and stop the simulation, request new runs at the previous flight condition (RERUN), or change data

Figure B. 2. A-7D Hybrid Simulation Block Diagram

146
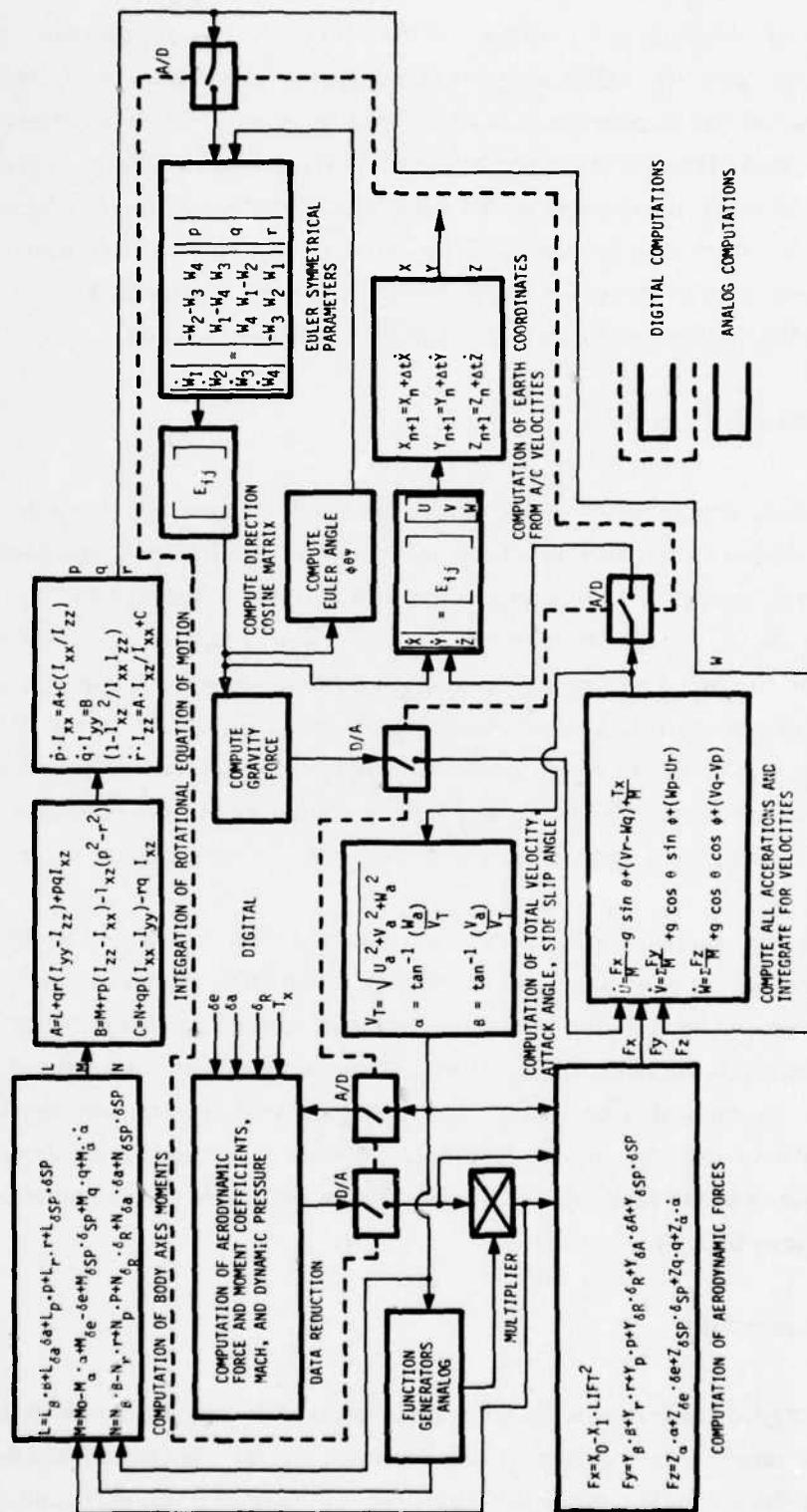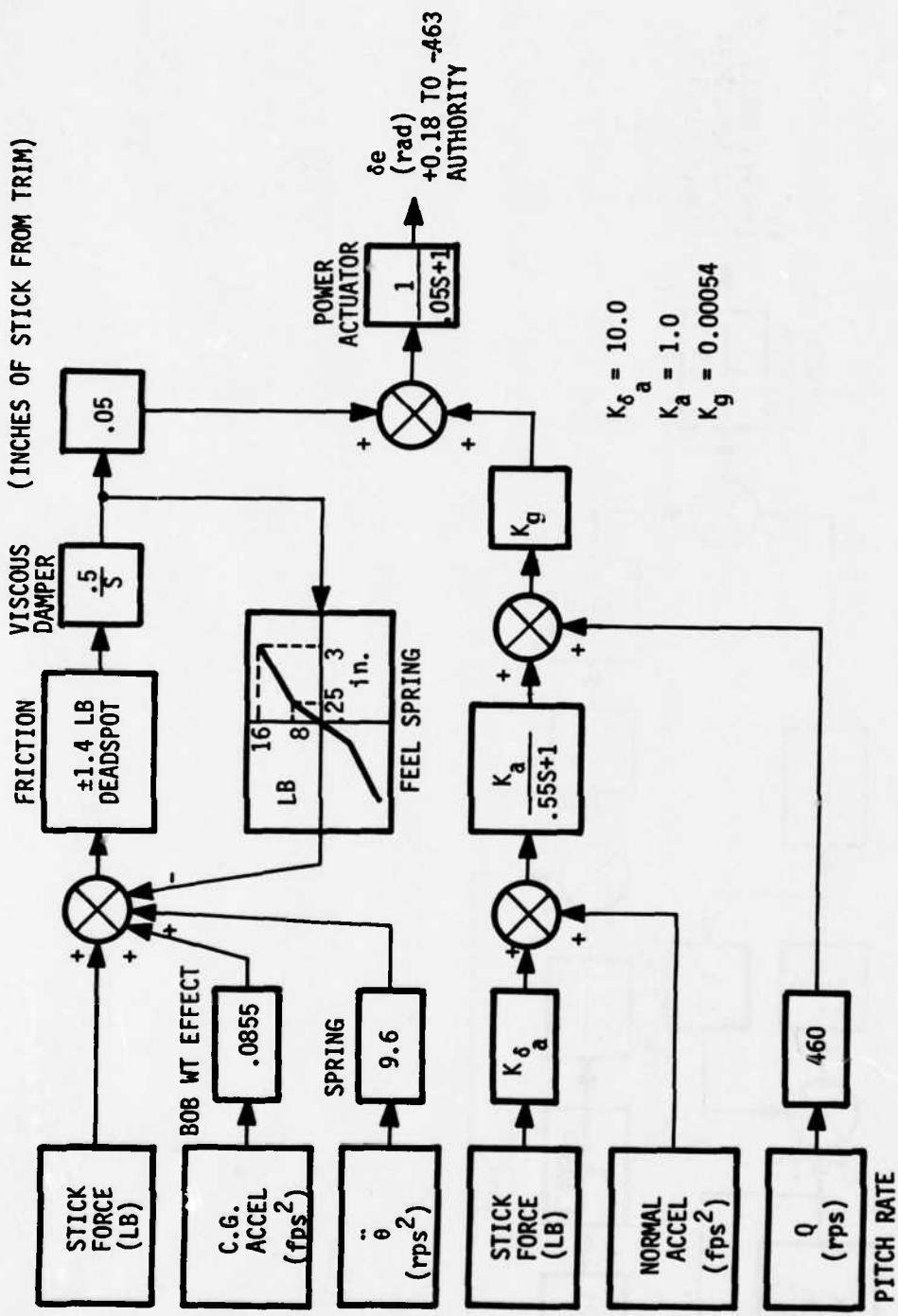
Figure B.3. Pitch Axis Control Laws for A-7D Aircraft Simulation
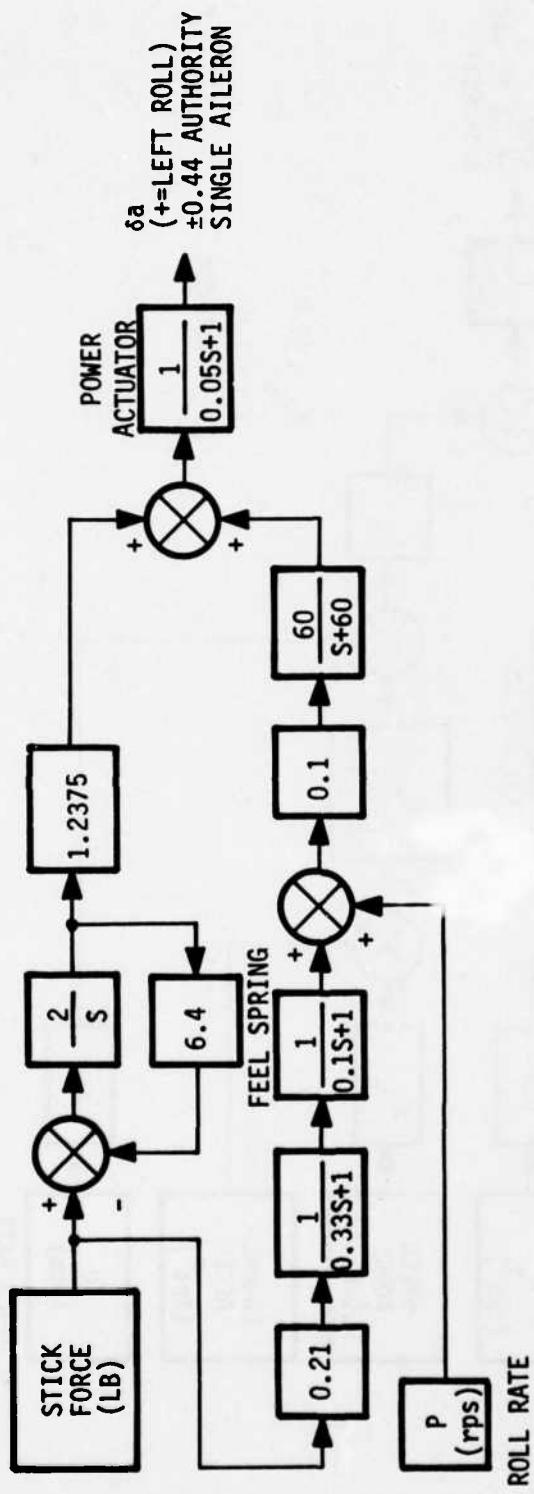
Figure B.4. Roll Axis Control Laws for A-7D Aircraft Simulation

148
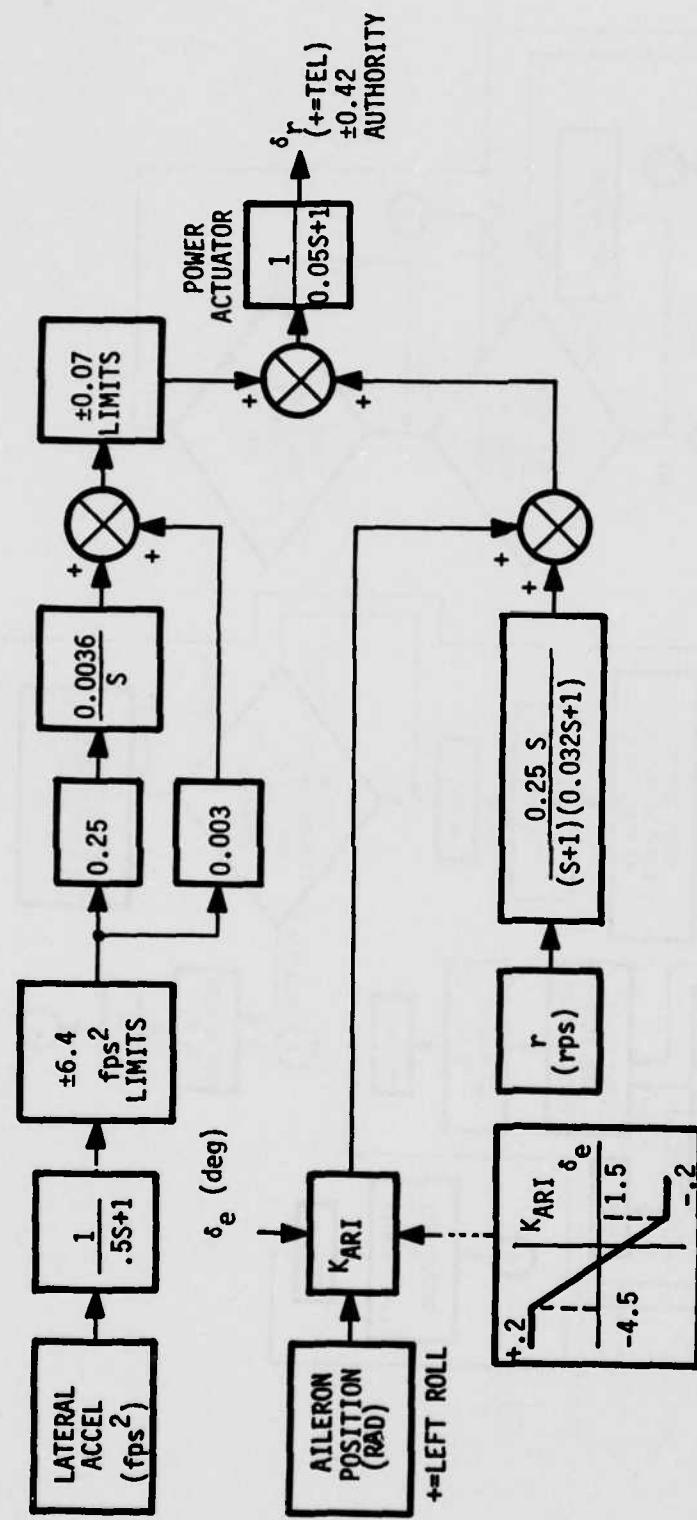
Figure B.5. Yaw Axis Control Laws for A-7D Aircraft Simulation

149
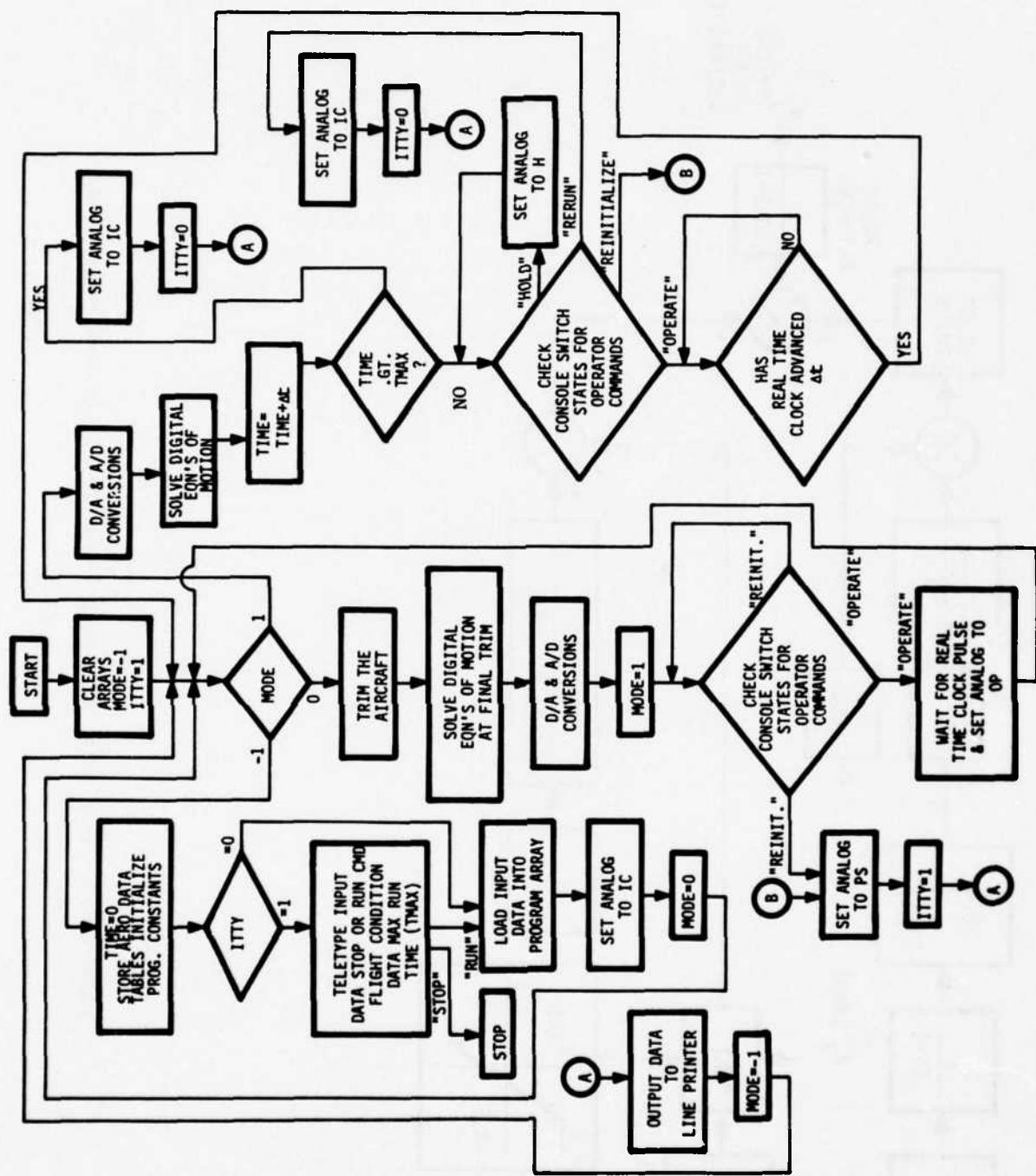
Figure B. 6. Program Operational Control Block Diagram for A-7D Simulation

150

for new runs (REINIT). An option for stopping and continuing the same run is also provided (HOLD). The controller responds to the operator commands by switching the analog into "PS" (pot set), "IC" (initial condition), "H" (hold), or "OP" (operate), and then branches to appropriate digital routines.

During initialization, the aerodynamic data tables are stored in memory and program constants are set. At this point new data can be entered through the console teletype; the minimum data for the first run require an initial altitude, velocity, and maximum run time. Communication within the system is accomplished through a single array which is common to all subroutines including the input and output routines. An iterative trim routine is used to set initial conditions on angle-of-attack, elevator position, and thrust.

Once the operate mode is entered, a computer cycle consists of momentarily "freezing" the A/D channels (not the analog) while data conversion is performed, followed by processing the digital equations of motion. Simulation time is updated and tests for run termination are performed. These computations require approximately 35 to 40 milliseconds. The computer is then cycled through a tight loop while waiting for a pulse from the real-time clock (every 50 msec), thus establishing real-time digital processing. The analog, of course, processes continuously during each and every digital cycle.

APPENDIX C

SENSOR FAULT DETECTION WITH QUATERNIONS

Euler angles (ϕ, θ, ψ) and body rates (P, Q, R) have well-defined relationships (see Equations (7) through (12)). The foregoing development uses quaternions to employ another set of relationships which offer some advantages over the standard equations.

C.1 ATTITUDE ESTIMATION AND FAULT DETECTION WITH QUATERNIONS

The use of generalized coordinates or quaternions for solving Euler angle rotations offers an alternate approach to construction of a Kalman filter innovations process. This provides an alternate approach for detecting faults in body angular rates and Euler angles.

Using definitions and (for the most part) development of Deyst and Deckert (Reference 37) and defining an attitude quaternion which rotates a vector from Reference Frame 1 to 2 as q_2^1, the following relationships can be observed:

$$q_3^1 = q_2^1 \; q_3^2 \tag{C1}$$

$$q_2^1 = q_3^1 \, (q_3^2)^* \tag{C2}$$

or

$$q_3^2 = (q_2^1)^* \; q_3^1 \tag{C3}$$

(* implies conjugate)

The error between the estimated body frame, $\overline{B}$, and the actual body frame, B, can be written as

$$q_B^{\overline{B}} = (q_{\overline{B}}^I)^* \; q_B^I \tag{C4}$$

where "I" is the inertial reference frame.

If the estimated body frame is close to the real body frame, then the estimation error quaternion is

$$q_B^{\overline{B}} = 1 + \frac{1}{2} \underline{e} \, \zeta \tag{C5}$$

$\underline{e}_\xi$ is a three-state vector

$$\underline{e}_\xi{}^T = (\bar{\phi}_b, \ \bar{\theta}_b, \ \bar{\psi}_b) \tag{C6}$$

where

$\bar{\phi}_b, \ \bar{\theta}_b, \ \bar{\psi}_b$ are small rotation angles from the estimated body frame to the actual
body frame

The error angles propagate according to

$$\underline{e}_\xi(t_{k+1}) = \underline{e}_\xi(t_k) + \underline{e}_\omega(t_k) \Delta T \tag{C7}$$

where

$\underline{e}_\omega$ is the body axis rotational velocity error

ΔT is the time increment

t_k is the current time

For our purposes, we can assume $\underline{e}_\omega$ is the noise term in the body rate gyros, i.e.,

$$\underline{e}_\omega \sim N(O, \ Q_e) \ \underline{white} \tag{C8}$$

In order to properly construct a Kalman filter, it is necessary to provide additional
quaternions for the filter to operate on. One is

$$q_{\tilde{B}}^{\bar{B}}$$

where

$\bar{B}$ is the estimated body frame before measurement update

$\tilde{B}$ is the measured body frame

This can be obtained by performing the following quaternion multiplication:

$$q_{\tilde{B}}^{\bar{B}} = (q_{\bar{B}}^I)^* \ q_{\tilde{B}}^I \tag{C9}$$

$q_{\tilde{B}}^I$ is available from the measuring device (attitude reference system or inertial measure-
ment unit). $q_{\bar{B}}^I$ is properly derived by integrating the upgraded previous quaternion, $q_{\hat{B}}^I$,
where $\hat{B}$ is the updated body estimate, i.e., newest measurement incorporated. This can
be accomplished by examining the quaternion differential equation. In continuous time

153

$$\underline{\dot{\lambda}} = A\underline{\lambda} \tag{C10}$$

$\underline{\lambda}$ is a four-state vector composed of elements of q_B^I, i.e.,

$$q_B^I \triangleq \lambda_0 + \lambda_1 \underline{i} + \lambda_2 \underline{j} + \lambda_3 \underline{k} \tag{C11}$$

where

$\underline{i}, \underline{j}, \underline{k}$ are unit basis elements

This is equivalent to

$$\underline{\lambda}^T \triangleq (\lambda_0, \lambda_1, \lambda_2, \lambda_3) \tag{C12}$$

$$A \triangleq -\frac{1}{2} \begin{bmatrix} O & P & Q & R \\ -P & O & -R & Q \\ -Q & R & O & -P \\ -R & -Q & P & O \end{bmatrix} \tag{C13}$$

Then

$$e^{A\Delta T} \triangleq \sum_{i=0}^{\infty} \frac{1 c^i \Delta T^{2i}}{(2i)!} I + \sum_{j=0}^{\infty} \frac{c^j \Delta T^{2j}}{(2j+1)!} A\Delta T \tag{C14}$$

where

$$c = -\frac{1}{4} (P^2 + Q^2 + R^2)/t_n \tag{C15}$$

t_n = time at the nth sample

This demonstrates the fairly easy way one can expand $e^{A\Delta T}$ into a sufficiently large number of terms by expanding two scalar power series. The result is that the prediction step can be carried out simply:

$$\lambda(t_{n+1}) = e^{A\Delta T} \lambda(t_n) \tag{C16}$$

This results in $q_{\overline{B}}^I (t_{n+1})$ from $q_{\hat{B}}^I (t_n)$ to complete the iteration

$$q_{\hat{B}}^I = q_{\overline{B}}^I q_{\hat{B}}^{\overline{B}} \tag{C17}$$

where $q_{\hat{B}}^{\overline{B}}$ is calculated with a Kalman filter applied to $q_{\overline{B}}^{\overline{B}}$. $q_{\overline{B}}^{\overline{B}}$ can be written

$$q_B^{\overline{B}} = 1 + \frac{1}{2} \underline{\tilde{e}}_\xi \tag{C18}$$

154

where

$$\underline{\mathfrak{T}}_\xi^{\ T} = (\tilde{\phi}_b, \ \tilde{\theta}_b, \ \tilde{\psi}_b) \text{ and } (1)^T = [1, \ \tilde{\phi}_b, \ \tilde{\theta}_b, \ \tilde{\psi}_b] \tag{C19}$$

Equation (C7) allows the filtering problem to be handled completely decoupled, i.e., three first-order filters. Defining the measurement error covariance

$$R_s(t_n) = \begin{bmatrix} R_\phi(t_n) & 0 & 0 \\ 0 & R_\theta(t_n) & 0 \\ 0 & 0 & R_\psi(t_n) \end{bmatrix} \tag{C20}$$

the error covariance (before measurement)

$$M_s(t_n) = \begin{bmatrix} M_\phi(t_n) & 0 & 0 \\ 0 & M_\theta(t_n) & 0 \\ 0 & 0 & M_\psi(t_n) \end{bmatrix} \tag{C21}$$

and the error covariance (after measurement)

$$P_s(t_n) = \begin{bmatrix} P_\phi(t_n) & 0 & 0 \\ 0 & P_\theta(t_n) & 0 \\ 0 & 0 & P_\psi(t_n) \end{bmatrix} \tag{C22}$$

the quantity $q_{\hat{B}}^{\overline{B}}$ becomes (Reference 37)

$$q_{\hat{B}}^{\overline{B}} = 1 - \frac{1}{4} \left[(P_\phi \tilde{\phi}_b / R_\phi)^2 + (P_\theta \tilde{\theta}_b / R_\theta)^2 + (P_\psi \tilde{\psi}_b / R_\psi)^2 \right]$$
$$+ \frac{1}{2} \left[\underline{i} P_\phi \tilde{\phi}_b / R_\phi + \underline{j} P_\theta \tilde{\theta}_b / R_\theta + \underline{k} P_\psi \tilde{\psi}_b / R_\psi \right] \tag{C23}$$

C.2 SIGNIFICANCE OF FORMULATION

The above representation has a number of features which make it inviting for analytical redundancy:

- It has a computationally simple filter although it has a higher order filter than a design based on standard relationships.

155

- It has increased stability.

- The scheme theoretically isolates body rates for individual residual fault detection (practical results are needed, however, to verify this).

APPENDIX D

SIMULATION STRIP CHARTS

This appendix contains a set of outputs in strip chart form for the fault runs on each of the three concepts. The strip charts show the following:

- **Flight Condition**

  $1 \Rightarrow h = 1000$ ft, $V_{AS} = 335.1$ fps (low $\bar{q}$)

  $2 \Rightarrow h = 15000$ ft, $V_{AS} = 750$ fps (medium $\bar{q}$)

  $3 \Rightarrow h = 2000$ ft, $V_{AS} = 1005$ fps (high $\bar{q}$)

- **Maneuver**--Pilot commands for either pitch or roll maneuvers.

- **Failed Sensor**--Either accelerometers (n_z, n_y), rate gyros (p, q, r), attitude sensors (ϕ, θ, ψ, α), airspeed indicator (V_{AS}), or altimeter (h).

- **Failure Types**

  $\pm$ H.O. $\Rightarrow$ Hardover--output is maximum reading for a given sensor.

  D $\Rightarrow$ Dead sensor--output is zero.

  B $\Rightarrow$ Bias error--output has a ramp bias.

  S.F.-L $\Rightarrow$ Low scale factor error--output equals 0.75 actual.

  S.F.-H $\Rightarrow$ High scale factor error--output equals 0.5 actual.

  D.R. $\Rightarrow$ Dynamic response--all signals low pass filtered at 1.0 rad/sec.

Table D.1 defines some special nomenclature used in labeling Figures D.1 through D.156. Tables D.2, D.3, and D.4 provide figure information concerning concept tested, maneuver, and fault inserted.

TABLE D.1 STRIP CHART LABELS

Strip Chart Label	Parameter	Definition
NZ	n_z	Normal Acceleration (actual)
NZM	n_{z_m}	Normal Acceleration (sensor reading)
Q	Q	Pitch Rate (actual)
QM	Q_m	Pitch Rate (sensor reading)
THETA	θ	Euler Pitch Angle (actual)
THETAM	θ_m	Euler Pitch Angle (sensor reading)
ALPHA	α	Angle-of-Attack (actual)
ALPHAM	α_m	Angle-of-Attack (sensor reading)
H	H	Altitude (actual)
HM	H_m	Altitude (sensor reading)
P	P	Roll Rate (actual)
PM	P_m	Roll Rate (sensor reading)
PHI	ϕ	Euler Roll Angle (actual)
PHIM	ϕ_m	Euler Roll Angle (sensor reading)
R	R	Yaw Rate (actual)
RM	R_m	Yaw Rate (sensor reading)
PSI	ψ	Euler Yaw Angle (actual)
PSIM	ψ_m	Euler Yaw Angle (sensor reading)
U	U	Velocity along X-axis (actual)
UM	U_m	Velocity along X-axis (sensor reading)
V P $\Big\}$ V Q $\Big\}$ V R $\Big\}$ etc.	v_p $\Big\}$ v_q $\Big\}$ v_r $\Big\}$	Residual Outputs from AR Computations

158

TABLE D.2 STRIP CHART RUN LEGEND--CONCEPT I

Figure Number	AR Test Concept	Flight Condition	Maneuver	Failed Sensor	Failure Type *
D.1	1	2	NONE	n_z	H.O.
D.2	1	2	NONE	n_z	D
D.3	1	2	PITCH	n_z	D
D.4	1	2	PITCH	n_z	D.R.
D.5	1	2	NONE	n_z	B
D.6	1	2	PITCH	n_z	S.F.
D.7	1	2	NONE	q	+H.O.
D.8	1	2	PITCH	q	D
D.9	1	2	NONE	q	B
D.10	1	2	PITCH	q	S.F.-L
D.11	1	2	PITCH	q	S.F.-L
D.12	1	2	PITCH	q	S.F.-H
D.13	1	2	NONE	θ	+H.O.
D.14	1	2	NONE	θ	D
D.15	1	2	NONE	θ	B
D.16	1	2	PITCH	θ	S.F.-L
D.17	1	2	NONE	θ	S.F.-H
D.18	1	1	NONE	α	+H.O.
D.19	1	1	PITCH	α	D
D.20	1	1	NONE	α	B
D.21	1	1	PITCH	α	S.F.-L
D.22	1	1	PITCH	α	S.F.-H
D.23	1	1	NONE	h	-H.O.
D.24	1	1	NONE	h	B
D.25	1	2	ROLL	p	+H.O.
D.26	1	2	ROLL	p	-H.O.
D.27	1	2	ROLL	p	D
D.28	1	2	NONE	p	B
D.29	1	2	ROLL	p	S.F.-L
D.30	1	2	ROLL	p	S.F.-H

*H.O. = Hardover, D = Dead, D.R. = Dynamic Response, B = Bias, S.F. = Scale Factor, L = 25% S.F., H = 50% S.F.

159

TABLE D.2 STRIP CHART RUN LEGEND--CONCEPT I (concluded)

Figure Number	AR Test Concept	Flight Condition	Maneuver	Failed Sensor	Failure Type*
D.31	1	2	ROLL	φ	+H.O.
D.32	1	2	ROLL	φ	D
D.33	1	2	NONE	φ	B
D.34	1	2	ROLL	φ	S.F.-L
D.35	1	2	ROLL	φ	S.F.-H
D.36	1	2	NONE	r	+H.O.
D.37	1	2	ROLL	r	D
D.38	1	2	NONE	r	B
D.39	1	2	ROLL	r	S.F.-L
D.40	1	2	ROLL	r	S.F.-H
D.41	1	2	NONE	ψ	+H.O.
D.42	1	2	ROLL	ψ	D
D.43	1	2	NONE	ψ	B
D.44	1	2	ROLL	ψ	S.F.-L
D.45	1	2	ROLL	ψ	S.F.-H

*H.O. = Hardover, D = Dead, D.R. = Dynamic Response, B = Bias, S.F. = Scale Factor, L = 25% S.F., H = 50% S.F.

TABLE D.3 STRIP CHART RUN LEGEND--CONCEPT II

Figure Number	AR Test Concept	Flight Condition	Maneuver	Failed Sensor	Failure Type*
D.46	2	3	NONE	n_z	+H.O.
D.47	2	3	NONE	n_z	-H.O.
D.48	2	3	PITCH	n_z	D
D.49	2	3	NONE	n_z	D.R.
D.50	2	3	PITCH	n_z	D.R.
D.51	2	2	NONE	n_z	B
D.52	2	2	PITCH	n_z	S.F.-L
D.53	2	2	PITCH	n_z	S.F.-H
D.54	2	2	PITCH	n_z	S.F.-H
D.55	2	2	NONE	q	+H.O.
D.56	2	2	NONE	q	-H.O.
D.57	2	2	NONE	q	D
D.58	2	2	PITCH	q	D
D.59	2	2	PITCH	q	D
D.60	2	2	NONE	q	B
D.61	2	2	NONE	q	S.F.-L
D.62	2	2	PITCH	q	S.F.-H
D.63	2	2	PITCH	q	S.F.-L
D.64	2	2	NONE	θ	+H.O.
D.65	2	2	PITCH	θ	D
D.66	2	2	NONE	θ	B
D.67	2	2	PITCH	θ	S.F.-L
D.68	2	2	PITCH	θ	S.F.-H
D.69	2	1	NONE	α	+H.O.
D.70	2	1	NONE	α	-H.O.
D.71	2	1	NONE	α	D
D.72	2	1	NONE	α	B
D.73	2	1	PITCH	α	S.F.-L
D.74	2	1	PITCH	α	S.F.-H
D.75	2	1	NONE	h	-H.O.

---

*H.O. = Hardover, D = Dead, D.R. = Dynamic Response, B = Bias, S.F. = Scale Factor, L = 25% S.F., H = 50% S.F.

TABLE D.3 STRIP CHART RUN LEGEND--CONCEPT II (continued)

Figure Number	AR Test Concept	Flight Condition	Maneuver	Failed Sensor	Failure Type*
D.76	2	1	NONE	h	B
D.77	2	1	NONE	h	D
D.78	2	1	NONE	V_{AS}	+H.O.
D.79	2	1	NONE	V_{AS}	+H.O.
D.80	2	1	NONE	V_{AS}	-H.O.
D.81	2	1	NONE	V_{AS}	D
D.82	2	2	ROLL	p	+H.O.
D.83	2	2	ROLL	p	-H.O.
D.84	2	2	ROLL	p	D
D.85	2	2	NONE	p	B
D.86	2	2	ROLL	p	S.F.-L
D.87	2	2	ROLL	p	S.F.-H
D.88	2	2	NONE	ϕ	+H.O.
D.89	2	2	ROLL	ϕ	+H.O.
D.90	2	2	ROLL	ϕ	-H.O.
D.91	2	2	ROLL	ϕ	D
D.92	2	2	NONE	ϕ	B
D.93	2	2	ROLL	ϕ	S.F.-L
D.94	2	2	ROLL	ϕ	S.F.-H
D.95	2	2	ROLL	r	+H.O.
D.96	2	2	ROLL	r	-H.O.
D.97	2	2	ROLL	r	+H.O.
D.98	2	2	ROLL	r	-H.O.
D.99	2	2	ROLL	r	D

*H.O. = Hardover, D = Dead, D.R. = Dynamic Response, B = Bias, S.F. = Scale Factor, L = 25% S.F., H = 50% S.F.

TABLE D.3 STRIP CHART RUN LEGEND--CONCEPT II (concluded)

Figure Number	AR Test Concept	Flight Condition	Maneuver	Failed Sensor	Failure Type*
D.100	2	2	ROLL	r	D
D.101	2	2	NONE	r	B
D.102	2	2	ROLL	r	S.F.-L
D.103	2	2	ROLL	r	S.F.-H
D.104	2	2	ROLL	ψ	+H.O.
D.105	2	2	ROLL	ψ	-H.O.
D.106	2	2	ROLL	ψ	D
D.107	2	2	ROLL	ψ	D
D.108	2	2	NONE	ψ	B
D.109	2	2	ROLL	ψ	S.F.-L
D.110	2	3	ROLL	n_y	-H.O.
D.111	2	3	ROLL	n_y	+H.O.
D.112	2	3	ROLL	n_y	D
D.113	2	3	NONE	n_y	B
D.114	2	3	ROLL	n_y	S.F.-L
D.115	2	3	ROLL	n_y	S.F.-H
D.116	2	3	ROLL	n_y	D.R.

*H.O. = Hardover, D = Dead, D.R. = Dynamic Response, B = Bias, S.F. = Scale Factor, L = 25% S.F., H = 50% S.F.

163

TABLE D.4 STRIP CHART LEGEND--CONCEPT III

Figure Number	AR Test Concept	Flight Condition	Maneuver	Failed Sensor	Failure Type*
D. 117	3	3	NONE	n_z	+H. O.
D. 118	3	3	PITCH	n_z	D
D. 119	3	3	PITCH	n_z	D
D. 120	3	3	PITCH	n_z	D
D. 121	3	3	PITCH	n_z	D
D. 122	3	3	PITCH	n_z	D. R.
D. 123	3	3	PITCH	n_z	S. F. -L
D. 124	3	3	PITCH	n_z	S. F. -H
D. 125	3	2	NONE	q	+H. O.
D. 126	3	2	PITCH	q	D
D. 127	3	2	PITCH	q	D
D. 128	3	2	PITCH	q	D
D. 129	3	2	PITCH	q	D
D. 130	3	2	PITCH	q	S. F. -L
D. 131	3	2	PITCH	q	S. F. -H
D. 132	3	1	PITCH	α	+H. O.
D. 133	3	1	NONE	α	D
D. 134	3	1	NONE	α	S. F. -L
D. 135	3	2	ROLL	p	+H. O.
D. 136	3	2	ROLL	p	D
D. 137	3	2	ROLL	p	-H. O.
D. 138	3	2	ROLL	p	S. F. -L

---

*H. O. = Hardover, D = Dead, D. R. = Dynamic Response, B = Bias, S. F. = Scale Factor,
L = 25% S. F. , H = 50% S. F.

TABLE D.4 STRIP CHART LEGEND--CONCEPT III (concluded)

Figure Number	AR Test Concept	Flight Condition	Maneuver	Failed Sensor	Failure Type*
D.139	3	2	ROLL	r	+H.O.
D.140	3	2	ROLL	r	-H.O.
D.141	3	2	ROLL	r	D
D.142	3	2	ROLL	r	S.F.-L
D.143	3	2	ROLL	r	S.F.-H
D.144	3	3	ROLL	n_y	-H.O.
D.145	3	3	ROLL	n_y	+H.O.
D.146	3	3	ROLL	n_y	S.F.-L
D.147	3	3	ROLL	n_y	D
D.148	3	3	ROLL	n_y	D.R.
D.149	3	3	NONE	n_y	-H.O.
D.150	3	3	NONE	n_y	+H.O.
D.151	3	3	NONE	p	D
D.152	3	3	ROLL	p	D
D.153	3	3	ROLL	p	S.F.-L
D.154	3	3	ROLL	p	S.F.-H
D.155	3	3	ROLL	n_y	-H.O.
D.156	3	3	ROLL	n_y	+H.O.

*H.O. = Hardover, D = Dead, D.R. = Dynamic Response, B = Bias, S.F. = Scale Factor, L = 25% S.F., H = 50% S.F.

Figure D.1

Figure D. 2

167

Figure D. 3

168

Figure D. 4

169

Figure D.5

170

Figure D. 6

Figure D. 7

172

Figure D. 8

173

Figure D. 9

Figure D.10

175

Figure D. 11

176

Figure D. 12

177

Figure D.13

178

Figure D. 14

179

Figure D. 15

Figure D. 16

Figure D. 17

182

Figure D. 18

Figure D. 19

184

Figure D. 20

Figure D. 21

186

Figure D. 22

187

Figure D.23

Figure D. 24

189

Figure D. 25

Figure D. 26

Figure D. 27

Figure D. 28

Figure D. 29

194

Figure D. 30

Figure D. 31

Figure D. 32

Figure D.33

198

Figure D. 34

199
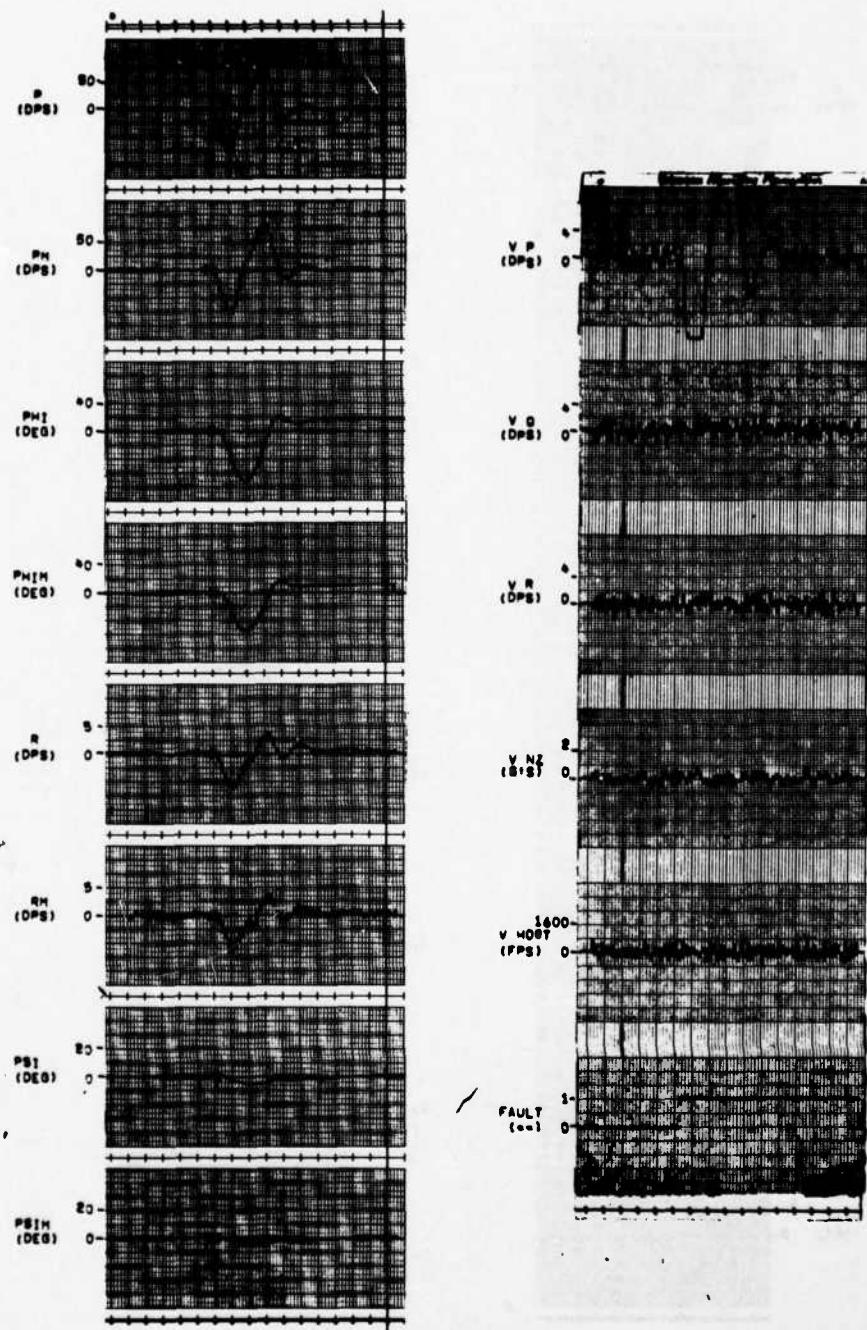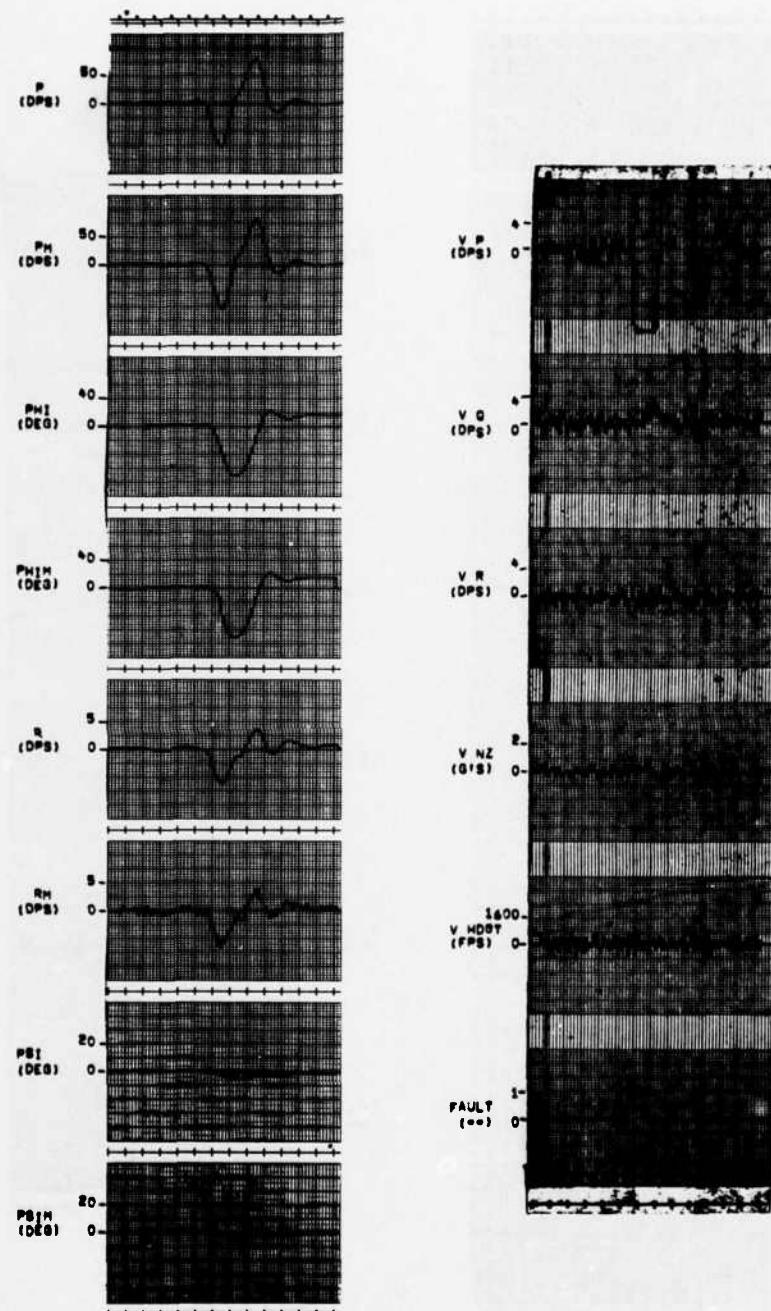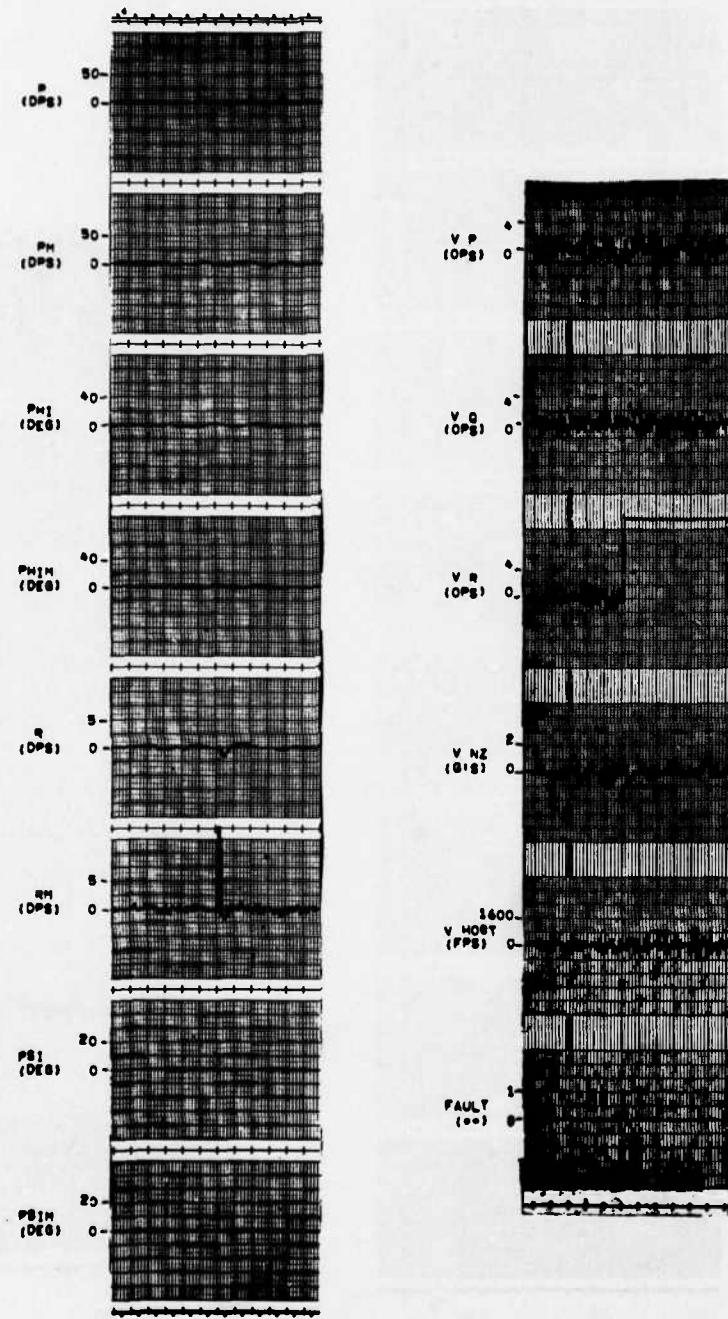
Figure D. 35

Figure D. 36
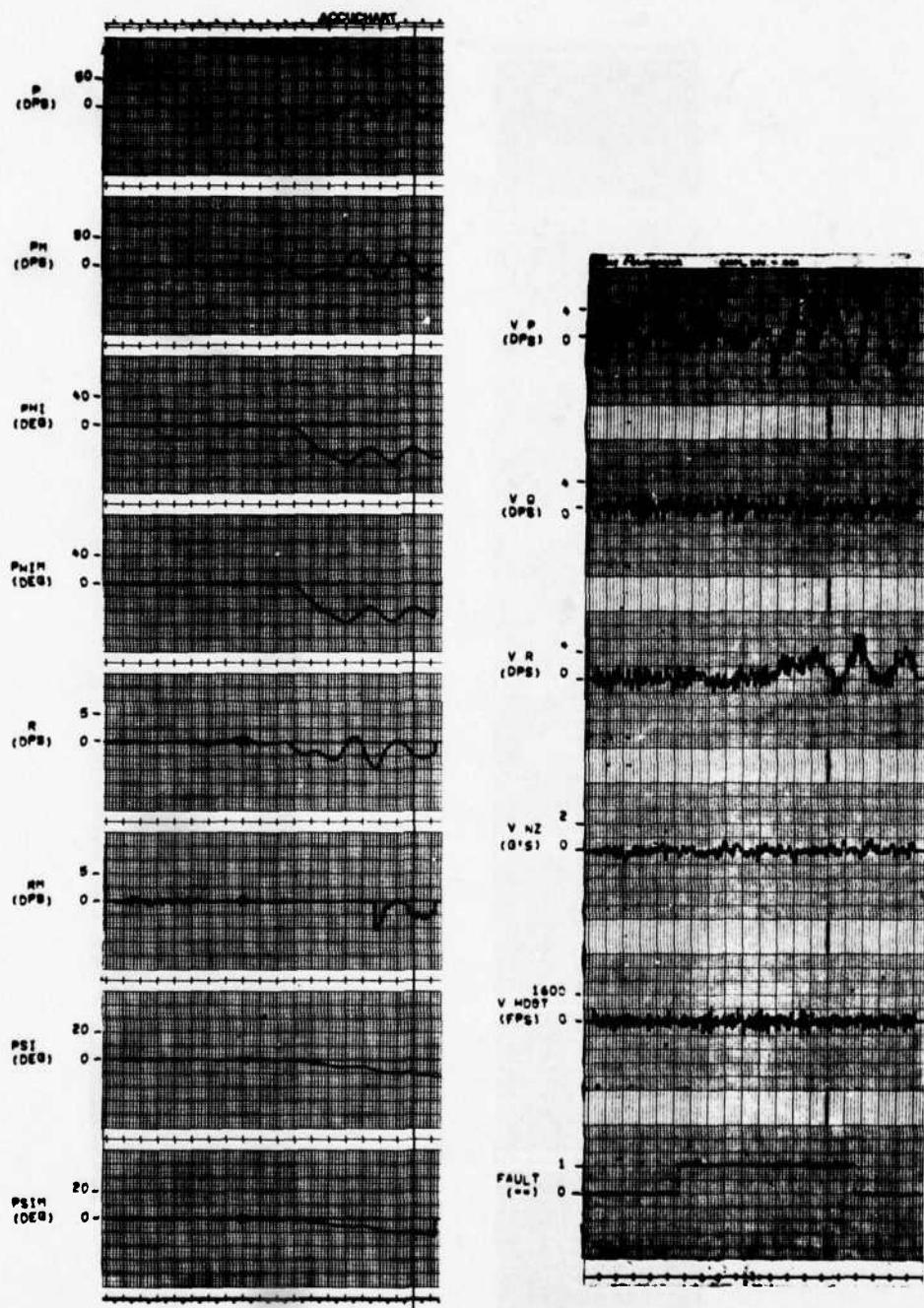
Figure D. 37
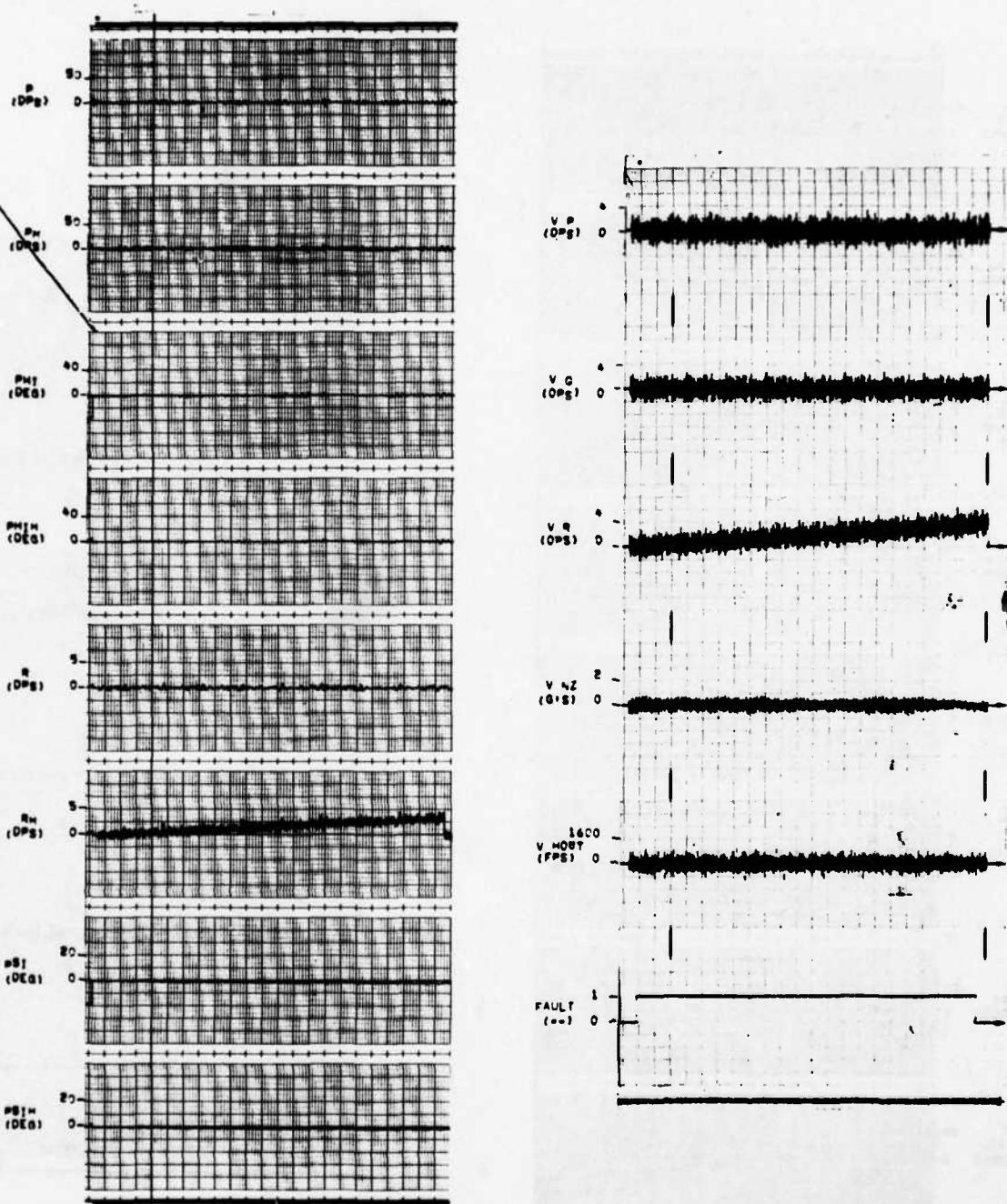
Figure D. 38

Figure D.39

204
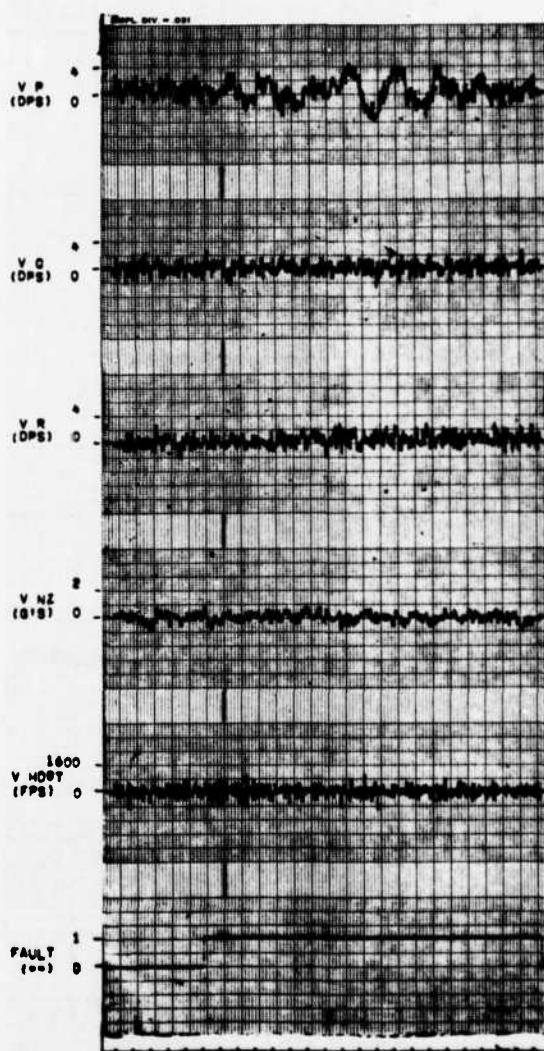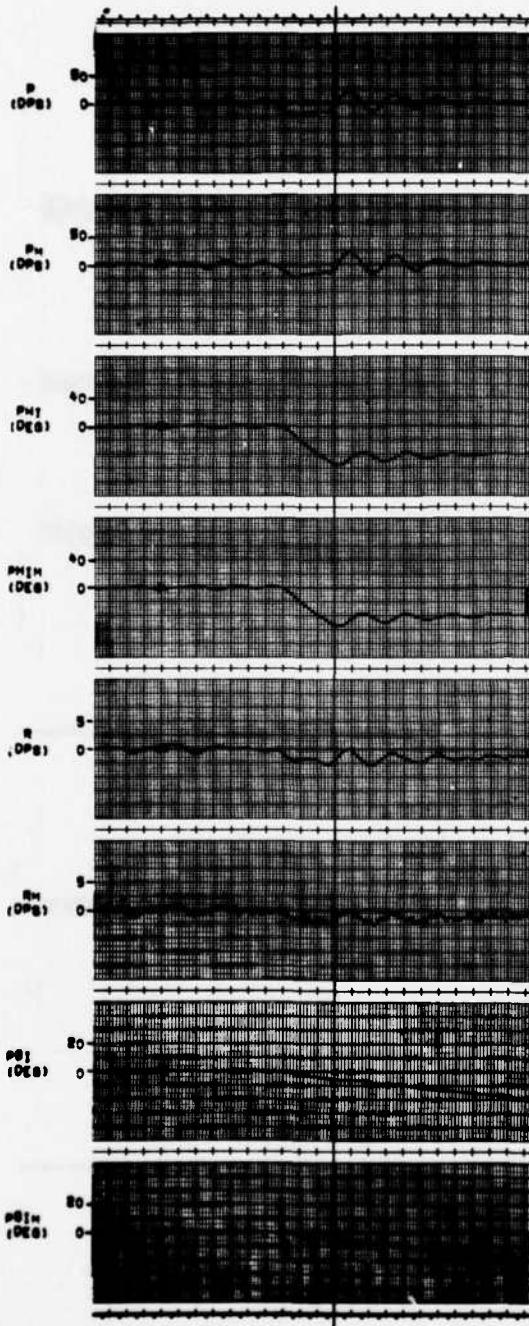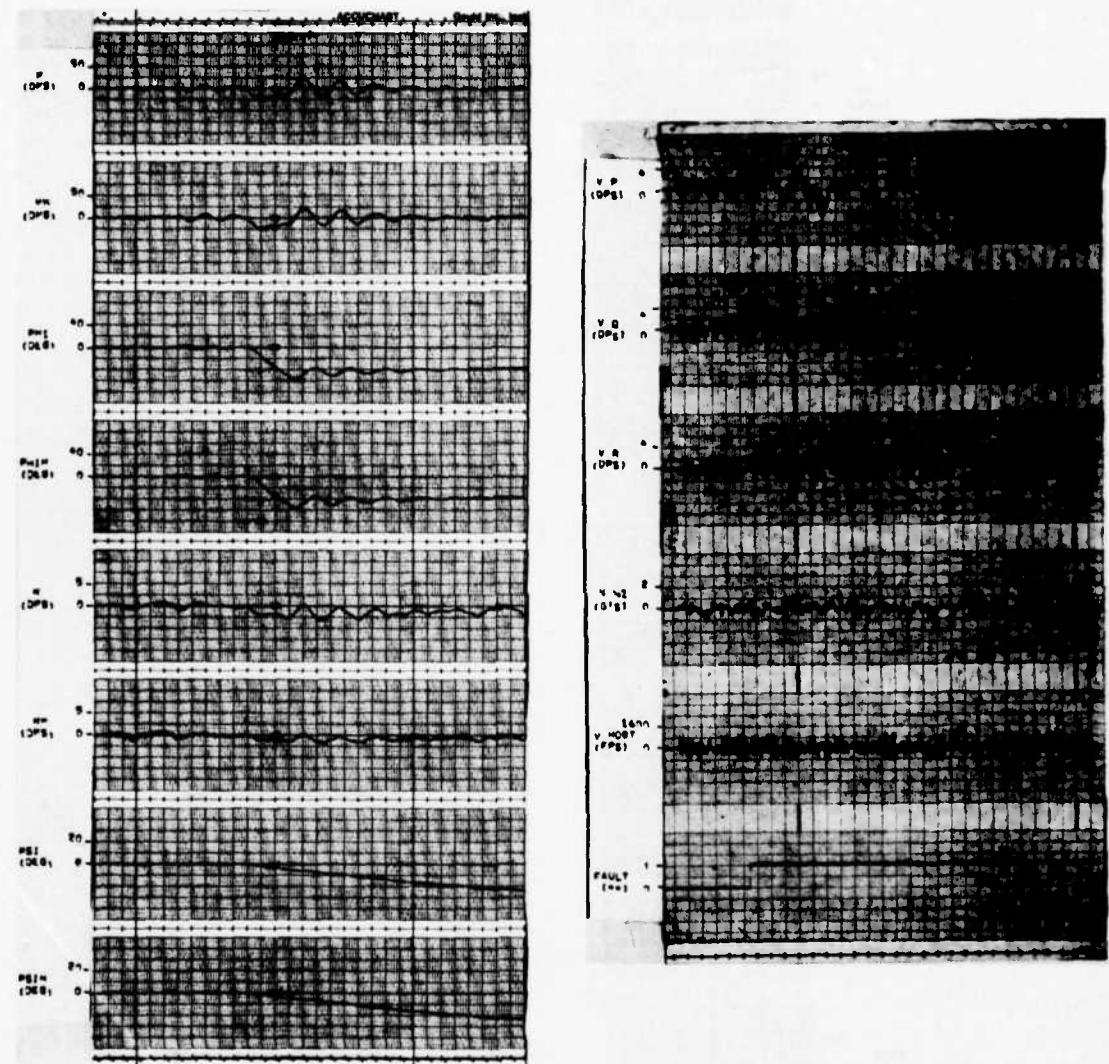
Figure D. 40

Figure D. 41

206
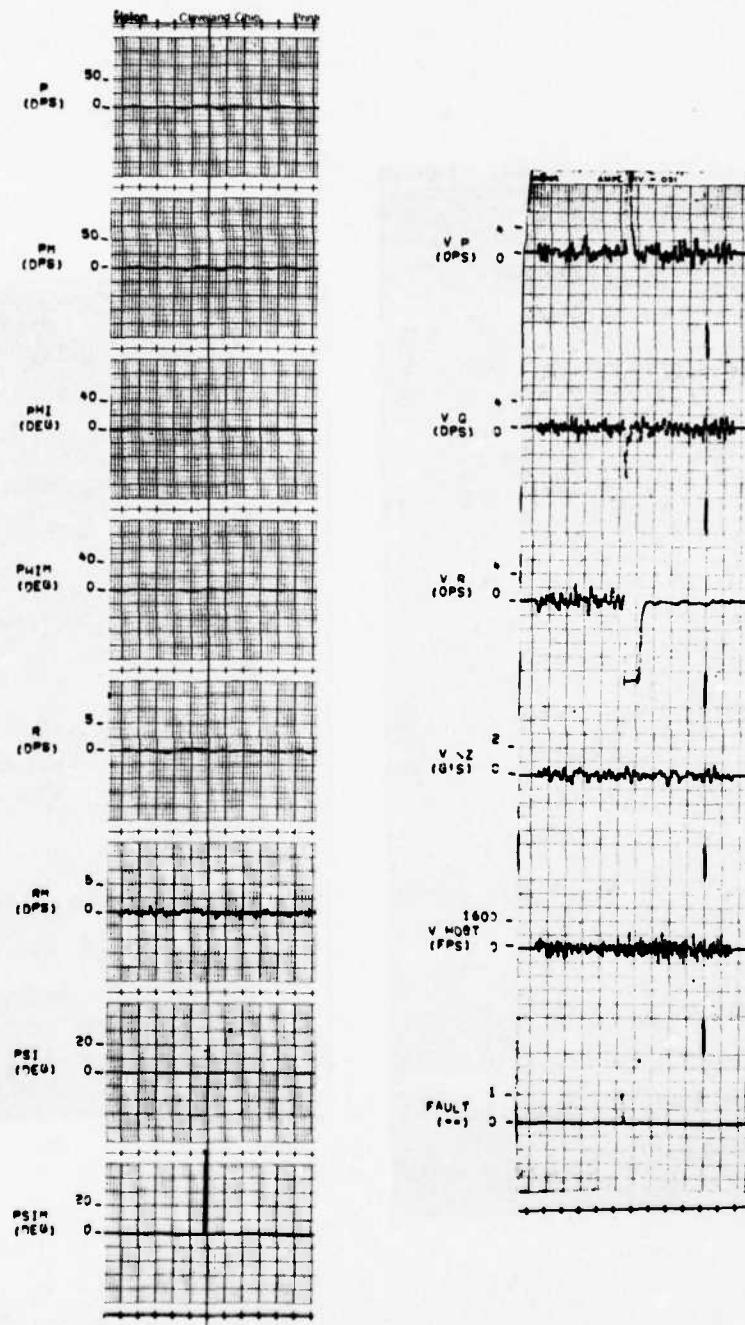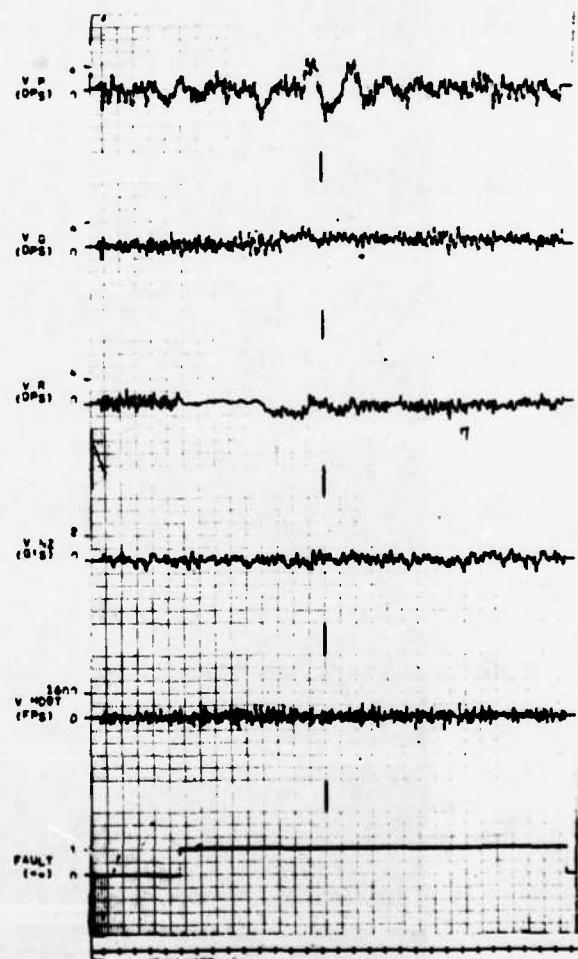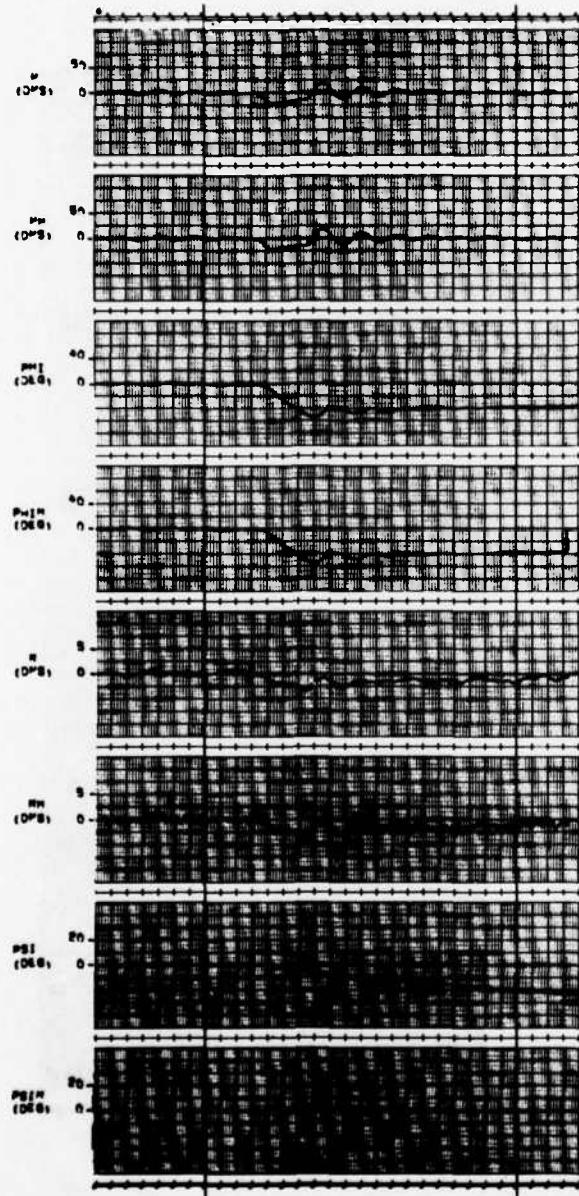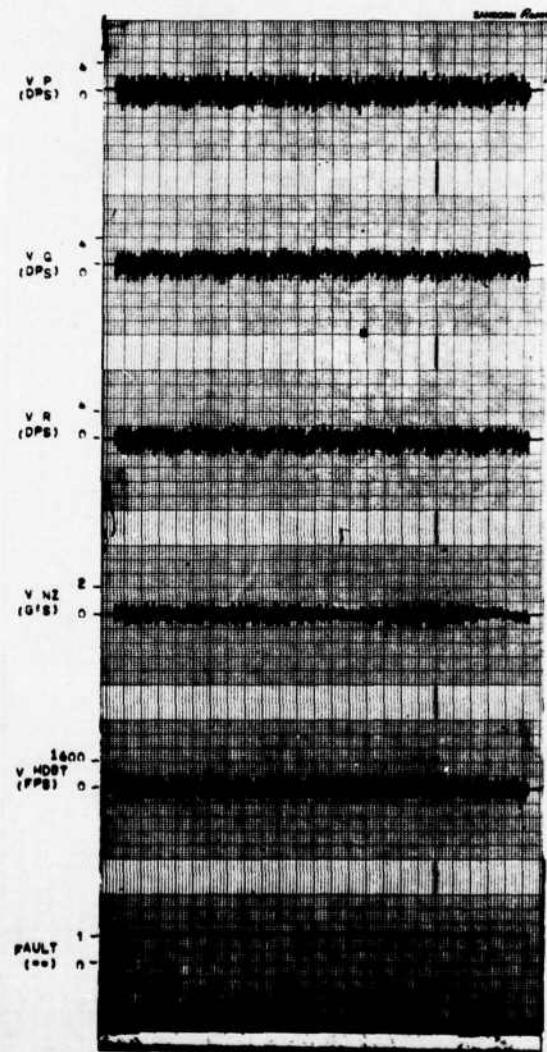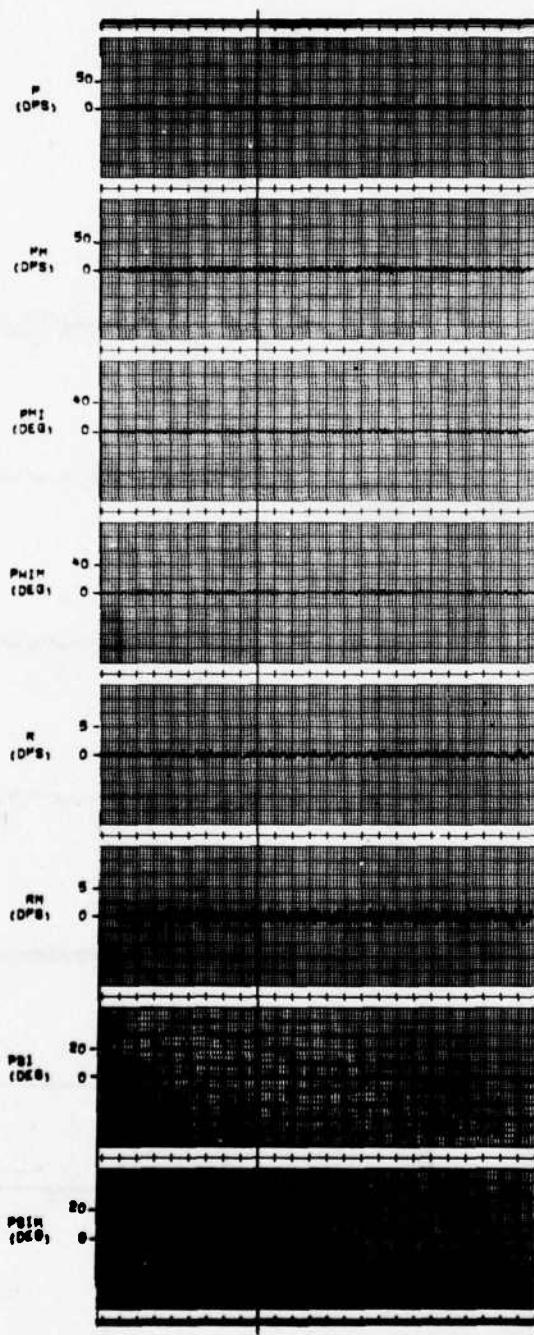
Figure D. 42

Figure D. 43
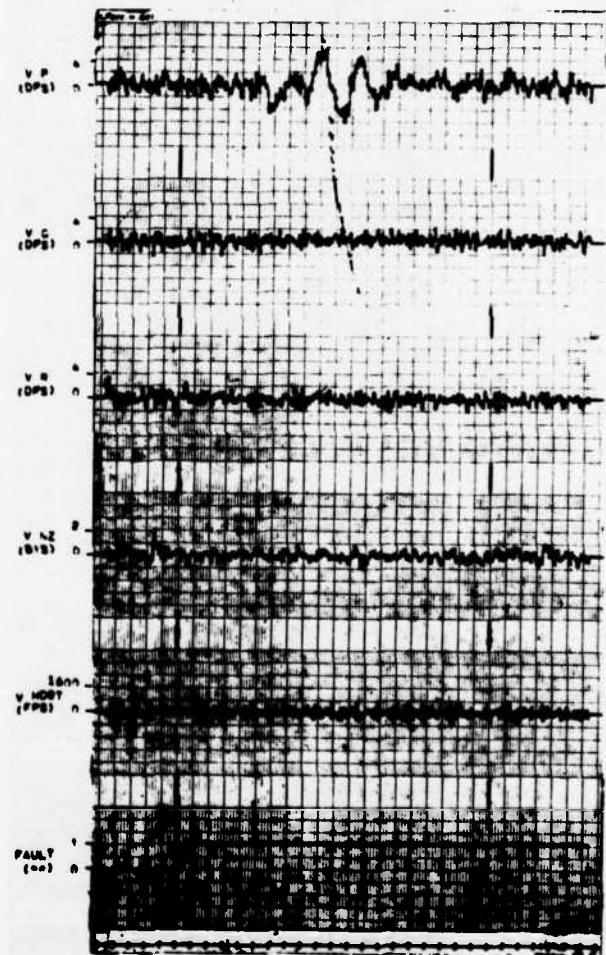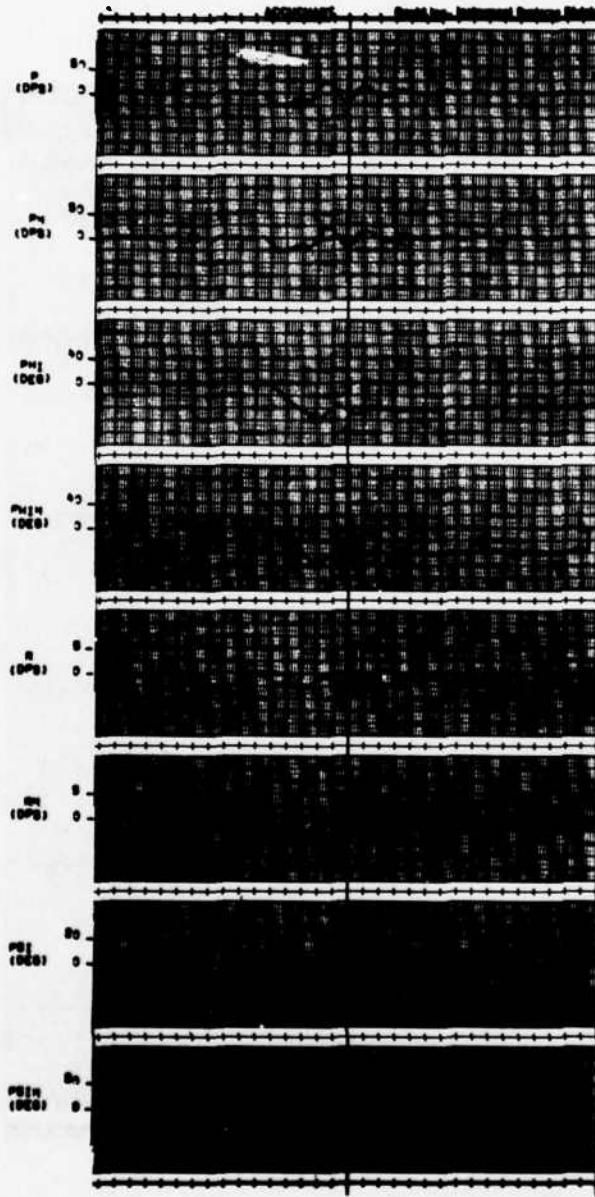
Figure D. 44

Figure D. 45

210
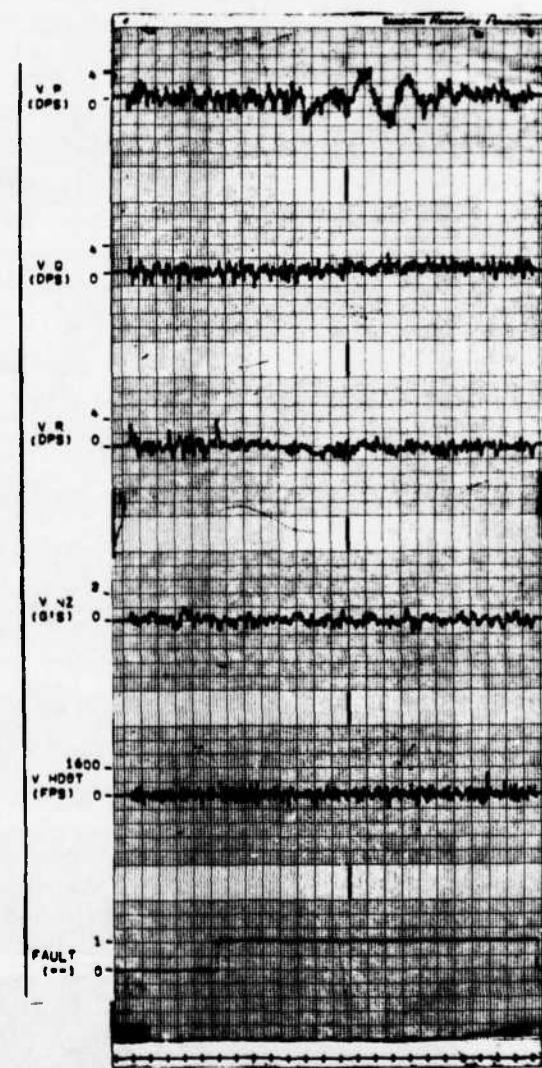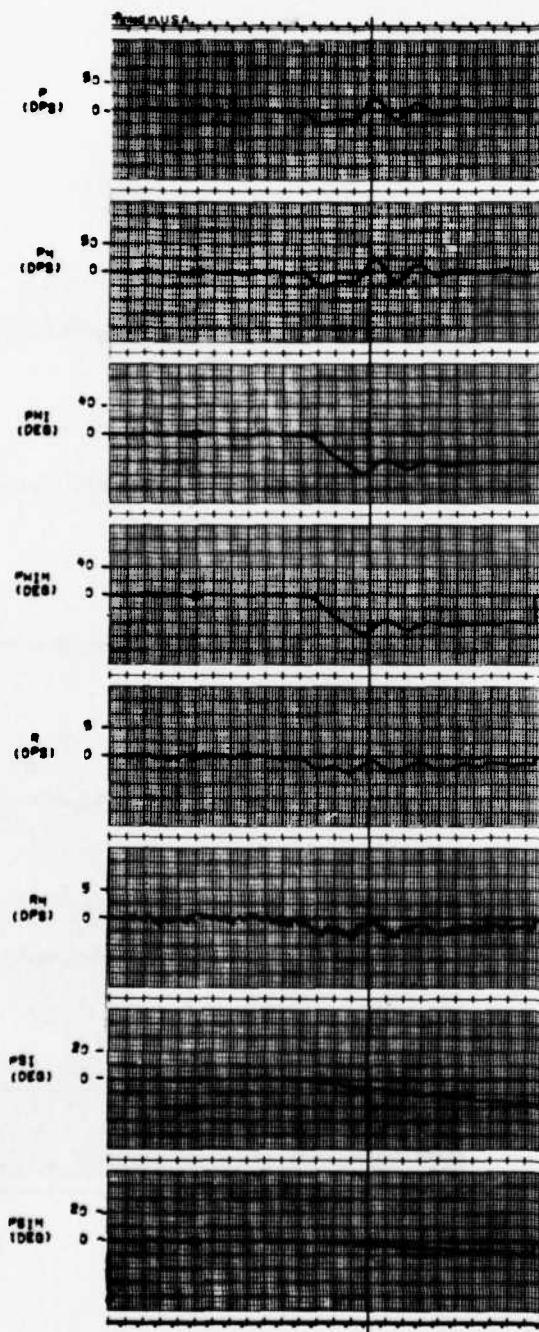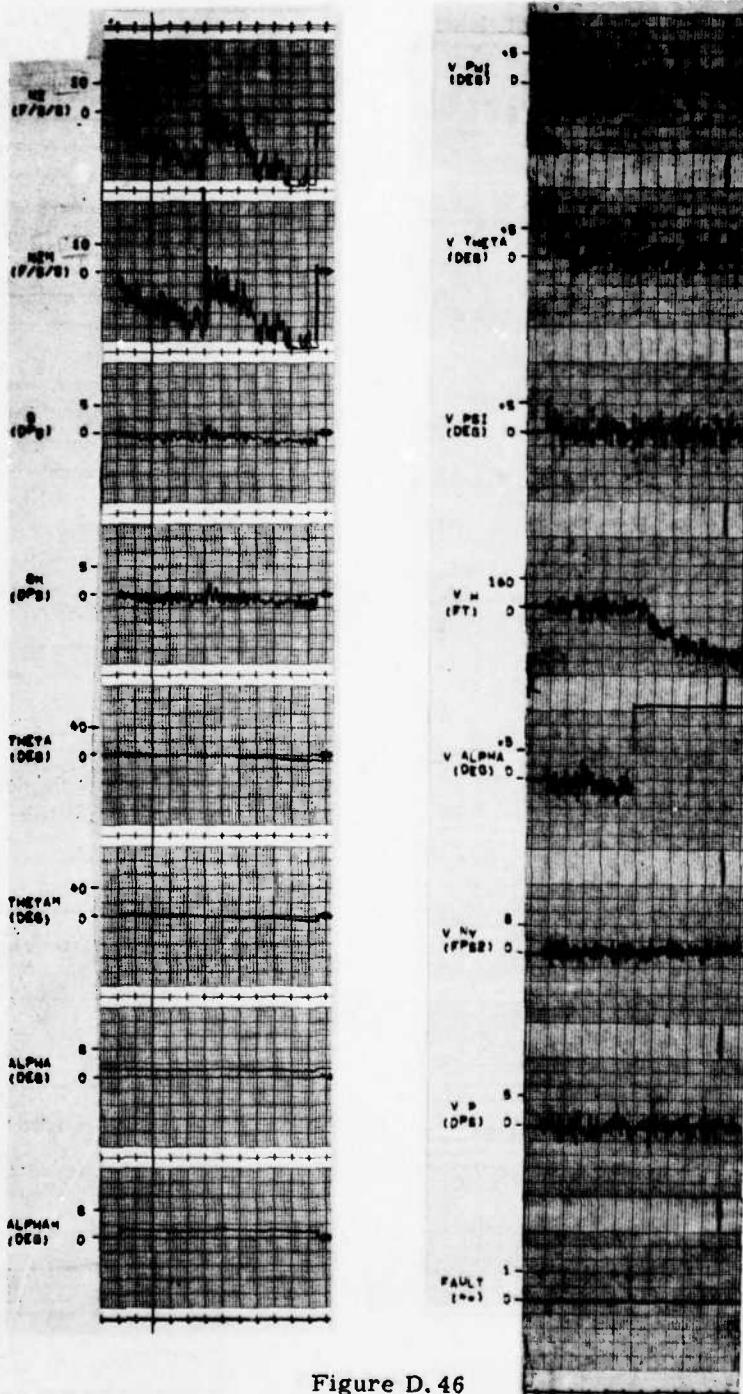
Figure D. 46

Figure D. 47

212
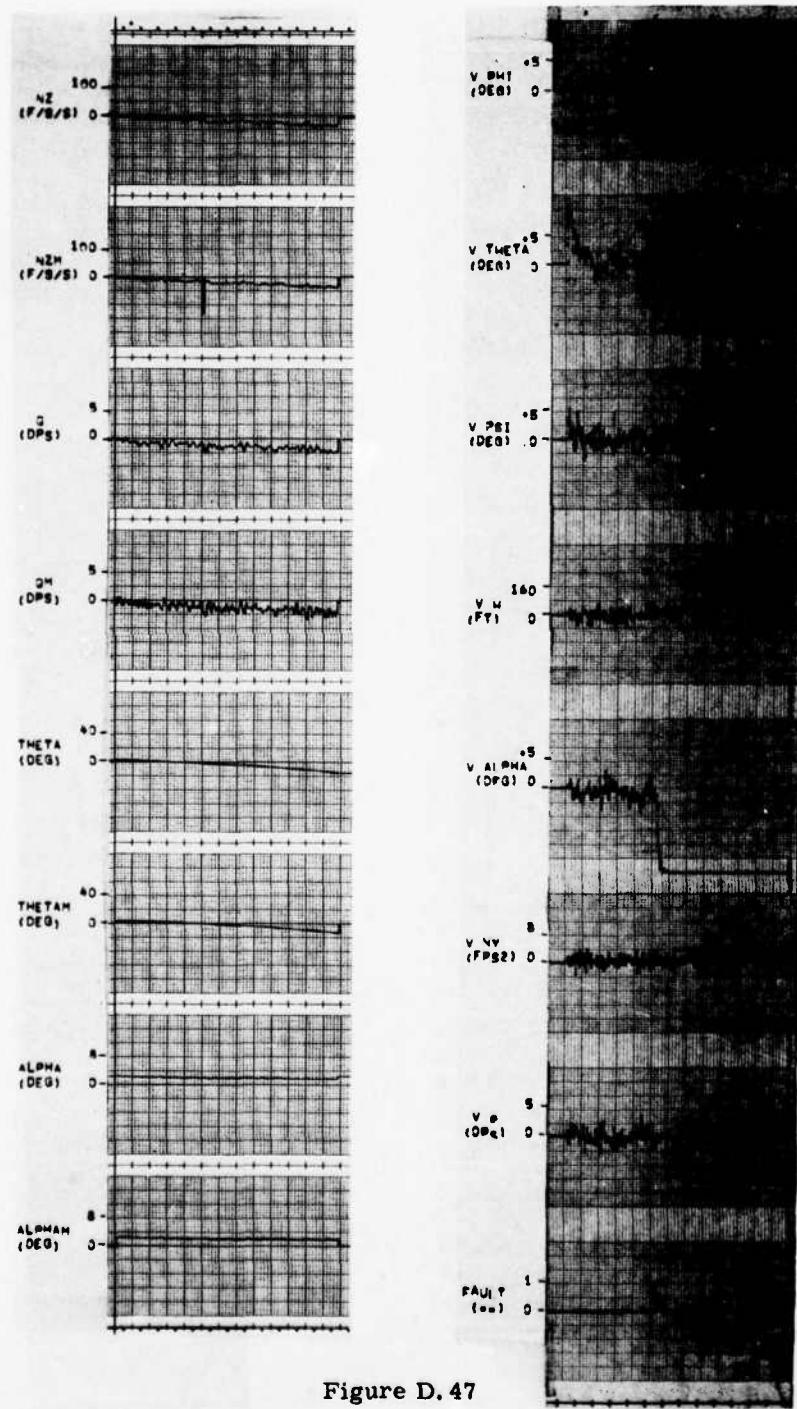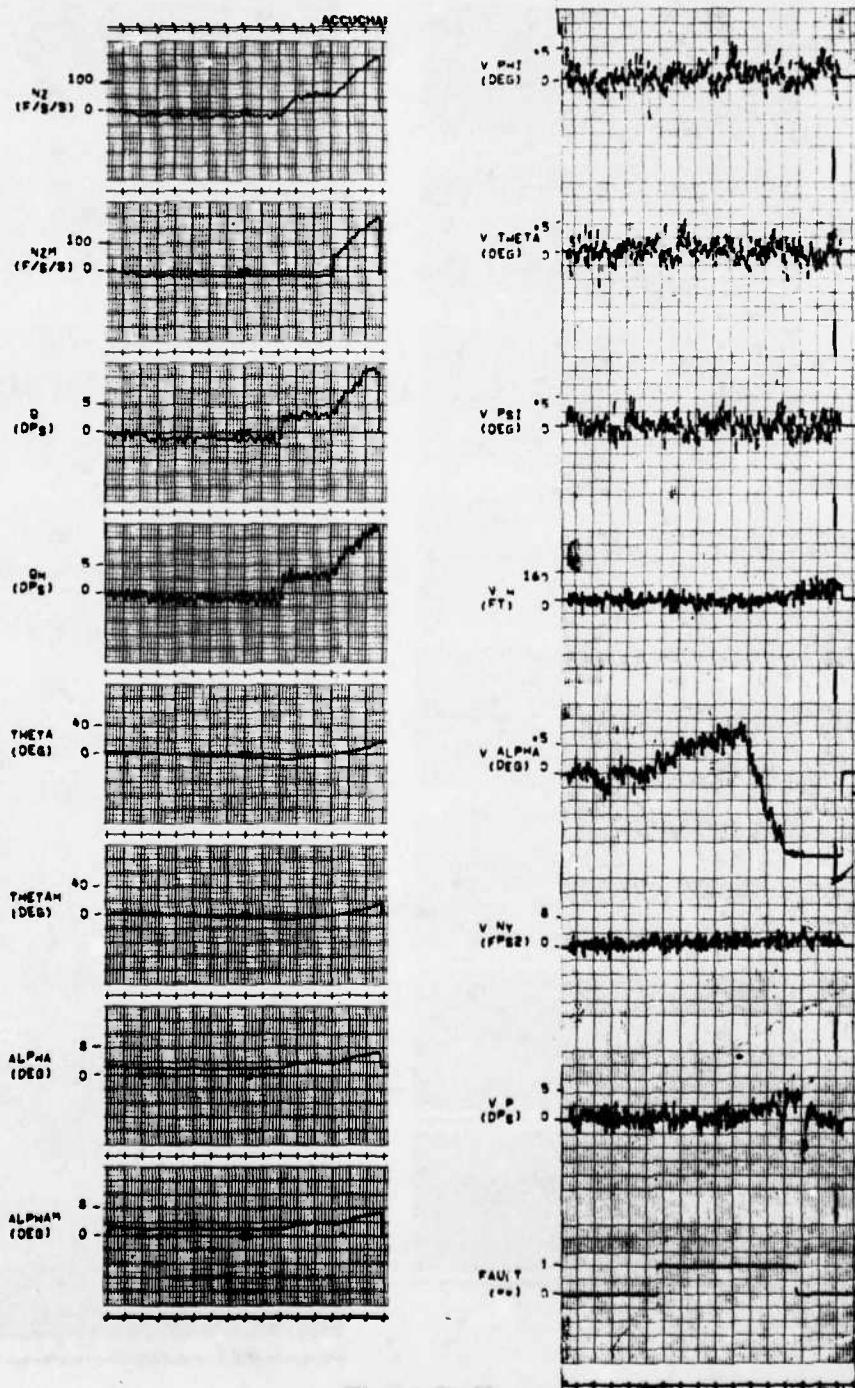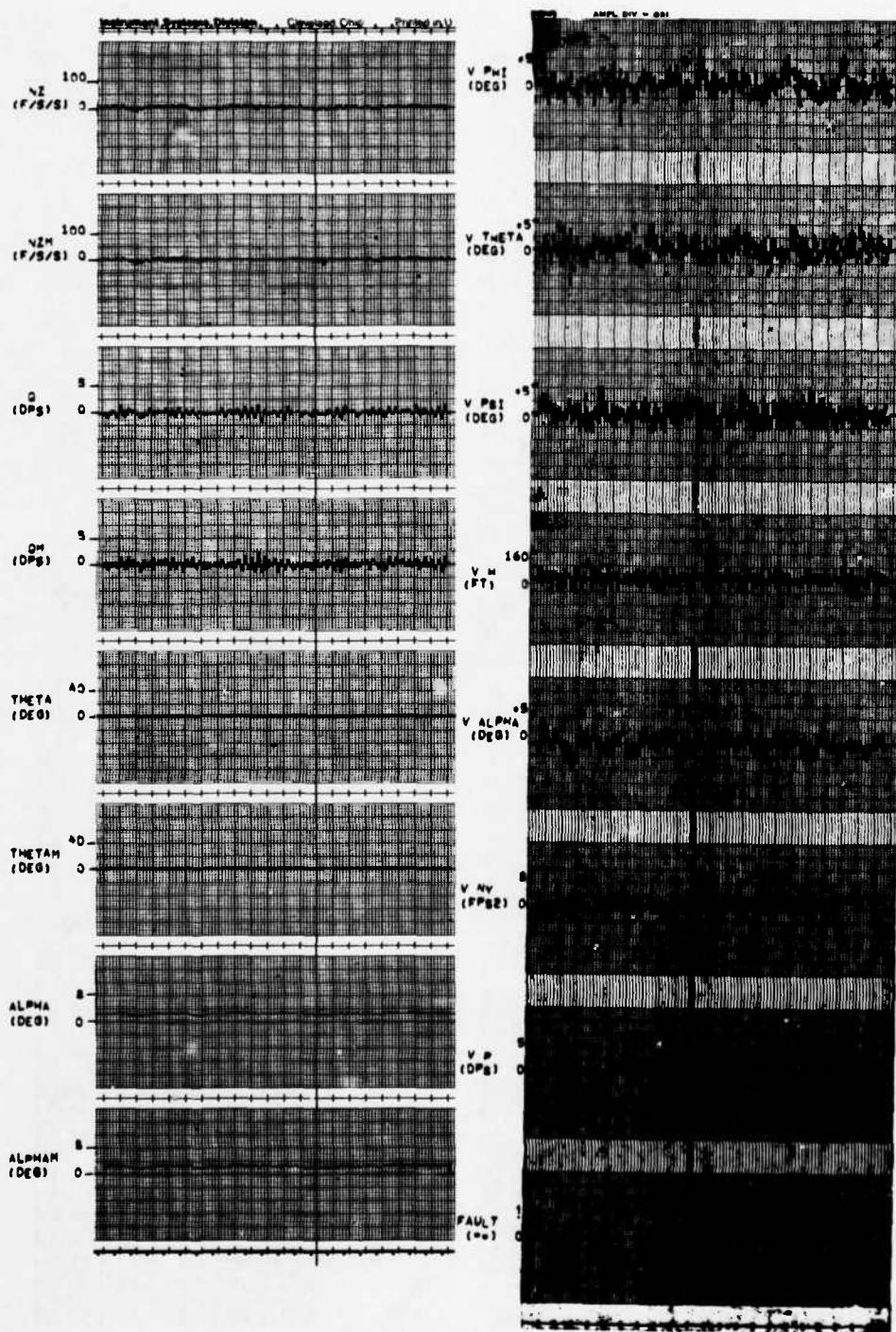
Figure D. 48

Figure D. 49

Figure D. 50

215

Figure D. 51

216

Figure D. 52

217
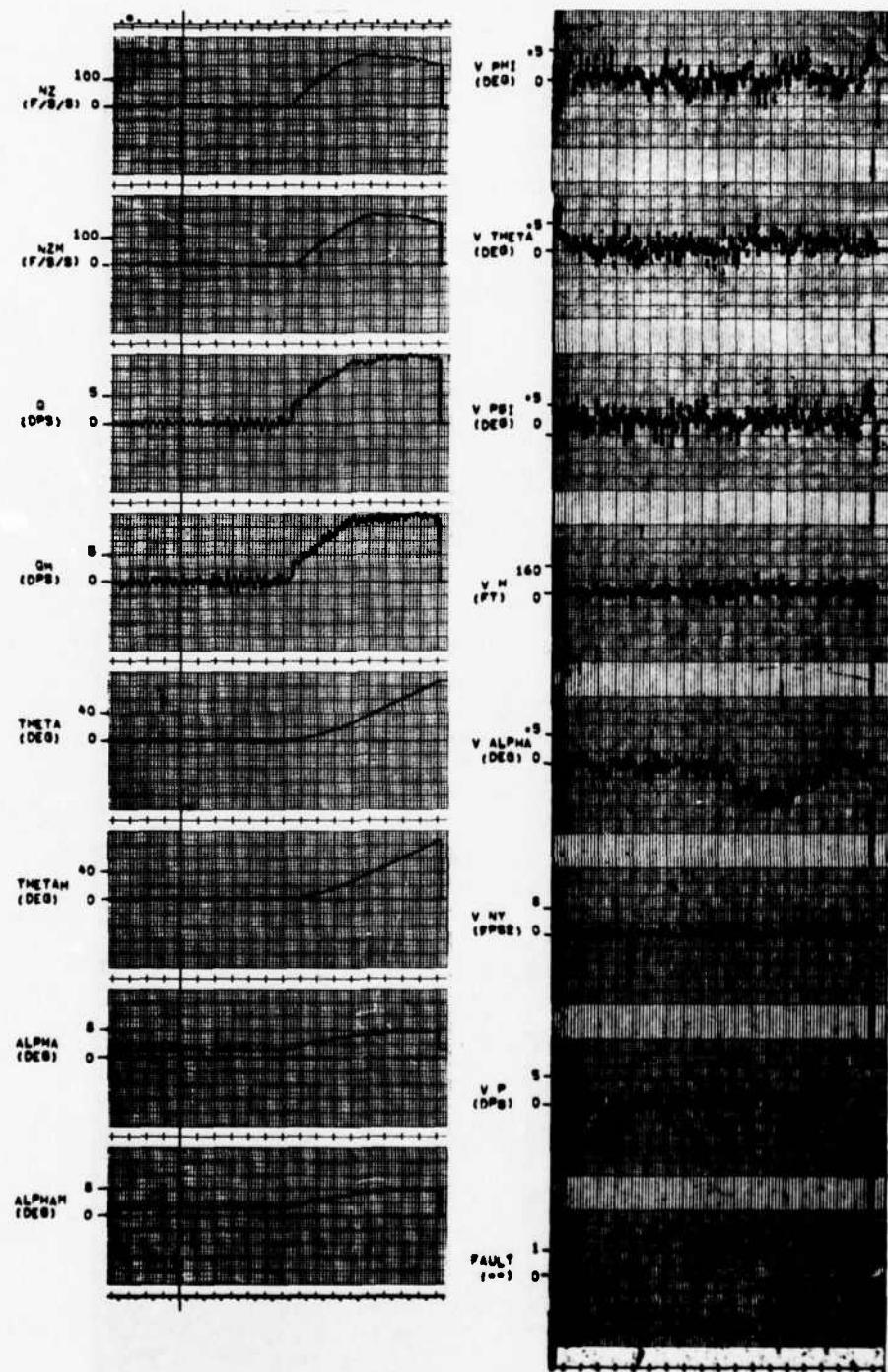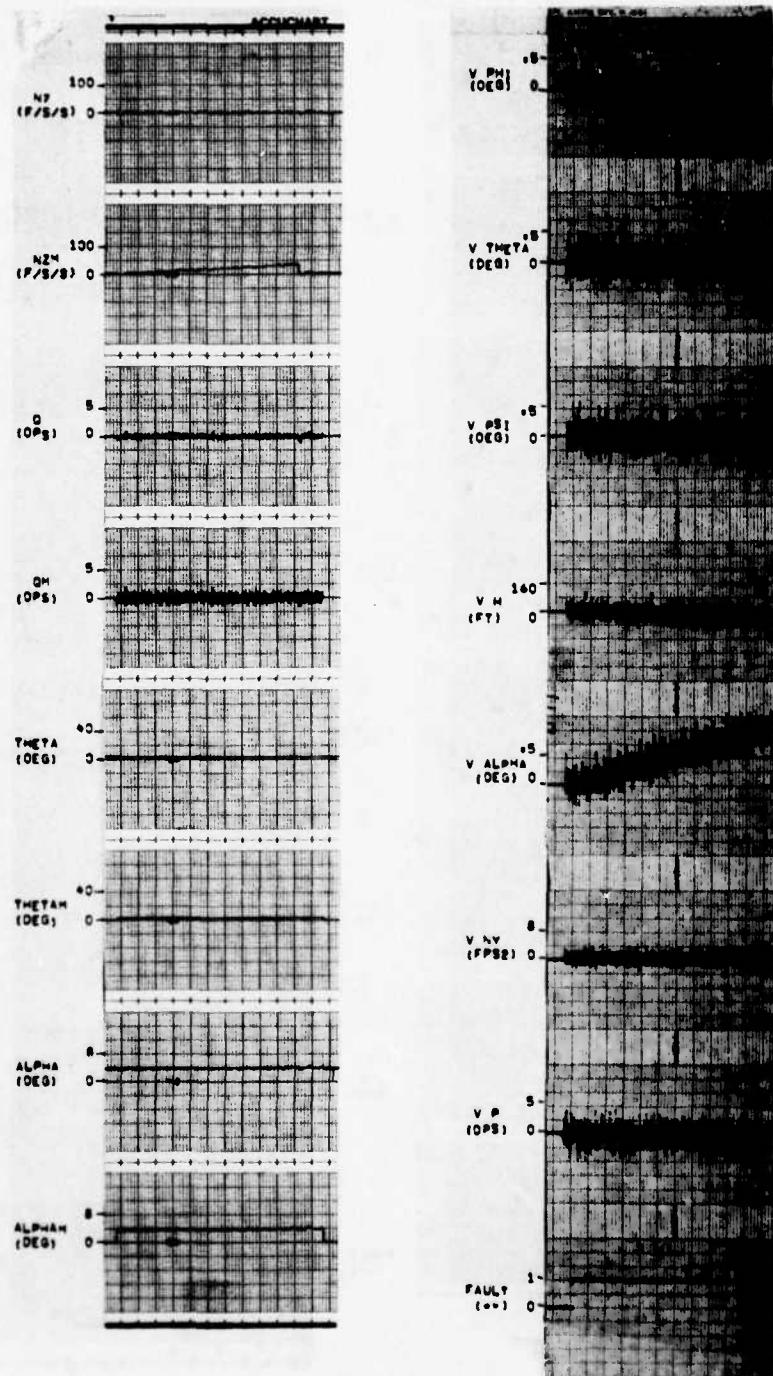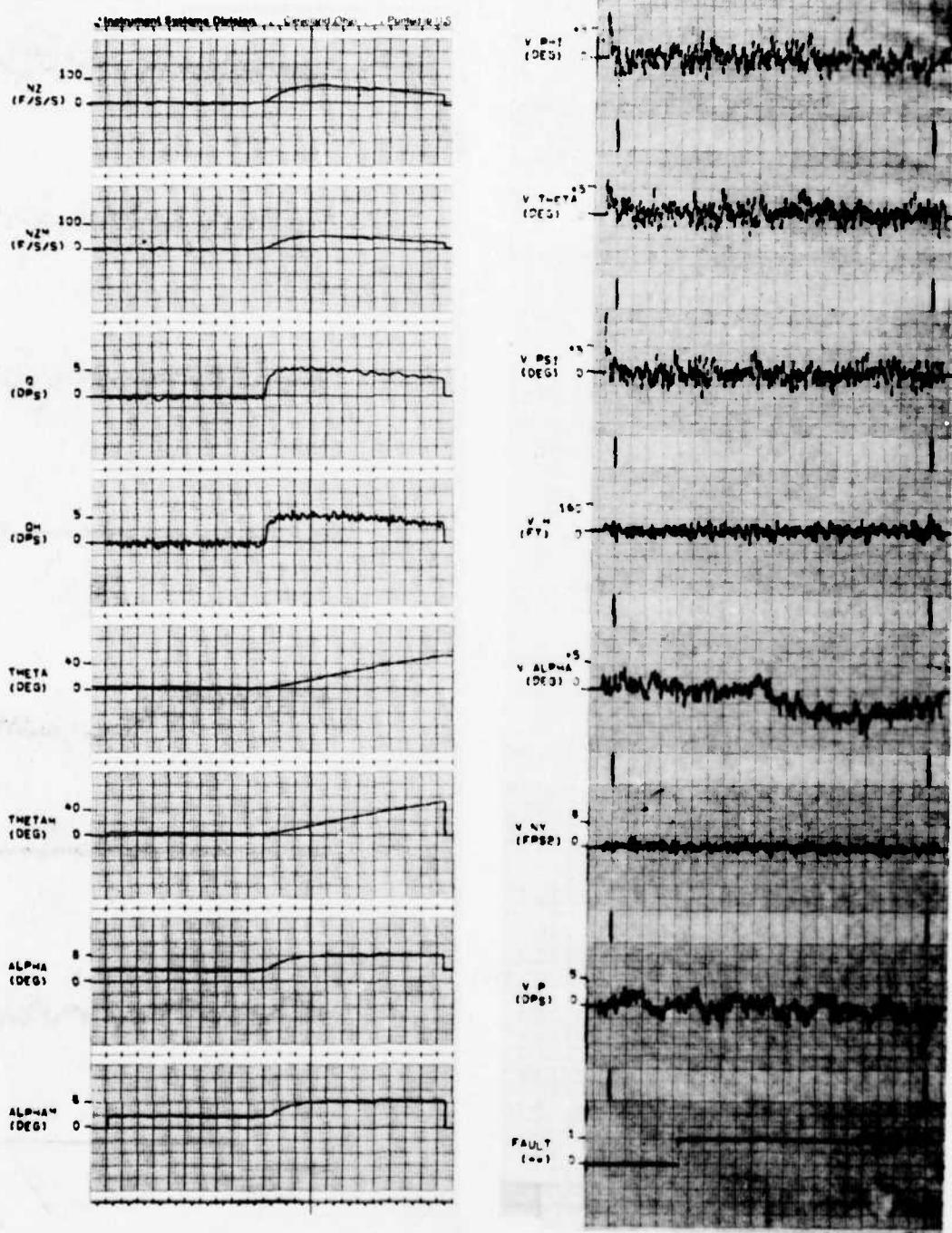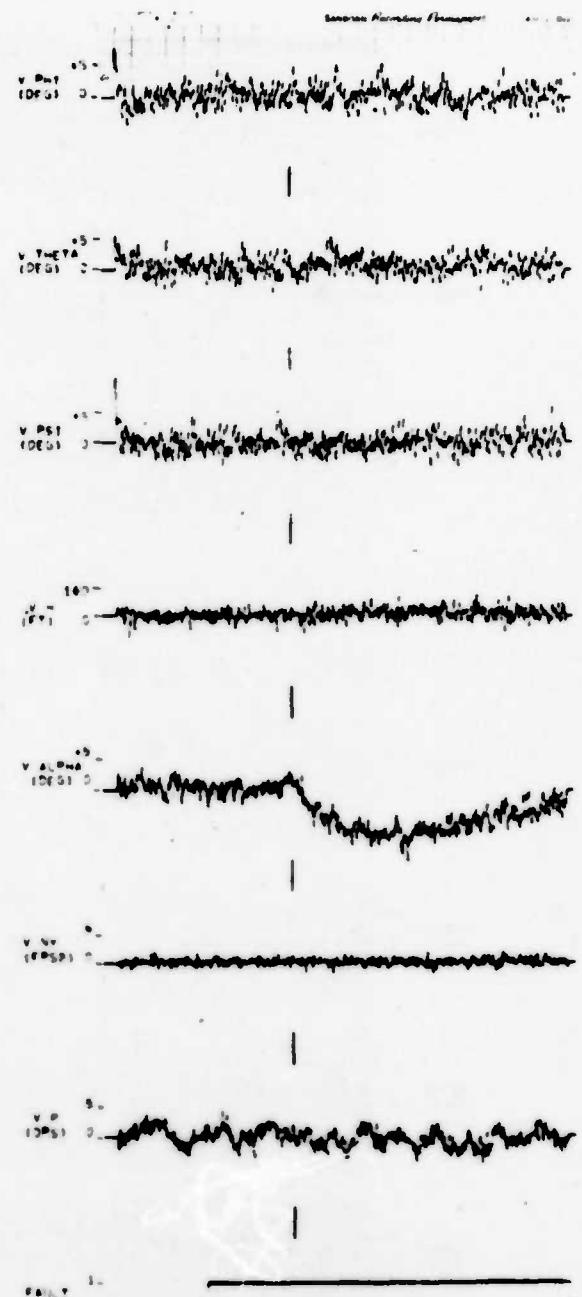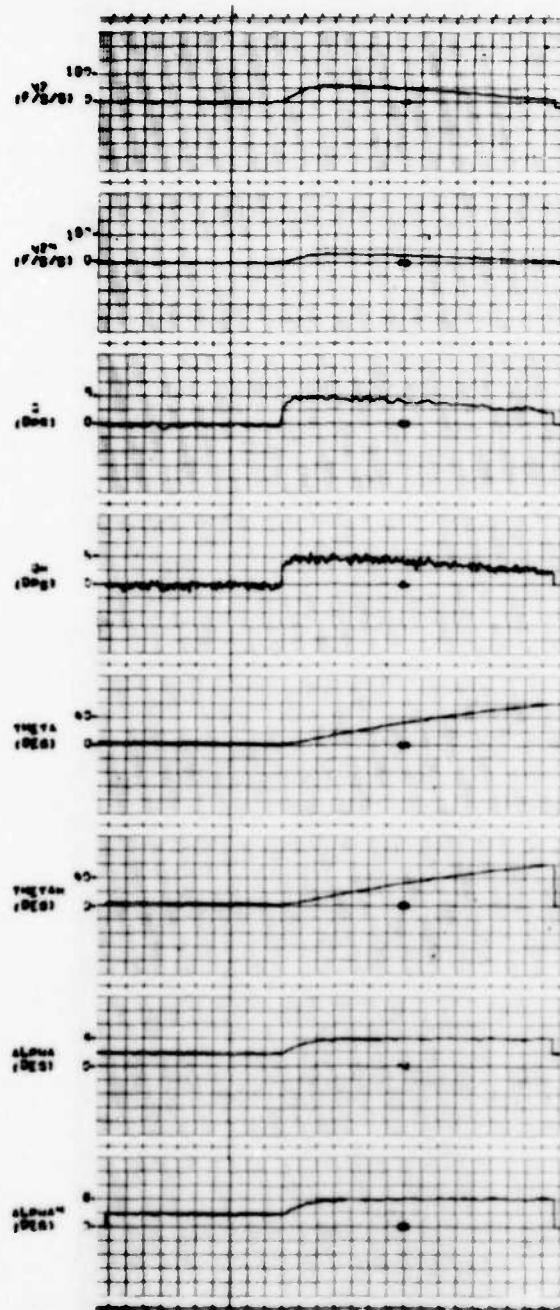
Figure D. 53

Figure D. 54

219
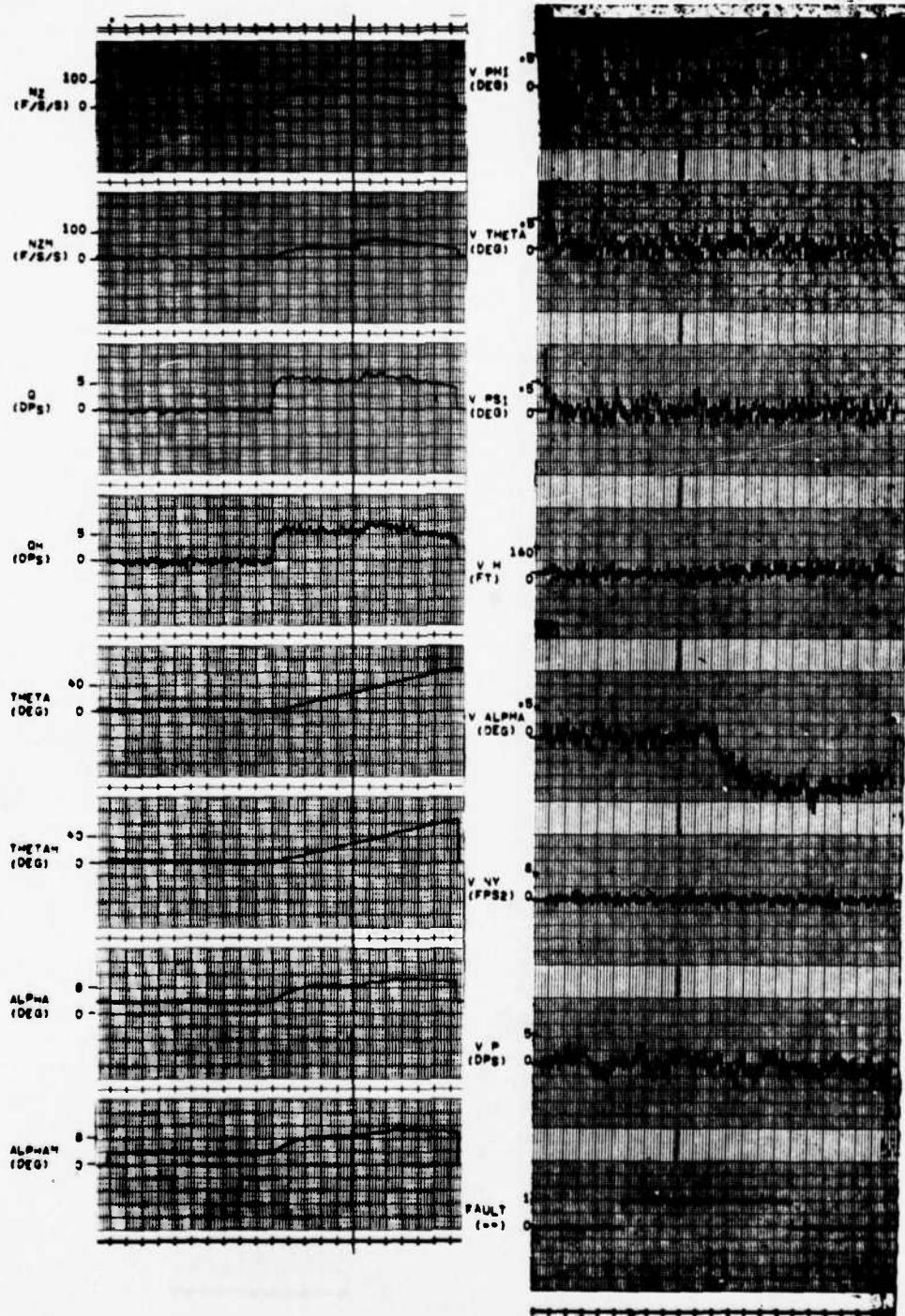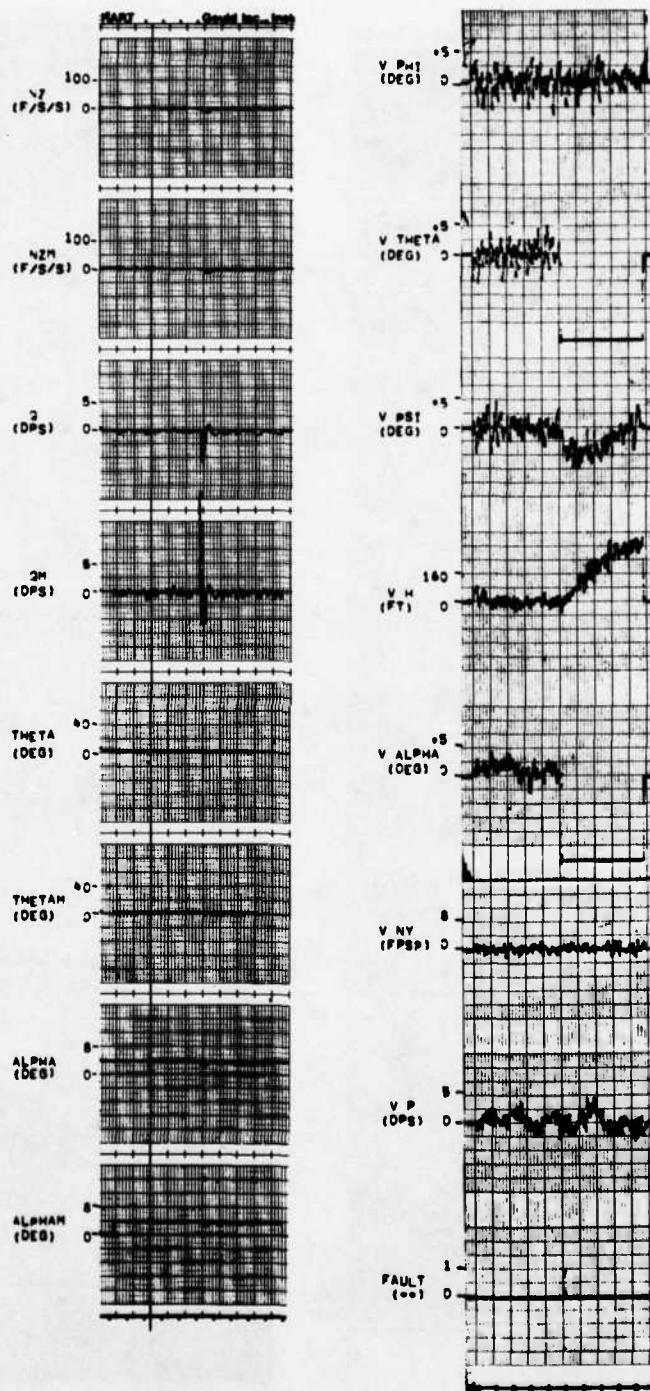
Figure D. 55

Figure D. 56

221

Figure D. 57

222

Figure D. 58

223
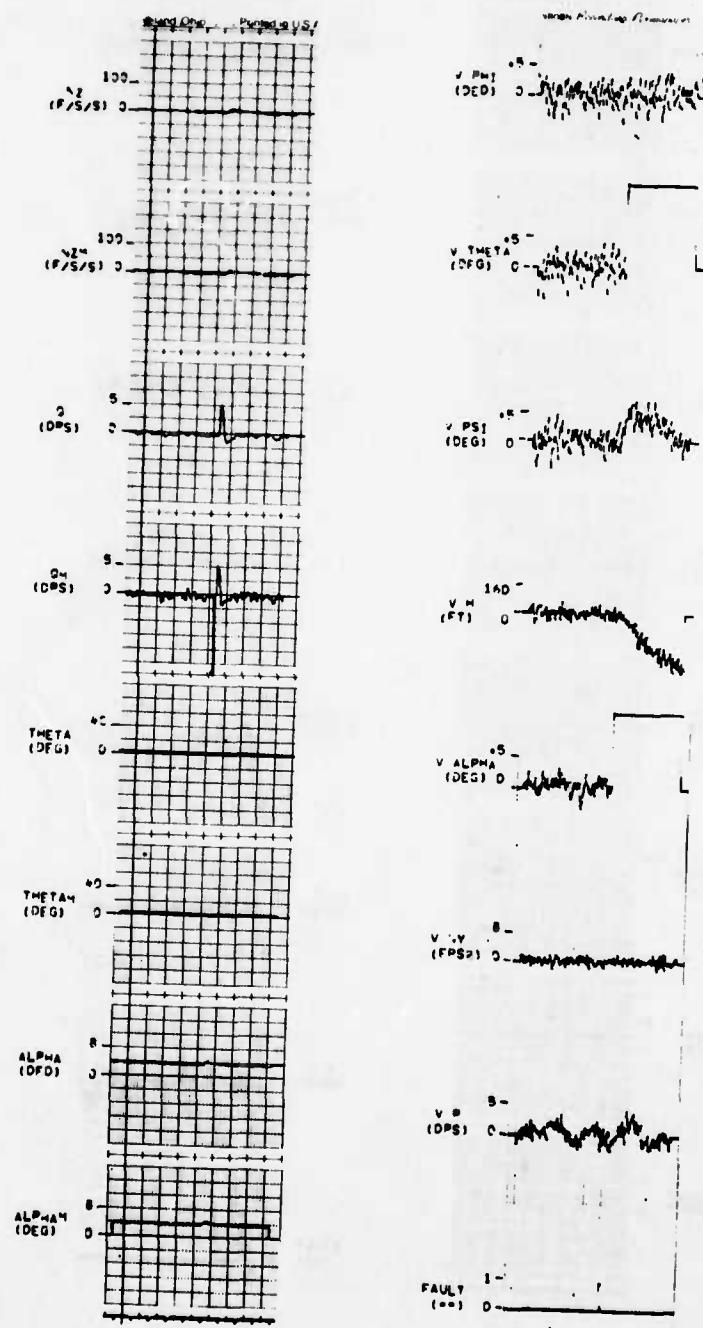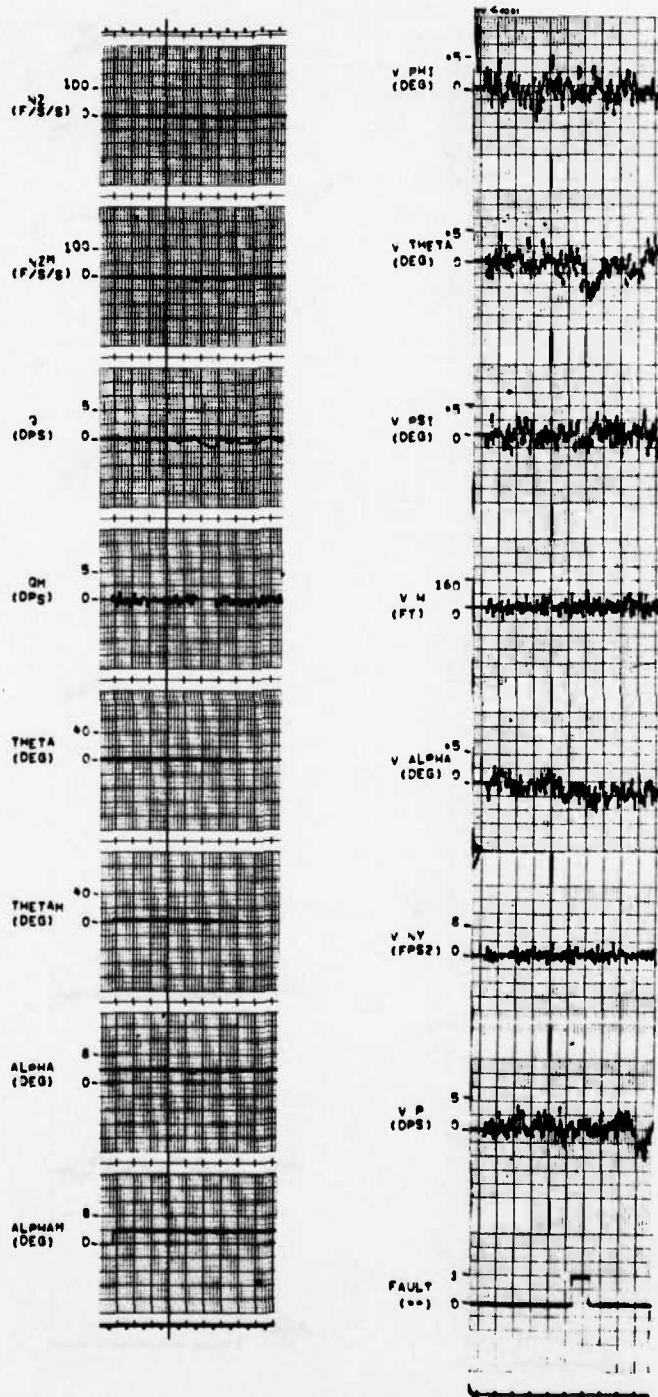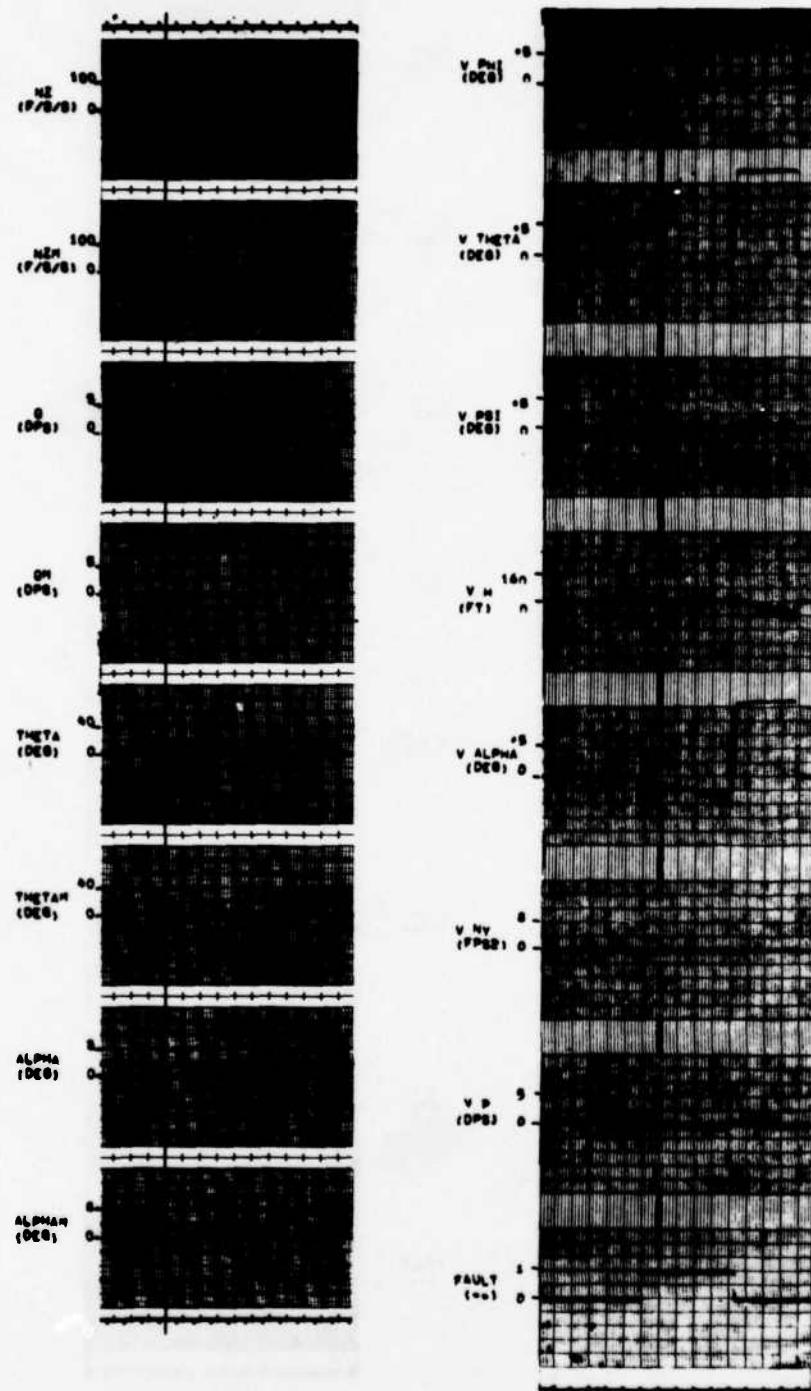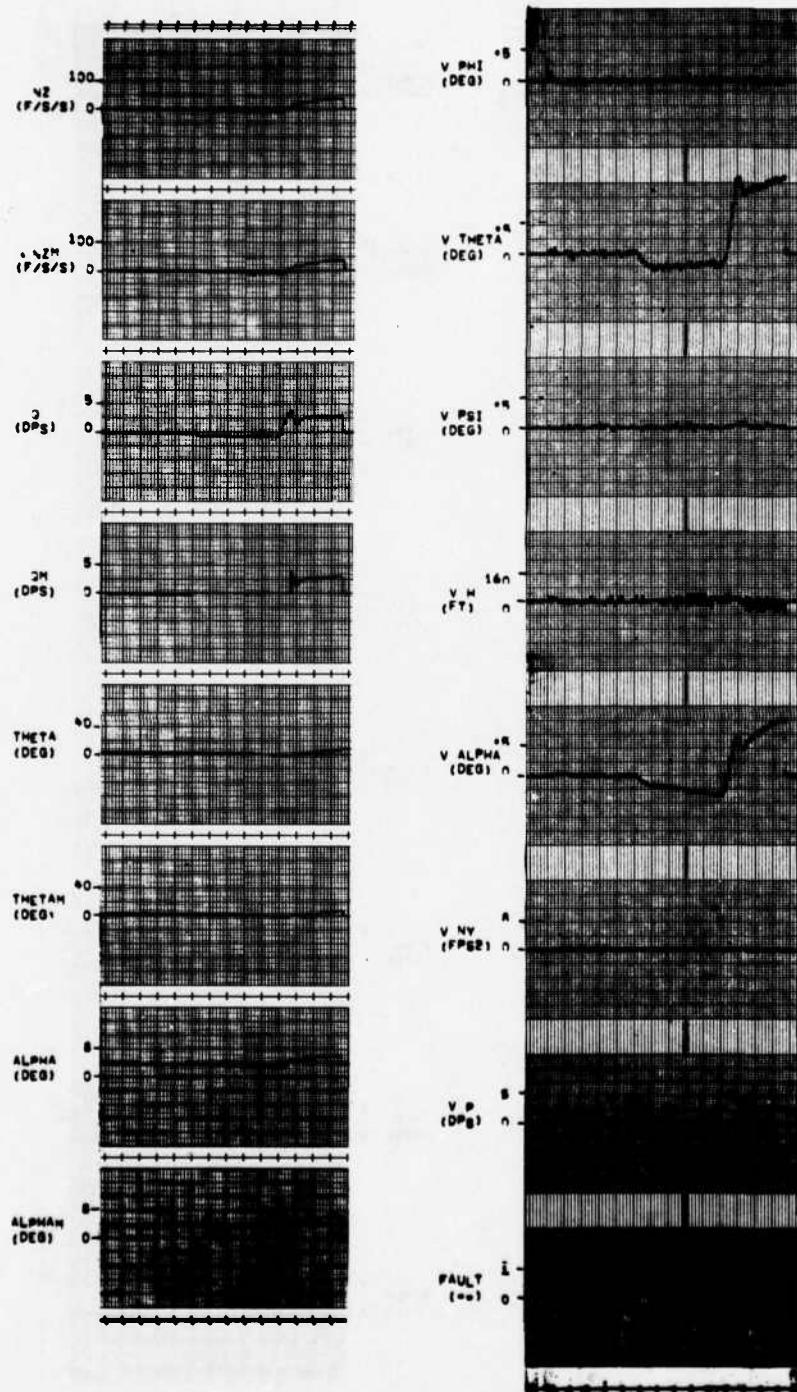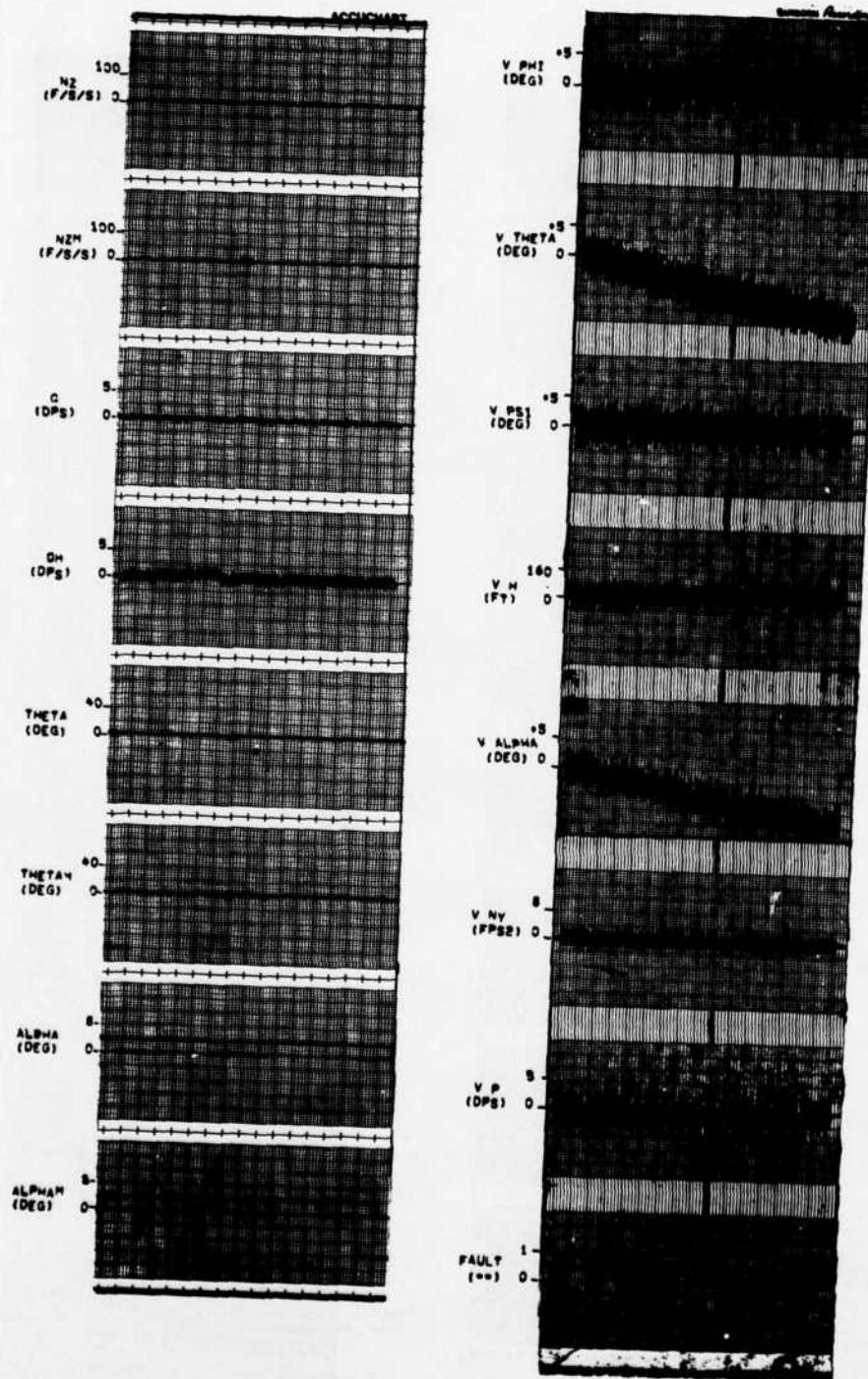
Figure D. 59

Figure D. 60
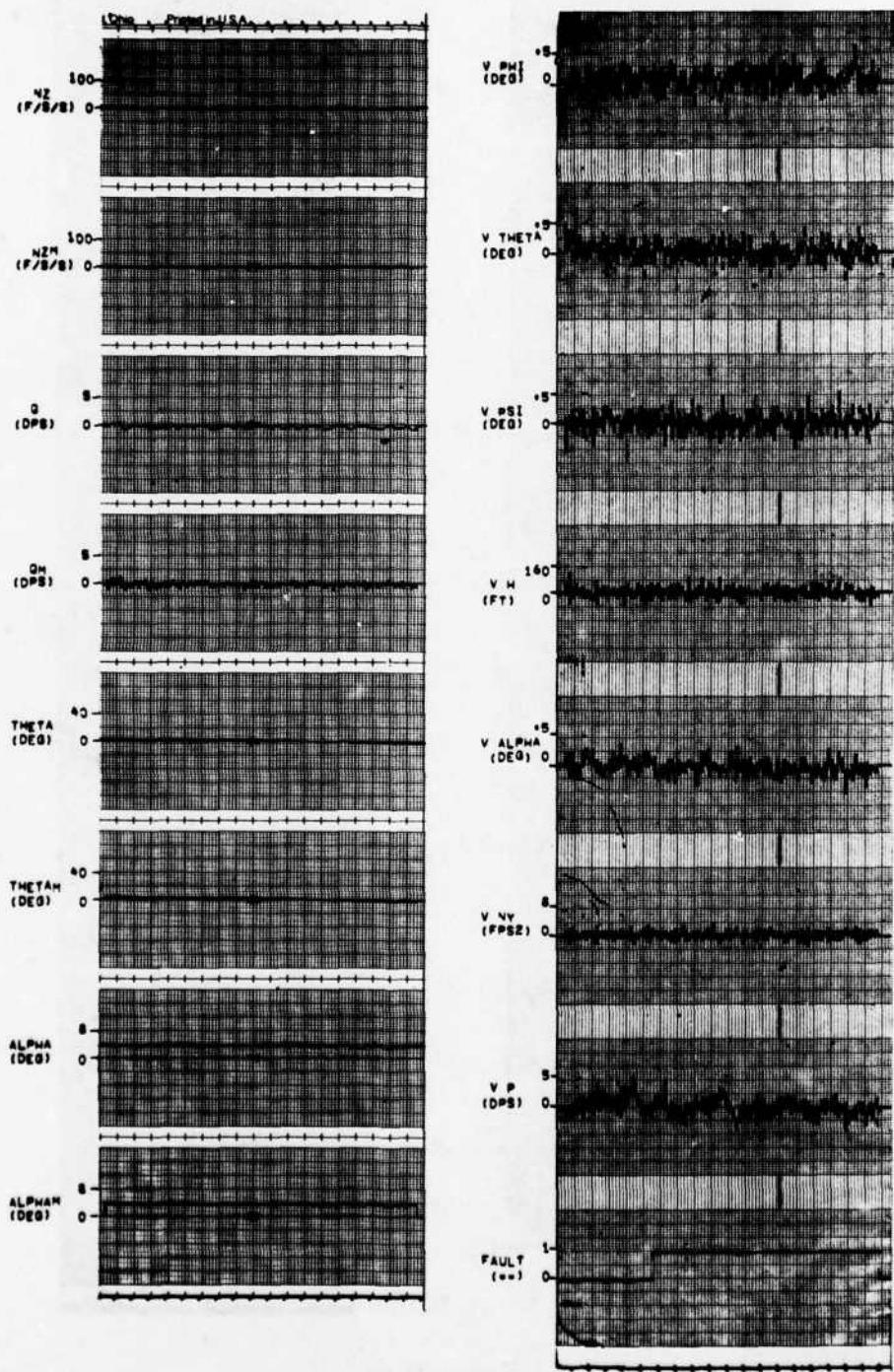
Figure D. 61

Figure D.62

Figure D. 63

228

Figure D. 64

Figure D. 65

Figure D. 66

231

Figure D. 67

232

Figure D. 68

233

Figure D. 69

Figure D. 70

Figure D. 71

Figure D. 72

237

Figure D. 73

Figure D. 74

239

Figure D. 75

240

Figure D. 76

241

Figure D. 77

Figure D. 78

243

Figure D. 79

244

Figure D. 80

245

Figure D. 81

246

Figure D. 82

Figure D. 83

Figure D. 84

Figure D. 85

250

Figure D. 86

Figure D. 87

252

Figure D. 88

253

Figure D. 89

254

Figure D. 90

255

Figure D. 91

Figure D. 92

257

Figure D. 93

258

Figure D. 94

Figure D. 95

260

Figure D. 96

261

Figure D. 97

262

Figure D. 98

263

Figure D. 99

Figure D. 100

265

Figure D.101

Figure D. 102

Figure D. 103

Figure D.104

269

Figure D. 105

Figure D. 106

271

Figure D. 107

272

Figure D.108

273

Figure D. 109

274

Figure D. 110

Figure D.111

Figure D. 112

Figure D. 113

Figure D.114

Figure D.115

280

Figure D.116

281

Figure D. 117

282

Figure D.118

Figure D. 119

284

Figure D. 120

285

Figure D. 121

Figure D. 122

287

Figure D.123

288

Figure D.124

289

Figure D. 125

Figure D.126

Figure D. 127

Figure D. 128

293

Figure D.129

Figure D. 130

Figure D. 131

296
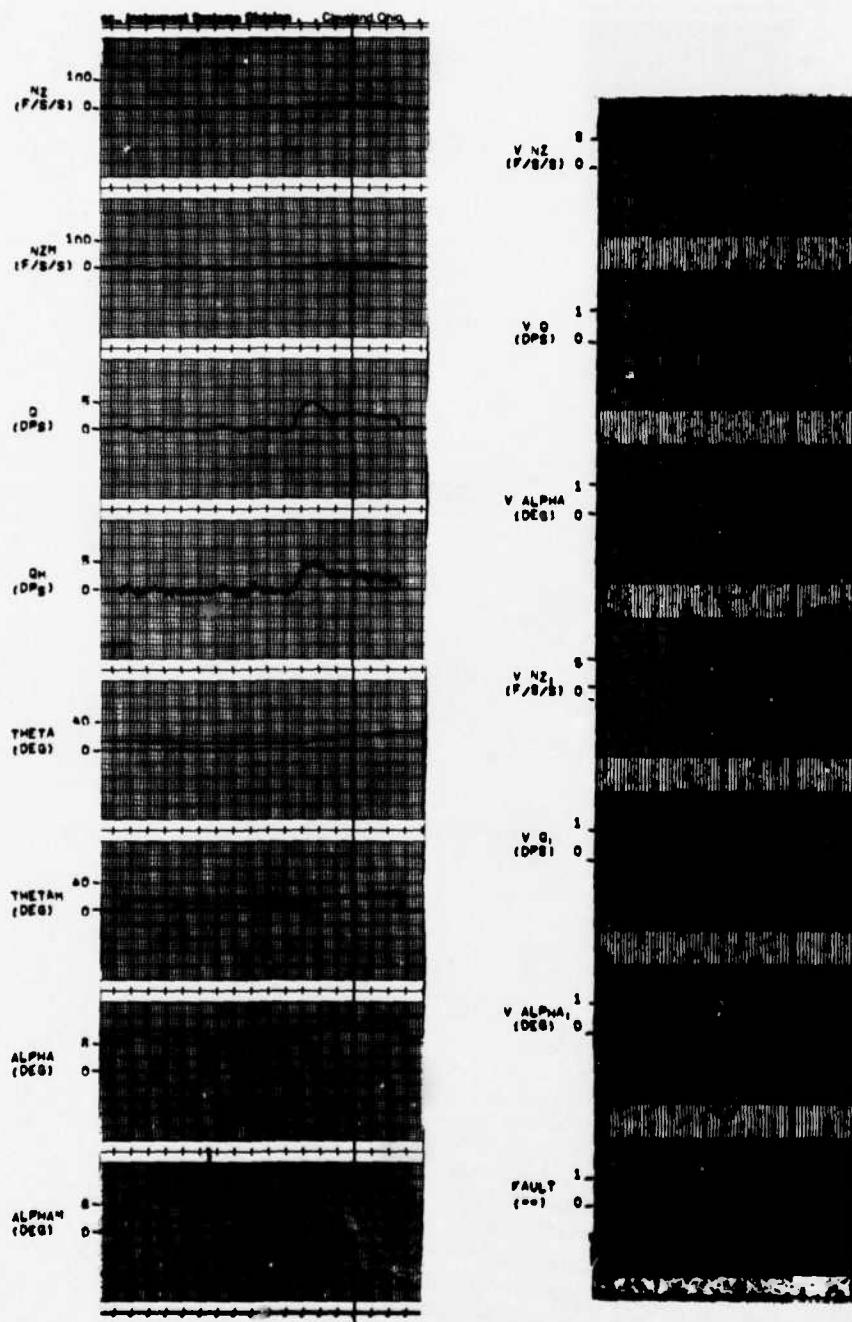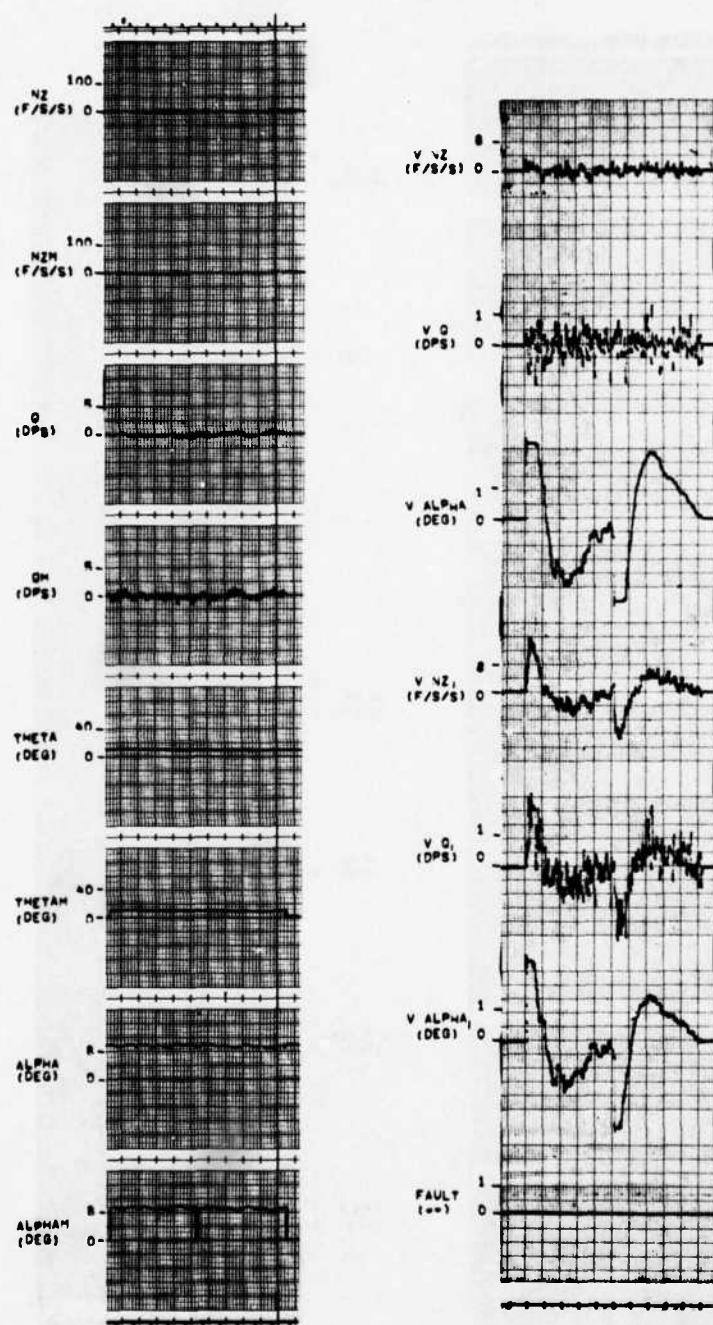
Figure D.132

Figure D. 133
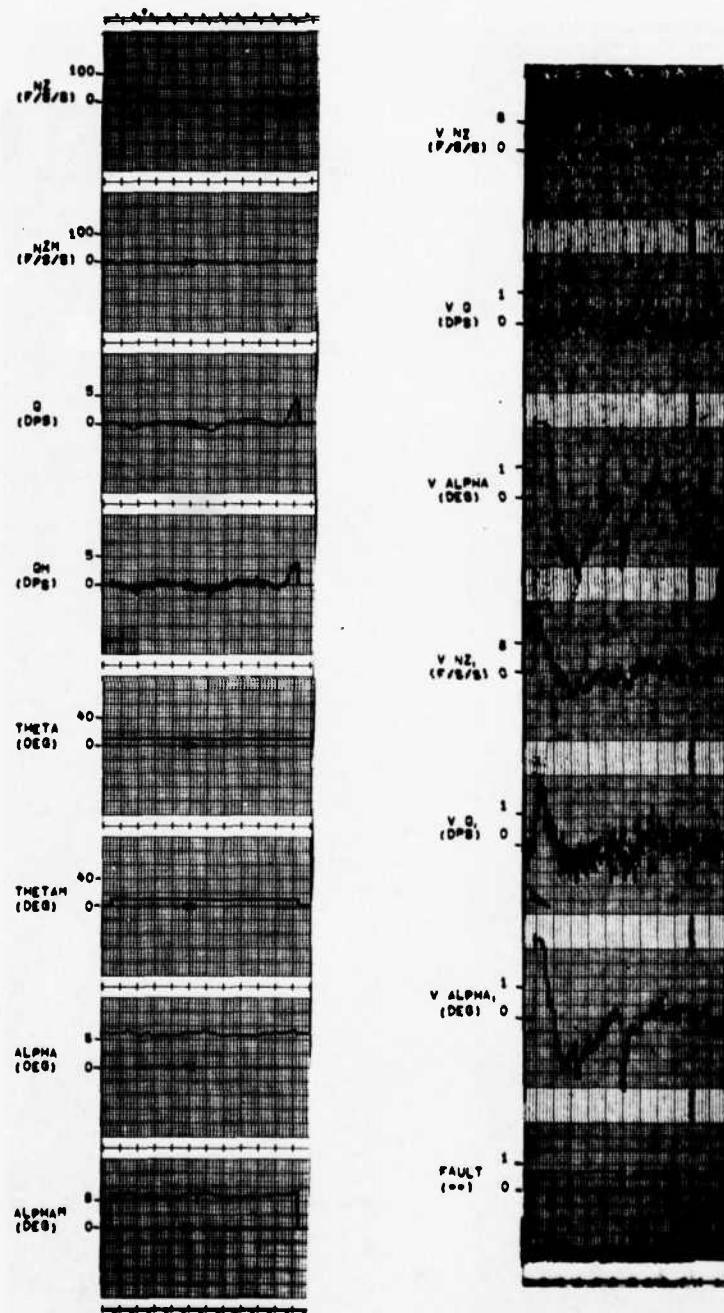
Figure D.134
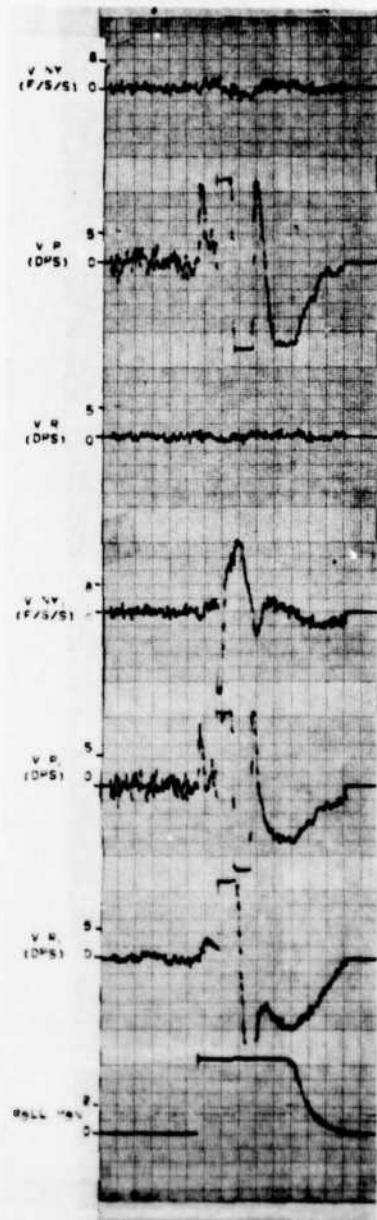
Figure D. 135

Figure D. 136

301
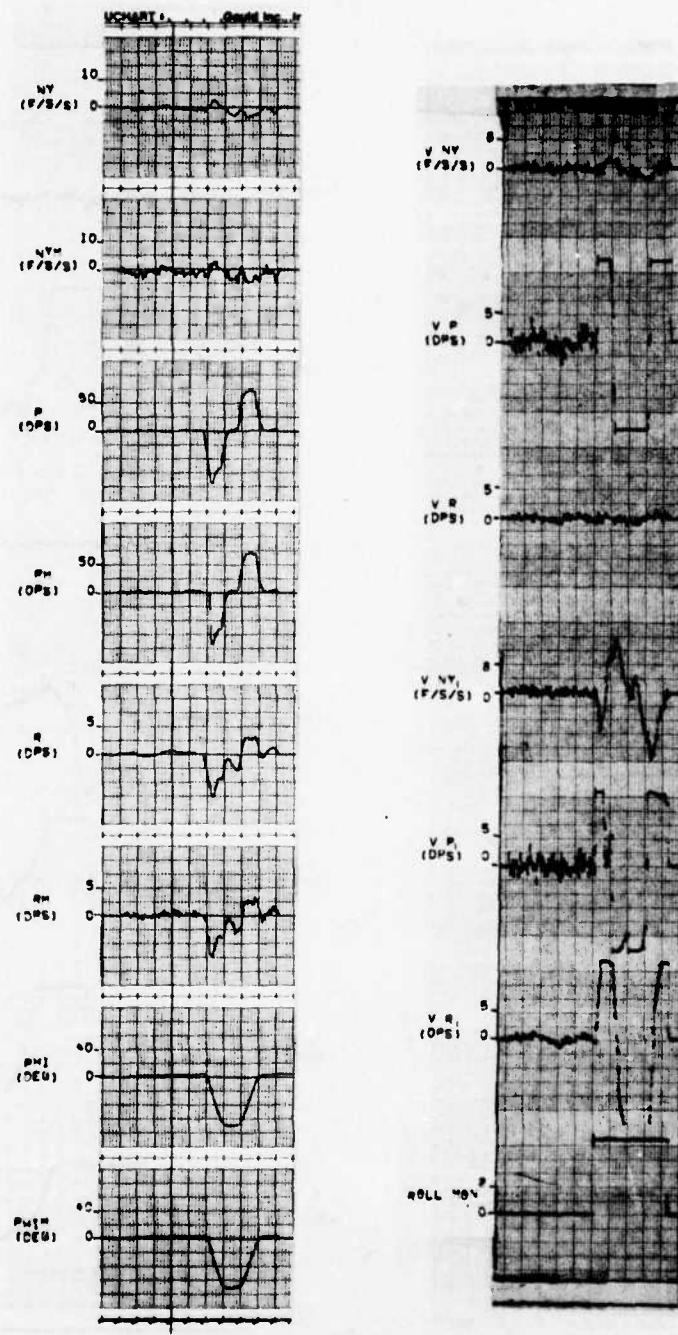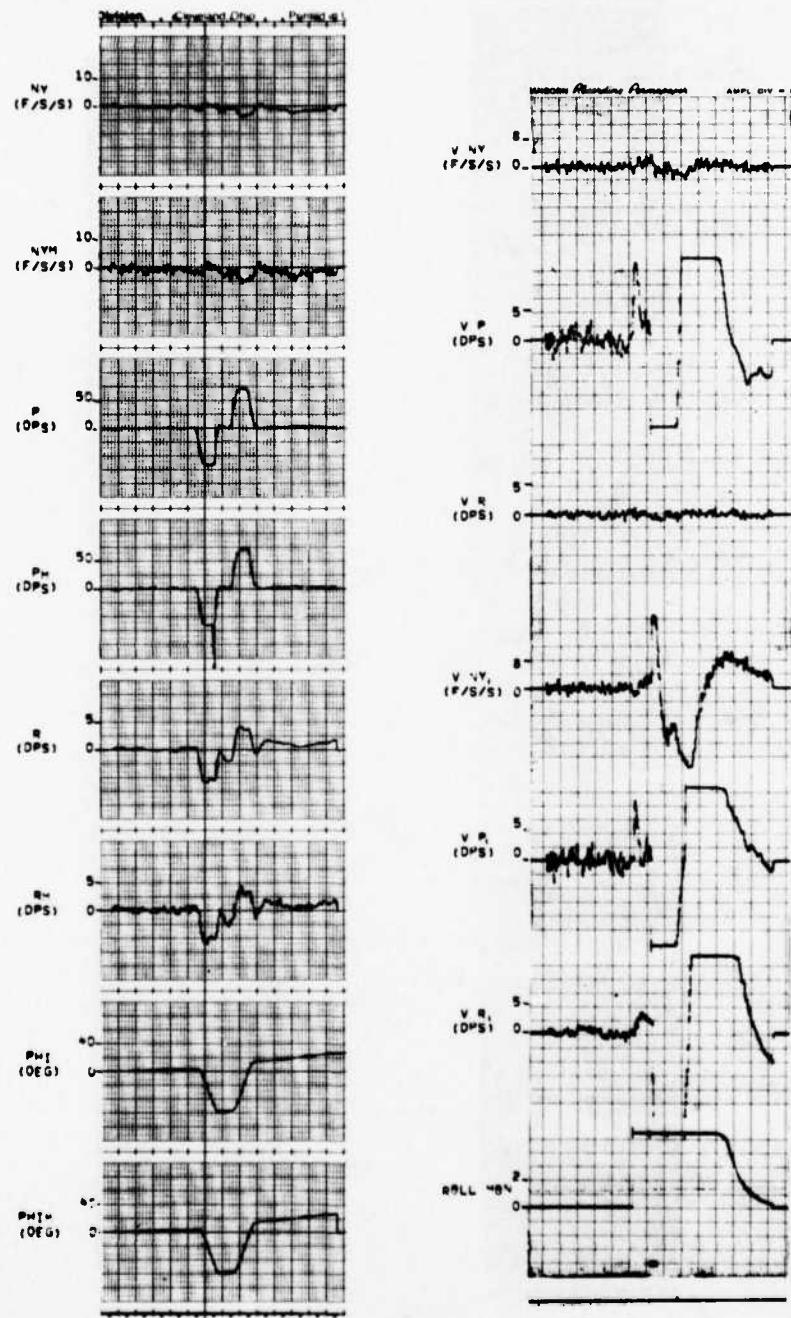
Figure D. 137

Figure D.138
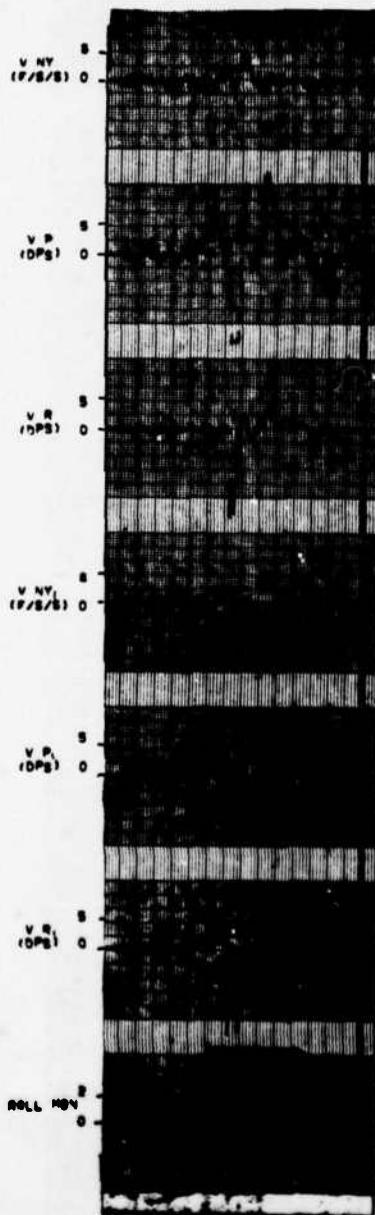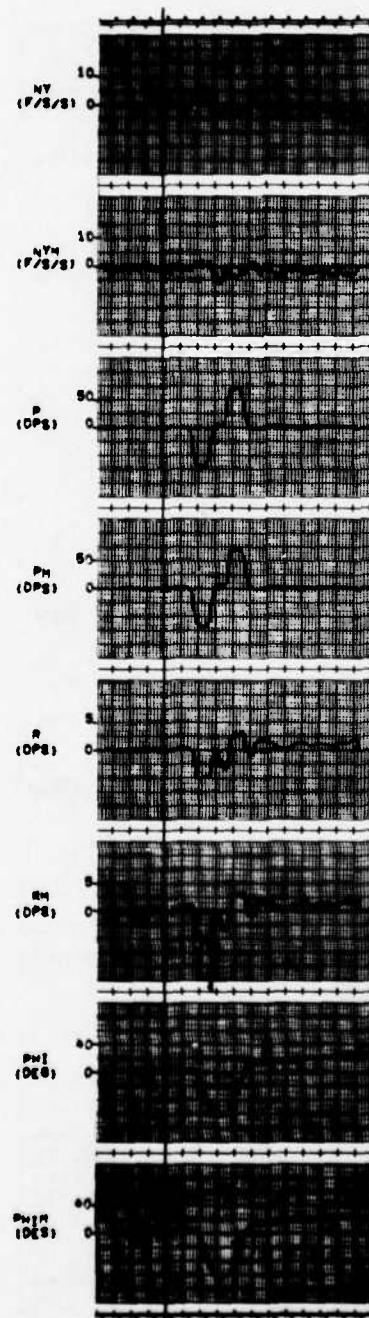
303

Figure D. 139

Figure D. 140
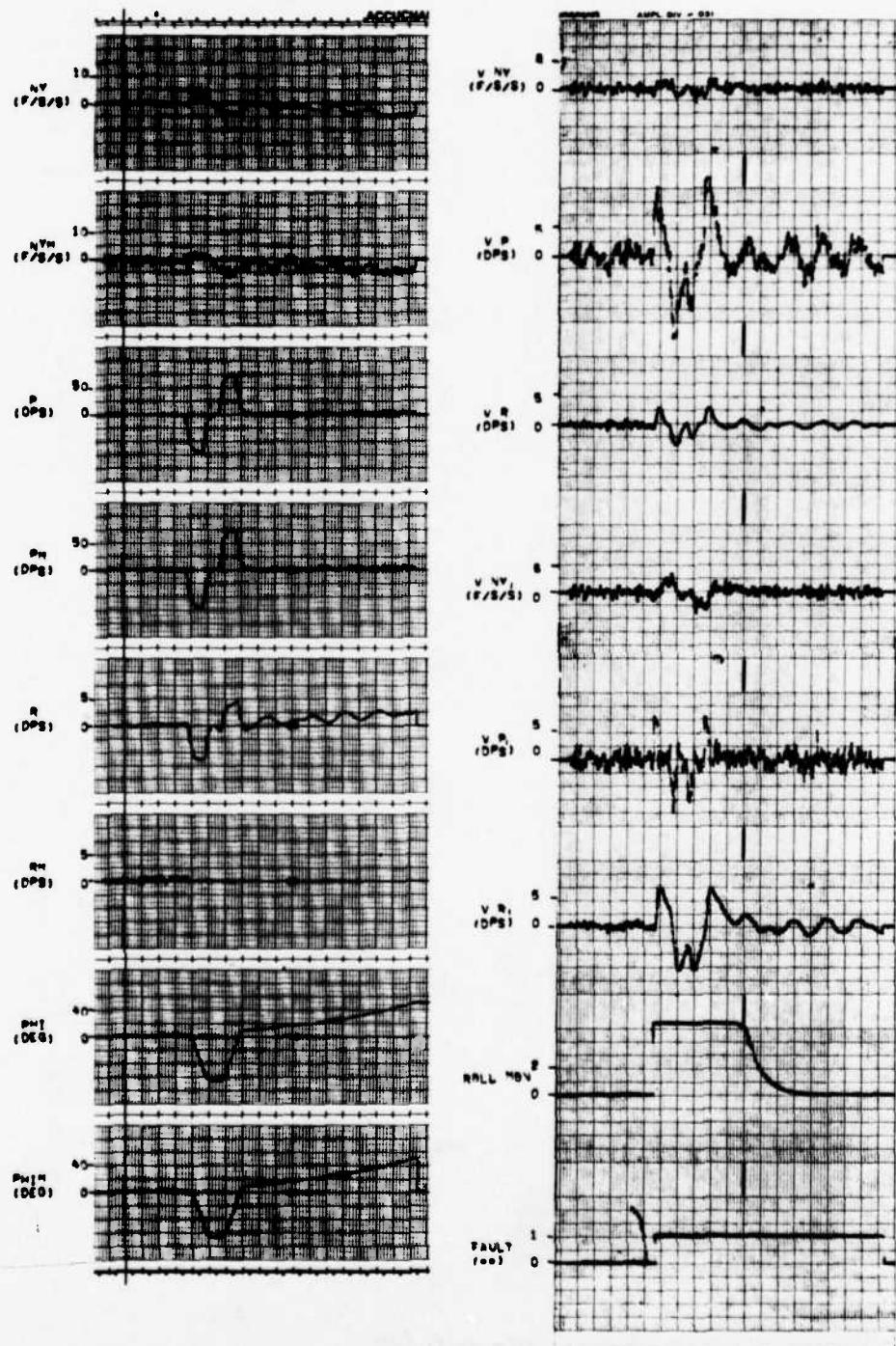
Figure D. 141

306

Figure D. 142

307

Figure D. 143

308

Figure D. 144

309

Figure D.145

310

Figure D. 146

311

Figure D. 147

312
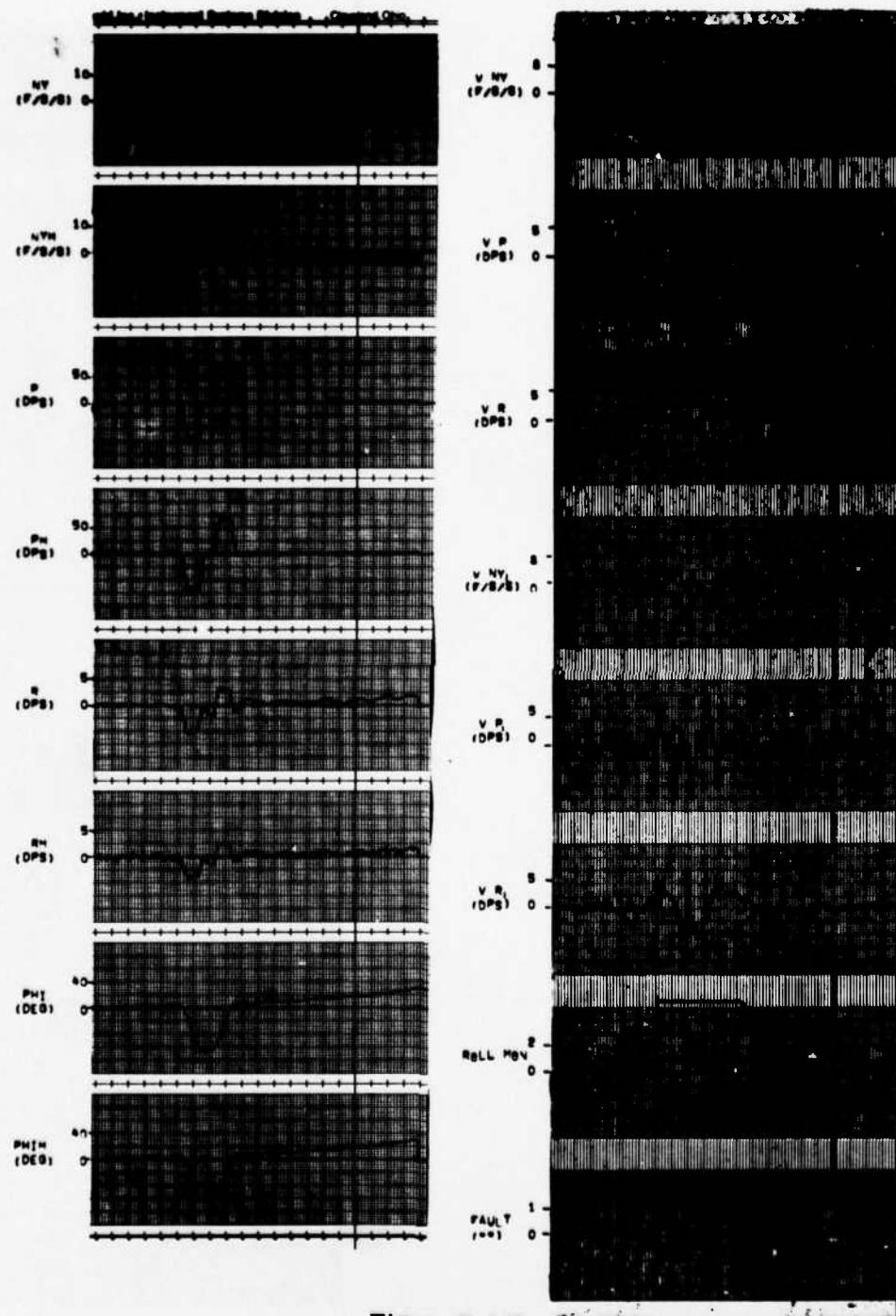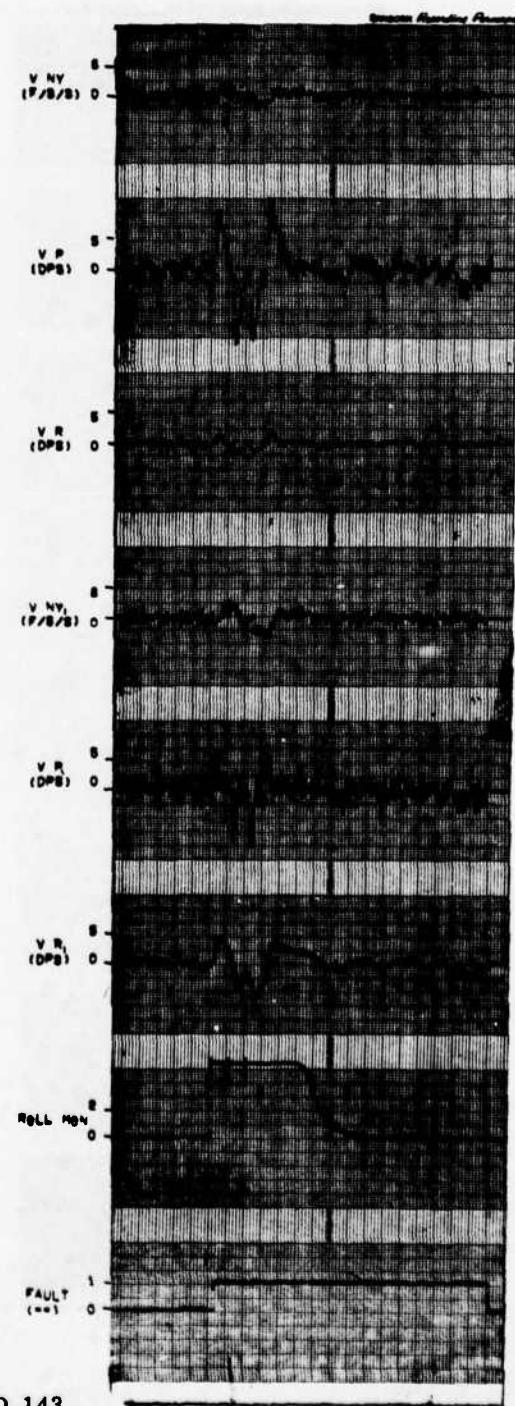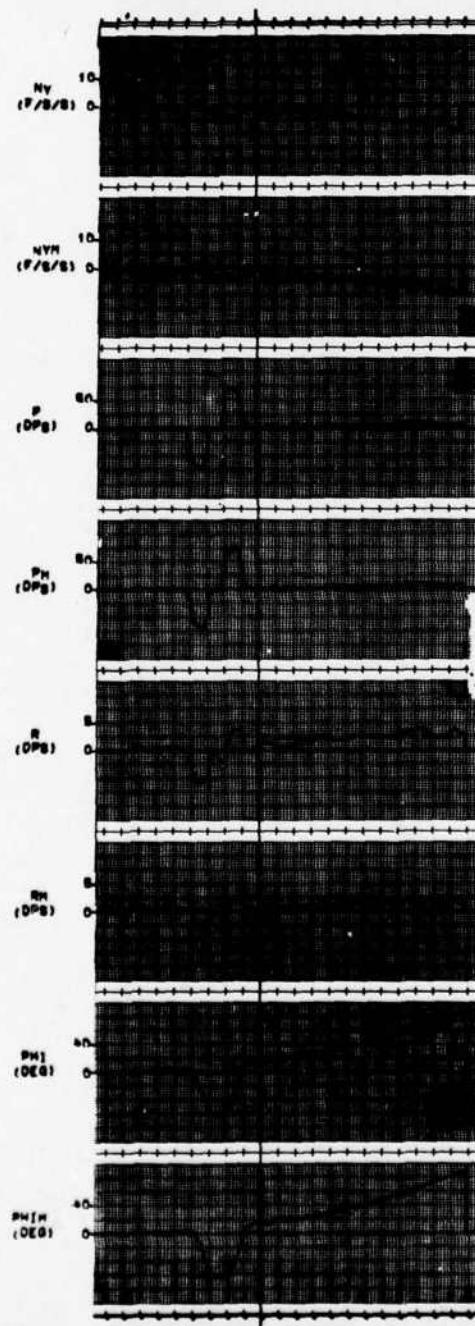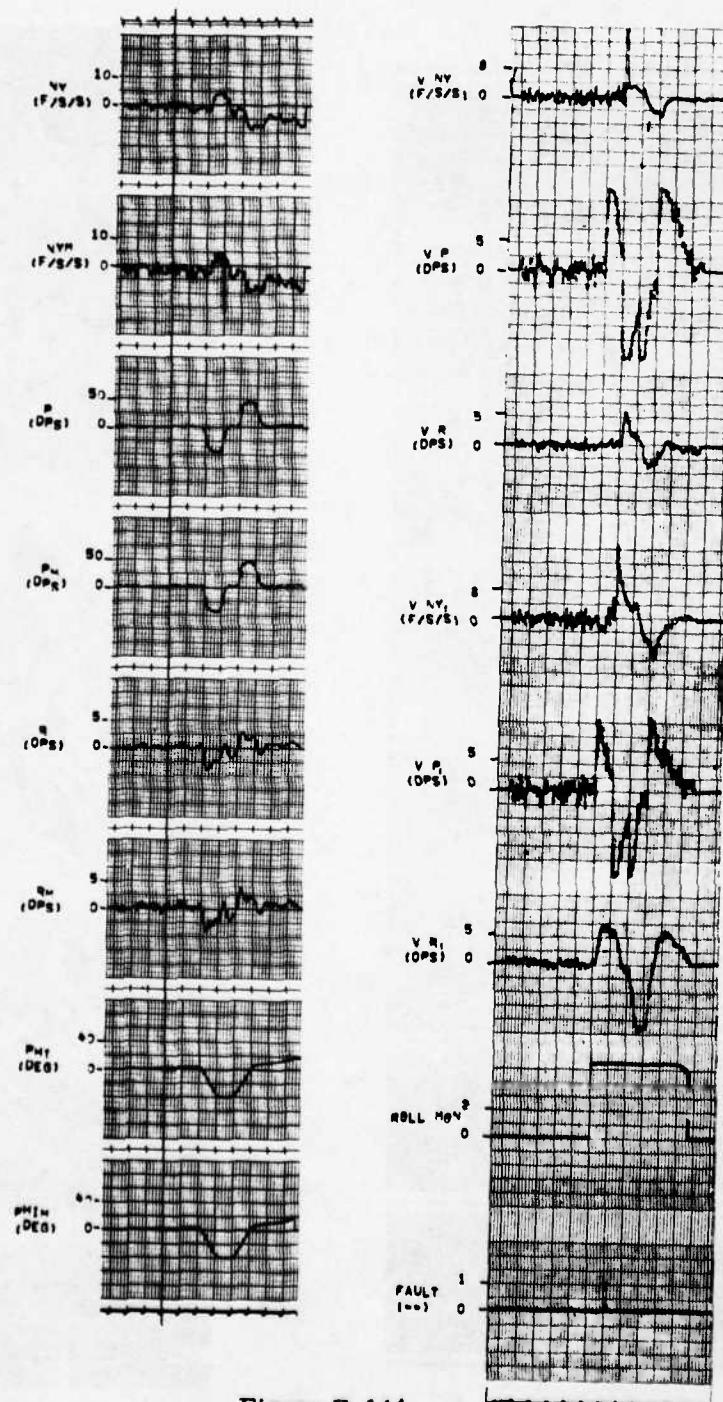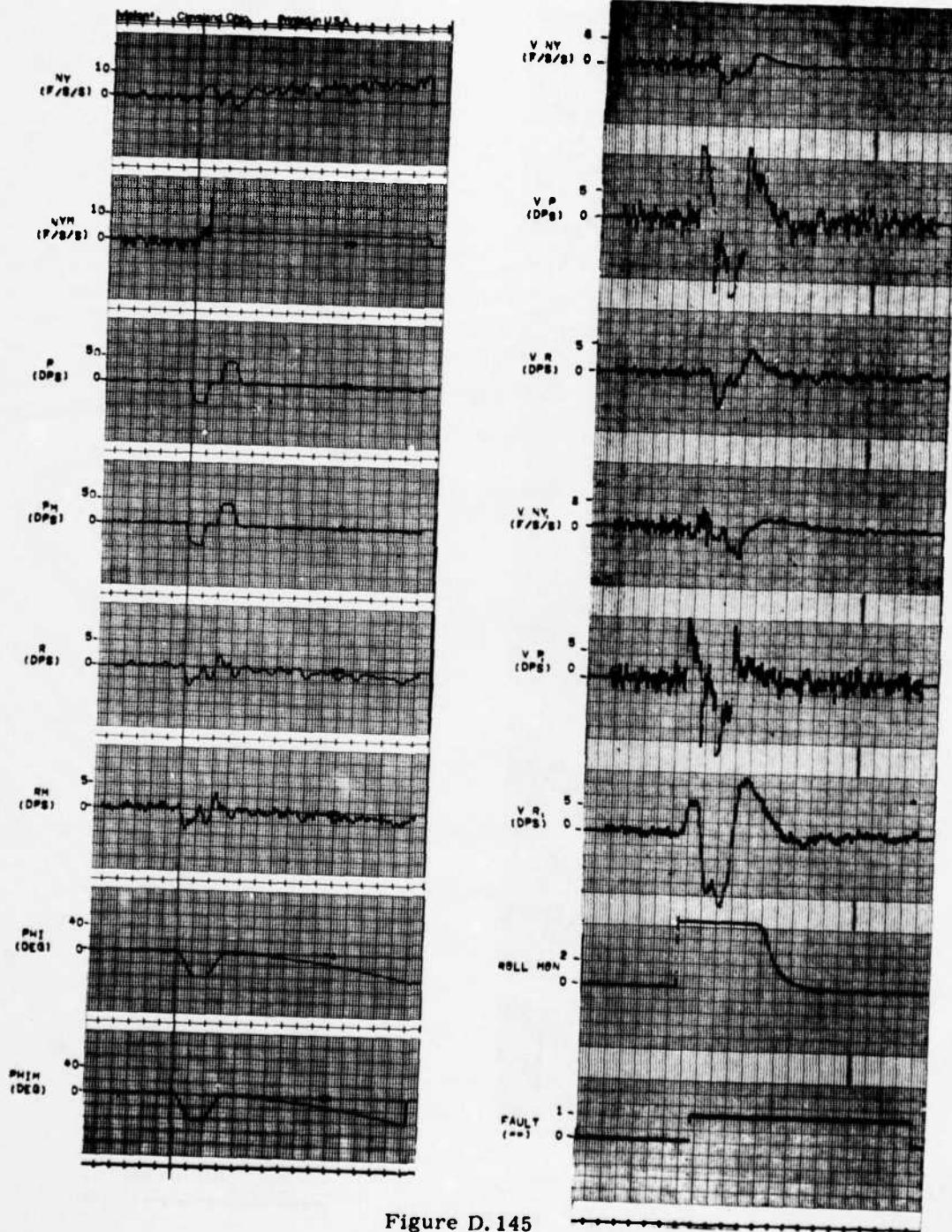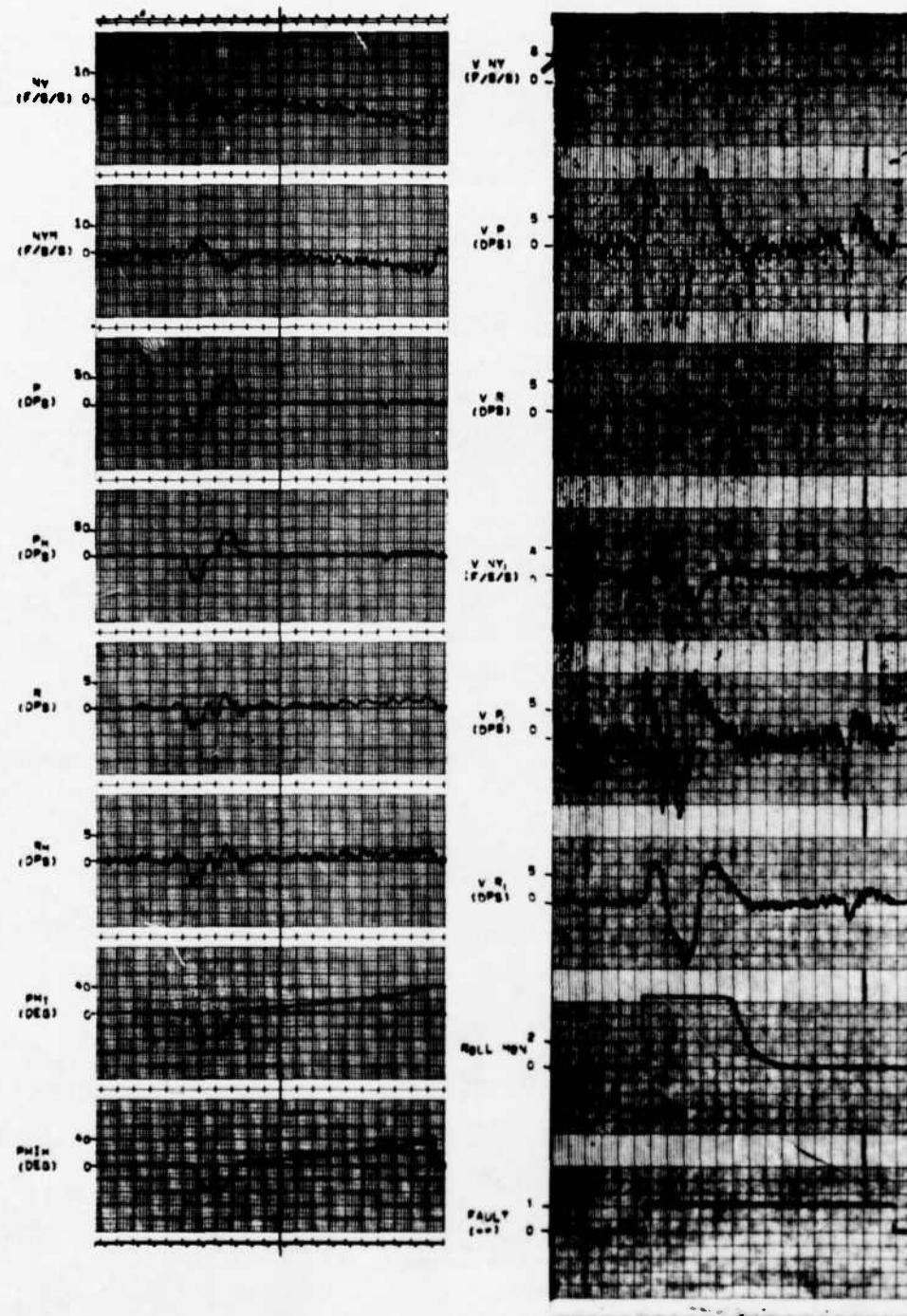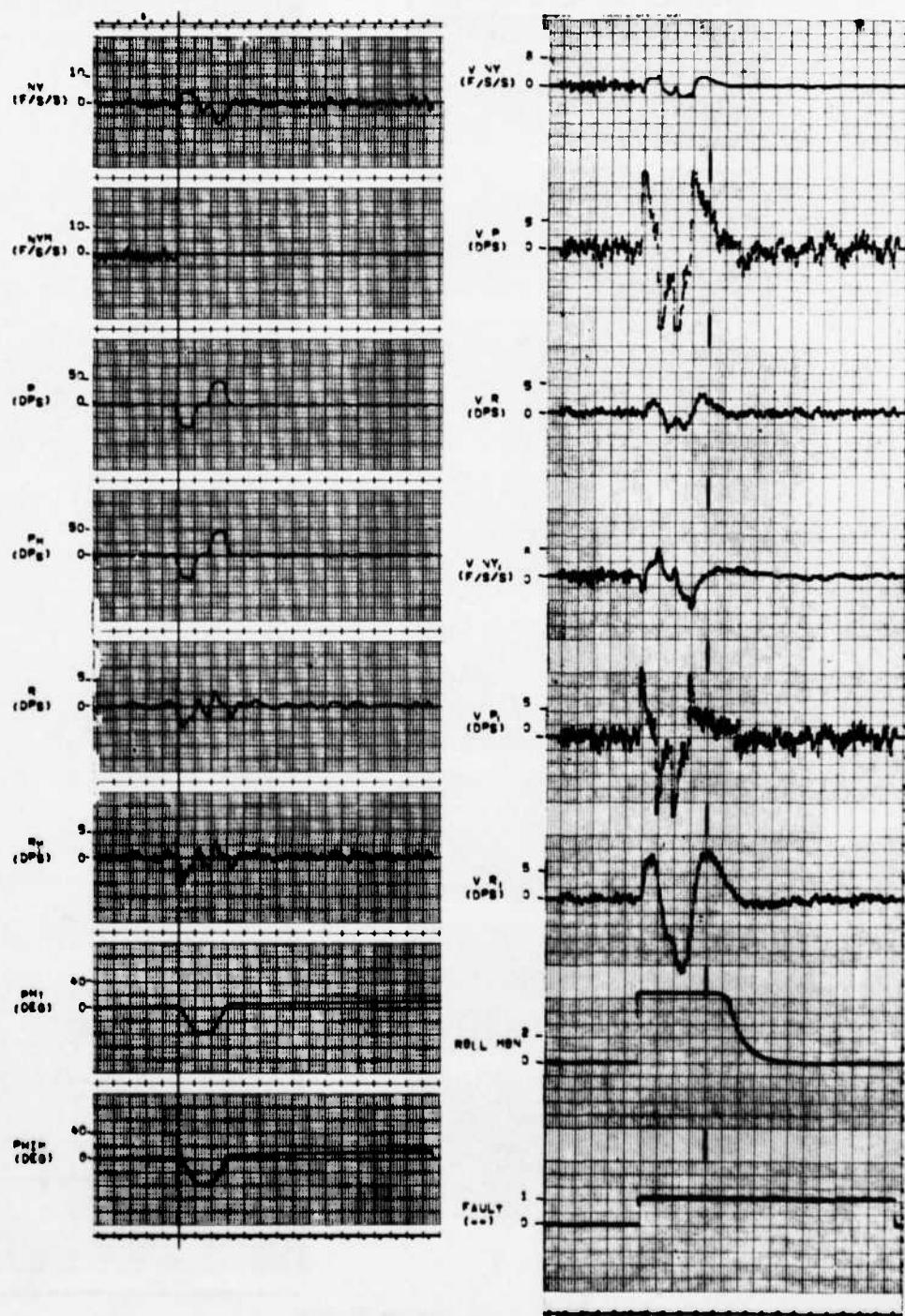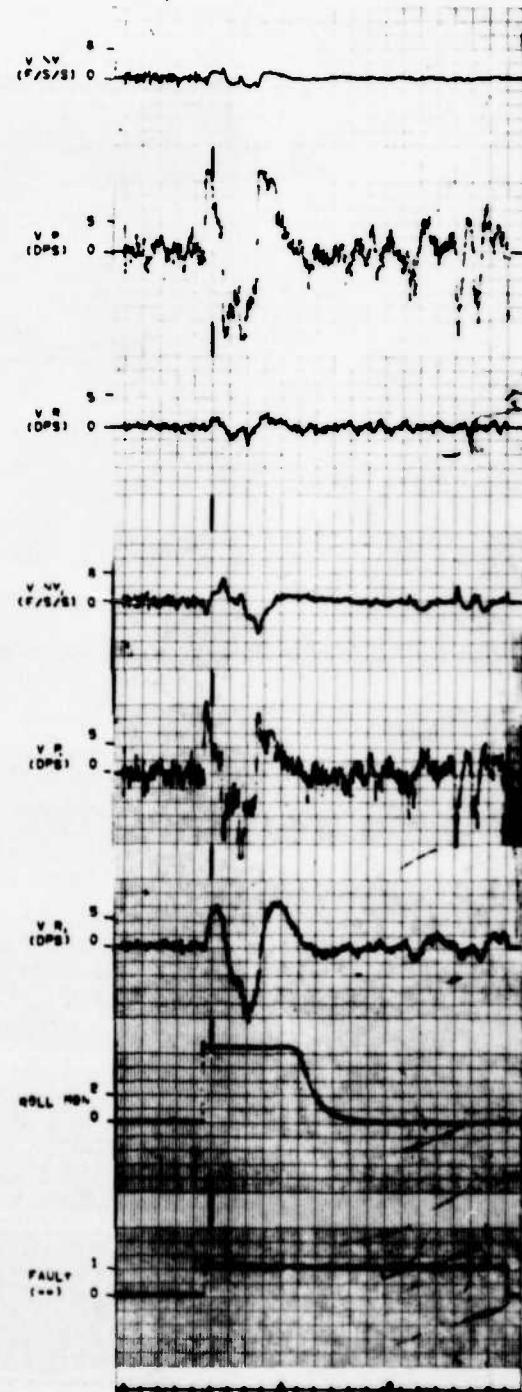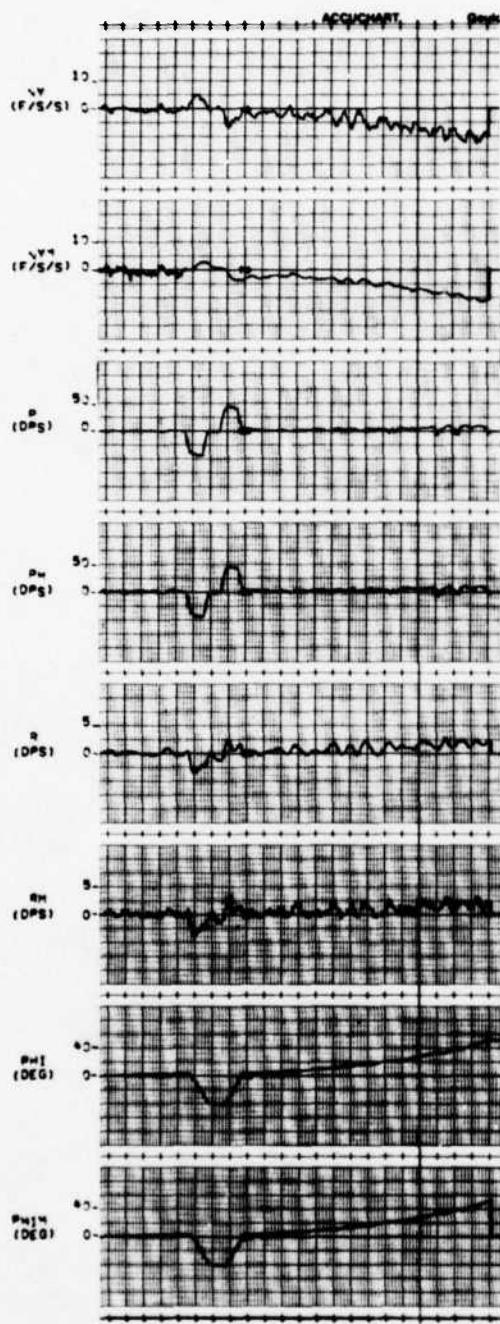
Figure D.148

Figure D. 149

314

Figure D.150

315
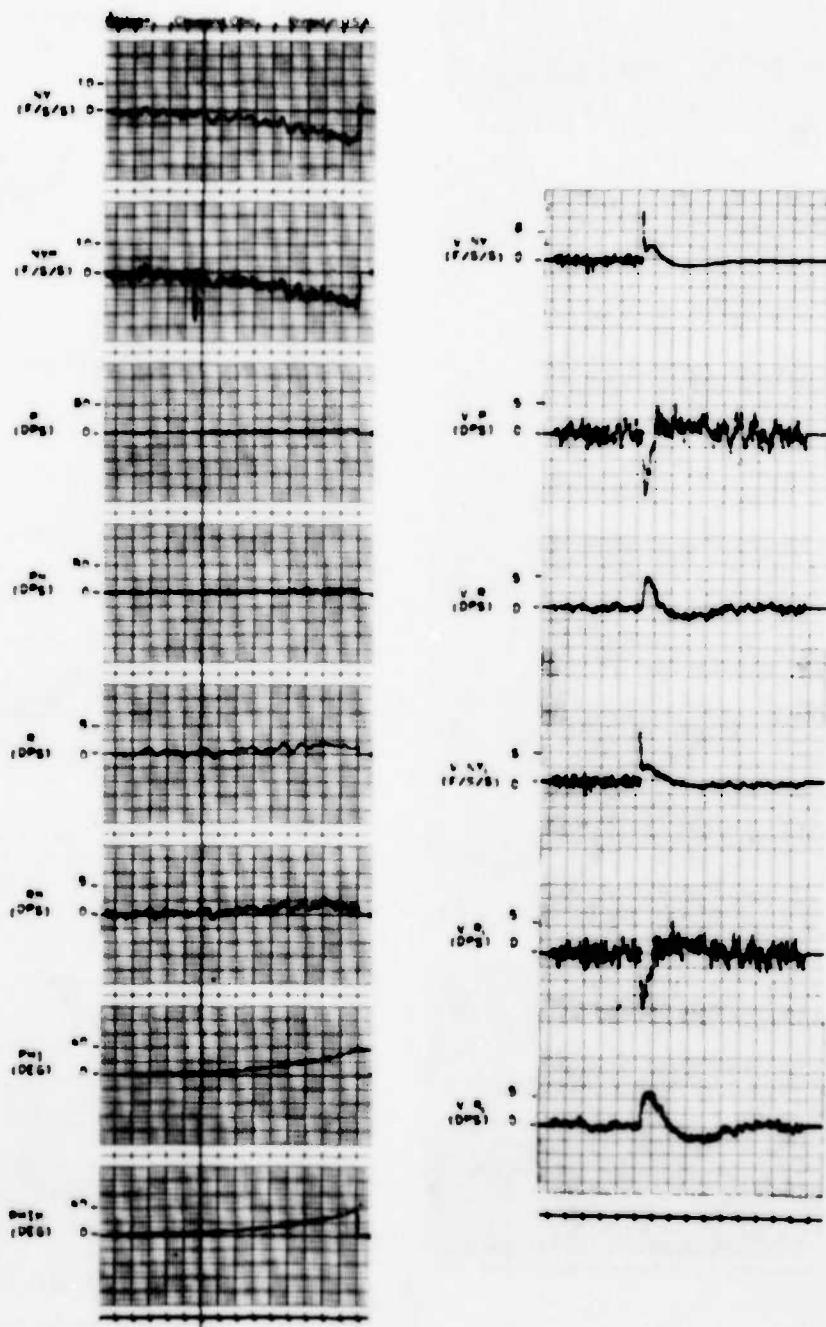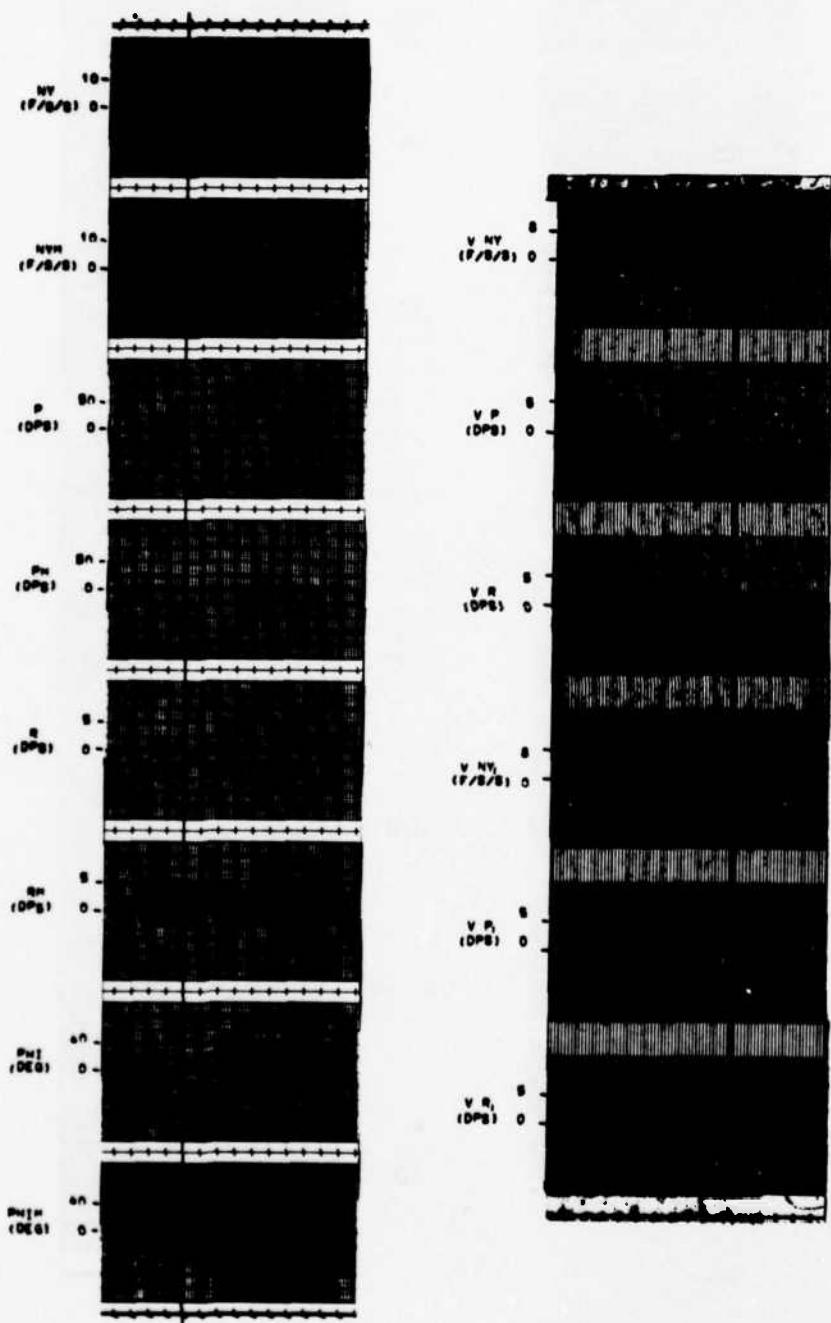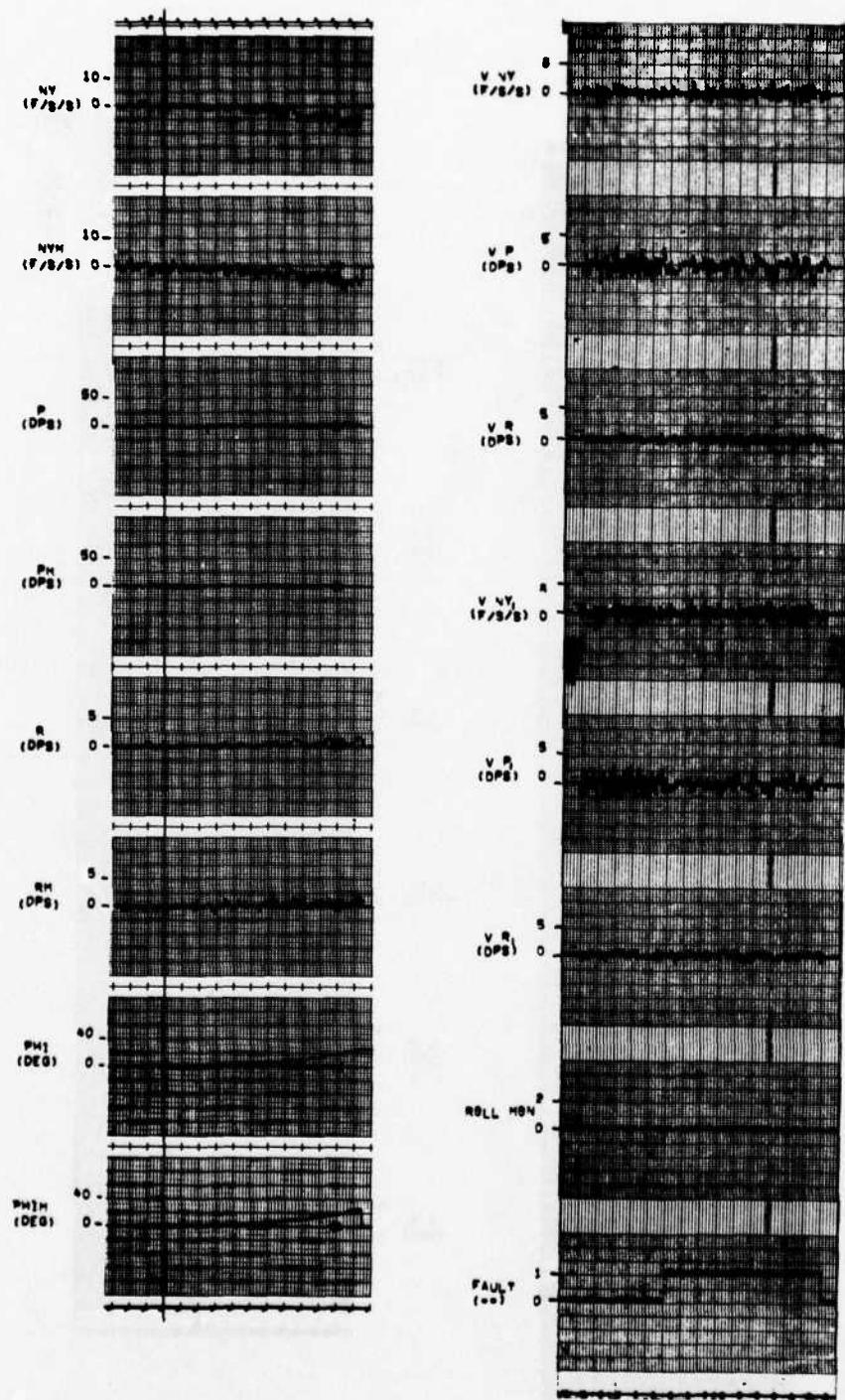
Figure D. 151

Figure D. 152

317

Figure D.153

318

Figure D. 154

319
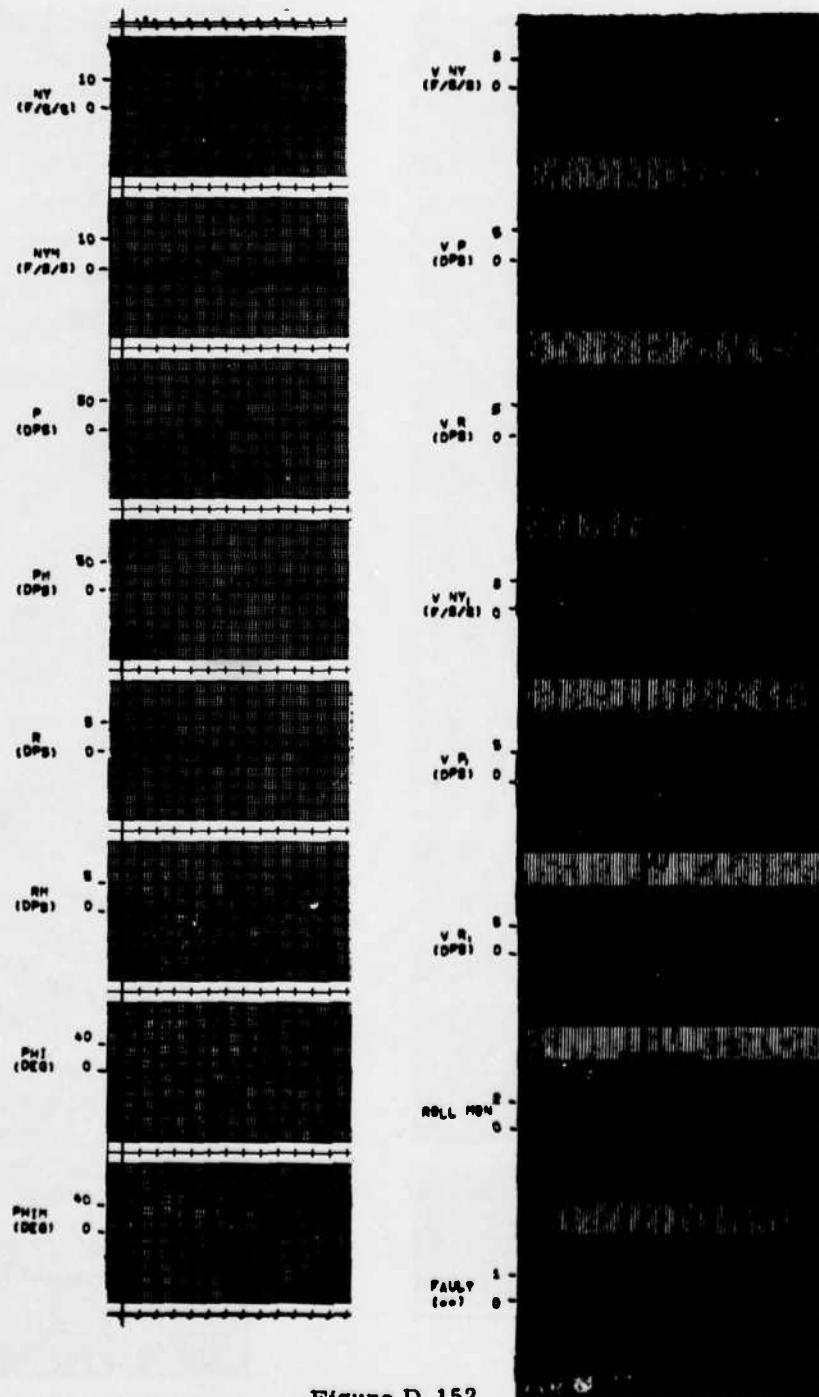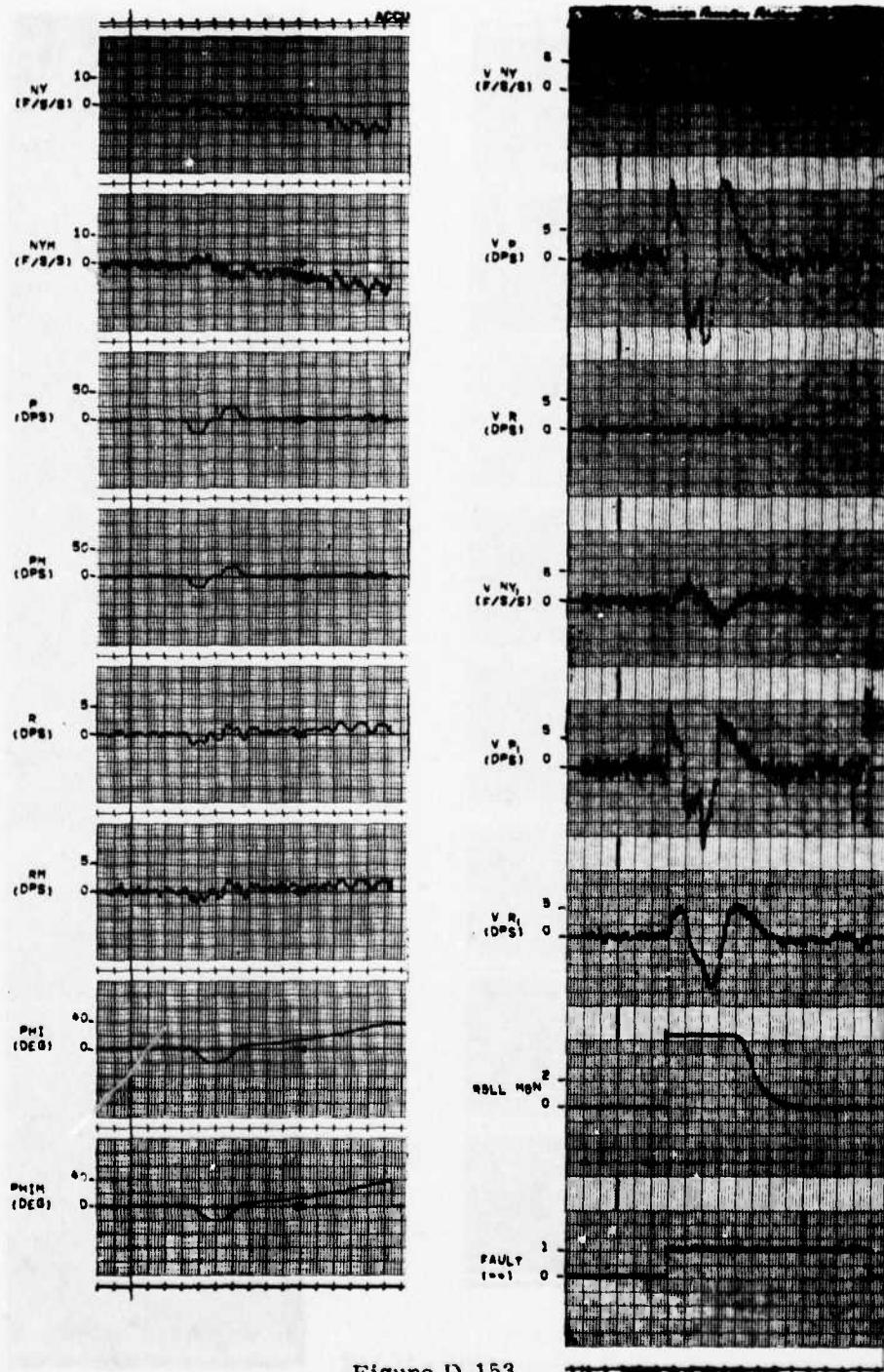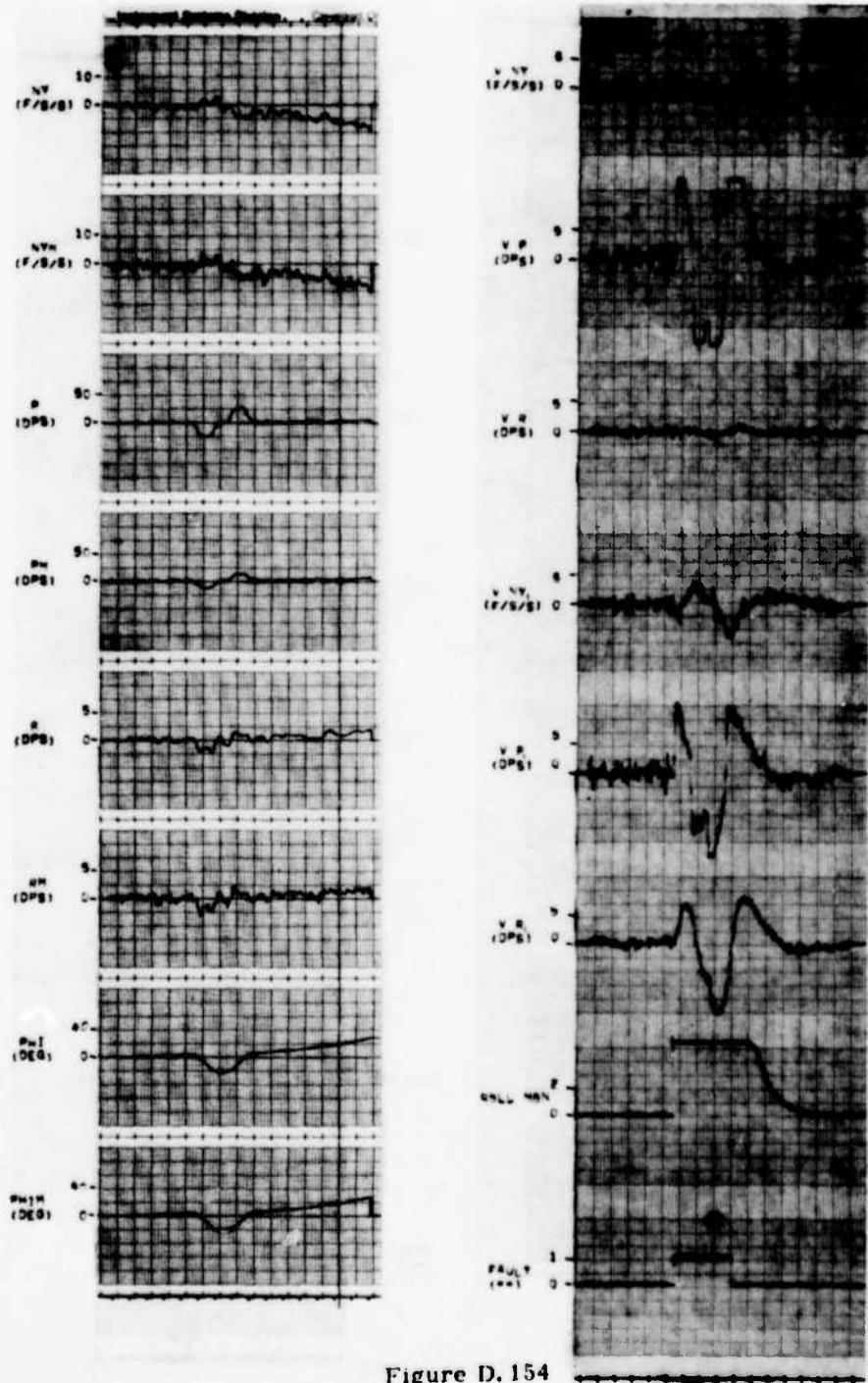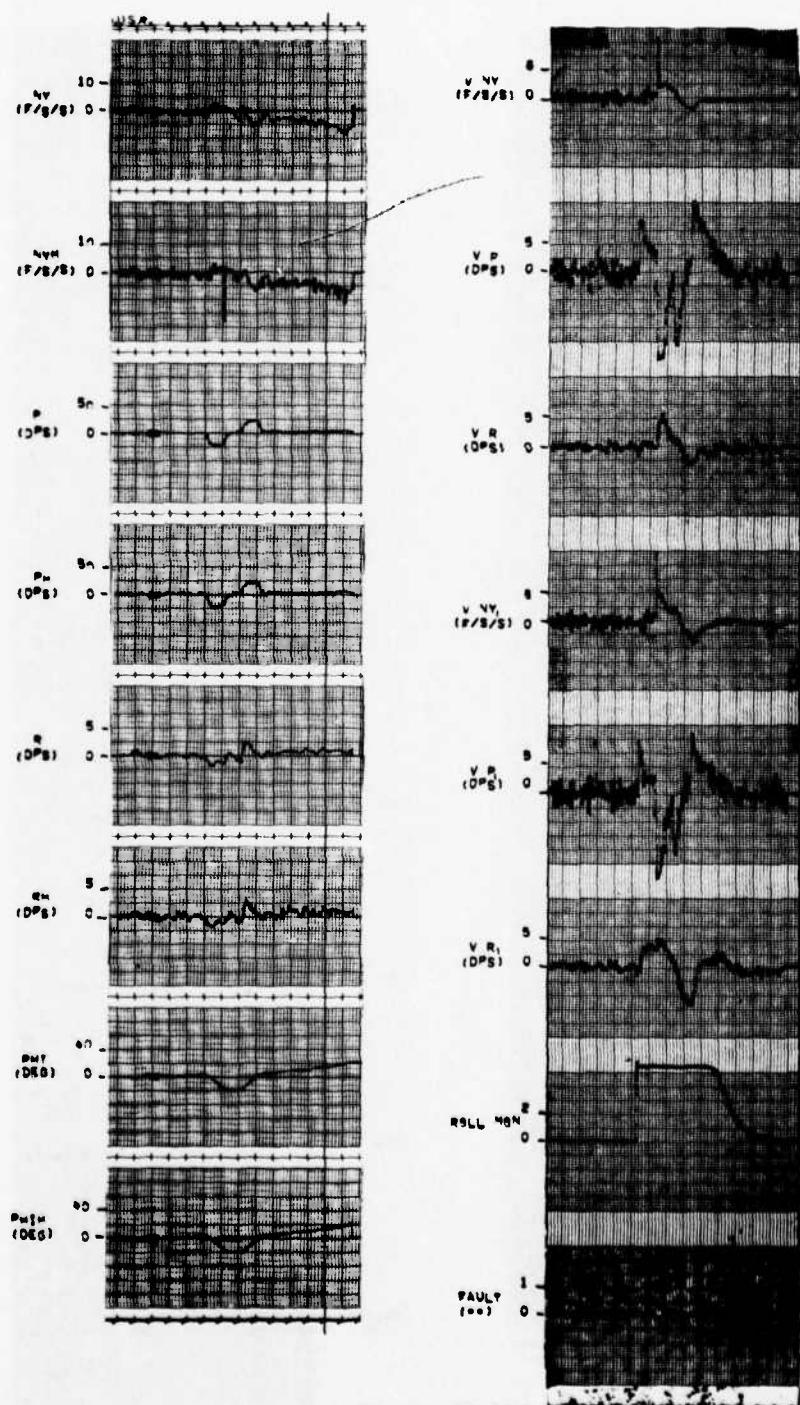
Figure D.155

Figure D.156

321
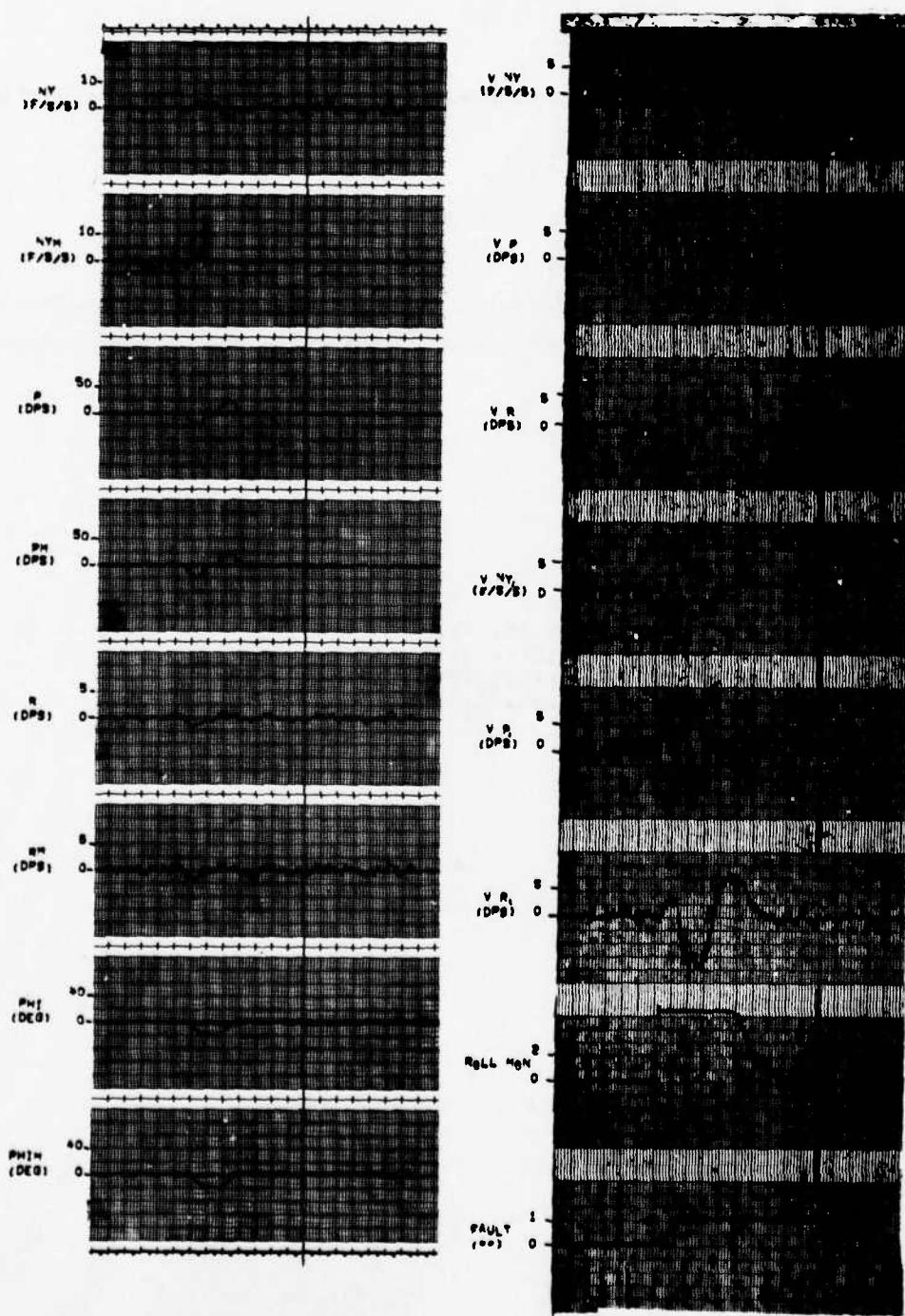
APPENDIX E

PROGRAM DOCUMENTATION

This appendix contains the routines used for the sensor fault evaluations examined in this study.

E.1 MAINLINE CALLING SEQUENCE

The implementation of the analytical redundancy schemes is made through a series of calls to modularized subroutines. The sequence of call statements for each concept is given in the subsections that follow.

E.1.1 Concept I Calling Sequence

```
C
C   CONCEPT 1
C
      CALL ROLLMON(DAC,V(30),1)
      CALL MONC(XMON1,XMONO,DMON,35,39,V(30))
      CALL DETECT(IFLAG1(35),V(35),V(36),V(37),V(38),V(39)
     1,XMON1(35),XMON1(36),XMON1(37),XMON1(38),XMON1(39))
      CALL FDELAY(IFLAG1,IFLAG2,35,39)
      CALL WHOA(Y)
```

```
┌─────────────────────┐
│   ENTER CONCEPT I   │
└─────────────────────┘
           │
           ▼
┌─────────────────────┐
│ APPLY ROLL MONITOR  │
│   UPLOGIC THROUGH   │
│  "ROLLMON" "MONC"   │
└─────────────────────┘
           │
           ▼
┌─────────────────────┐
│      EVALUATE       │
│      FAULTS.        │
│     "DETECT"        │
│       RLIM          │
│     "FOLAG"         │
│     "HIPASS"        │
└─────────────────────┘
           │
           ▼
┌─────────────────────┐
│    DELAY FAULT      │
│    DECLARATION      │
│     "FDELAY"        │
└─────────────────────┘
           │
           ▼
┌─────────────────────┐
│    APPLY SENSOR     │
│    CONSISTENCY      │
│        TEST         │
│       "WHOA"        │
└─────────────────────┘
           │
           ▼
┌─────────────────────┐
│   DISPLAY RESULTS   │
└─────────────────────┘
```
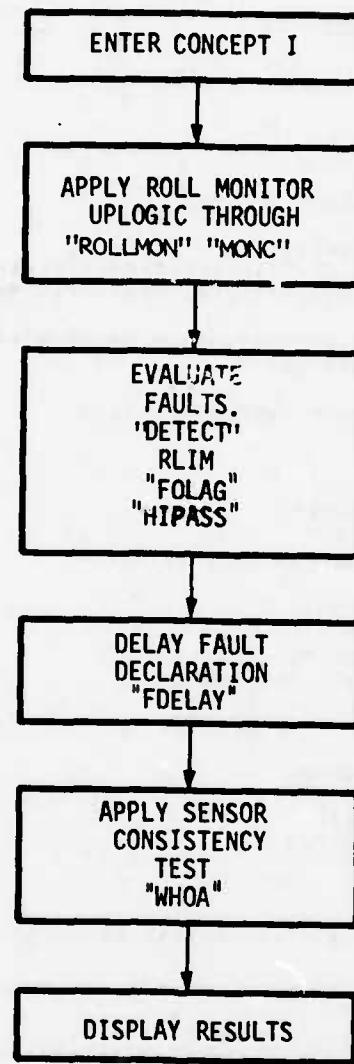
Figure E.1.   Concept I

323

E.1.2   Concept II Calling Sequence

```
C
C    CONCEPT 2 CALLING SEQUENCE
C
     CALL ROLLMON(DAC,V(30),1)
     CALL AR21(Y(6),Y(3),SP,CP,ST,CT,XBAR,XHAT,V,DT)
     CALL AR22(ALTM,ALM,NZM,Y(3),SP,CP,ST,CT,UOM,0.0,XBAR(4),XHAT(10)
    1,V(4),DT,T)
     CALL AR23(NYM,PM,RM,DRT,DAT,UOM,ALTM,QBARM,ALM,CT,SP,XBAR(7)
    1,XHAT(13),V(6),DT,OPTION)
C
C    SET MONITORS FOR MULTIPLE TRIP EVALUATION
C
     DO 86 I=1,8
  86 XMON1(I)=XMONO(I)
     CALL MONQ(XMON1,QBARM,T)
     CALL MONH(XMON1,ALTM)
     CALL MONC(XMON1,XMON1,DMON,1,8,V(30))
C
C    MULTIPLE TRIP EVALUATION
C
     CALL MON3(V,XMON1,IFLAG3,1,NV)
     CALL FDELAY(IFLAG3,IFLAG2,1,NV)
C
C    ADJUST MONITORS FOR SLRT EVALUATION
C
     XMON1(5)=XMON1(5)+.002
     XMON1(6)=XMON1(6)+0.2
     XMON1(7)=XMON1(7)+.01
     XMON1(8)=XMON1(8)+0.003
C
C    SLRT EVALUATION
C
     CALL MON1(V(1),XMON1(1),IFLAG1(1),NV,20,1)
C
C    SET-UP DUAL BODY-RATE SIGNALS FOR FAIL-OP EVALUATION
C
     CALL AR24(Y(6),Y(3),Y(12),SP,CP,ST,CT,XBAR(11),XHAT(17),V(9)
    1,DT,VLIKE)
C
C    EVALUATE COMPARISON MONITORS OF DUAL SIGNALS
C
     CALL MON3(V,XMON1,IFLAG1,31,33)
     CALL FDELAY(IFLAG1,IFLAG2,31,33)
C
C    APPLY SLRT FOR FAILURE ISOLATION
C
     CALL MON2(VLIKE,IFLAG1(31),IFLAG2(31),IFLAG1(34),IFLAG2(34)
    1,XMON1(34))
C
C    EXTRA, EVALUATE BODY-RATE BIAS ESTIMATION FOR BIAS FAULTS
C
     V(40)=XHAT(2)
     V(41)=XHAT(5)
     V(42)=XHAT(8)
     CALL MON3(V,XMON1,IFLAG1,40,42)
     CALL FDELAY(IFLAG1,IFLAG2,40,42)
     CALL WHOA(Y)
```
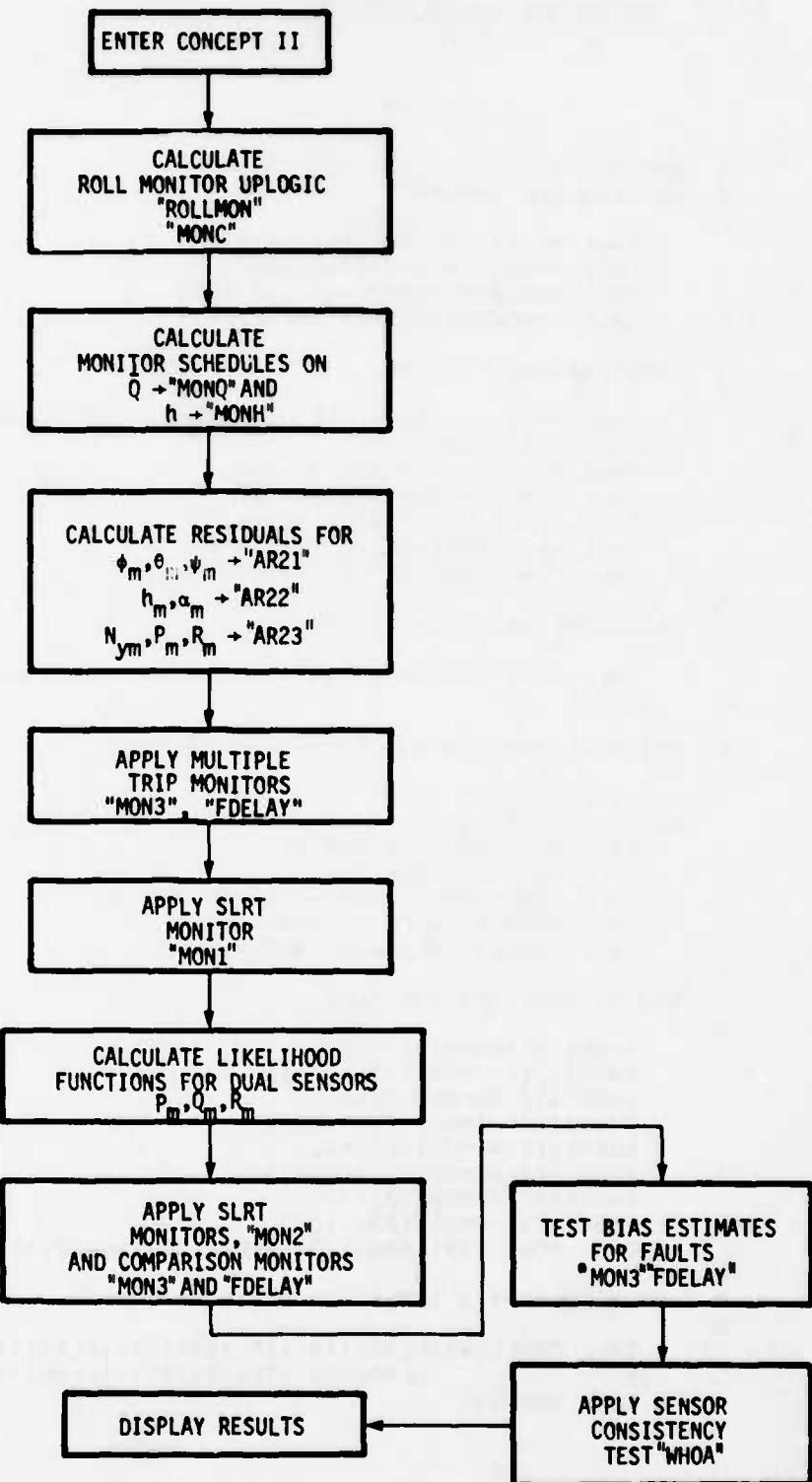
Figure E.2. Concept II

E.1.3   Concept III Calling Sequence

```
C  CONCEPT 3
C  HI-PASS ALL INPUTS
C
      CALL HPAS2(NZM,NZH,Z(1),Z(2))
      CALL HPAS2(QM,QH,Z(7),Z(8))
      CALL HPAS2(ALM,ALH,Z(11),Z(12))
      CALL HPAS2(DET,DEH,Z(13),Z(14))
C
C  LONGITUDINAL FILTERS
C
      CALL AR31(NZH,QH,ALH,DEH,UOM,ALTM,QBARM,XBAR(11),XHAT(17)
     1,V(9),DT,ICON)
      CALL HPAS2(NYM,NYH,Z(3),Z(4))
      CALL HPAS2(PM,PH,Z(5),Z(6))
      CALL HPAS2(RM,RH,Z(9),Z(10))
      CALL HPAS2(DAT,DAH,Z(15),Z(16))
      CALL HPAS2(DRT,DRH,Z(17),Z(18))
C
C  LATERAL-DIRECTIONAL FILTERS
C
      CALL AR32(NYH,PH,RH,DRH,DAH,UOM,ALTM,QBARM,XBAR(20),XHAT(26)
     1,V(18),DT)
C
C  SET MONITORS FOR MULTIPLE TRIP CRITERIA
C
      DO 85 I=9,29
   85 XMON1(I)=XMONO(I)
      CALL MONQ(XMON1,QBARM,T)
      CALL MONH(XMON1,ALTM)
      CALL MONC(XMON1,XMON1,DMON,9,29,V(30))
      CALL MON3(V,XMON1,IFLAG3,9,NV+8)
      CALL FDELAY(IFLAG3,IFLAG2,9,NV+8)
C
C  ADJUST MONITORS FOR SLRT
C
      XMON1(9)=XMON1(9)+.5
      XMON1(11)=XMON1(11)+.0015
      XMON1(12)=XMON1(12)+.5
      XMON1(14)=XMON1(14)+.0030
      XMON1(15)=XMON1(15)+1.0
      XMON1(17)=XMON1(17)+.0015
      XMON1(21)=XMON1(21)+.5
      XMON1(23)=XMON1(23)+.003
      CALL MON1(V(9),XMON1(9),IFLAG1(9),NV,20,1)
C
C  APPLY CONCEPT 3 ISOLATION LOGIC
C
      CALL C3RECOV(IFLAG1(12),IFLAG1(13),IFLAG1(16),IFLAG1(17)
     1,        IFLAG1(24),IFLAG1(26),IFLAG1(27),IFLAG1(28),ISENF,1)
      CALL WHOA(Y)
```

326
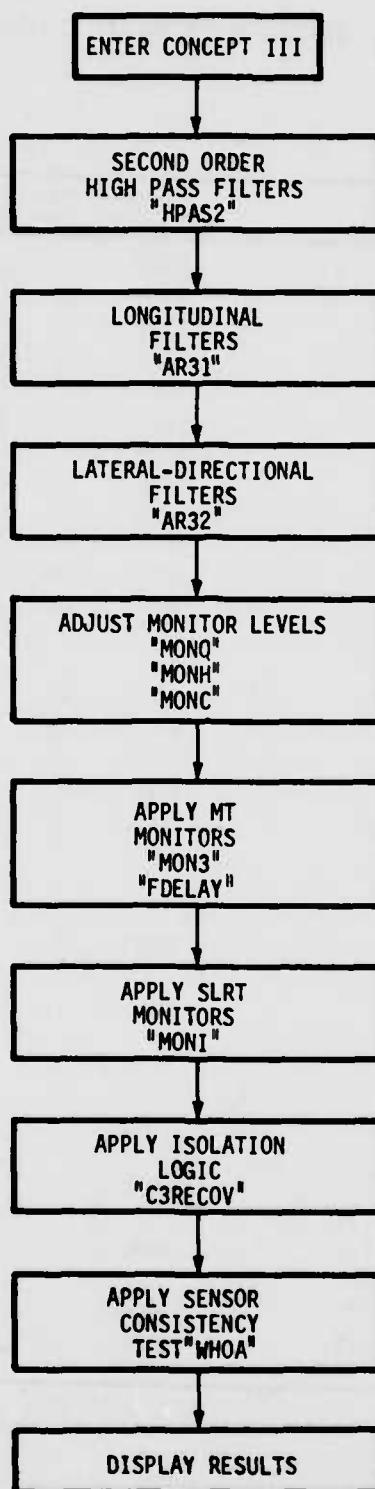
Figure E. 3.   Concept III

TABLE E.1. MAINLINE VARIABLE DEFINITIONS

Program Variable	Physical Quantity	Description	Program Variable	Physical Quantity	Description
Y(1)	n_{z_m}		V(22)	v_p	
Y(2)	n_{y_m}		V(23)	v_p	
Y(3)	P_m		V(24)	v_{n_y}	
Y(4)	Q_m		V(25)	v_p	Concept III Residuals
Y(5)	R_m		V(26)	v_R	
Y(6)	ϕ_m		V(27)	v_{n_y}	
Y(7)	θ_m	Measurements	V(28)	v_p	
Y(8)	ψ_m		V(29)	v_r	
Y(9)	U_m		V(30)	y	Roll Monitor
Y(10)	α_m		V(31)	ERR(1)	Dual Body Rate
Y(11)	H_m		V(32)	ERR(2)	Sensor Error
Y(12)	P_{m2}		V(33)	ERR(3)	Signals
Y(13)	Q_{m2}		V(34)	VLIKE	Likelihood Difference Function
Y(14)	R_{m2}				
V(1)	v_ϕ		V(35)	e_p	
V(2)	v_θ		V(36)	e_Q	
V(3)	v_ψ		V(37)	e_R	Concept I Error Signals
V(4)	v_H	Concept II Residuals	V(38)	e_{n_z}	
V(5)	v_α		V(39)	e_R	
V(6)	v_{n_y}		XHAT	$\hat{x}$	Concepts II and III updated Estimates
V(7)	v_p				
V(8)	v_R				
V(9)	v_{n_z}		XBAR	$\bar{x}$	Concepts II and III Predictions
V(10)	v_Q				
V(11)	v_α		DAC	δ_{a_c}	Aileron Command Signal
V(12)	v_{n_z}				
V(13)	v_Q		DT	Δt	Sample Time (.05 sec)
V(14)	v_α	Concept III Residuals			
V(15)	v_{n_z}		OPTION	-	Gain Schedule Option
V(16)	v_Q				
V(17)	v_α		XMONO	-	Initial Monitor Levels
V(18)	v_{n_y}				
V(19)	v_p		XMONI	-	Scheduled Monitor Levels
V(20)	v_R				
V(21)	v_{n_y}		IFLAGI, IFLAG2	-	Trip Flags

E.2 ANALYTICAL REDUNDANCY SUBROUTINES

E.2.1 __MONQ__--This routine schedules certain monitors with lagged $\bar{q}$.
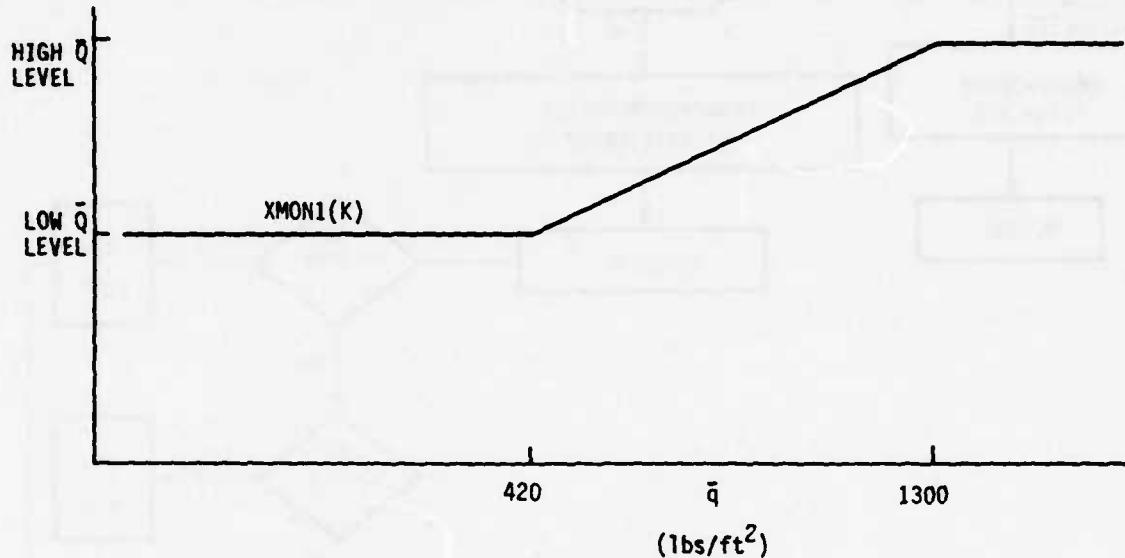

```
1:          SUBROUTINE MONQ(XMON1,QBARM,T)
2:          DIMENSION XMON1(1)
3:          IF(T.GT.0.) GO TO 1
4:          QBARF=QBARM
5:          PHIQ=.975
6:          RETURN
7:        1 CONTINUE
8:          QBARF=QBARF*PHIQ+(1.0-PHIQ)*QBARM
9:          SQ=QBARF
10:         IF(SQ.GT.1300.)SQ=1300.
11:         IF(SQ.LT.420.)SQ=420.
12:         RAT=(SQ-420.)/780.
13:         XMON1( 6)=( 2.0-XMON1( 6))*RAT+XMON1( 6)
14:         XMON1( 9)=( 6.2-XMON1( 9))*RAT+XMON1( 9)
15:         XMON1(12)=( 6.2-XMON1(12))*RAT+XMON1(12)
16:         XMON1(15)=(10.0-XMON1(15))*RAT+XMON1(15)
17:         XMON1(18)=( 2.0-XMON1(18))*RAT+XMON1(18)
18:         XMON1(21)=( 2.5-XMON1(21))*RAT+XMON1(21)
19:         XMON1(24)=( 2.0-XMON1(24))*RAT+XMON1(24)
20:         XMON1(27)=( 2.5-XMON1(27))*RAT+XMON1(27)
21:         RETURN
22:         END
```
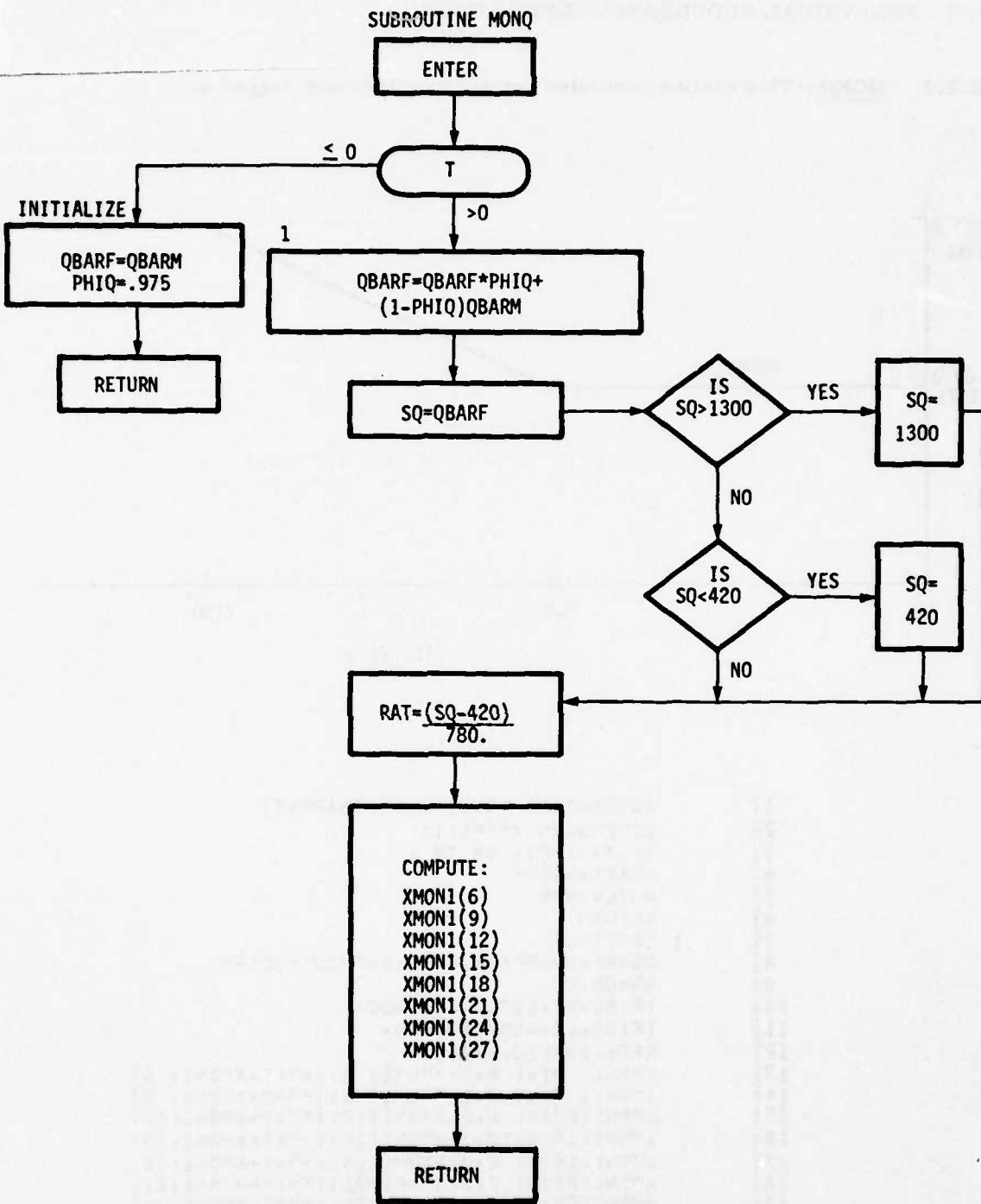
Figure E. 4. Subroutine MONQ

330

E.2.2 <u>ROLLMON</u>--This routine is used to increase monitors during roll maneuvers commanded by the roll stick.
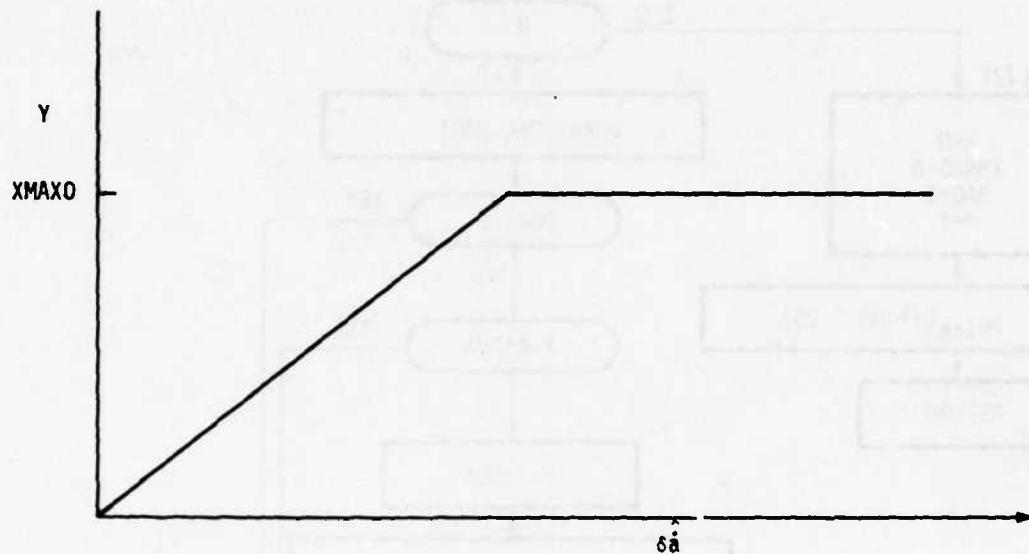
XMAXO ~ LARGEST $\delta\hat{a}$ ENCOUNTERED IN A GIVEN MANEUVER.

```
 1:          SUBROUTINE ROLLMON(DAC,Y,N)
 2:          IF(N.GT.0)GO TO 1
 3:          X=0.0
 4:          XMAX0=0.0
 5:          DA0=0.0
 6:          A=3.0
 7:          PHI=EXP(-ALOG(A)**05)
 8:          RETURN
 9:        1 CONTINUE
10:          DDA=3.0*ABS(DAC-DA0)
11:          IF(DDA.LT.0.2)GO TO 2
12:          IF(X.GT.A*DDA)GO TO 2
13:          X=A*DDA
14:          XMAX=AMIN(DDA,2.0)
15:          XMAX=AMAX(XMAX,XMAX0)
16:          XMAX0=XMAX
17:        2 CONTINUE
18:          Y=X
19:          IF(Y.GT.XMAX)Y=XMAX
20:          DA0=DAC
21:          X=X*PHI
22:          IF(X.LT.0.2)XMAX0=0.0
23:          RETURN
24:          END
```
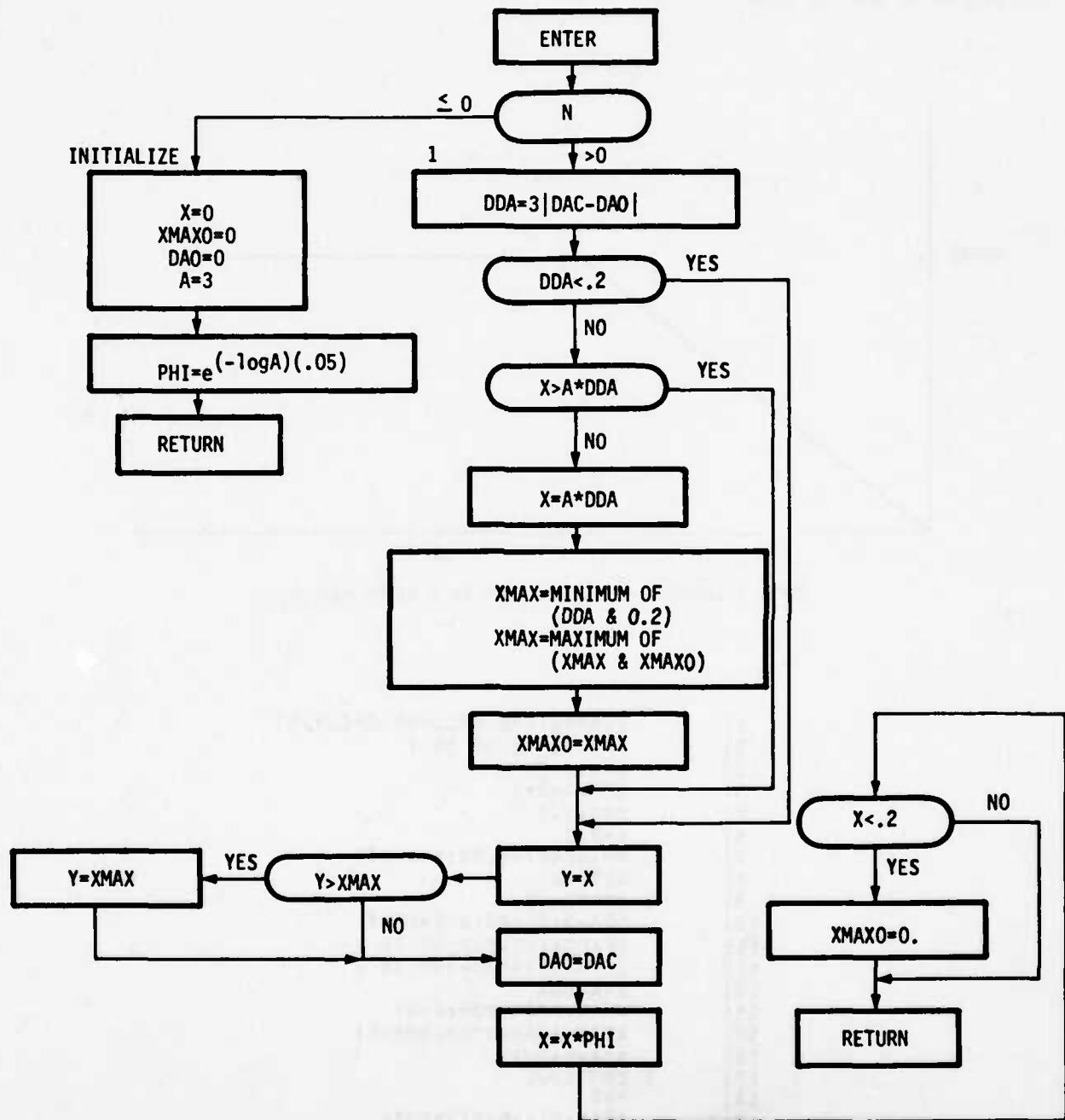
Figure E.5. Subroutine ROLLMON

332

E.2.3   MONC--Apply ROLL UPLOGIC calculated in ROLLMON.

```
1:        SUBROUTINE MONC(XMON1,XMONO,DMON,N1,N2,Y)
2:        DIMENSION XMON1(1),XMONO(1),DMON(1)
3:        DO 2 I=N1,N2
4:      2 XMON1(I)=XMONO(I)+DMON(I)*Y
5:        RETURN
6:        END
```
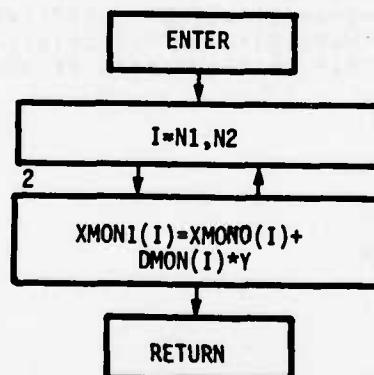

Figure E.6.   Subroutine MONC

333

E.2.4   <u>DETECT</u>--Complete Concept I algorithm (not including multiple trip delay).

```
 1:         SUBROUTINE DETECT(IFAIL,PE,QE,RE,NZE,HDE,KP1,KQ1,KR1,KNZ1,KHD1)
 2: C  SENSOR FAILURE DETECTION LOGIC
 3: C  CONCEPT 1
 4:         DIMENSION IFAIL(1)
 5:         COMMON /FILTIC/MODE,DT
 6:         COMMON /FILTER/XP(20),YP(20),C1(20),C2(20),XPP(10),DTI
 7:         COMMON /SENS/Y(17),LLIM(11),ULIM(11),SIGB(11),SIGSF(11),SIGSN(11)
 8:       1,BIAS(11),SFBR(3)
 9:         REAL LLIM
10:         REAL NZS,NZE,NZEA
11:         REAL NZM,NYM
12:         REAL KP1,KP2
13:         REAL KQ1,KQ2,KQ3,KQ4
14:         REAL KR1,KR2,KR3,KR4
15:         REAL KNZ1,KNZ2,KNZ3,KNZ4,KNZ5,KNZ6
16:         REAL KHD1,KHD2,KHD3,KHD4
17:         DATA KP2/.055/
18:         DATA KQ2,KQ3,KQ4/.055,.0053,0.0/
19:         DATA KR2,KR3,KR4/.055,.0050,0.0/
20:         DATA KNZ2,KNZ3,KNZ4,KNZ5,KNZ6/.015,.35,.54,.0342,.0353/
21:         DATA KHD2,KHD3,KHD4/.028,.35,21./
22:         DATA RTD/57.3/
23: C
24: C  DIGITAL INPUTS
25:         EQUIVALENCE (NZM,Y(1)),(NYM,Y(2)),(PM,Y(3)),(QM,Y(4)),(RM,Y(5))
26:       1             ,(PHIM,Y(6)),(THETAM,Y(7)),(PSIM,Y(8)),(UOM,Y(9))
27:       2             ,(ALM,Y(10)),(ALTM,Y(11)),(DEO,Y(12)),(DAO,Y(13))
28:       3             ,(DRO,Y(14)),(UG,Y(15)),(VG,Y(16)),(WG,Y(17))
29: C
30:         NZS=NZM/32.17
31:         PDS=PM*RTD
32:         QDS=QM*RTD
33:         RDS=RM*RTD
34:         PHIDS=PHIM*RTD
35:         THDS=THETAM*RTD
36:         PSIDS=PSIM*RTD
37:         VELS=UOM
38:         ALDS=ALM*RTD
39:         HS=ALTM
40:         SPHIS=SIN(PHIM)
41:         CPHIS=COS(PHIM)
42:         STHS=SIN(THETAM)
43:         CTHS=COS(THETAM)
44:         PDSA=ABS(PDS)
45:         QDSA=ABS(QDS)
46:         RDSA=ABS(RDS)
```

334

```
47: C
48: C    ROLL RATE MECHANIZATION
49:         T1=DERIV(7,PHIDS) + DERIV(1,PSIDS)*STHS
50:         T2=PDS - RLIM(T1,-200.,200.)
51:         PE=FOLAG(1,.1,T2)
52:         PEA=ABS(PE)
53:         T3=KP1 + KP2*PDSA
54:         IFAIL(1)=0
55:         IF(PEA.GE.T3) IFAIL(1)==1
56: C
57: C    PITCH RATE MECHANIZATION
58:         T4=DERIV(2,THDS)*CPHIS
59:         T5=DERIV(3,PSIDS)*SPHIS*CTHS
60:         T6=T4 + T5
61:         T7=QDS - RLIM(T6,-30.,30.)
62:         QE=FOLAG(2,.1,T7)
63:         QEA=ABS(QE)
64:         T8=KQ1 + KQ2*QDSA + KQ3*PDSA + KQ4*RDSA
65:         IFAIL(2)=0
66:         IF(QEA.GE.T8) IFAIL(2)==1
67: C
68: C    YAW RATE MECHANIZATION
69:         T9=DERIV(4,PSIDS)*CPHIS*CTHS
70:         T10=DERIV(5,THDS)*SPHIS
71:         T11=RDS - T9 + T10
72:         RE=FOLAG(3,.1,T11)
73:         REA=ABS(RE)
74:         T12=KR1 + KR2*RDSA + KR3*PDSA + KR4*QDSA
75:         IFAIL(3)=0
76:         IF(REA.GE.T12) IFAIL(3)==1
77: C
78: C    NORMAL ACCEL MECHANIZATION (NO. 1)
79:         T13=QDS - DERIV(6,ALDS)
80:         T14=VELS*T13/(57.3*32.17)
81:         T15=T14 + CTHS*CPHIS - 1.
82:         T16=NZS - RLIM(T15,-4.,10.)
83:         NZE=FOLAG(4,.1,T16)
84:         NZEA=ABS(NZE)
85:         T17=KNZ1 + KNZ2*QDSA + KNZ3*ABS(NZS) +
86:        1           VELS*(KNZ4 + KNZ5*QDSA + KNZ6*PDSA)/(57.3*32.17)
87:         IFAIL(4)=0
88:         IF(NZEA.GE.T17) IFAIL(4)==1
89: C
90: C    ALTITUDE MECHANIZATION
91:         T18=STHS - CPHIS*CTHS*ALDS/57.3
92:         T19=VELS*T18
93:         HDS=HIPASS(5,.1,HS)
94:         HDE=HDS - FOLAG(6,.1,T19)
95:         HDEA=ABS(HDE)
96:         T20=KHD1 + KHD2*ABS(VELS) + KHD3*ABS(HDS) + KHD4
97:         IFAIL(5)=0
98:         IF(HDEA.GE.T20) IFAIL(5)==1
99:         RETURN
100:        END
```

ENTER

CONVERT SENSOR INPUTS
TO DEGREES & "G'S"

ROLL RATE
MECHANIZATION   CONCEPT 1

$IFAIL(1)=0$
$P_e=P-\dot{\phi}+\dot{\psi}\sin\theta$

$IFAIL(1)=-1$ if:
$|P_e|\geq KP_1+KP_2|P|$

PITCH RATE
MECHANIZATION   CONCEPT 1

$IFAIL(2)=0$
$Q_e=Q-\dot{\theta}\cos\phi-\dot{\psi}\sin\phi\cos\theta$

$IFAIL(2)=-1$ if:
$|Q_e|\geq KQ_1+KQ_2|Q|+KQ_3|P|+KQ_4|R|$

YAW RATE
MECHANIZATION   CONCEPT 1

$IFAIL(3)=0$
$R_e=R-\dot{\psi}\cos\phi\cos\theta+\dot{\theta}\sin\phi$

$IFAIL(3)=-1$ if:
$|R_e|\geq KR_1+KR_2|R|+KR_3|P|+KR_4|Q|$

NORMAL ACCEL.
MECHANIZATION   CONCEPT 1

$IFAIL(4)=0$
$N_{ze}=N_z-V_T(Q-\dot{\alpha})-g(\cos\theta\cos\phi-1)$

$IFAIL(4)=-1$ if:
$|N_{ze}|\geq KN_{z1}+KN_{z2}|Q|+KN_{z3}|N_z|+$
$(V_T/57.3)(KN_{z4}+KN_{z5}|Q|+KN_{z6}|P|)$

ALTITUDE RATE
MECHANIZATION   CONCEPT 1

$IFAIL(5)=0$
$\dot{H}_1=SH$

$\dot{H}_2=V_T(\sin\theta-\sin\alpha\cos\phi\cos\theta)$
$\dot{H}_e=\dot{H}_1-\dot{H}_2$

$IFAIL(5)=-1$ if:
$|\dot{H}_e|\geq KHD_1+KHD_2|V_T|+KHD_4|\dot{H}_1|+KHD_4$

RETURN

Figure E.7. Subroutine DETECT

E. 2. 5   <u>FOLAG</u>--First order lag filter, used in Concept I.

```
 1:          FUNCTION FOLAG(I,TAU,X)
 2:  C  MODELS  1/(TS + 1) FILTERS
 3:          COMMON /FILTIC/MODE,DT
 4:          COMMON /FILTER/XP(20),YP(20),C1(20),C2(20),XPP(10),DTI
 5:  C
 6:          IF(MODE) 100,100,300
 7:      100 CONTINUE
 8:          C1(I)=DT/(2.*TAU + DT)
 9:          C2(I)=(2.*TAU - DT)/(2.*TAU + DT)
10:          XP(I)=X
11:          YP(I)=X
12:      300 FOLAG=C1(I)*(X + XP(I)) + C2(I)*YP(I)
13:          XP(I)=X
14:          YP(I)=FOLAG
15:          RETURN
16:          END
```
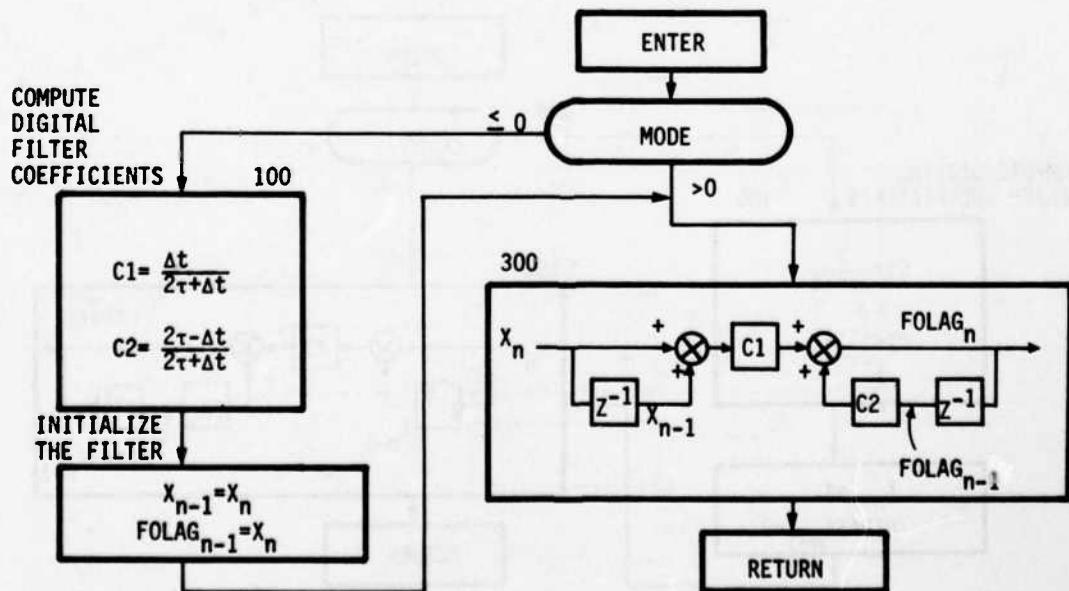

Figure E. 8.   Subroutine FOLAG

337

E.2.6   HIPASS--First order high-pass filter, used in Concept I.

```
 1:        FUNCTION HIPASS(I,TAU,X)
 2: C  MODELS  S/(TS + 1) FILTER
 3:        COMMON /FILTIC/MODE,DT
 4:        COMMON /FILTER/XP(20),YP(20),C1(20),C2(20),XPP(10),DTI
 5: C
 6:        IF(MODE) 100,100,300
 7:    100 CONTINUE
 8:        C1(I)=2./(2.*TAU + DT)
 9:        C2(I)=(2.*TAU - DT)/(2.*TAU + DT)
10:        XP(I)=X
11:        YP(I)=0.
12:    300 HIPASS=C1(I)*(X - XP(I)) + C2(I)*YP(I)
13:        XP(I)=X
14:        YP(I)=HIPASS
15:        RETURN
16:        END
```
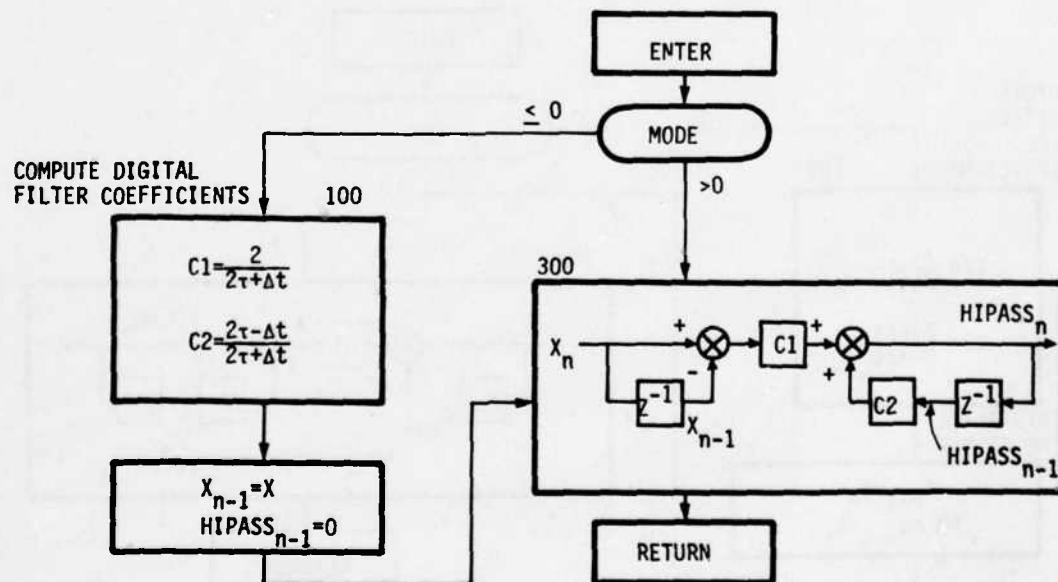

Figure E.9.   Subroutine HIPASS

338

E.2.7 <u>DERIV</u>--Digital derivative calculation, used in Concept I.

$$\dot{X} = (X - XLAST)/DT$$

```
1:        FUNCTION DERIV(I,X)
2: C  COMPUTES DERIVATIVE OF X
3:        COMMON /FILTIC/MODE,DT
4:        COMMON /FILTER/XP(20),YP(20),C1(20),C2(20),XPP(10),DTI
5: C
6:        IF(MODE) 100,100,300
7:    100 DTI=1./DT
8:        XPP(I)=X
9:    300 DERIV=(X - XPP(I))*DTI
10:       XPP(I)=X
11:       RETURN
12:       END
```
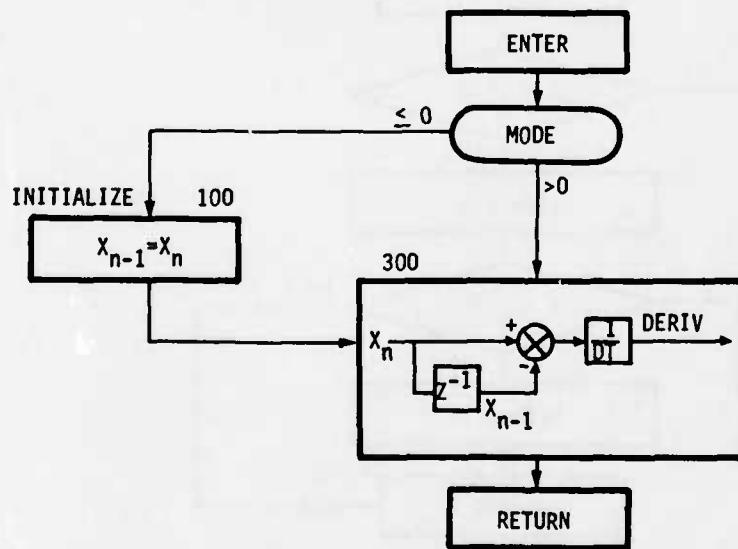

Figure E.10. Subroutine DERIV

339

E.2.8   RLIM--Apply prescribed limits on monitor movement, used in Concept I.

```
1:          FUNCTION RLIM(X,LLIM,ULIM)
2: C  LIMIT UPPER AND LOWER VALUES OF X
3:          REAL LLIM
4:          RLIM=X
5:          IF(X.GT.ULIM) RLIM=ULIM
6:          IF(X.LT.LLIM) RLIM=LLIM
7:          RETURN
8:          END
```
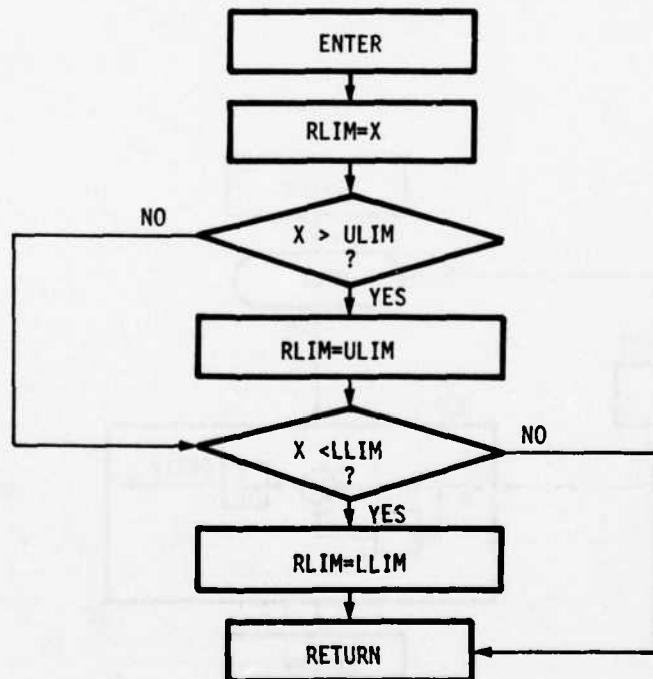

Figure E.11. Subroutine RLIM

E.2.9   <u>FDELAY</u>--Counts single trips for three-trip fault declaration.

```
 1:         SUBROUTINE FDELAY(IFAIL,JFAIL,N1,N2)
 2: C
 3: C  3 CONSECUTIVE IFAIL  INDICATORS WILL SET JFAIL INDICATOR
 4: C
 5:         DIMENSION IFAIL(1),JFAIL(1),TEMP(42)
 6:         COMMON/FILTIC/MODE,DT
 7:         INTEGER TEMP
 8: C
 9:         IF(MODE) 5,5,10
10: C
11:       5 DO 6 I=N1,N2
12:       6 TEMP(I)=0
13: C
14:      10 CONTINUE
15:         DO 20 I=N1,N2
16:         JFAIL(I)=0
17:         TEMP(I)=TEMP(I) + IFAIL(I)
18:         IF(IFAIL(I).GE.0) TEMP(I)=0
19:         IF(TEMP(I).LE.-3) JFAIL(I)=-1
20:      20 CONTINUE
21:         RETURN
22:         END
```
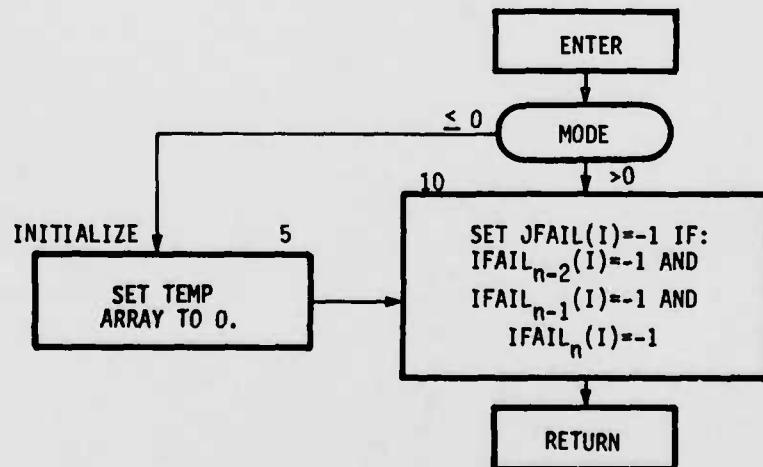

Figure E.12.   Subroutine FDELAY

341

E.2.10   <u>MON1</u>--Sequential likelihood ratio test of residual mean value used in Concepts
II and III.

```
 1:        SUBROUTINE MON1(V,XMON,IFLAG,NV,NMAX,MODE)
 2:        DIMENSION V(1),XMON(1),IFLAG(1)
 3:        DIMENSION SUM(42),N(42)
 4:        DATA SF1/2.00/,SF2/3.13/
 5:        IF(MODE) 10,10,20
 6:     10 DO 11 I=1,42
 7:        SUM(I)=0.
 8:     11 N(I)=0
 9:        RETURN
10:     20 DO 1 I=1,NV
11:        IFLAG(I)=0
12:        SUM(I)=SUM(I) + V(I)
13:        N(I)=N(I) + 1
14:        XN=N(I)
15:        IF(ABS(SUM(I)).LT.(SF2+SF1*XN)*XMON(I).OR.N(I).GT.NMAX)GO TO 2
16:        IFLAG(I)=-1
17:        GO TO 1
18:      2 CONTINUE
19:        IF(ABS(SUM(I)).GT.(SF2+SF1*(XN=2))*XMON(I).AND.N(I).LT.NMAX)GOTO 1
20:        SUM(I)=0.
21:        N(I)=0
22:      1 CONTINUE
23:        RETURN
24:        END
```
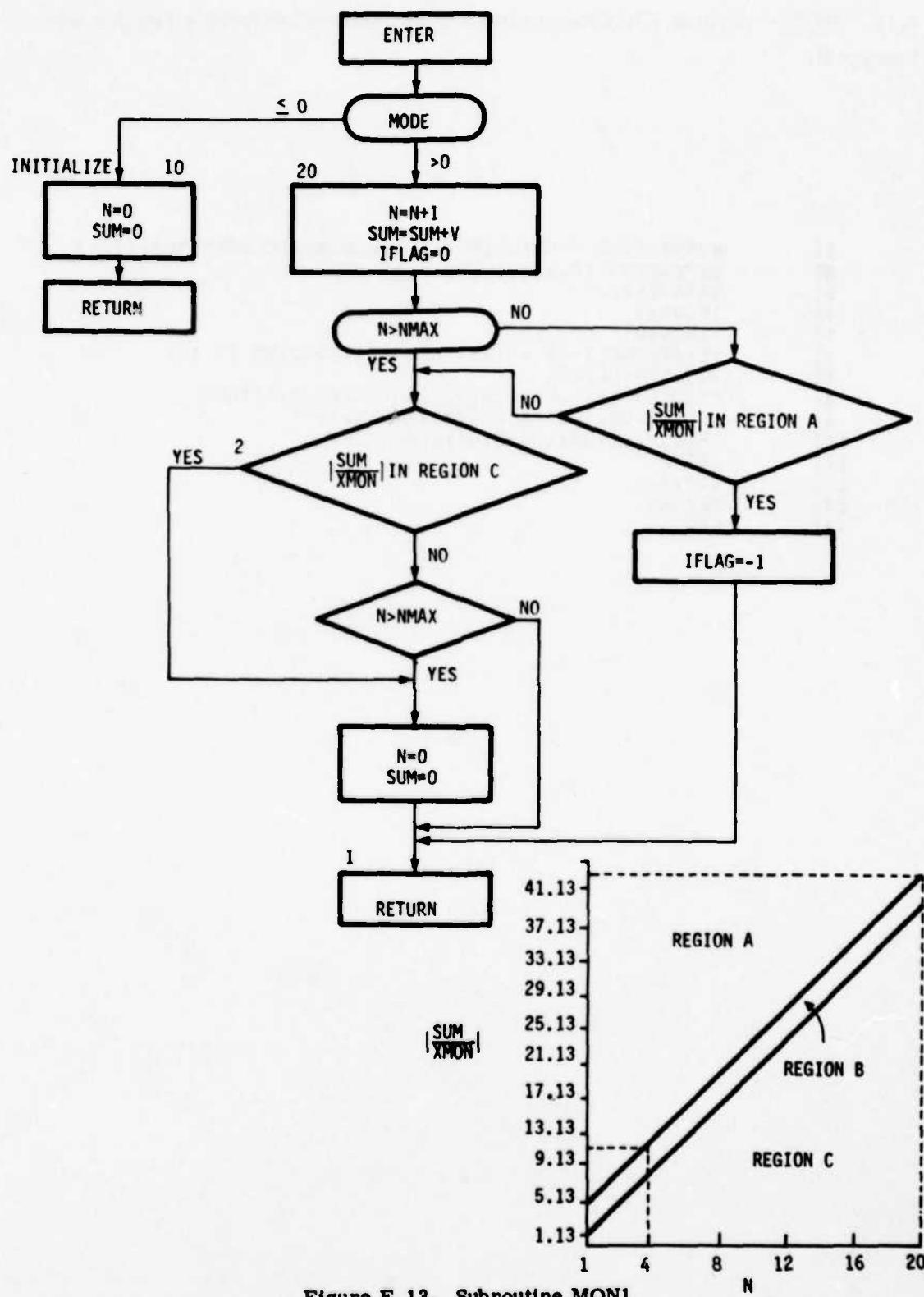
Figure E.13. Subroutine MON1

343

E.2.11   <u>MON2</u>--Sequential likelihood ratio test of likelihood difference function used
in Concept II.

```
 1:          SUBROUTINE MON2(VLIKE,IFLAG,JFLAG,IPLUS,MINUS,SIGV)
 2:          DIMENSION IFLAG(1),JFLAG(1)
 3:          DATA SF/1.0/
 4:          IPLUS=0
 5:          MINUS=0
 6:          IF(IFLAG(1)+IFLAG(2)+IFLAG(3).EQ.0)GO TO 1
 7:          SUM=SUM+VLIKE
 8:          IF(JFLAG(1)+JFLAG(2)+JFLAG(3).EQ.0)RETURN
 9:          IF(SUM.GT.3.455*SIGV*SF)IPLUS==1
10:          IF(SUM.LT.=3.455*SIGV*SF)MINUS==1
11:          RETURN
12:        1 SUM=0.0
13:          RETURN
14:          END
```

344
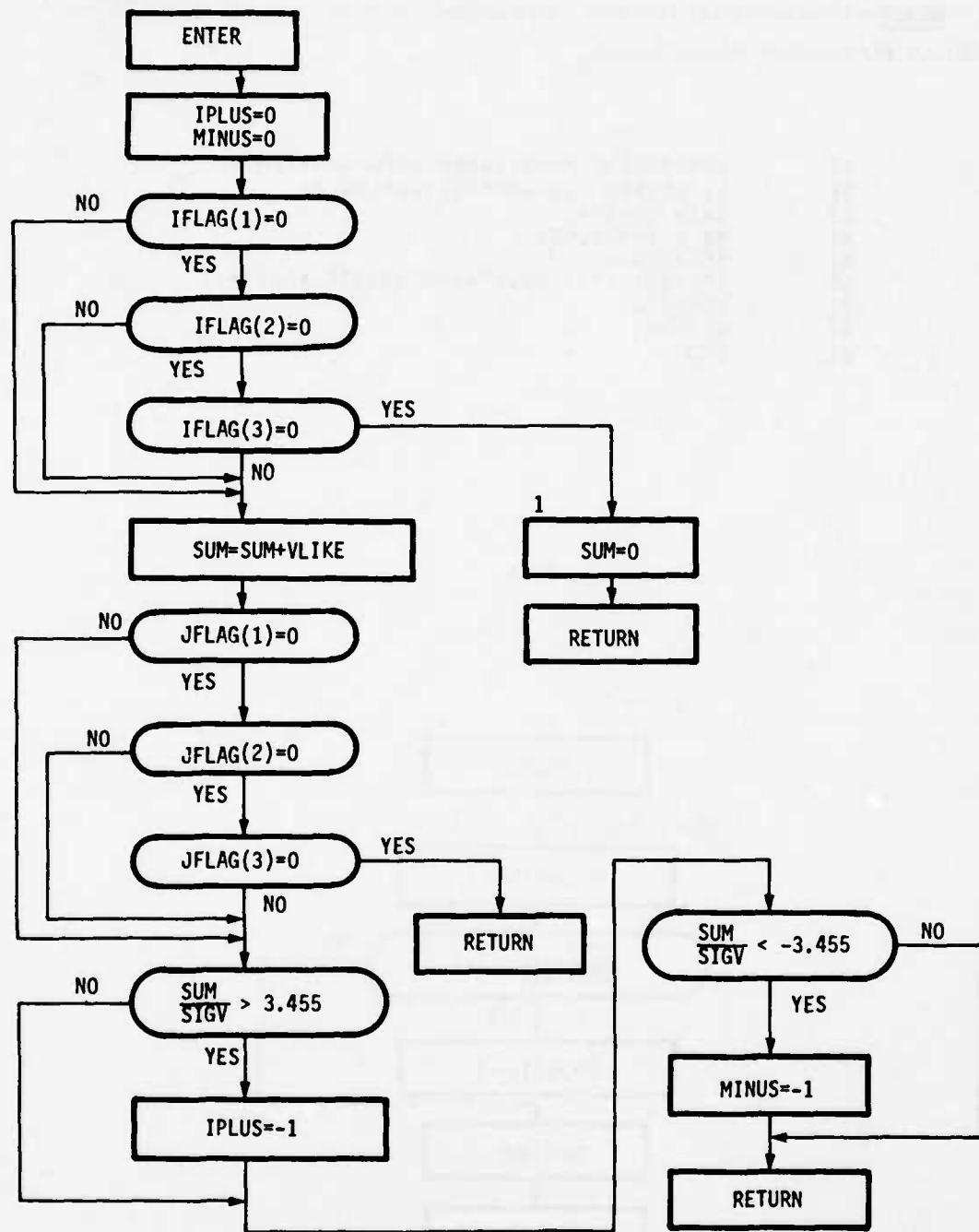
Figure E. 14. Subroutine MON2

345

E.2.12   MON3--Constant level residual trip monitor, used in Concepts II and III (used with FDELAY for multiple trip criteria).

```
1:        SUBROUTINE MON3(V,XMON,IFLAG,NV1,NV2)
2:        DIMENSION V(1),XMON(1),IFLAG(1)
3:        DATA SF/3.4/
4:        DO 1 I=NV1,NV2
5:        IFLAG(I)=0
6:        IF(ABS(V(I)).GT.SF*XMON(I))IFLAG(I)=-1
7:      1 CONTINUE
8:        RETURN
9:        END
```
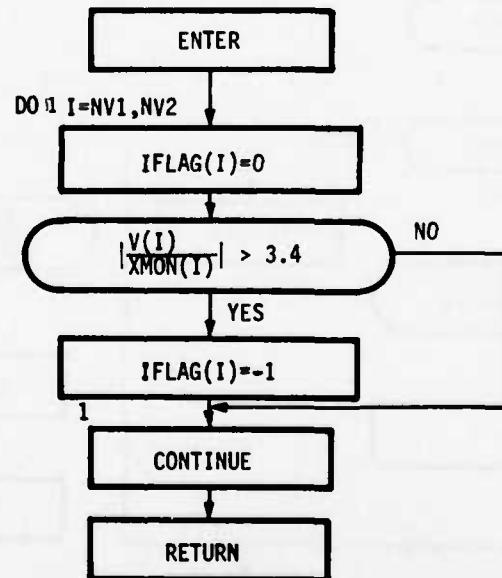

Figure E.15.   Subroutine MON3

346

E.2.13　AR21--Concept II Euler angle-body rate diagnostic filter.

```
 1:       SUBROUTINE AR21(EA,BR,SP,CP,ST,CT,XBAR,XHAT,V,DT)
 2:       REAL KF
 3:       DIMENSION EA(3),BR(3),XBAR(3),XHAT(3,3),KF(2,3)
 4:      1,EACK(3),BRCK(3),B(3,3),V(3),T(3)
 5:       DATA EACK/2*0.05,100.0/,BRCK/3*0.1/,B/1.0,8*0.0/
 6:      1,KF/0.229,-0.075,0.1131,-0.03,0.15627,-0.05/
 7:       B(1,2)=SP*ST/CT
 8:       B(1,3)=CP*ST/CT
 9:       B(2,2)=CP
10:       B(2,3)=-SP
11:       B(3,2)=SP/CT
12:       B(3,3)=CP/CT
13:       DO 6 J=1,3
14:       V(J)=EA(J)-XBAR(J)
15:       XHAT(1,J)=XBAR(J)+KF(1,J)*V(J)
16:       IF(ABS(BR(J)).GT.BRCK(J))GO TO 5
17:       IF(ABS(EA(J)).GT.EACK(J))GO TO 6
18:       XHAT(2,J)=XHAT(2,J)+KF(2,J)*V(J)
19:       GO TO 6
20:     5 XHAT(3,J)=XHAT(3,J)+KF(2,J)*V(J)/BR(J)
21:     6 T(J)=BR(J)-XHAT(2,J)-XHAT(3,J)*BR(J)
22:       DO 1 J=1,3
23:       TEMP=0.0
24:       DO 7 K=1,3
25:     7 TEMP=TEMP+B(J,K)*T(K)
26:     1 XBAR(J)=XHAT(1,J)+DT*TEMP
27:       RETURN
28:       END
```

ENTER

$$B = \begin{bmatrix} 1 & SIN\phi TAN\theta & COS\phi TAN\theta \\ 0 & COS\phi & -SIN\phi \\ 0 & SIN\phi/COS\theta & COS\phi/COS\theta \end{bmatrix}$$

J=1

COMPUTE RESIDUALS, V(J)

UPDATE EULER ANGLE ESTIMATES, XHAT(1,J)

ARE BODY RATES, BR(J) > BODY RATE CHECKS, BRCK(J) ?

YES

J=J+1

NO

ARE EULER ANGLES, EA(J) > EULER ANGLE CHECKS, EACK(J) ?

NO

ESTIMATE BIASES, XHAT(2,J)

YES

ESTIMATE SCALE FACTORS, XHAT(3,J)

PREDICT EULER ANGLES, XBAR(J)

J = 3 ?

NO

YES

RETURN
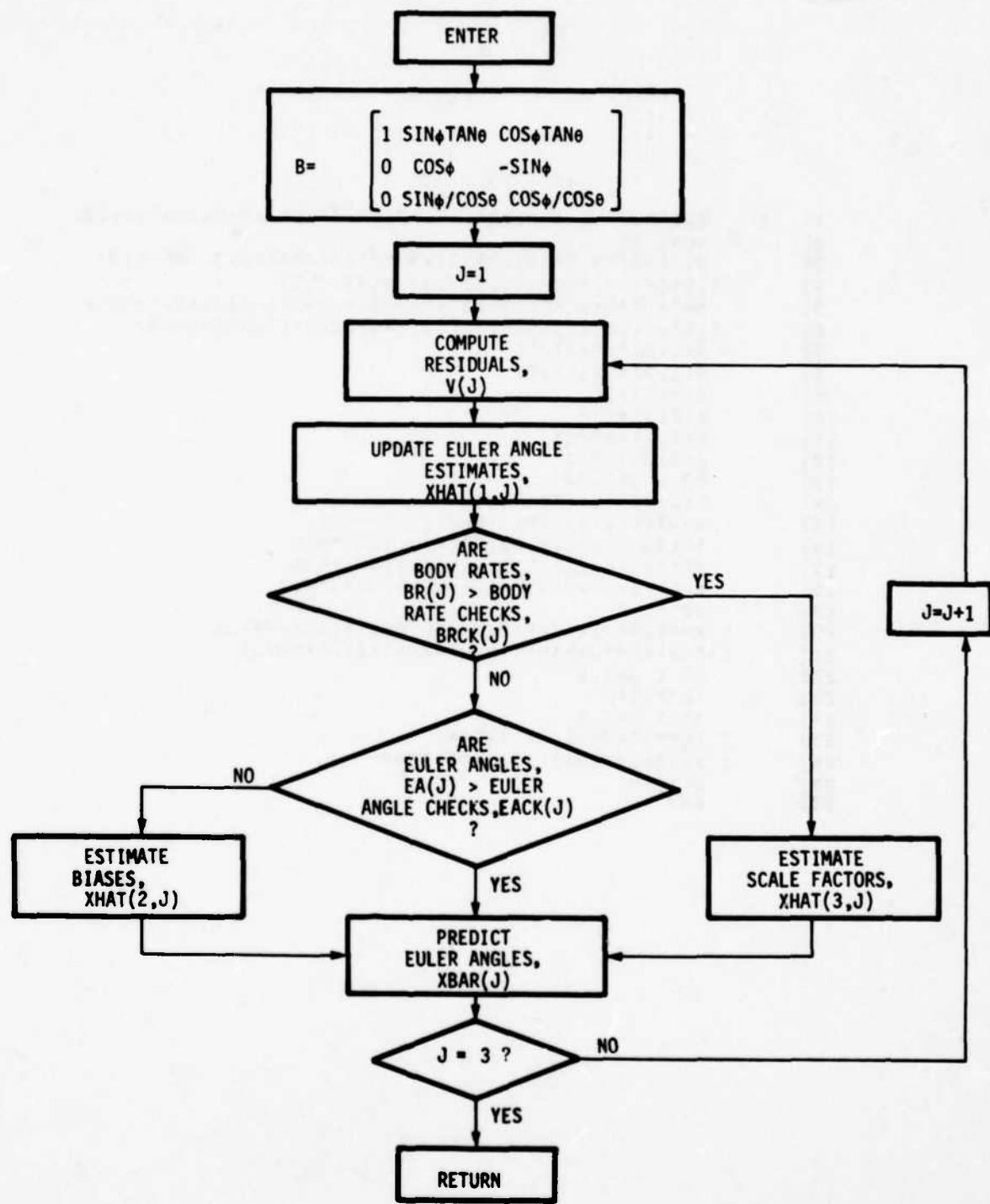
Figure E.16. Subroutine AR21

348

E.2.14   <u>AR22</u>--Concept II U, n_z, α, h, θ diagnostic filter.

```
 1:         SUBROUTINE AR22(ALT,AL,NZ,BR,SP,CP,ST,CT,UM,VS,XBAR,XHAT,V,DT,T)
 2:         REAL BR(3),XBAR(3),XHAT(3),V(2)
 3:        1,KF(3,2),LW,NZ
 4: C          GAIN SET NØ 2, INCREASED H = REDUCED AL
 5:         DATA G/32.17/
 6:        1,KF/.11482,-.046154,.043185,-3.9599,17.764,174.17/
 7:         V(1)=ALT-XBAR(1)
 8:         V(2)=AL-(XBAR(2)+XBAR(3))/UM
 9:         LW=1750.
10:         IF(ALT.LT.1750.)LW=ALT
11:         IF(ALT.LT.30.)LW=30.
12:         PHIG=1.0-DT*UM/LW
13:         DØ 2 I=1,3
14:         XHAT(I)=XBAR(I)
15:         DØ 2 J=1,2
16:       2 XHAT(I)=XHAT(I)+KF(I,J)*V(J)
17:         XBAR(1)=XHAT(1)+DT*(UM*ST-XHAT(2)*CT*CP*VS*CT*SP)
18:         XBAR(2)=XHAT(2)+DT*(-NZ+G*CT*CP-G*BR(1)*VS+BR(2)*UM)
19:         XBAR(3)=PHIG*XHAT(3)
20:         RETURN
21:         END
```
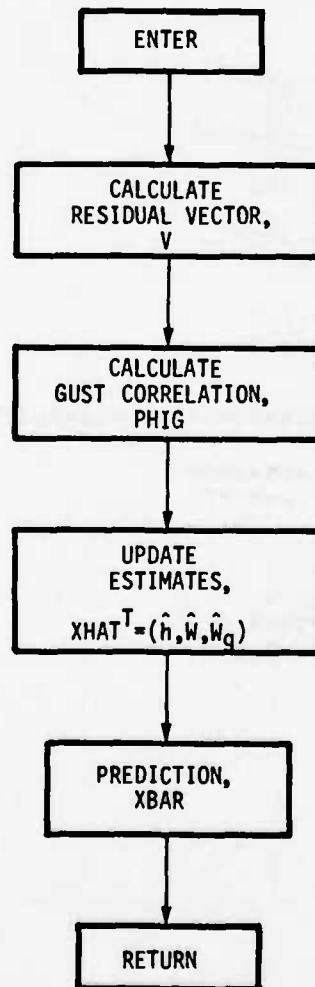

Figure E.17.   Subroutine AR22

349

E.2.15   AR23--Concept II n_y, P, R, ϕ diagnostic filter.

```
 1:         SUBROUTINE AR23(NY,P,R,DR,DA,U0,ALT,QBAR,AL,CT,SP,XBAR,XHAT
 2:        1,V,DT,OPTION)
 3:          REAL NY,V(1),XBAR(1),XHAT(1),KF(4,3)
 4:          INTEGER OPTION
 5:          DATA G/32.17/,KF
 6:        1/-1.7898E-04,2.9915E-03,-5.2628E-04,-1.5129E-03
 7:        2,-3.2498E-03,1.8832E-01,-4.2338E-02,-4.1000E-02
 8:        3,-2.4176E-02,-3.2073E-01,1.0432E-01,8.3344E-02/
 9:          DATA A11,A21,A31,A41,A12,A22,A32,A42,A13,A23,A33,A43,A14
10:        1,A24,A34,A44
11:        2/.97779,-1.7691,.34428,0.0,3.5414E-06,.78701,1.6985E-03
12:        3,0.0,-0.048333,.10048,.95026,0.0,-0.021674,-1.7184
13:        4,.33472,.94568/
14:          IF(OPTION.EQ.2)GO TO 4
15:          A14=-.00625-3.0E-05*QBAR
16:          A11=A14+1.0
17:          A12=0.0
18:          A13=-0.05
19:          A21=-.2-2.625E-03*QBAR
20:          A22=.940-2.5E-04*QBAR
21:          A23=5.25E-02+8.35E-05*QBAR
22:          A24=A21
23:          A31=0.115+6.7E-04*QBAR
24:          A32=-.004
25:          A33=.985-5.417E-05*QBAR
26:          A34=A31
27:          LW=1750.
28:          IF(ALT.LT.1750.)LW=ALT
29:          IF(ALT.LT.600.0)LW=600.
30:          A44=1.0-DT*U0/LW
31:        4 CONTINUE
32:          C11=(-0.12-2.583E-04*QBAR+2.0E-06*ALT)*U0
33:          C14=C11
34:          B11=2.0E-03+2.038E-05*QBAR
35:          IF(B11.GT..0127)B11=.0127
36:          B12=0.0
37:          B13=DT*32.17/U0
38:          B21=7.62E-04*QBAR
39:          IF(B21.GT.0.4)B21=0.4
40:          B22=-0.25-4.1E-03*QBAR
41:          IF(B22.LT.-2.4)B22=-2.4
```

350

```
42:       B31=-0.025-6.88E-04*QBAR
43:       IF(B31.LT.-0.4)B31=-0.4
44:       B32=0.10-4.375E-04*QBAR
45:       IF(B32.LT.-.075)B32=-.075
46:       D1=.0862*QBAR
47:       IF(D1.GT.43.7)D1=48.7
48:       D2=.0207*QBAR
49:       IF(D2.GT.15.0)D2=15.0
50:       V(1)=NY-C11*XBAR(1)-C14*XBAR(4)-D1*DR-D2*DA
51:       V(2)=P-XBAR(2)
52:       V(3)=R-XBAR(3)
53:       DO 2 J=1,4
54:       TEMP=XBAR(J)
55:       DO 3 K=1,3
56:     3 TEMP=TEMP+KF(J,K)*V(K)
57:     2 XHAT(J)=TEMP
58:       XBAR(1)=A11*XHAT(1)+A12*XHAT(2)+A13*XHAT(3)
59:      1+A14*XHAT(4)+B11*DR+B12*DA
60:      2+DT*P*AL+B13*CT*SP
61:       XBAR(2)=A21*XHAT(1)+A22*XHAT(2)+A23*XHAT(3)
62:      1+A24*XHAT(4)+B21*DR+B22*DA
63:       XBAR(3)=A31*XHAT(1)+A32*XHAT(2)+A33*XHAT(3)
64:      1+A34*XHAT(4)+B31*DR+B32*DA
65:       XBAR(4)=A44*XHAT(4)
66:       RETURN
67:       END
```
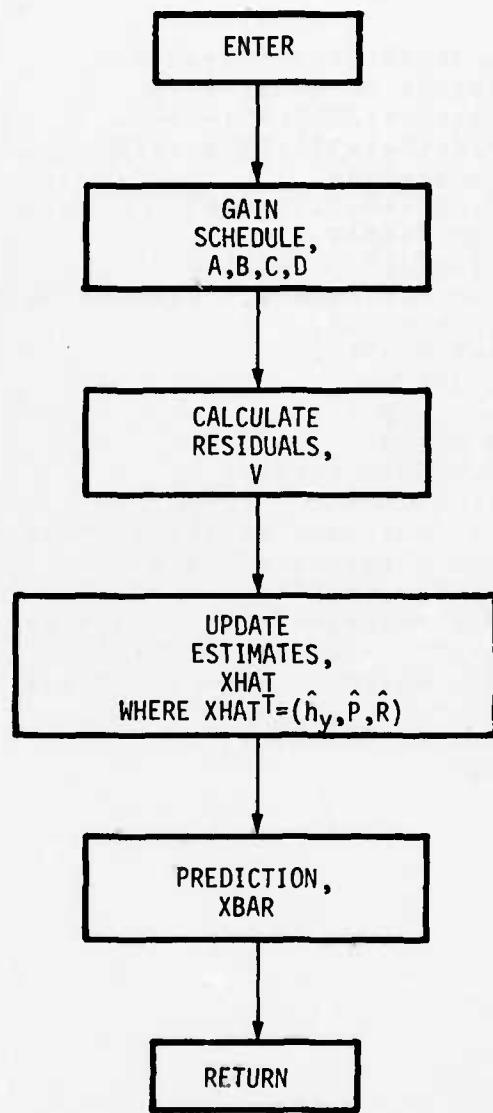
Figure E.17. Subroutine AR23

352

E. 2.16 AR24--Concept II dual body rate fail-op diagnostic filters.

```
 1:        SUBROUTINE AR24(EA,BR1,BR2,SP,CP,ST,CT,XBAR,XHAT,V,DT,VLIKE)
 2:        REAL KF(3),EA(3),BR1(3),BR2(3),V(6),XHAT(6),XBAR(6)
 3:       1,B(3,3),SIGS(3)
 4:        DATA KF/.229,.1131,.1567/,B/1.0,8*0.0/
 5:        DATA SIGS/.0198,2*.00698/
 6:        B(1,2)=SP*ST/CT
 7:        B(1,3)=CP*ST/CT
 8:        B(2,2)=CP
 9:        B(2,3)=-SP
10:        B(3,2)=SP/CT
11:        B(3,3)=CP/CT
12:        DO 1 I=1,3
13:        V(I)=EA(I)-XBAR(I)
14:        V(I+3)=EA(I)-XBAR(I+3)
15:        XHAT(I)=XBAR(I)+KF(I)*V(I)
16:        XHAT(I+3)=XBAR(I+3)+KF(I)*V(I+3)
17:        VLIKE=0.0
18:        DO 2 K=1,3
19:      2 VLIKE=VLIKE+B(I,K)*BR1(K)
20:        XBAR(I)=XHAT(I)+DT*VLIKE
21:        VLIKE=0.0
22:        DO 3 K=1,3
23:      3 VLIKE=VLIKE+B(I,K)*BR2(K)
24:      1 XBAR(I+3)=XHAT(I+3)+DT*VLIKE
25:        VLIKE=0.0
26:        DO 4 I=1,3
27:      4 VLIKE=VLIKE+(V(I)*V(I)-V(I+3)*V(I+3))/(SIGS(I)*SIGS(I))
28:        RETURN
29:        END
```

ENTER

PRECOMPUTE SIN
AND COS FUNCTIONS
REQUIRED FOR
EQN'S 7,8,9

CONCEPT 2   CONCEPT 2

EULER ANGLE-BODY
RATE KALMAN FILTER
USING BODY RATES
FROM SET 1

EULER ANGLE-BODY
RATE KALMAN FILTER
USING BODY RATES
FROM SET 2

$(\nu_\phi, \nu_\theta, \nu_\psi)_1$ $(\nu_\phi, \nu_\theta, \nu_\psi)_2$

COMPUTE VLIKE:

$$= \frac{\nu_{\phi_1}^2 - \nu_{\phi_2}^2}{\sigma_{\nu_\phi}^2} + \frac{\nu_{\theta_1}^2 - \nu_{\theta_2}^2}{\sigma_{\nu_\theta}^2} + \frac{\nu_{\psi_1}^2 - \nu_{\psi_2}^2}{\sigma_{\nu_\psi}^2}$$

RETURN
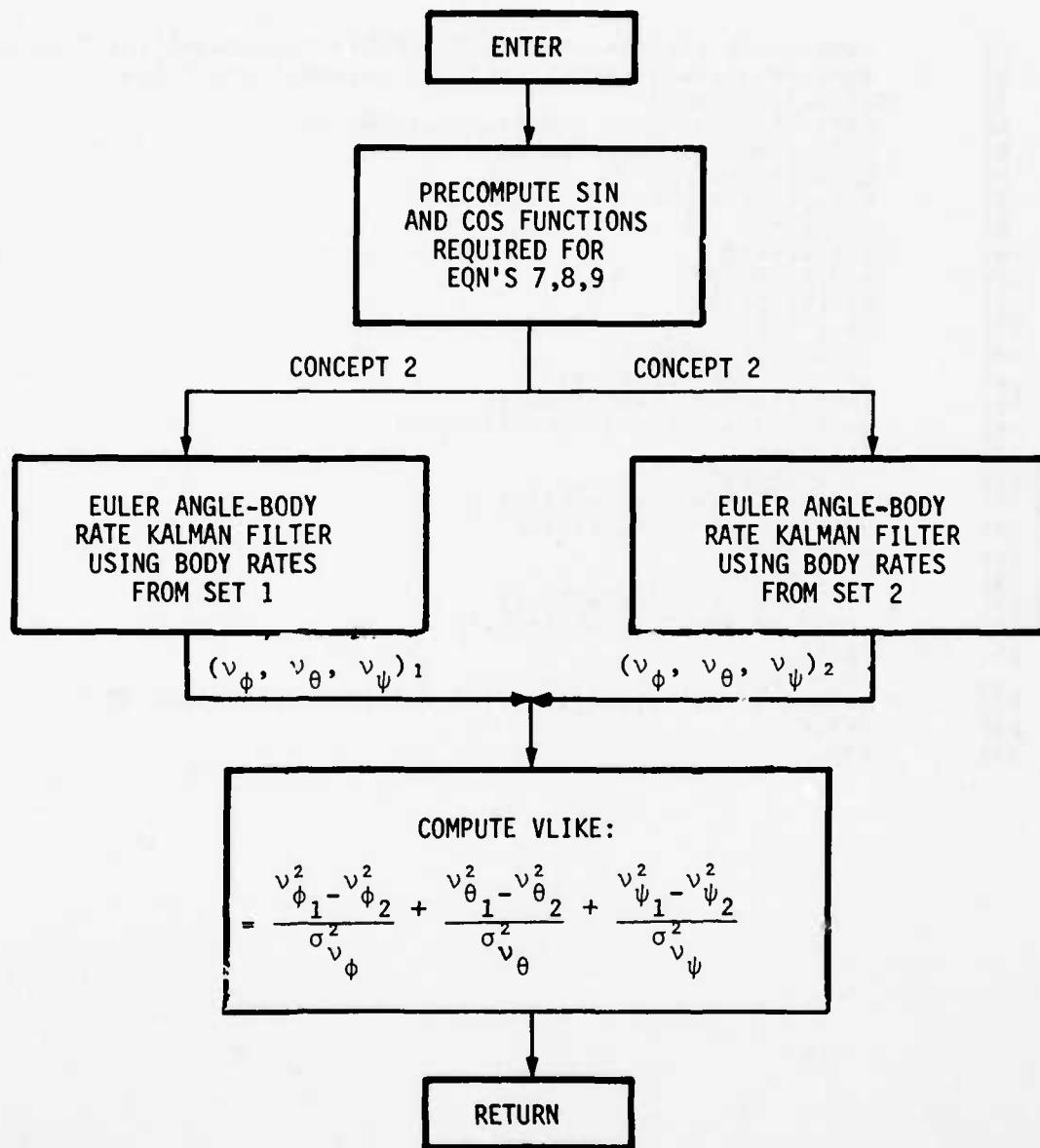
Figure E.18.   Subroutine AR24

E.2.17   AR31--Concept III, 3 n_z, Q, α linear short period filters.

```
 1:          SUBROUTINE AR31(NZ,Q,AL,DE,U0,ALT,GBAR,XBAR,XHAT,V,DT)
 2:          REAL NZ,V(1),XBAR(1),XHAT(1),KF(9,3),LW
 3: C           GAIN SET NO 2, REDUCED AL . INCREASED NZ AND Q
 4:          DATA KF
 5:          1/-2.3552E-05,1.6226E-04,-2.7967E-04
 6:          2,-2.5408E-05,1.8176E-04,-3.0519E-04
 7:          3,3*0.0
 8:          4,4.9818E-02,2.3288E-01,-1.2503E-01
 9:          5,5.0423E-02,2.4851E-01,-1.3468E-01
10:          6,5.2303E-02,3.5566E-01,-2.0825E-01
11:          7,5.3190E-03,-3.6643E-02,5.3158E-02
12:          8,3*0.0
13:          9,8.5222E-03,-7.5977E-02,1.1090E-01/
14:           A11=1.0+DT*(-.35-.002667*QBAR)
15:           A12=DT
16:           A13=A11-1.0
17:           A21=DT*(1.0-.031667*QBAR)
18:           A22=1.0+DT*(-.35-.0018333*QBAR)
19:           A23=A21
20:           LW=1750.
21:           IF(ALT.LT.1750.)LW=ALT
22:           IF(ALT.LT.30.)LW=30.
23:           A33=1.0-DT*U0/LW
24:           C11=-2.375*QBAR
25:           C13=C11
26:           B1=-.005-6.0E-05*QBAR
27:           B2=-.01-.002125*QBAR
28:           D=-.2583*QBAR
29:           DO 1 I=1,7,3
30:           V(I)=-NZ-C11*XBAR(I)-C13*XBAR(I+2)-D*DE
31:           V(I+1)=Q-XBAR(I+1)
32:           V(I+2)=AL-XBAR(I)-XBAR(I+2)
33:           DO 2 J=1,3
34:           IJ1=I+J-1
35:           TEMP=XBAR(IJ1)
36:           DO 3 K=1,3
37:           IK1=I+K-1
38:         3 TEMP=TEMP+KF(IJ1,K)*V(IK1)
39:         2 XHAT(IJ1)=TEMP
40:           XBAR(I)=A11*XHAT(I)+A12*XHAT(I+1)+A13*XHAT(I+2)
41:          1+B1*DE
42:           XBAR(I+1)=A21*XHAT(I)+A22*XHAT(I+1)+A23*XHAT(I+2)
43:          1+B2*DE
44:         1 XBAR(I+2)=A33*XHAT(I+2)
45:           RETURN
46:           END
```

355
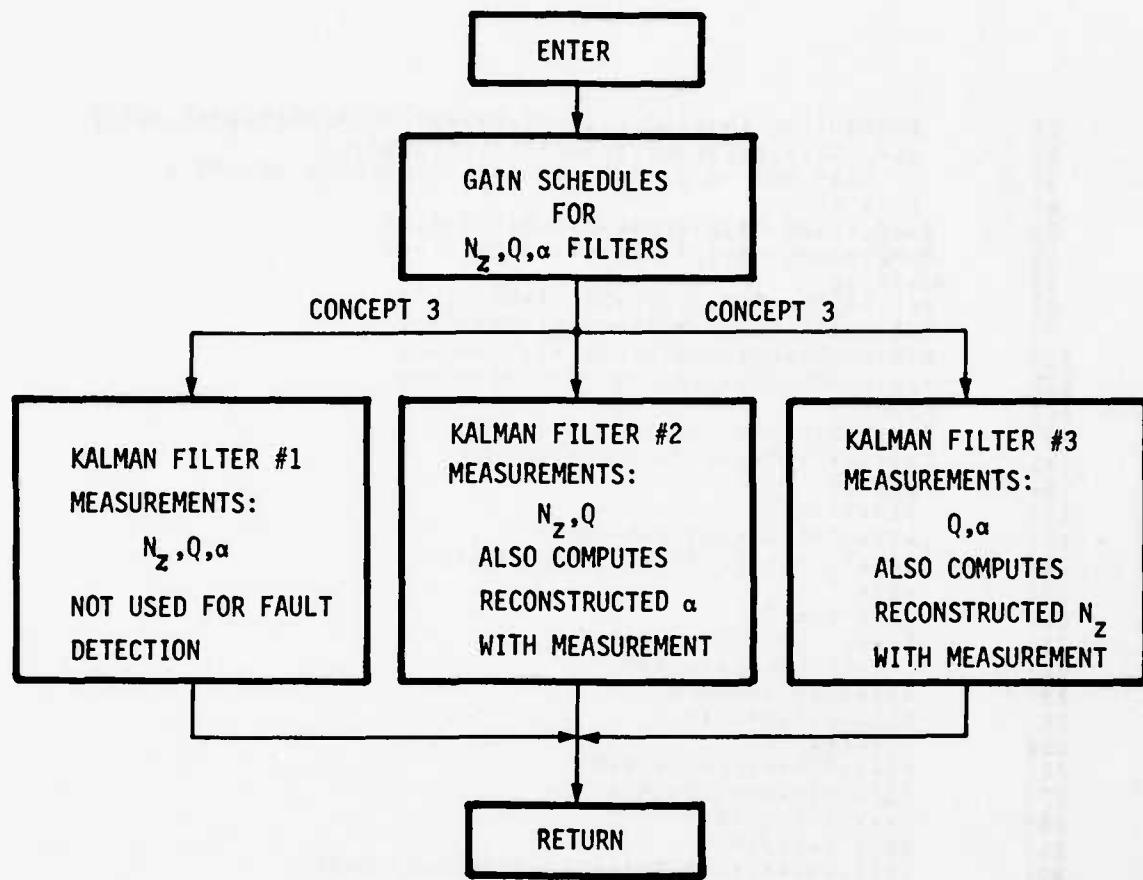
Figure E. 19. Subroutine AR31

E.2.18   <u>AR32</u>--Concept III, 4 n_y, P, R, lateral-directional filters.

```
 1:          SUBROUTINE AR32(NY,P,R,DR,DA,U0,ALT,QBAR,XBAR,XHAT,V,DT)
 2:          REAL NY,V(1),XBAR(1),XHAT(1),KF(4,3),LW
 3:          DATA KF
 4:          1/-1.7898E-04,2.9915E-03,-5.2628E-04,-1.5129E-03
 5:          2,-3.2498E-03,1.8832E-01,-4.2388E-02,-4.1000E-02
 6:          3,-2.4176E-02,-3.2073E-01,1.0432E-01,8.3344E-02/
 7:          A14=-.00625-3.0E-05*QBAR
 8:          A11=A14+1.0
 9:          A12=0.0
10:          A13=-0.05
11:          A21=-.2-2.625E-03*QBAR
12:          A22=.940-2.5E-04*QBAR
13:          A23=5.25E-02+8.35E-05*QBAR
14:          A24=A21
15:          A31=0.115+6.7E-04*GBAR
16:          A32=.004
17:          A33=.985-5.417E-05*QBAR
18:          A34=A31
19:          LW=1750.
20:          IF(ALT.LT.1750.)LW=ALT
21:          IF(ALT.LT.600.0)LW=600.
22:          A44=1.0-DT*U0/LW
23:          C11=(-0.12-2.583E-04*QBAR+2.0E-06*ALT)*U0
24:          C14=C11
25:          B11=2.0E-03+2.038E-05*QBAR
26:          IF(B11.GT..0127)B11=.0127
27:          B12=0.0
28:          B21=7.62E-04*QBAR
29:          IF(B21.GT.0.4)B21=0.4
30:          B22=-0.25-4.1E-03*QBAR
31:          IF(B22.LT..2.4)B22=-2.4
32:          B31=-0.025-6.88E-04*QBAR
33:          IF(B31.LT..-0.4)B31=-0.4
34:          B32=0.10-4.375E-04*QBAR
35:          IF(B32.LT...075)B32=-.075
36:          D1=.0862*QBAR
37:          IF(D1.GT.48.7)D1=48.7
38:          D2=.0207*QBAR
39:          IF(D2.GT.15.0)D2=15.0
40:          II=0
```
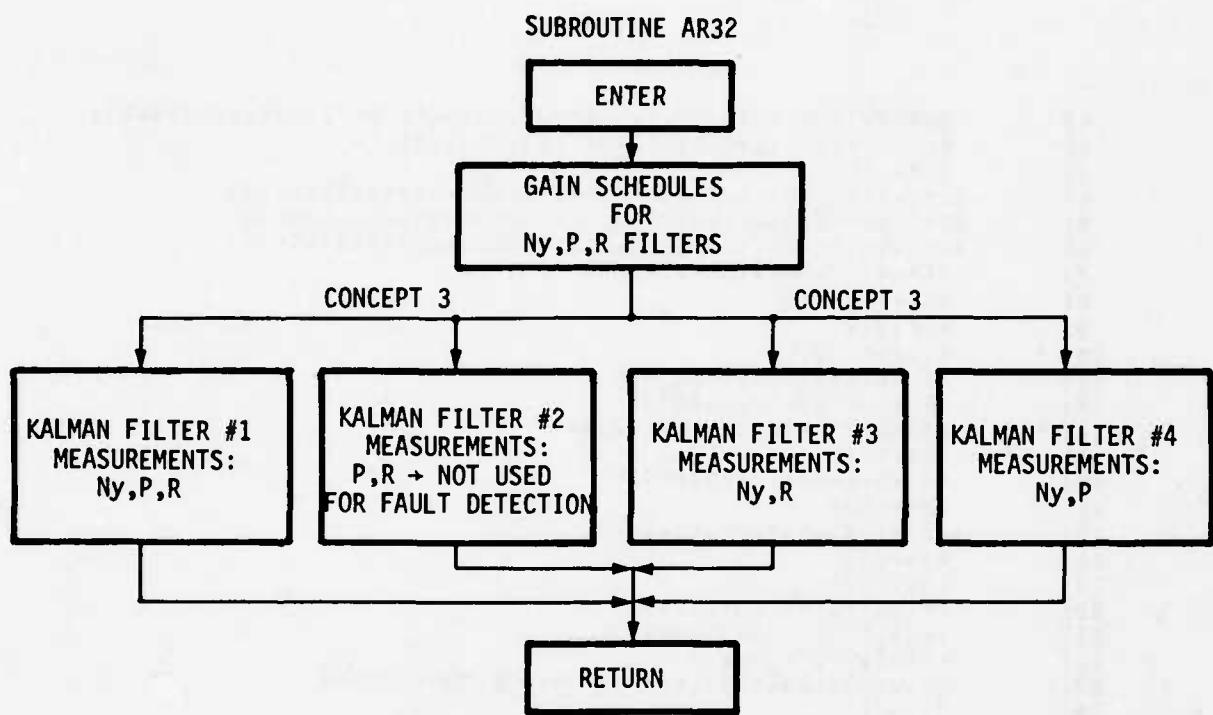
Figure E.20.   Subroutine AR32

E.2.19   <u>WHOA--Sensor consistency monitor.</u>

```
 1:          SUBROUTINE WHOA(X)
 2: C  IF SENSORS RATE OF CHANGE EXCEEDS A LIMIT THE LAST
 3: C  GOOD OUTPUT REPLACES IT
 4:          COMMON /FICTIC/MODE,DT
 5:          DIMENSION X(1),XP(11),XLIM(11)
 6:          DATA XLIM/16.00,6.00,1.00,.25,.25,.20,.07,.07,100.00,.10,200.00/
 7: C
 8:          IF(MODE) 100,100,200
 9: C
10:      100 DO 110 I=1,11
11:      110 XP(I)=X(I)
12:          RETURN
13:      200 DO 220 I=1,11
14:          TEMP=X(I) - XP(I)
15:          IF(ABS(TEMP).LT.XLIM(I)) GO TO 210
16:          X(I)=XP(I)
17:          GO TO 220
18:      210 XP(I)=X(I)
19:      220 CONTINUE
20:          RETURN
21:          END
```
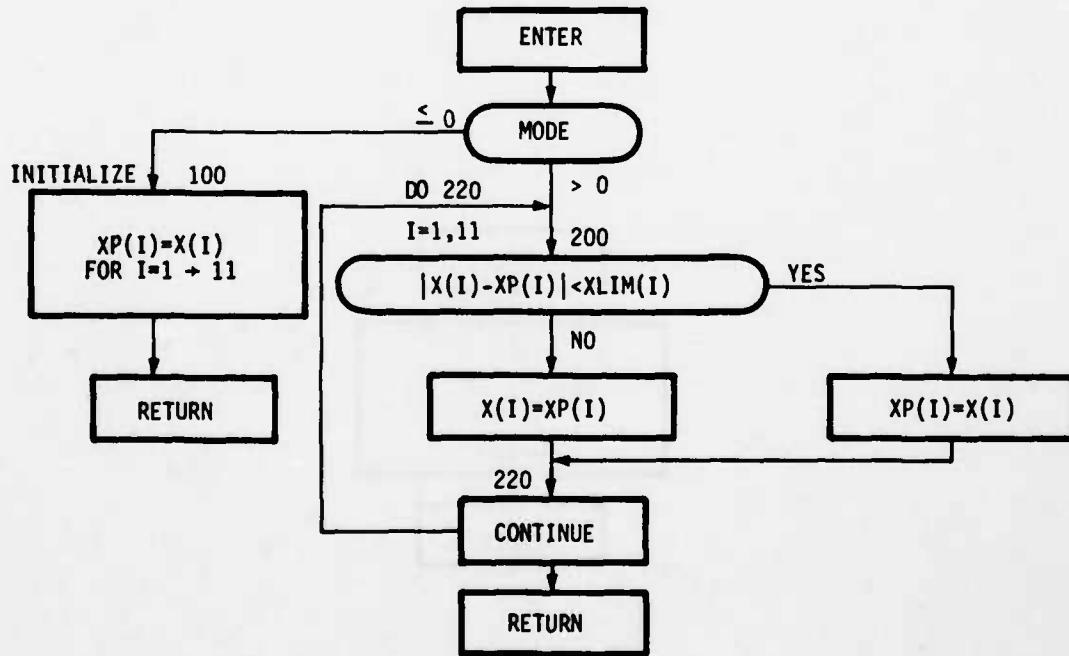

Figure E.21.   Subroutine WHOA

E.2.20　HPAS2--Second order high-pass filter--used in Concept III.

```
1:        SUBROUTINE HPAS2(YIN,YOUT,X1,X2)
2:        DATA A11,A21,A12,A22/.99378,-.04827,0.04827,.9312/
3:       1    ,B1,B2/.0012211,.04827/,C1,C2/-.9656,-1.376/,D/.9656/
4:        YOUT=C1*X1+C2*X2+D*YIN
5:        TEMP=A11*X1+A12*X2+B1*YIN
6:        X2=A21*X1+A22*X2+B2*YIN
7:        X1=TEMP
8:        RETURN
9:        END
```

$$\frac{s^2}{s^2+2\zeta\omega s+\omega^2}$$
$$\zeta=.7$$
$$\omega=1.0$$

ENTER → RETURN
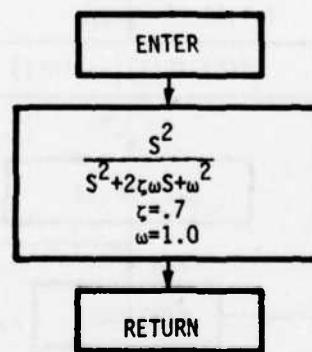
Figure E.22.　Subroutine HPAS2

E.2.21   <u>C3RECOV</u>--This routine performs the necessary isolation logic for Concept III. The following table describes this in more detail:

TABLE E.2.   CONCEPT III ISOLATION LOGIC DEFINITIONS

Flags	Concept II Filter (table)	Residual	Failed Sensor
IF1	KF #1	n_{z_m}	n_{z_m}
IF2	KF #1	Q_m	n_{z_m}
JF1	KF #2	Q_m	α_m
JF2	KF #2	α_m	α_m
(IF1 or IF2) and (JF1 or JF2)	KF #1 and KF #2	n_{z_m}, Q_m, α_m	Q_m
IF3	KF #3	n_{y_m}	R_m
IF4	KF #3	R_m	R_m
JF3	KF #4	n_{y_m}	P_m
JF4	KF #4	P_m	P_m
(IF3 or IF4) and (JF3 or JF4)	KF #3 and KF #4	n_{y_m}, P_m, R_m	n_{y_m}

```
1:        SUBROUTINE C3RECOV(IF1,IF2,JF1,JF2,IF3,IF4,JF3,JF4,ISENF,MODE)
2:        IF(MODE.GT.0)GO TO 1
3:        IFLP=0
4:        JFLP=0
5:        IFLR=0
6:        JFLR=0
7:        ISENF=0
8:        RETURN
9:      1 CONTINUE
10:       IF(IF1+IF2.LT.0)IFLP=IFLP+1
11:       IF(JF1+JF2.LT.0)JFLP=JFLP+1
12:       IF(IF3+IF4.LT.0)IFLR=IFLR+1
13:       IF(JF3+JF4.LT.0)JFLR=JFLR+1
14:       IF(IFLP.GT.0)ISENF=1
15:       IF(JFLP.GT.0)ISENF=10
16:       IF(IFLP.GT.0.AND.JFLP.GT.0)ISENF=4
17:       IF(IFLR.GT.0)ISENF=5
18:       IF(JFLR.GT.0)ISENF=3
19:       IF(IFLR.GT.0.AND.JFLR.GT.0)ISENF=2
20:       RETURN
21:       END
```
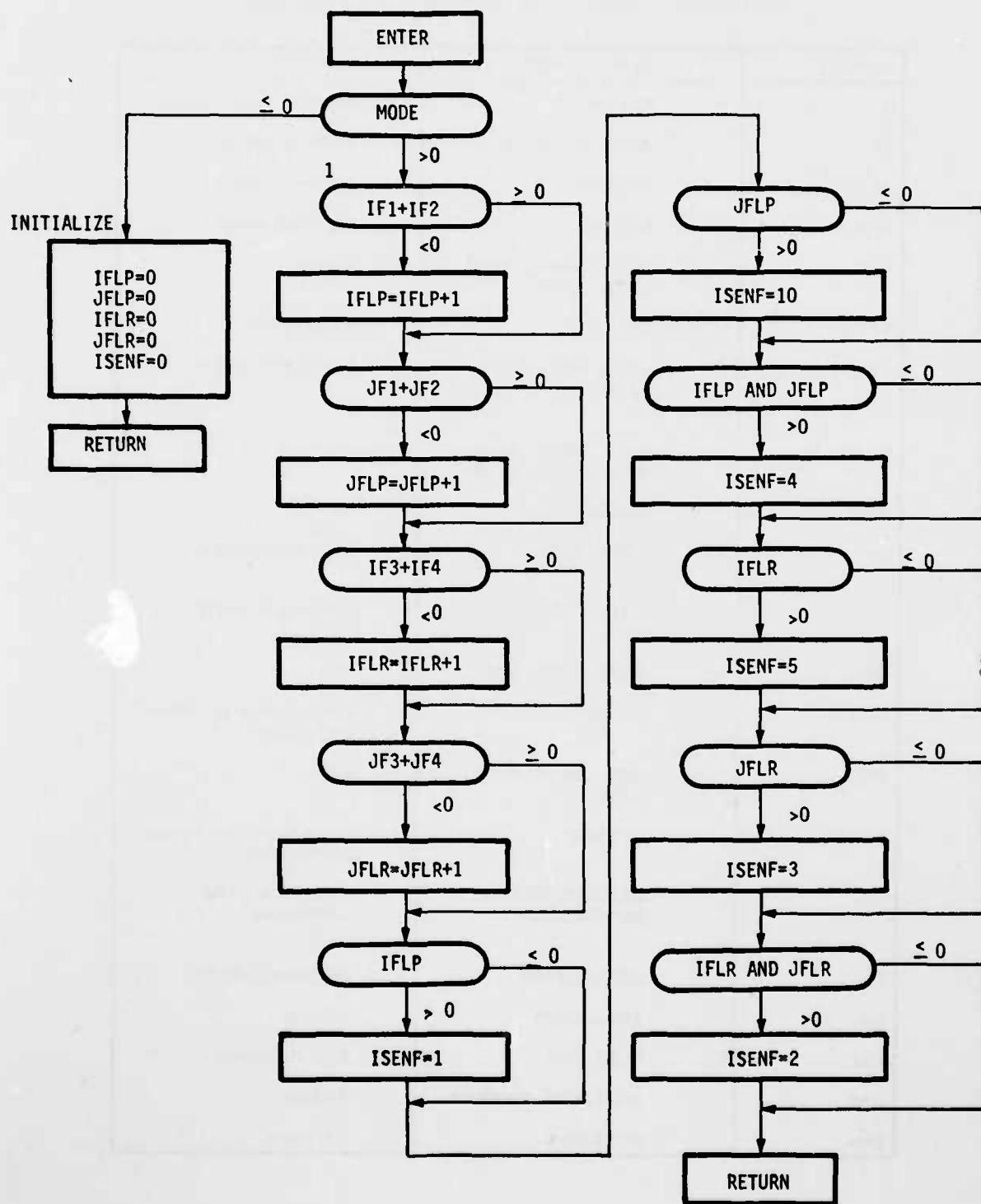
Figure E. 23.   Subroutine C3RECOV

363

TABLE E.3. COMPUTER VARIABLE DEFINITIONS

Variable	Routines Used	Definition
A	ROLLMON	Uplogic Decay Constant
AL	AR22, AR23, AR31	Angle-of-Attack
ALDS	DETECT	Angle-of-Attack
ALM	DETECT	Angle-of-Attack
ALT	MONH, AR22, AR23, AR31, AR32	Altitude
ALTM	DETECT	Altitude (ft)
A11, A12,...	AR23, AR31, AR32, HPAS2	Discrete A Matrix
B, B1, B2	AR21, AR24, AR33, AR31, AR23, HPAS2	Discrete B Matrix
BIAS	DETECT	Bias
BR	AR21, AR22	Body Rate Vector
C	AR23, AR31, AR32, HPAS2	Discrete C Matrix
CP	AR21, AR22, AR24	$\cos \phi$
CPHIS	DETECT	$\cos \phi$ (cosine of sensed roll angle)
CT	AR21, AR22, AR23, AR24	$\cos \theta$
CTHS	DETECT	$\cos \theta$ (cosine of sensed pitch angle)
C1	DETECT, FOLAG, HIPASS, DERIV	First Order Lag Coefficient
D	AR31, HPAS2	Discrete D Matrix
DA	AR23, AR32	Aileron
DAC	ROLLMON	Roll Command
DA0	ROLLMON, DETECT	Aileron
DDA	ROLLMON	Δ Aileron

TABLE E.3. COMPUTER VARIABLE DEFINITIONS

Variable	Routines Used	Definition
DE	AR31	Elevator
DEθ	DETECT	Elevator
DMON	MONC	Monitor Change
DR	AR23, AR32	Radar
DR0	DETECT	Rudder
DT	DETECT, FOLAG, HIPASS, DERIV, FDELAY, AR21, AR22, AR23, AR24, AR31, AR32, WHOA	Sampling Time (Simulation Sample Time)
DTI	DETECT, FOLAG, HIPASS, DERIV	Sampling Time
EA	AR21, AR24	Euler Angle Vector
EACK	AR21	Euler Angle Magnitude Check Vector
G	AR22, AR23	Gravity
H	MONH	Altitude
HDE	DETECT	Altitude Rate Error
HDEA	DETECT	Altitude Rate Error
HDS	DETECT	Filtered Altitude Rate
HS	DETECT	Filtered Altitude Rate
ICON	AR31, AR32	Gain Schedule Option
IFAIL	DETECT	Monitor Trip Flags
IFLP	C3RECOV	Concept III Logic Parameter
IFLR	C3RECOV	Concept III Logic Parameter
ISENF	C3RECOV	Concept III Isolated Failed Sensor
IF	C3RECOV	Concept III Logic Parameter

AD-A045 671　HONEYWELL INC　MINNEAPOLIS MINN SYSTEMS AND RESEARCH --ETC　F/G 1/3
FAULT TOLERANT DIGITAL FLIGHT CONTROL WITH ANALYTICAL REDUNDANC--ETC(U)
MAY 77　T CUNNINGHAM, D CARLSON, R HENDRICK　F33615-76-C-3031
AFFDL-TR-77-25　NL

UNCLASSIFIED

5 OF 5
ADA
045671

END
DATE
FILMED
11-77
DDC

TABLE E.3. COMPUTER VARIABLE DEFINITIONS

Variable	Routines Used	Definition
JFAIL	FDELAY, MON2	Monitor Trip Flags
JFLP	C3RECOV	Concept III Logic Parameter
JFLR	C3RECOV	"
JF	C3RECOV	"
KHD1	DETECT	Altitude Rate Mechanization Gain
KHD2	DETECT	Altitude Rate Mechanization Gain
KHD3	DETECT	Altitude Rate Mechanization Gain
KHD4	DETECT	Altitude Rate Mechanization Gain
KNZ1	DETECT	Normal Acceleration Mechanization Gain
KNZ2	DETECT	Normal Acceleration Mechanization Gain
KNZ3	DETECT	Normal Acceleration Mechanization Gain
KNZ4	DETECT	Normal Acceleration Mechanization Gain
KNZ5	DETECT	Normal Acceleration Mechanization Gain
KNZ6	DETECT	Normal Acceleration Mechanization Gain
KP1	DETECT	Roll Rate Mechanization Gain
KP2	DETECT	Roll Rate Mechanization Gain
KQ1	DETECT	Pitch Rate Mechanization Gain
KQ2	DETECT	Pitch Rate Mechanization Gain
KQ3	DETECT	Pitch Rate Mechanization Gain

TABLE E.3. COMPUTER VARIABLE DEFINITIONS

Variable	Routines Used	Definition
KQ4	DETECT	Pitch Rate Mechanization Gain
KR1	DETECT	Yaw Rate Mechanization Gain
KR2	DETECT	Yaw Rate Mechanization Gain
KR3	DETECT	Yaw Rate Mechanization Gain
KR4	DETECT	Yaw Rate Mechanization Gain
LLIM	RLIM, DETECT	Lower Limit To Be Imposed on Input Parameter
LW	AR22, AR23, AR31, AR32	Gust Scale Length
MINUS	MON2	SLRT Logic Output
MODE	C3RECOV, DETECT, FOLAG, HIPASS, DERIV, FDELAY, MON1, WHOA	Flag To Indicate Program Initialization or Run Segment
N	ROLLMON	Initialization
N(1-42)	MON1	Sum Numbers
NMAX	MON1	Maximum Sequence in Sum
NV	MON1	Number of Residuals Being Tested
NV1	MON3	Test Index Limits or Residuals
NV2	MON3	Test Index Limits or Residuals
NY	AR23, AR32	Lateral Acceleration
NYM	DETECT	Measured Lateral Acceleration
NZ	AR22 AR31	Normal Acceleration (ft/s/s) Sensed Lateral Acceleration

TABLE E.3. COMPUTER VARIABLE DEFINITIONS

Variable	Routines Used	Definition
NZE	DETECT	Difference between Sensed and Reconstructed Normal Acceleration
NZEA	DETECT	Absolute Value of NZE
NZM	DETECT	Sensed Normal Acceleration
NZS	DETECT	Sensed Normal Acceleration
N1	MONC, FDELAY	Starting Location in IFAIL for Applying Triple Trip Delay
N2	MONC, FDELAY	Ending Location in IFAIL for Applying Triple Trip Delay
P	AR23, AR32	Roll Rate
PDS	DETECT	Sensed Roll Rate
PDSA	DETECT	Absolute Value of PDS
PE	DETECT	Difference between Sensed and Reconstructed Roll Rates
PEA	DETECT	Absolute Value of PE
PHI	ROLLMON	Roll Angle
PHIDS	DETECT	Sensed Roll Angle
PHIG	AR22	Gust Correlation
PHIM	DETECT	Sensed Roll Angle
PHIQ	MONQ	Dynamic Pressure Delay Parameter
PM	DETECT	Sensed Roll Rate
PSIDS	DETECT	Sensed Yaw Angle (deg)
PSIM	DETECT	Sensed Yaw Angle (rad)
Q	AR31	Pitch Rate
QBAR	AR23, AR31, AR32	Dynamic Pressure

TABLE E.3. COMPUTER VARIABLE DEFINITIONS

Variable	Routines Used	Definition
QBARF	MONQ	Lased Dynamic Pressure
QDS	DETECT	Sensed Pitch Rate
QDSA	DETECT	Absolute Value of QDS
QE	DETECT	Difference between Sensed and Reconstructed Pitch Rate
QEA	DETECT	Absolute Value of QE
QM	DETECT	Sensed Pitch Rate
R	AR23, AR32	Yaw Rate
RAT	MONQ	Ratio
RDS	DETECT	Sensed Yaw Rate
RDSA	DETECT	Absolute Value of RDS
RE	DETECT	Difference between Sensed and Reconstructed Yaw Rate (dps)
REA	DETECT	Absolute Value of RE
RM	DETECT	Sensed Yaw Rate
RTD	DETECT	Radian-to-Degrees Conversion Constant (= 57.3) (d/r)
SF	MON2, MON3	Scaling Factor
SFBR(1-3)	DETECT	Sensor Parameters in Labeled Common--Not Used in DETECT
SIGB(1-11)	DETECT	Sensor Parameters in Labeled Common--Not Used in DETECT
SIGS(1-3)	AR24	Likelihood RMS Values
SIGSF(1-11)	DETECT	Sensor Parameters in Labeled Common--Not Used in DETECT

TABLE E.3. COMPUTER VARIABLE DEFINITIONS

Variable	Routines Used	Definition
SIGSN(1-11)	DETECT	Sensor Parameters in Labeled Common--Not Used in DETECT
SIGV	MON2	Residual RMS
SP	AR21, AR22, AR23, AR24	$\sin \phi$
SPHIS	DETECT	$\sin \phi$ (Sine of Sensed Roll Angle)
SQ	MONQ	Dynamic Pressure
ST	AR21, AR22, AR24	$\sin \theta$
STHS	DETECT	$\sin \theta$ (Sine of Sensed Pitch Angle)
SUM	MON1, MON2	Sum of Residuals
T	MONQ, AR22	Time
T(1-3)	AR21	Temporary Variables
TAU	FOLAG, HIPASS	Filter Time Constant
TEMP	AR21	Temporary Variables
TEMP	AR23	"
TEMP	AR31	"
TEMP	AR32	"
TEMP	WHOA	Difference between Current and Previous Sensor Outputs
TEMP	HPAS2	Counts the Number of Consecutive Trip Flags in IFAIL
THDS	DETECT	Sensed Pitch Angle
THETAM	DETECT	Sensed Pitch Angle
T1, T2, ⋮ T20	DETECT	Miscellaneous Intermediate Computations

TABLE E.3. COMPUTER VARIABLE DEFINITIONS

Variable	Routines Used	Definition
UG	DETECT	Gust Velocity along Longitudinal Axis (fps)
ULIM	RLIM	Upper Limit To Be Imposed on Input Parameter
ULIM(1-11)	DETECT	Upper Limits Imposed on Sensor Outputs
UM	AR22	Airspeed Measurement
UO	AR23, AR31, AR32	Airspeed
UOM	DETECT	Sensed Velocity along Longitudinal Axis (fps)
V(1-42)	MON1, MON3, AR21, AR22, AR23, AR24, AR31, AR32	Residual Vector
VELS	DETECT	Sensed Total Velocity (fps)
VG	DETECT	Gust Velocity along Lateral Axis (fps)
VLIKE	MON2, AR24	Likelihood Difference
VS	AR22	Sideslip Velocity
WG	DETECT	Vertical Gust Velocity (fps)
X	ROLLMON	Roll Uplogic State
X	FOLAG	Parameter to Which Lag Will Be Applied
X	HIPASS	Parameter That Will Be High-Passed
X	DERIV	Parameter from Which the Derivative Will Be Computed
X	RLIM	Parameter to Which Limits Will Be Applied
XBAR(1-42)	AR21, AR22, AR23, AR24, AR31, AR32	$\bar{x}$, Predicted State Vector
XHAT(1-42)	AR21, AR22, AR23, AR24, AR31, AR32	$\hat{x}$, Estimate Vector

TABLE E.3. COMPUTER VARIABLE DEFINITIONS

Variable	Routines Used	Definition
XMAX	ROLLMON	Maximum Roll Uplogic State
XMAXO	ROLLMON	Initial Roll Uplogic State
XMON(1-42)	MON1, MON3	Current Monitor Level
XMONO(1-42)	MONC	Initial Monitor Level
XMON1(1-42)	MONQ, MONH, MONC	Monitor Level
XN	MON1	Sum Count (real)
XP(1-6)	DETECT, FOLAG, HIPASS, DERIV	Value of Filter Input at the Previous Sample Point
XP(7-20)	DETECT, FOLAG, HIPASS, DERIV	Not Used
XPP(1-7)	DETECT, FOLAG, HIPASS, DERIV	Value of Input to DERIV at the Previous Sample Point
XPP(8-10)	DETECT, FOLAG, HIPASS, DERIV	Not Used
Y	ROLLMON, MONC	Roll Uplogic Variable
Y(1)	DETECT	Sensed Normal Acceleration (ft/s/s)
Y(2)	DETECT	Sensed Lateral Acceleration (ft/s/s)
Y(3)	DETECT	Sensed Roll Rate (rps)
Y(4)	DETECT	Sensed Pitch Rate (rps)
Y(5)	DETECT	Sensed Yaw Rate (rps)
Y(6)	DETECT	Sensed Roll Angle (rad)
Y(7)	DETECT	Sensed Pitch Angle (rad)
Y(8)	DETECT	Sensed Yaw Angle (rad)
Y(9)	DETECT	Sensed Longitudinal Velocity (fps)
Y(10)	DETECT	Sensed Angle-of-Attack (rad)
Y(11)	DETECT	Sensed Altitude (ft)

TABLE E.3. COMPUTER VARIABLE DEFINITIONS

Variable	Routines Used	Definition
Y(12-17)	DETECT	Not Used in DETECT
YP(1-6)	DETECT, FOLAG, HIPASS, DERIV	Value of Filter Output at the Previous Sample Point
YP(7-20)	DETECT, FOLAG, HIPASS, DERIV	Not Used

373

REFERENCES

1. Eberlein, A. and Lahn, T., "Failure Detection and Isolation Investigation for Strap Down Skewed Redundant Tetrad Laser Gyro Inertial Sensor Arrays," NASA Ames HI-CR-137730, 1975.

2. Abrahms, C. R. and Weinstein, W. D., "A Concept for Angular Rate Flight Control Sensors," AIAA Paper No. 74-868, Mechanics and Control of Flight Conference, August 1974.

3. Pejsa, A., "Optimum Skewed Redundant Inertial Navigation," AIAA Guidance and Control Conference, Paper No. 73-850, August 1973.

4. Pejsa, A., "Optimum Orientating and Accuracy of Redundant Sensor Arrays," 9th Aerospace Sciences Meeting, Paper No. 71-59, January 1971.

5. Advanced Fighter Digital Flight Control Definition Study, MCAIR Purchase Order Z40020, Honeywell, Inc., March 1975.

6. Meier, L., Ross, D. W., and Glaser, M. B., Evaluation of the Feasibility of Using Internal Redundancy to Detect and Isolate On-Board Control Data Instrumentation Failures, AFFDL-TR-70-172, January 1971.

7. Maybeck, Peter S., Failure Detection Through Functional Redundancy, AFFDL-TR-74-3, January 1974.

8. Hartmann, G. L., Harvey, C. A., Stein, G. et al., Digital Adaptive F-8C Control Laws, Final Report NAS 1-13358, July 1975.

9. Clark, R. N. et al., "Detecting Instrument Malfunctions in Control Systems," IEEE Transactions on Aerospace and Electronic Systems, Vol. AES-11, No. 4, July 1975.

10. Kerr, T. H., "A Two Ellipsoid Overlap Test for Real-Time Failure Detection and Isolation by Confidence Regions," IEEE Conference on Decision and Control, Phoenix, Arizona, November 1974.

11. Mehra, R. K. and Peschon, J., "An Innovations Approach to Fault Detection and Diagnosis in Dynamic Systems," <u>Automatica</u>, Vol. 7, 1971, pp. 637-640.

12. Montgomery, R. C. and Caglayan, A. K., "A Self-Reorganizing Digital Flight Control System for Aircraft," <u>AIAA 12th Aerospace Sciences Meeting</u>, Washington, D. C., January 30-February 1, 1974.

13. Montgomery, R. C. and Price, D. B., "Management of Analytical Redundancy in Digital Flight Control Systems for Aircraft," <u>AIAA Mechanics and Control of Flight Conference</u>, Anaheim, California, August 5-9, 1974.

14. Athans, M. and Willner, D., "A Practical Scheme for Adaptive Aircraft Flight Control Systems," <u>Symp. on Parameter Estimation Techniques and Applications in Aircraft Flight Testing</u>, NASA Flt. Res. Center, Edwards AFB, April 24 and 25, 1973.

15. Lainiotis, D. G., "Joint Detection, Estimation, and System Identification," <u>Information and Control</u>, Vol. 19, No. 1, August 1971, pp. 75-92.

16. Buxbaum, P. J. and Haddad, R. A., "Recursive Optimal Estimation for a Class of Nongaussian Processes," <u>Proc. of Symp. on Computer Processing in Communications</u>, Polytech Inst. of Brooklyn, April 8-10, 1969.

17. Stein, G. and Hartmann, G. L., <u>F-8C Adaptive Control Extensions</u>, NASA Contract NAS 1-13383, June 1976.

18. Willsky, A. S., Deyst, J. J. and Crawford, B. S., "Adaptive Filtering and Self-Test Methods for Failure Detection and Compensation," <u>Proc. of the 1974 JACC</u>, Austin, Texas, June 19-21, 1974.

19. Willsky, A. S. and Jones, H. L., "A Generalized Likelihood Ratio Approach to State Estimation in Linear Systems Subject to Abrupt Changes," <u>Proc. of the 1974 IEEE Conference on Decision and Control</u>, Phoenix, Arizona, November 1974.

20. Deyst, J. J. and Deckert, J. C., "RCS Jet Failure Identification for the Space Shuttle," <u>Proc. of IFAC '75</u>, Cambridge, Massachusetts, August 1975.

21. McAulay, R. J. and Denlinger, E., "A Decision-Directed Adaptive Tracker," <u>IEEE Trans. on Aero. and Elec. Sys.</u>, Vol. AES-9, March 1973, pp. 229-236.

22. Sanyal, P. and Shen, C. N., "Bayes' Decision Rule for Rapid Detection and Adaptive Estimation Scheme with Space Applications," IEEE Trans. on Automatic Control, Vol. AC-19, June 1974, pp. 228-231.

23. Jones, H. L., Failure Detection in Linear Systems, PhD Thesis, Lept. of Aeronautics and Astronautics, MIT, Cambridge, Massachusetts, September 1973.

24. Beard, R. V., Failure Accommodation in Linear Systems Through Self-Reorganization, Report MVT-71-1, Man-Vehicle Laboratory, Cambridge, Massachusetts, February 1971.

25. Sworder, D. D. and Robinson, V. G., "Feedback Regulators for Jump Parameter Systems with State and Control Dependent Transition Rates," IEEE Trans. on Automatic Control, Vol. AC-18, No. 4, August 1973, pp. 355-360.

26. Sworder, D. D., "Bayes' Controllers with Memory for a Linear System with Jump Parameters," IEEE Trans. on Automatic Control, Vol. AC-17, February 1972, pp. 118-121.

27. Ratner, R. S. and Luenberger, D. G., "Performance-Adaptive Renewal Policies for Linear Systems," IEEE Trans. on Automatic Control, Vol. AC-14, No. 4, August 1969, pp. 344-351.

28. Pierce, B. D. and Sworder, D. D., "Bayes and Minimax Controllers for a Linear System with Stochastic Jump Parameters," IEEE Trans. on Automatic Control, Vol. AC-16, No. 4, August 1971, pp. 300-307.

29. Davis, M. H. A., "The Application of Nonlinear Filtering to Fault Detection in Linear Systems," IEEE Trans. on Automatic Control, Vol. AC-20, No. 2, April 1975, pp. 257-259.

30. McGarty, T. P., "State Estimation with Faulty Measurements: An Application of Bayesian Outlier Rejection," Proc. of the Fifth Symposium on Nonlinear Estimation and Its Applications, San Diego, California, September 1974.

31. Chien, T. T., An Adaptive Technique for a Redundant-Sensor Navigation System, Report T-560, Draper Labs, Cambridge, Massachusetts, February 1972.

32. Sage, A. P., *Optimum Systems Control*, Prentice-Hall, Englewood Cliffs, N.J., 1968.

33. Chalk, T. P. and Harris, T. M., "Background Information and User Guide for MIL-F-8785B (ASG), Military Specification-Flying Qualities of Piloted Airplanes," AFFDL-TR-69-72, August 1969.

34. Hendrick, R. et al., *Flight Test Evaluation of a Digital Multimode Flight Control System for the A-7D Aircraft: Volume I--Design, Analysis, and Ground Test Phase*, AFFDL-TR-75-97, August 1975.

35. Cramer, H. and Leadbetter, M. R., *Stationary and Related Stochastic Processes*, John Wiley & Sons, New York, 1967.

36. Lindgren, B. W., *Statistical Theory*, MacMillan, London, 1968.

37. Deyst, J. J. and Deckert, J. C., *Shuttle Orbiter Reaction Control Subsystem Jet Failure Detection Using a Generalized Likelihood Ratio Technique*, The Charles Stark Draper Laboratory, Inc., Report No. R-848, Cambridge, Massachusetts, November 1974.